Molecular Engineering of Porphyrins as Organocatalysts and Methods Development for New Highly Substituted Porphyrins

Submitted by

Marc Kielmann (M.Sc.)

Trinity College Dublin, the University of Dublin

A thesis submitted to Trinity College Dublin, the University of Dublin, for the degree of

Doctor of Philosophy

August 2019

Under the supervision of Prof. Dr. Mathias O. Senge

„Da steh ich nun, ich armer Tor,

und bin so klug als wie zuvor.“

Johann Wolfgang von Goethe (Werk: Faust)

Declaration

I declare that this thesis has not been submitted as an exercise for a degree at this or any other university and it is entirely my own work.

I agree to deposit this thesis in the University's open access institutional repository or allow the Library to do so on my behalf, subject to Irish Copyright Legislation and Trinity College Library conditions of use and acknowledgement.

Where work was carried out jointly, this is duly acknowledged in the text wherever included.

Signed:

_____(Marc Kielmann)

August 2019 Trinity College Dublin

Summary of Work

Chapter 1 introduces the N–H···X binding motif in tetrapyrroles, which forms the basis of the research carried out on organocatalytically active porphyrins in Chapters 3.1–3.3. Specifically, the role of porphyrin(oid) ligands in various coordination-type complexes, means to access the core for hydrogen bonding, and the concept of conformational control are discussed. As will be shown, a good understanding of these aspects is vital to promote emerging applications for porphyrins, such as organocatalysis and sensors.

Chapters 3.1 and 3.2 focus on the synthesis of potential nonplanar porphyrin organocatalysts and their application in Michael additions and Henry reactions. This was propelled by the idea that the bifunctional core of tetrapyrroles should be accessible for intermolecular interactions upon sufficient distortion of the macrocycles. An underlying principle is that in planar porphyrins, the inner core system, which has basic imine and acidic amine groups, is buried within the macrocycle plane. As a result, a molecular engineering approach was perused in order to reshape the vector of N/N–H orientation outwards and allow these functional groups to activate appropriate small molecules. This was successfully transformed into a first case study where highly substituted porphyrins, such as 2,3,7,8,12,13,17,18-octaethyl-5,10,15,20-tetraphenylporphyrin (H_2OETPP, **74**) acted as efficient organocatalysts. In Chapter 3.3, a series of 5,10,15,20-tetraphenylporphyrins with graded degrees of β-ethyl substitution was applied in sulfa-Michael test reactions to correlate the degree of nonplanarity with their catalytic activity. The aim was to provide a better understanding and additional proof for the likely bifunctional mode of activation, accompanied by density functional theory (DFT) calculations.

Chapters 3.4 and 3.5 focus on methods development to produce new highly substituted porphyrins with tailored properties. First, in Chapter 3.4, a series of porphyrin thioethers was synthesized from 2,3,7,8,12,13,17,18-octaethyl-5,10,15,20-tetranitroporphyrin (H_2OETNP, **95**) in straightforward substitution reactions followed by their thorough structural evaluation in the solid state. At the same time, a new

methodology for the stepwise denitration of **95** was elaborated and accompanied by single crystal X-ray structural analyses of all 2,3,7,8,12,13,17,18-octaethylporphyrins with 1–4 meso-nitro groups. Therein, the goal was to to deduce interrelationships between substituent pattern, specific conformations, and potential for new applications. Next, in Chapter 3.5, it was attempted to introduce a new general-purpose method for preparing regioisomerically pure, highly substituted type I porphyrins based on steric considerations. Through rational choice of easily accessible aldehyde and pyrrole components with tailored steric bulk, it was possible to synthesize several type I porphyrins that were not contaminated by other type isomers. This is important because porphyrin type isomers have synthetic and biological relevance. Therefore, a reliable route to access a broad range of such compounds is an important step towards the design and engineering of systems for biomedical studies.

Publications

1 M. Kielmann, N. Grover, W. W. Kalisch, M. O. Senge, Incremental Introduction of Organocatalytic Activity into Conformationally Engineered Porphyrins, *Eur. J. Org. Chem*. **2019**, 2448–2452.
Invited for journal front cover of issue 14/2019.

2 M. Kielmann, M. O. Senge, Molecular Engineering of Free Base Porphyrins as Ligands—The N–H···X Binding Motif in Tetrapyrroles, *Angew. Chem*. **2019**, *131*, 424–448; *Angew. Chem. Int. Ed*. **2019**, *58*, 418–441.

3 M. Kielmann, C. Prior, M. O. Senge, Porphyrins in Troubled Times: A Spotlight on Porphyrins and Their Metal Complexes for Explosives Testing and CBRN Defense, *New J. Chem*. **2018**, *42*, 7529–7550.
Invited for journal back cover of issue 10/2018.

4 M. Roucan, M. Kielmann, S. J. Connon, S. S. R. Bernhard, M. O. Senge, Conformational Control of Nonplanar Free Base Porphyrins: Towards Bifunctional Catalysts of Tunable Basicity, *Chem. Commun*. **2018**, *54*, 26–29.
Invited for journal front cover of issue 01/2018.

5 M. Kielmann, K. J. Flanagan, K. Norvaiša, D. Intrieri, M. O. Senge, Synthesis of a Family of Highly Substituted Porphyrin Thioethers via Nitro Displacement in 2,3,7,8,12,13,17,18-Octaethyl-5,10,15,20-tetranitroporphyrin, *J. Org. Chem*. **2017**, *82*, 5122–5134.

Notes on Publications

Chapter 1 contains details from papers 2 and 3.

Chapter 2 contains details from papers 2 and 4.

Chapter 3 contains details from papers 1, 4, and 5.

Chapter 4 contains details from papers 1, 2, 4, and 5.

Acknowledgements

First and foremost, I would like to thank my supervisor, Prof. Dr. Mathias O. Senge. I am grateful for having been given the opportunity to work on the colorful and multifaceted world of porphyrins, to conduct cutting-edge research, develop my synthetic, analytical, critical thinking, project management, and scientific writing skills and, not least, my character. On countless occasions, Prof. Dr. Senge provided guidance in the form of scientific advice and beyond, which, as I have recognized, were essential prerequisites to kickstart my Ph.D. studies and to spend four successful years abroad. One paragraph cannot give an account of all that could be said but on a personal note, I would like to thank Prof. Dr. Senge for providing a productive and well-funded environment for an aspiring scientist like myself, for always being upfront, and for teaching me his ways; this will be cherished.

A big thanks goes out to all my current and former labmates, or as I would say, friends, (in no particular order): Keith, Alina, Ganapathi, Marie, Bhavya, Dáire, Piotr, Stefan, Harry, Jessica, Zoi, Karolis, Gemma, Mikhail, Elisabeth, Susan, Nitika, Ayman, Yasser, Aoife, and the many visiting students, especially those who worked under my supervision. Thanks again for keeping up with me, for inspiration, help with troubleshooting, friendship, and appreciation. I am also thankful to all previous group members whose achievements and dedication allowed me to go beyond.

Many thanks are due to the technical staff of the chemistry department, particularly Dr. John O'Brien, Dr. Manuel Ruether, Dr. Gary Hessman, and Dr. Martin Feeney.

I am grateful to all my coauthors, eminently Marie Roucan for her teamwork in catalyst design and screening, Dr. Nitika Grover for help with quantum chemical modelling methods, Dr. Keith J. Flanagan for crystal structure analyses, and Karolis Norvaiša for help with the synthesis of porphyrin thioethers and nitroporphyrins. I am also indebted to Prof. Stephen J. Connon for his collaboration on porphyrin organocatalysis.

Besides, I would like to express my eternal gratitude to my family and friends. Danke an meine Eltern, die mich immer unterstützt haben. Meine

Mutter steht hierbei an erster Stelle, denn sie hat mir immer einen sicheren Hafen geboten. Dies gilt auch für meine Großeltern—nach wie vor zwei der inspirierendsten Menschen in meinem Leben. Danke an meine Freunde aus der Heimat, ganz besonders Antonio, Alex, André, Ogi, Anna und Thomas. And thanks to Maryia for supporting me in Dublin.

With this, after having spent 22 years in the educational system, I am closing a chapter of my life in order to turn over a new leaf. It would go beyond the constraints of this section to name all the events and people that played a part in contributing to this, but I trust that those intended will know.

List of Abbreviations

Å	Angstrom
A/A^{n-}	analyte/anion
Ac	Acetyl
acac	acetylacetonate
ADP	adenosine diphosphate
APCI	atmospheric-pressure chemical ionization
Ar	aryl
ATP	adenosine triphosphate
ATR	attenuated total reflectance
av.	average
B3	Becke's three-parameter hybrid exchange functional
B3LYP	Becke's three-parameter hybrid exchange functional, Lee-Yang-Parr correlation functional
$BnPy^{+}–C_6H_4CO_2^{-}$	*N*-benzyl-4-carboxyphenylpyridinium
C_α	α-positions/α-carbon atom
calcd.	calculated
cat.	catalyst
C_β	β-position/β-carbon atom
CCDC	Cambridge Crystallographic Data Centre (deposition reference)
C_m	meso-position/meso-carbon atom
conv.	conversion
CSA	colorimetric sensor assay
δ	chemical shift
Δ24	average deviation from the 24-atom mean-plane (of the porphyrin)
ΔC_α	average deviation of the α-carbon atoms from the 24-atom mean-plane
ΔC_β	average deviation of the β-carbon atoms from the 24-atom mean-plane
ΔC_m	average deviation of the meso-carbon atoms from the 24-atom mean-plane

Δ_{ip}	simulated total in-plane distortion
ΔN	simulated displacement of the four internal nitrogen atoms from the 24-atom mean-plane
Δ_{oop}	simulated total out-of-plane distortion
d	day or doublet
DBU	1,8-diazabicyclo(5.4.0)undec-7-ene
DCTB	*trans*-2-[3-(4-*tert*-butylphenyl)-2-methyl-2-propenylidene]-malononitrile
DCM	dichloromethane
DDQ	2,3-dichloro-5,6-dicyanobenzoquinone
dec.	decomposition
DFT	density functional theory
DMAP	4-dimethylaminopyridine
DMF	dimethylformamide
DMNB	2,3-dimethyl-2,3-dinitrobutane
DMSO	dimethyl sulfoxide
DSSC	dye-sensitized solar cell
ε	extinction coefficient
ee	enantiomeric excess
E/E^+	electrophile
equiv	equivalent
Et	ethyl
FTIR	Fourier-transform infrared
GPER-1	G protein-coupled estrogen receptor 1
h	hour
H_2DPP	2,3,5,7,8,10,12,13,15,17,18,20-dodecaphenylporphyrin
HMX	1,3,5,7-tetranitro-1,3,5,7-tetrazocane
H_2OEP	2,3,7,8,12,13,17,18-octaethylporphyrin
H_2OETNP	2,3,7,8,12,13,17,18-octaethyl-5,10,15,20-tetranitroporphyrin
H_2OETPP	2,3,7,8,12,13,17,18-octaethyl-5,10,15,20-tetraphenylporphyrin
HOF	hydrogen-bonded organic framework

H_2OMTPP	2,3,7,8,12,13,17,18-octamethyl-5,10,15,20-tetraphenylporphyrin
HPLC	high-performance liquid chromatography
HRMS	high resolution mass spectrometry
H_2TPP	5,10,15,20-tetraphenylporphyrin
H_2TFPPBr$_8$	2,3,7,8,12,13,17,18-octabromo-5,10,15,20-tetrakis(2,3,4,5,6-pentafluorophenyl)-porphyrin
H_2TPPBr$_8$	2,3,7,8,12,13,17,18-octabromo-5,10,15,20-tetraphenylporphyrin
i-Bu	isobutyl
IR	infrared
J	coupling constant
λ	wavelength
L	liter
LYP	Lee-Yang-Parr correlation functional
m	multiplet
M	molar (mol/L)
M/M^{n+}	metal/metal ion
M$^+$	molecular cation
μL	microliter
μmol	micromole
MALDI	matrix-assisted laser desorption ionization
Me	methyl
MHz	megahertz
min	minute
MM	molecular mechanics
mmol	millimole
MOF	metal–organic framework
mol%	mole fraction
mp	melting point
MS	mass spectrometry
MS−MS	tandem mass spectrometry
m/z	mass-to-charge ratio
NBS	*N*-bromosuccinimide
n-Bu	*n*-butyl

NLA	nonlinear absorption
NLO	nonlinear optics
NSD	normal structural decomposition
Nu/Nu^-	nucleophile
PCM	polarizable continuum model
Ph/Ph	phenyl
pK_a/pK_{aH}	acid dissociation constant
PPIX	protoporphyrin IX (3,7,12,17-tetramethyl-8,13-divinyl-2,18- porphyrin dipropionic acid)
ppb	parts-per-billion
ppm	parts-per-million
q	quartet
QM/MM	quantum mechanics/molecular modelling
Q-TOF	quadrupole time-of-flight
quant.	quantitative
R_f	retention factor
rac	racemic
RDX	1,3,5-trinitro-1,3,5-triazinane
RGB	red, green, and blue
ROS	reactive oxygen species
RT	room temperature (25 °C)
s	singlet
SAM	self-assembled monolayer
SEC	size-exclusion chromatography
sept	septet
SET	single electron transfer
S_NAr	nucleophilic aromatic substitution
STM	scanning tunneling microscopy
t	time
T	temperature
t-Bu	*tert*-butyl
TDDFT	time-dependent density functional theory
TEA	triethylamine
TFA	trifluoroacetic acid
THF	tetrahydrofuran

TLC	thin-layer chromatography
TMS	trimethylsilyl
TNT	2,4,6-trinitrotoluene
Tol	tolyl
TON	turnover number
UV	ultraviolet
$\tilde{\nu}$	wavenumber
vis	visible
VOC	volatile organic compound
(VT) NMR	(variable temperature) nuclear magnetic resonance
v/v	volume-to-volume ratio
X/X^{n-}	H-bond acceptor/acid anion

Table of Contents

1. Introduction

1.1 The N–H···X Binding Motif in Tetrapyrroles

1.1.1 Porphyrins: State of the Art

Porphyrins **1** are often discussed as macrocyclic compounds *par excellence*. They are heteroaromatic systems with a rich metal coordination chemistry (**2**) and high functional versatility (**3**, Figure 1). As a result of their conformational flexibility, manipulation of the macrocycle conformation allows a fine-tuning of their physicochemical characteristics, including binding properties and chemical reactivity in general.[1] This manifests, for example, in tetrapyrrole-containing proteins, one of the most fundamental classes of enzymes in nature where a multitude of chemically distinct reactions involves the same porphyrin cofactor, which is largely attributed to protein-induced macrocyclic distortion.[2,3] Enhancement of the capability of porphyrins to undergo non-covalent interactions (*i.e*. hydrogen bonding) in enzymes or artificial systems is to a significant part an effect of macrocycle nonplanarity. As such, nonplanar free base tetrapyrroles can form hydrogen-bonded complexes N–H···X (**5**) under participation of the pyrrolic N–H groups in the core and suitable substrates X while often, the planar counterparts (**4**) remain inert as the core is in-plane (Figure 1).[3]

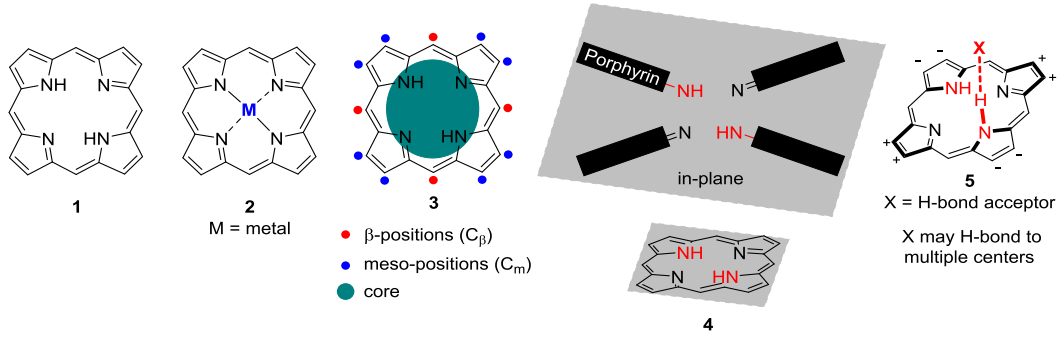

Figure 1. (Metallo)porphyrin macrocycles **1** and **2** and functionalities of a free base porphyrin **3** as well as N–H orientation in a planar porphyrin **4** and the N–H···X-type H-binding motif in a nonplanar porphyrin **5** (+ and − indicate displacements above and below the 24-atom mean-plane (Δ24), respectively).

Research on (nonplanar) porphyrins has exploded in recent decades and these days, they are used to test and illustrate advances in almost any area of chemistry, such as analytics,[4] physical chemistry,[5] biomedicine[6] as well as optics and materials science.[7] Their organic chemistry has given rise to a bewildering multitude of porphyrinoid macrocycles, which are isomeric, expanded, or contracted in relation to the parent 18 π-electron system.[8] Total synthesis of symmetrical porphyrins has finally made it to a scale suitable for practical applications and unsymmetrical substituted porphyrins are now available *en gros* in many cases *via* short syntheses or through functionalization reactions.[9] The size of oligoporphyrins has reached the realm of polymer chemistry[10] with the field coming to a point where more publications use scanning tunneling microscopy (STM) rather than classical CHN analysis for characterization.[11] However, the importance of the latter for determining a substance's purity remains undisputed.

One area, which has escaped significant attention relates to the coordination chemistry of free base porphyrins. Interest in porphyrins has been driven to a large extent by their ability to chelate almost any metal in the core. Many of the metal complexes are catalytically active and/or exhibit a rich axial coordination chemistry.[12,13] This is most prominently exemplified in nature, recalling, for example, hemes (iron complexes)[14] and their role in respiration in the electron transport chain and in a plethora of catalytic reactions or the chlorophylls (magnesium complexes) as the photoactive pigments in photosynthesis.[15] Furthermore, the cobalt complex vitamin B_{12} is essential for the functioning of the brain and nervous system and the formation of red blood cells.[16] As a result, there is a rich coordination chemistry involving the central metals and/or peripheral substituents.[12,17]

In this context, the pyrrole N–H units in the core of so-called free base porphyrins often appear in discussions solely as the precursor for metal insertion (**1**→**2**). The pyrrole N–H moieties are most often thought of as 'hidden' in the core and inaccessible for any meaningful use in supramolecular chemistry (*e.g.*, as in **4**, Figure 1). Detailed studies involving these groups have mostly been physical organic chemistry investigations on

the N–H tautomerism, *i.e*. studies on the behavior of the N–H units *within* the porphyrin plane.[18]

While traditionally in chemistry, a ligand is considered an ion or neutral molecule that binds to metal centers, in the following, scenarios more akin to the situation and definition of ligands and receptors used in biochemistry will be shown.[19] Therein, the tetrapyrrole is usually bound to a much larger unit, which qualifies all porphyrins in pigment–protein complexes and metalloproteins as ligands. However, as it is the major partition of this thesis, the emerging functional porphyrin chemistry where the targeted use of weak interactions, *i.e*. (out-of-plane) H-bonding (of the N4 porphyrin core) is utilized will be introduced at this point.

1.1.2 Coordination Types in Porphyrins

Peripheral H-bonding. Hydrogen bonds are a type of attractive electrostatic interaction (weak interaction) between two polar groups, *i.e*. covalently bound and polarized hydrogen atoms and electronegative atoms or groups.[20] They are common and important non-covalent forces in biological systems, such as proteins, enzymes, and nucleic acids and utilized as structural and functional principles in biomolecules and to control the microenvironment around metal centers in tetrapyrrole-containing enzymes. Additionally, H-bonds are partly responsible for the secondary and tertiary structures of proteins and nucleic acids and play an important role in the structure of natural and synthetic polymers. Given the porphyrin motif's pronounced role both in nature and artificial systems, it is inevitable to stress the role of hydrogen bonding in porphyrin-based assemblies.[21]

In this context, it seems rational to define two major categories of H-bonds: those involving the tetrapyrrole core and those involving peripheral groups. Both types are vital but found often in substantially different contexts. Peripheral H-bonding is a major driving force in supramolecular chemistry since the resulting frameworks are usually highly organized and exploit the structural flexibility and diversity that lies in the tunable hydrogen bonding strength.[22] On the other hand, hydrogen bonds of the tetrapyrrole core are

often discussed where porphyrins act as ligands. While peripheral H-bonding will be introduced briefly at this point, central (N–H···X-type) hydrogen bonding is discussed later in more detail. As will be shown in this chapter, the former and the latter may also interplay, producing unique porphyrinic architectures.

Hydrogen bonds play an important role in the self-assembly and stabilization of porphyrin J-aggregates. For example where peripheral hydroxy groups interact with the central nitrogen atoms of an adjacent macrocycle (**6** and **7**, Figure 2).[23] However, it should be noted that the specific arrangement in dimer **7** was proposed on the base of calculations, and additional studies would be necessary in order to confirm if this model is sustainable both in solution and in the solid state.

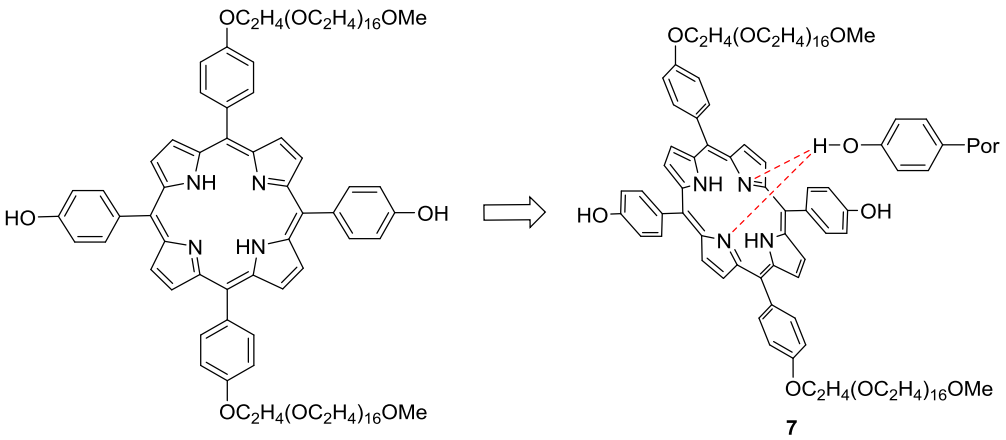

Figure 2. Supramolecular porphyrin complex **7** that formed through peripheral H-bonding and core interactions between units of **6**, as suggested by molecular mechanics (MM) calculations. Therein, the presence of hydrogen bonds between the porphyrin core and the hydrogen of the O–H group of the adjacent macromolecule was proposed.[23]

Further examples of the directing and reinforcing characteristics of hydrogen bonds are found in porphyrinic solids,[24] self-assembled monolayers (SAMs),[25] nanofibers and nanorods,[26] and nanochannels of 2,3,5,7,8,10,12,13,15,17,18,20-dodecaphenylporphyrin (H_2DPP, **64**) derivatives.[27] It has also been shown that protoporphyrin IX (PPIX, **71**) adsorbed on a Cu surface at low temperature forms adlayers stabilized by

tetragonal H-bonds between the nitrogen atoms of the macrocycle core and peripherally bound carboxyl groups.[28]

Looking at examples in nature, the malaria pigment hemozoin, a disposal product from the digestion of blood by malaria parasites, is an insoluble, peripherally hydrogen-bonded dimer of β-hematin.[29] And in chlorosomes, photosynthetic antenna complexes found in some anaerobic bacteria, hydrogen bonding can have a critical influence on exciton dynamics and as such, the light-harvesting process itself.[30] In the future, these findings may motivate new ventures into a bionic supramolecular chemistry.

Applications of peripherally hydrogen-bonded tetrapyrroles are found in material science, molecular electronics, nanotechnology, and solar technology. Representative examples are hydrogen-bonded organic frameworks (HOFs) based on porphyrins for selective gas separation,[31] and H-bonding mediated reversible self-assembly of porphyrin on a surface for the construction of dye-sensitized solar cells (DSSCs).[32]

Peripheral Covalent Bonding/Porphyrin Ligands in Biochemistry. In addition to weaker non-covalent bonds, nature also utilizes covalent bonding to fixate and regulate porphyrin cofactors in defined arrangements. The archetypical case is heme proteins, an indispensable class of porphyrin cofactors involved in a wide range of functions in nature, such as oxygen storage and transport, electron transfer, catalysis, gas sensing, and gene regulation.[33] Moreover, they pose an interesting case study to deduce the effects of different coordination types (covalent linkage to proteins: *e.g.*, heme c in cytochrome *c*[34] *vs.* axial coordination: *e.g.*, heme a in cytochrome *c* oxidase, heme b in hemoglobin and myoglobin) in tetrapyrroles.

A comparison of hemes in various binding situations underlines the functional and physicochemical differences originating from the several binding modes, *e.g.*, robustness,[35] fine-tuning of reduction potentials over a wide range,[36] interaction with proximal amino acids, metal–ligand interactions, metal spin state[37] and oxidation state,[38] and potentially kinetics and thermodynamics of electron transfer reactions itself. Notably, covalent attachment of a protein often results in heme c undergoing

conformational changes *(i.e.* nonplanarity),[36b,39] which effects, for example, the tetrapyrrole's redox properties (*vide infra*).[37,40] As such, nature highlights the critical role of binding types in porphyrins and provides one of the most interesting case studies on molecular engineering of tetrapyrroles. Historically, many tetrapyrroles were involved in studies on the biological role of nonplanar porphyrin/porphyrinoid conformations[41] and conformational control in enzymes.[3a,42] To date, numerous protein crystal structures were solved, in which the tetrapyrroles exhibit distorted macrocycles[43] along with considerable movement and flexibility.[44] As such, a rich landscape of structural studies revolves around porphyrin–protein complexes with a focus on weak interactions and tunable properties.[45]

1.1.3 Nonaromatic Porphyrinoids

Before focusing on 'true' porphyrins, a look must be taken at a number of nonaromatic tetrapyrroles, in which the N–H units have been utilized extensively to bind ions and small molecules through hydrogen bonds.[46] Macrocyclic conjugation in such systems is interrupted due to sp^3-hybridized meso-carbon atoms, giving rise to macrocycles with isolated pyrrole units that form what can be considered as cavities. The isolated pyrrole units can easily tilt out of the mean-plane and are therefore accessible as hydrogen bond donors as opposed to the situation in more rigid and often planar porphyrins. Overall, this is a main prerequisite for the rich coordination chemistry that revolves around these ligands.

Calix[4]pyrroles. Since their first description by Baeyer ('acetonepyrrole'), in which a tetrapyrrole with four sp^3-hybridized meso-carbon atoms, octamethylcalix[4]pyrrole (**8**), was synthesized from acetone and pyrrole (Figure 3).[47] Calix[4]pyrroles (porphyrinogens) and their analogues, including metal complexes, have been extensively studied and stand now as versatile and often used ligands for the complexation of anions and neutral molecules through H-bonding with the central pyrrole moieties.[48]

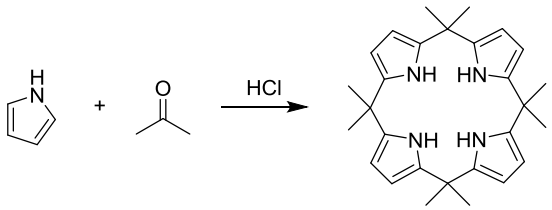

8

Figure 3. The first synthesis of a calixpyrrole **8** by Baeyer *via* acid-catalyzed condensation of acetone and pyrrole.[47] Note, that in cobtrast to porphyrins, calixpyrroles are nonaromatic due to the presence of sp^3-hybridized meso-like positions.

However, it was more than a century after the initial discovery that a 'gold rush' regarding the use of calixpyrroles and related compounds in ligand-based applications ensued, which yielded hundreds of analogues and a multitude of sensing methods.[49] Given the presence of pyrrolic hydrogen bond donor groups, they were considered as 'old yet new' anion binding agents and have been found to frequently complex halides, dihydrogen phosphate, carboxylate, and others, both in solution and in the solid state.[50–52] This is accompanied by a preference towards complexation of small fluoride anions over other guests, which is attributed to the spatial demands of the central cavity (*i.e*. size exclusion).[51,53] Notably, ligation can occur even in the solid state.[54]

In distinction to most porphyrins where conformational flexibility is limited,[55] calix[4]pyrroles modify their shape to accommodate guests. They often adopt a 1,2-alternate conformation (↑↑↓↓) in the absence of substrates and switch to cone-like shapes (↑↑↑↑) when bound to anions[51a] or 1,3- (↑↓↑↓) and 1,2-alternate forms with neutral substrates (Figure 4).[56] The result is the formation of aromatic voids defined by the four pyrrole rings within the host molecules and may be considered as a conformational response towards substrates.[57]

Many qualitative, quantitative, and theoretical studies have been performed on such tetrapyrroles. Examples include compounds **9–15** to compare binding constants and their dependence on electronic properties and stereochemistry, resulting in a better mechanistic insights into the host–

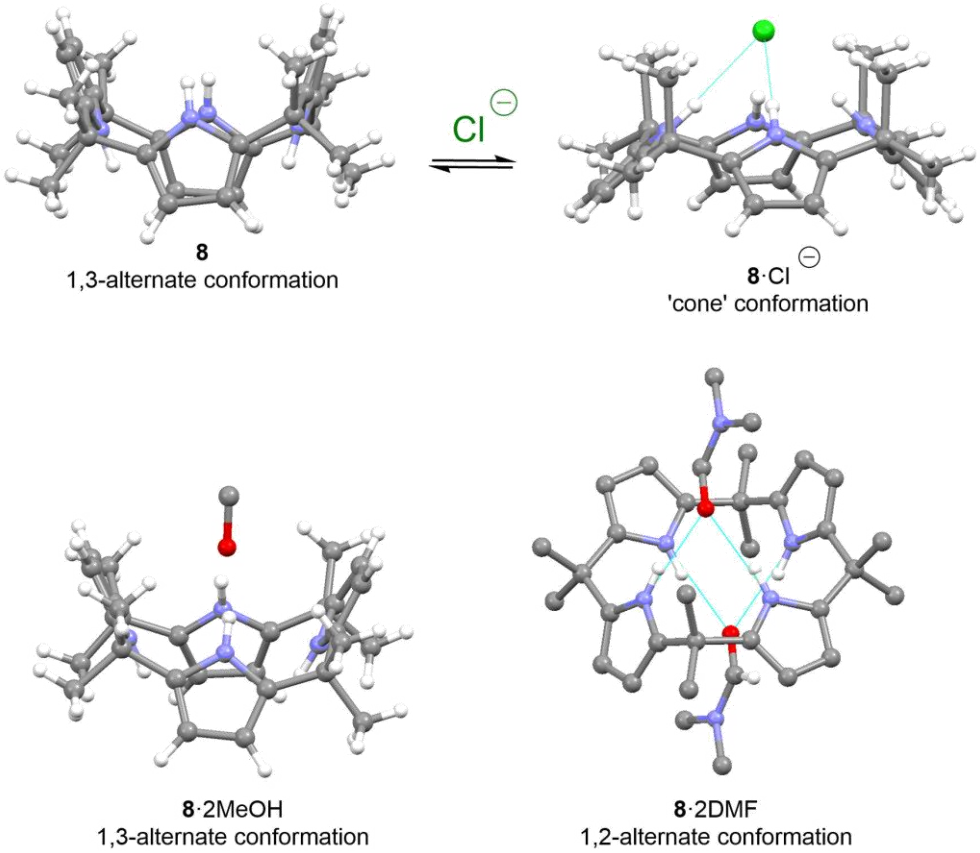

Figure 4. Typical conformations of calix[4]pyrroles and their crystal structures. Top: while the discrete ligand **8** (CCDC: VUSFIY01) is 1,3-alternate with regard to the pyrrole rings, the tetrapyrrole switches to a 'cone' in **8**·N(*n*-Bu)$_4$Cl (CDDC: TEQKIJ) to accommodate anions. The tetrabutylammonium counter ion has been omitted.[51a] Bottom: the complexes **8**·2MeOH (RECPEU) and **8**·2DMF (RECPIY, noncritical hydrogen atoms omitted) with neutral ligands are 1,3- and 1,2-alternate, respectively.[56a,58] CCDC = Cambridge Crystallographic Data Centre deposition reference.[58c] DMF = dimethylformamide.

guest chemistry involved (Figure 5).[51a,59] At the same time, complexation of neutral molecules is usually more challenging due to modest association constants.[56a]

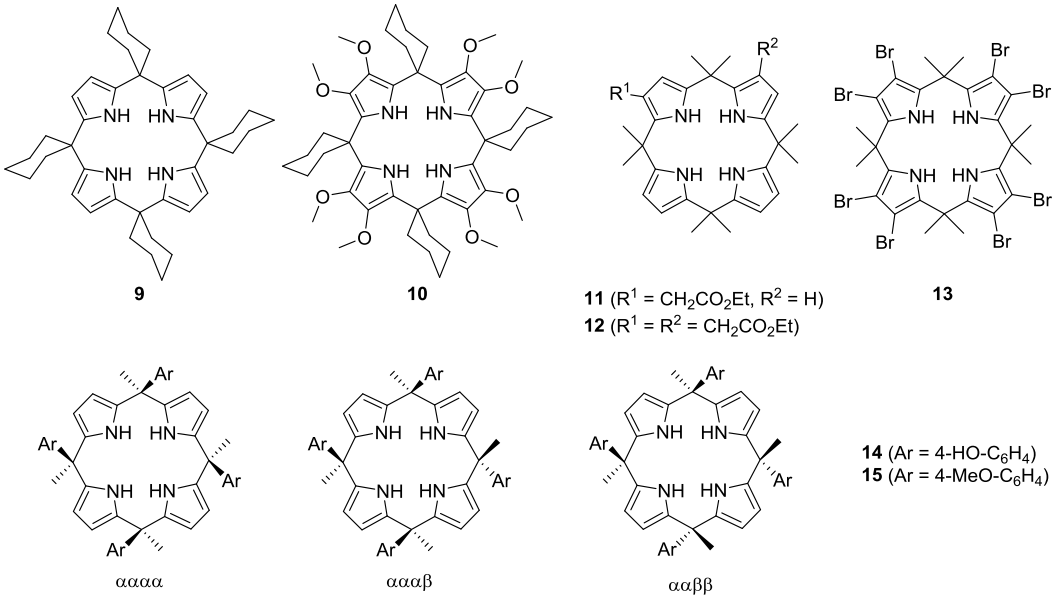

Figure 5. Some functionalized and stereoisomeric calix[4]pyrroles used in binding studies to compare the effects of both C_β- and C_m-substitution.[51a,59] The tags α and β describe the orientation of the aryl substituents ('up' or 'down').

Nevertheless, a large number of neutral receptor–substrate H-bonded complexes of calix[4]pyrroles were described, *e.g.*, with alcohols, amides, a broad range of oxygen-containing species, and pyridyl-*N*-oxides.[56,60] Based on relatively simple calix[4]pyrroles, numerous more sophisticated receptors have been prepared through an ever-growing toolbox of functionalization techniques (*e.g.*, **16**–**19**, Figure 6).[53b,c,56b,60–64]

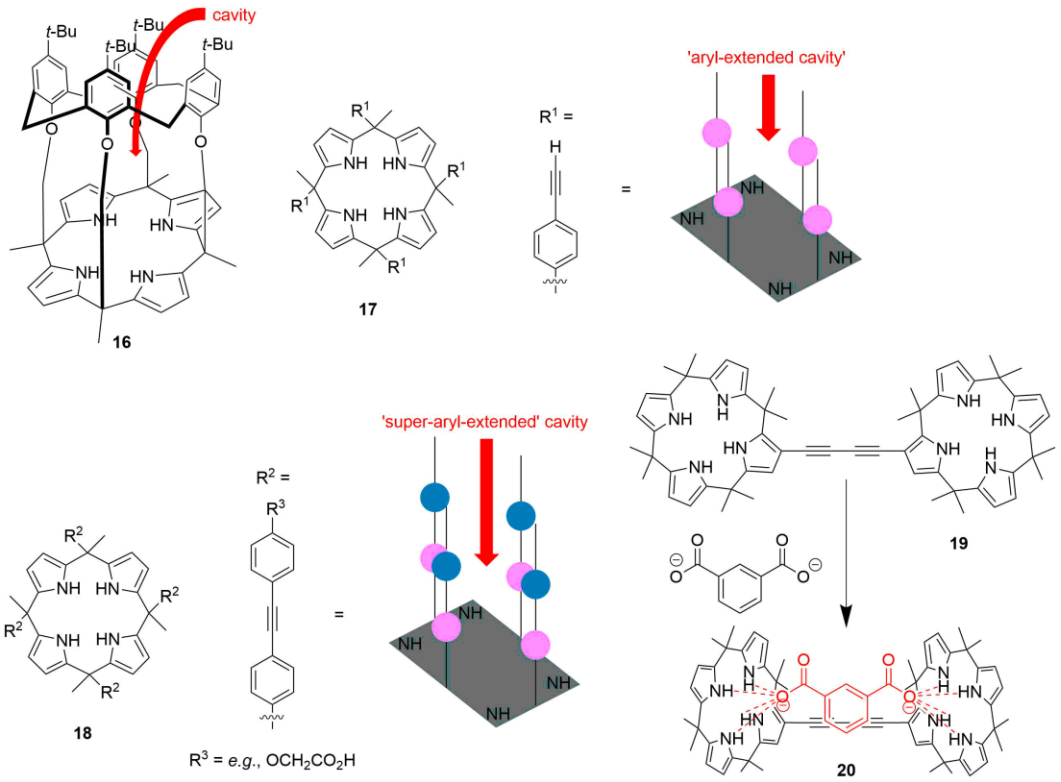

Figure 6. Selected examples of structurally advanced tetrapyrrole receptors: calix[4]arene–calix[4]pyrrole pseudo dimer **16**,[64] 'aryl-extended' and 'super-aryl-extended' systems **17** and **18**,[60] and the dimeric anion binding complex **19** when binding an isophthalate dianion to form **20**.[62c]

The various calixpyrrole-dependent recognition techniques were reviewed extensively by Gale and Sessler.[65] Optical sensors are often based on covalently linked colorimetric or fluorescent reporter groups where perturbation of the electronic properties upon complexation results in a visual or fluorescence-based signal (fluorescence quenching/'turn off' or 'turn on').[52,66] A second approach involves a displacement assay where an initial host–guest complex dissociates upon addition of a more strongly coordinating analyte, which results in a color change (Figure 7).[53a] On the other hand, electrochemical sensing utilizes ion-selective electrodes,[67] discrete redox-active molecular receptors,[68] and chemically modified electrodes.[69]

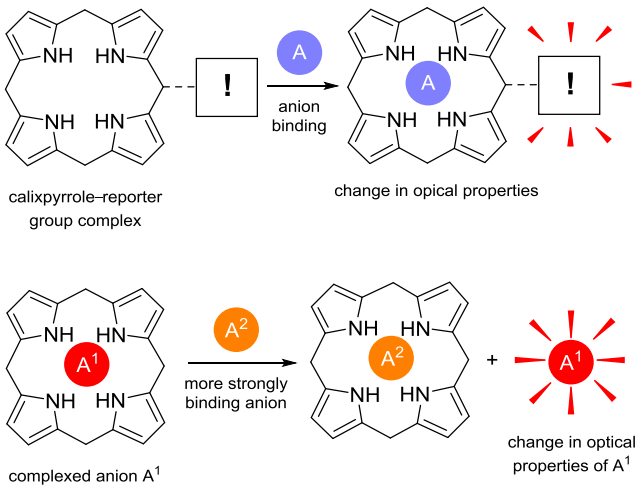

Figure 7. Illustration of common calixpyrrole-based optical sensors. Left: covalently attached tetrapyrrole–reporter conjugate. Right: displacement assay.

H-bonding calix[4]pyrroles have also been utilized as solid high-performance liquid chromatography (HPLC) supports in the form of modified silica gels for the separation of anions and neutral substrates, such as amino acids and (oligo)nucleotides.[70] As potent Lewis acidic multi-hydrogen bond donors, they possess organocatalytic properties and activate substrates by H-bonding, as illustrated by Diels–Alder and aldol reactions and diastereoselective vinylogous additions (Figure 8).[71] Furthermore, calix[4]pyrroles can aid regioselective *O*-alkylations and -acylations, likely through H-bonding catalysis.[72]

A recent review by Kim and Sessler discusses calix[4]pyrroles as molecular containers for ion transport, recognition, and molecular switching functions[73] that are often based on weak interactions. Used in this capacity, they stand as selective receptors and extractants for anions and ion pairs across phase boundaries and membranes and as building blocks for stimulus-responsive materials.[74] Due to their remarkable non-covalent binding properties and ability to form dimers, trimers,[62b,75] and aggregates of higher order for selective encapsulation[76] and allosteric binding of guests, such as nitroaromatic explosives and fullerenes,[77] they are now well-established in the realms of supramolecular chemistry (Figure 9A). Furthermore, calix[4]pyrroles were transformed into drug delivery vehicles,

enzyme mimics and made an entry as potential anti-tumor agents when it was observed that such synthetic ion carriers can trigger cell death by facilitating chloride anion transport into cells.[78] Even the simple calix[4]pyrrole **8** has been shown to act as an agonist to the G protein-coupled estrogen receptor 1 (GPER-1).[79]

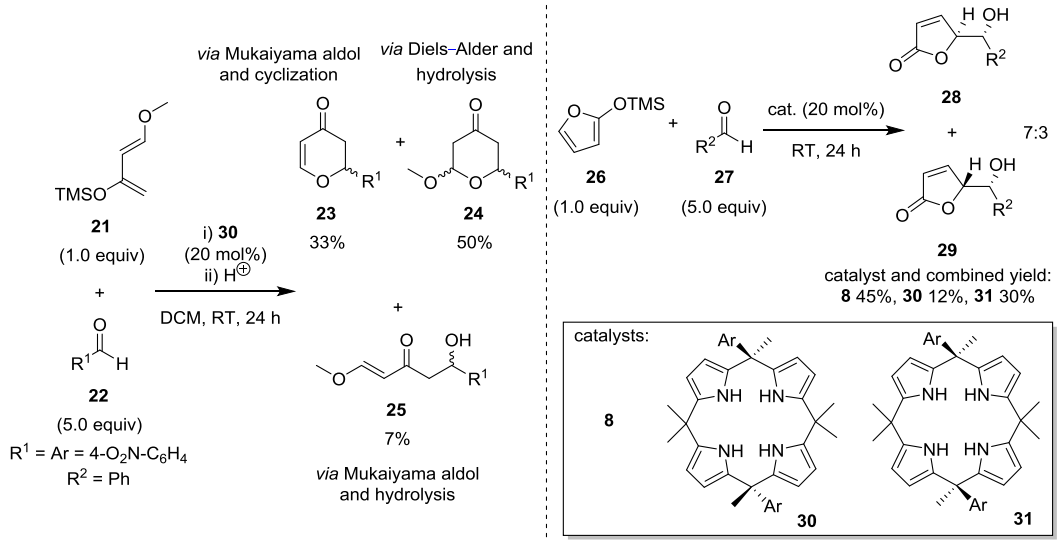

Figure 8. Calix[4]pyrrole organocatalysts. Left: reaction of Danishefsky's diene **21** and aromatic aldehyde **22** in the presence of **30**, yielding a mixture of **23**–**25**.[71a] Right: synthesis of γ-butenolides **28** and **29** *via* vinylogous addition of **26** and **27** in the presence of calixpyrroles **8**, **30**, and **31**, respectively.[71b] DCM = dichloromethane, TMS = trimethylsilyl.

Calix[4]phyrins: Phlorins, Porphomethenes, and Porphodimethenes. Formal two-, four-, or six-electron oxidation of these nonaromatic macrocycles leads to calix[4]phyrins, which bear analogy to both porphyrins and calix[4]pyrroles by containing a mixture of sp^2- and sp^3-hybridized meso-like positions. The partial interruptions in the conjugation introduce a number of unique structural features since the sp^3 carbon atoms perturb the π-system and significantly modify the molecular shape and flexibility. Likewise, far-range electronic induction effects still exist so that functional groups may be used for fine-tuning of conformational and chemical properties.[80]

Early examples of rational calixphyrin syntheses include acid-catalyzed cyclization reactions between ketones and pyrrolic precursors followed by

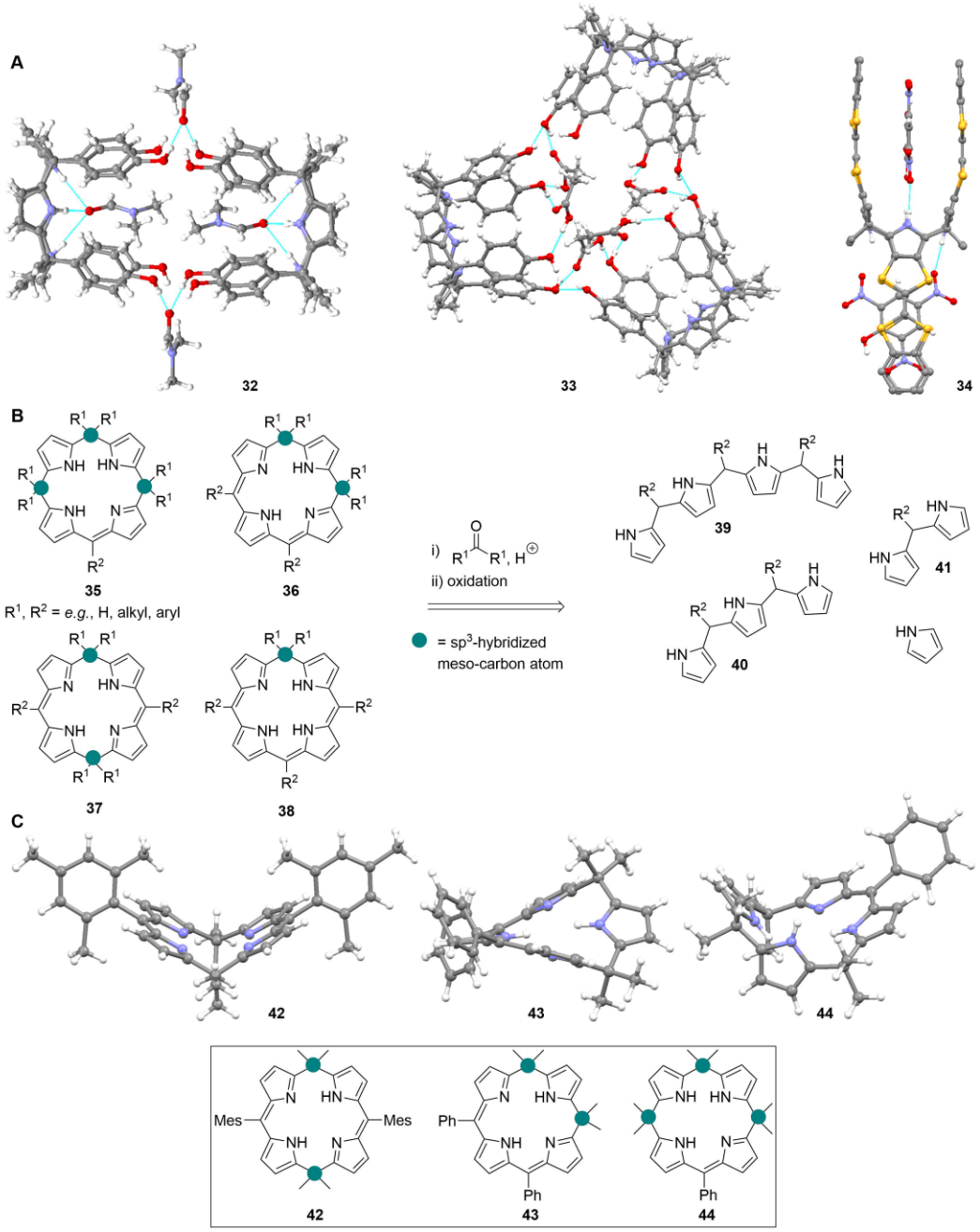

Figure 9. A: views[58] of selected calix[4]pyrrole-based supramolecules in the crystal. Dimer **32** (CCDC: MAVZIS) linked by hydrogen bonds with DMF and trimer **33** (CCDC: MAVZOY) linked by hydrogen bonds with AcOH[62b] as well as homotropic allosteric calix[4]pyrrole receptor **34** (GUNDUP) with hydrogen-bonded 2,4,6-trinitrophenol.[72] B: acid-catalyzed condensation of pyrrole and pyrrolic synthons **39**–**41** with ketones followed by partial oxidation as an efficient sequence to synthesize calixphyrins **35**–**38**. The differentiation of calix[4]phyrins into porphomethenes **35**, 5,10-porphodimethenes **36**, 5,15-porphodimethenes **37**, and phlorins **38** is also highlighted. C: structures[58] of nonplanar calix[4]phyrins in the crystal: **42** (CCDC: LISSIP), **43** (QENDOC), and **44** (QENDIW).[81]

partial oxidation (Figure 9B)[81] and Buchler's reductive methylation to yield metalloporphodimethenes[82] or substitution reactions.[83] The products are usually distorted and feature structural cavities and accessible inner nitrogen atoms (Figure 9C), which may aid the binding of substrates.

However, it should be noted that the calixphyrin core, like porphyrins, consists of both amine and imine groups and effectively has a lower number of N–H units to interact with guest molecules as compared to the analogous calixpyrroles. This may account for a less pronounced receptor chemistry revolving around this class of macrocycles, leaving the option of core protonation to introduce more N–H motifs and to increase the anion binding capabilities.[84] Nevertheless, a number of H-bonding complexes between (expanded) calixphyrins and various substrates have been observed (Figure 10).[85] As such, they provide a potential avenue towards a rich, but as of yet underdeveloped receptor chemistry up to enantiorecognition.[86]

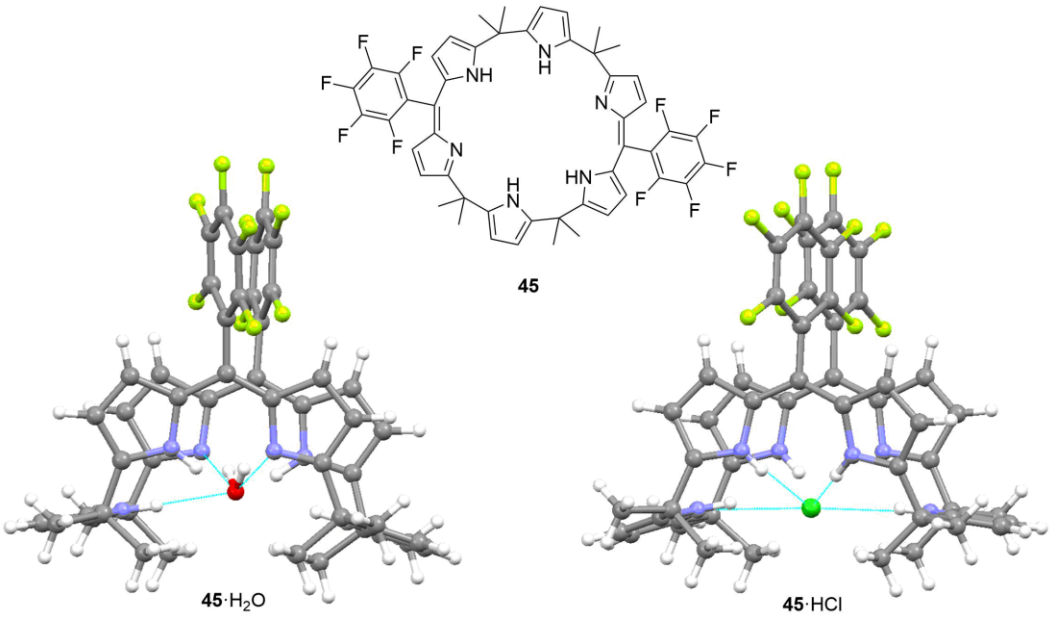

Figure 10. Expanded calixphyrin **45** and the structures of two of its hydrogen-bonding complexes in the crystal: **45**·H_2O (CCDC: XETYUQ) and **45**·HCl (XETZAX).[58,85]

Much like porphyrins, calixphyrins are basic and bind protons at their imine functions but intriguingly, the corresponding dications are more conjugated and thus more stable than the neutral species.[86b] This again highlights the

diverse character of calixphyrins as macrocycles with partial traits of both calixphyrins and porphyrins. In practical terms, core-protonated calix[4]phyrins form in the presence of acids where acid anions are subsequently hydrogen-bonded to the (protonated) core. In such complexes, *e.g.*, **46**, the pyrrole cycles are tilted significantly out of the mean-plane, and depending on the molecular geometry, the meso-hydrogen atoms can participate in further stabilization of those salts (Figure 11).[87]

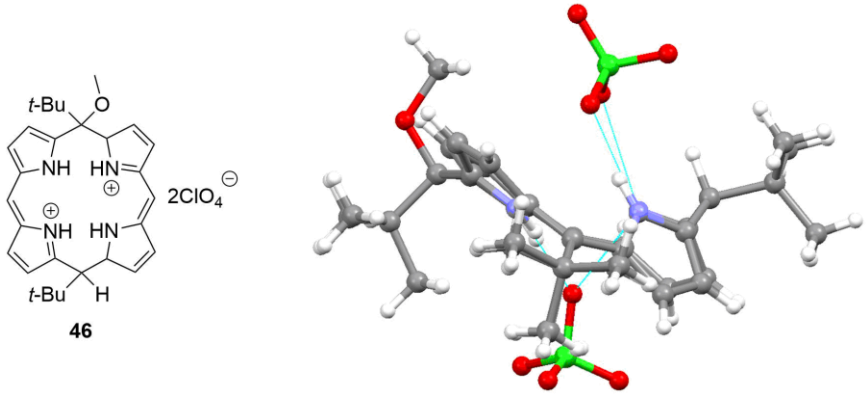

Figure 11. View of the molecular structure of calix[4]phyrin salt **46** in the crystal (CCDC: HETDEP).[58,87]

This identifies tetrapyrrole core protonation as an opportunity to enhance the molecules' receptor potential through out-of-plane distortion and exposure of the central nitrogen atoms. Hence, hereafter it will be shown in detail how this promising strategy has been utilized to exercise conformational control on porphyrins.

1.1.4 Accessing N–H Units in Porphyrins

A brief look at nonaromatic porphyrin analogues shows that they are to a large extent involved in many applications that are desirable for porphyrins, including organocatalysis and a rich receptor chemistry. However, due to the porphyrin motif's planarity, rigidness, and the presence of 'only' two N–H donors as opposed to up to four in tetrapyrrolic porphyrinoids, it is traditionally more challenging to apply them in the same manner and to the same extent. But an increased availability and therefore reactivity of the core

amine and imine moieties can be achieved through rationally altering their orientation within the mean-plane *via* molecular engineering. While various methods to deform the molecular skeleton in such a way exist (Figure 12),[1,88] a case study of two of the most feasible and widely used strategies will be conducted in this chapter, namely core protonation and high peripheral substitution while the various other ways are outside the scope of this introduction. Additionally, these approaches will be compared to the mode of action of the natural chelatases; enzymes that can induce porphyrin ring distortion.

Note, that corroles, expanded-, *N*-confused porphyrins, and various other analogues show an ample (chemo)receptor chemistry, too, paralleling that of 'true' porphyrins. However, this has recently been reviewed[4a] and will therefore be omitted at this point.

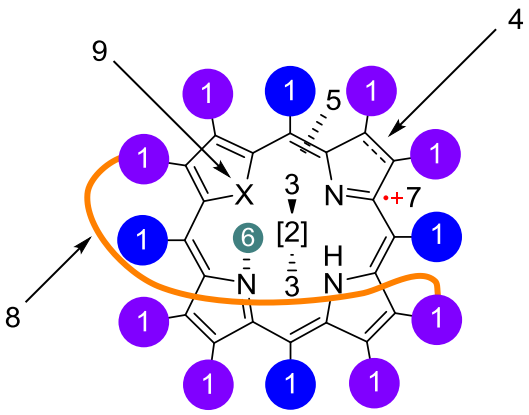

Figure 12. Possibilities to alter the macrocycle's conformation: (1) introduction of sterically demanding substituents, (2) metallation, (3) axial ligands, (4) degree of reduction, (5) interruption of the conjugated system (*vide supra*), (6) *N*-alkylation, -arylation, or protonation, (7) cation radical formation, (8) 'strapping' of the macrocycle *via* covalent linkage of the meso- or β-pyrrole positions, and (9) heteroatom substitution. Core and skeleton transformations are possible, too.[88]

Porphyrin (Di)cations. Porphyrin cations are readily produced in the form of core diacids through protonation of the internal imine groups (Figure 13A). This is accompanied by distortion of the macrocycle, which increases the vector of N–H outwards orientation (Figure 13B). At the same time, such

conformational manipulation dramatically boosts the amine groups' capacity to contact appropriate small molecules and anions. Accordingly, porphyrin cations can be considered as large anion sensors due to their capability to form hydrogen bonds with counterions (Figure 13C).[3]

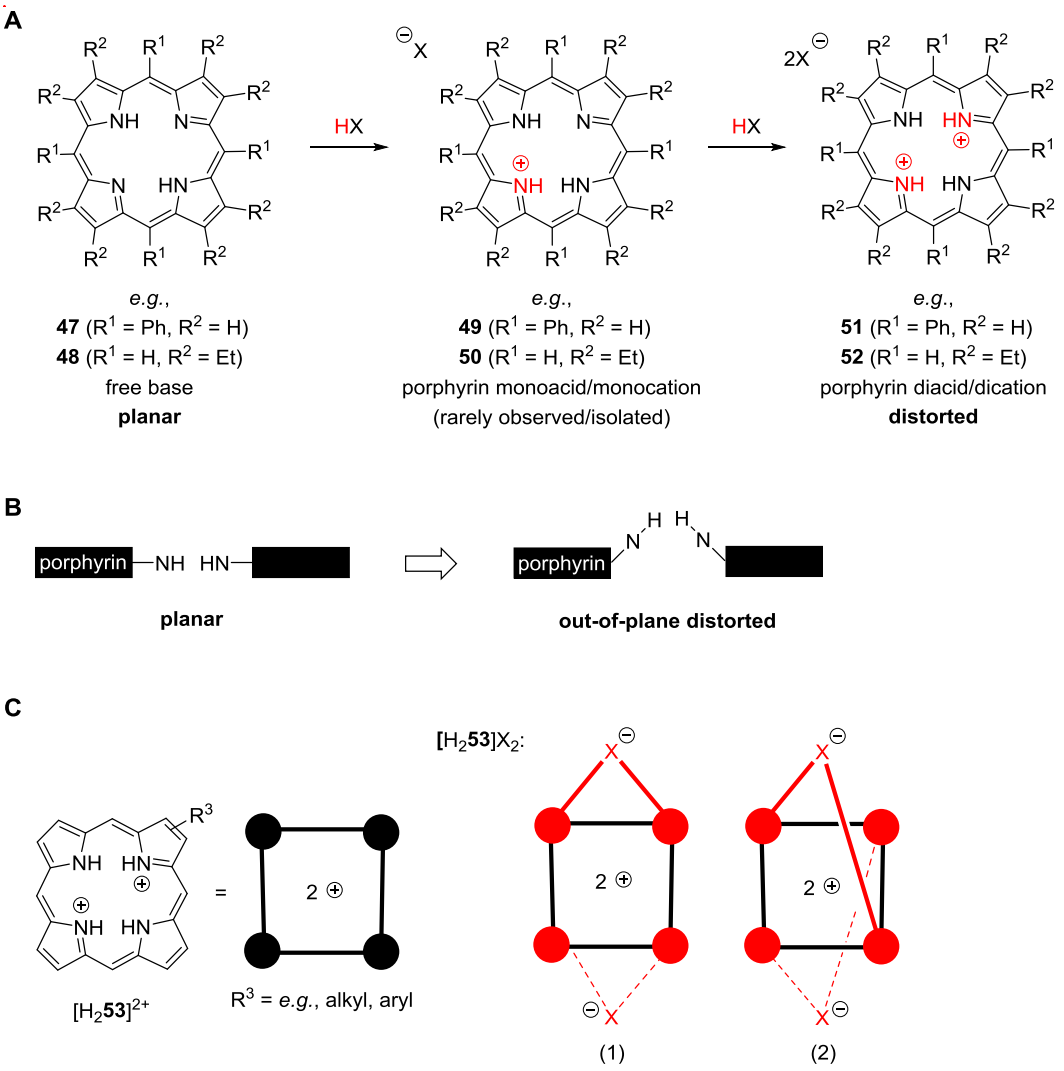

Figure 13. A: protonation of free base porphyrins, *e.g.*, 5,10,15,20-tetraphenylporphyrin (H_2TPP, **47**) or 2,3,7,8,12,13,17,18-octaethylporphyrin (H_2OEP, **48**) by acids HX results in the formation of porphyrin dications and their salts, *e.g.*, $[H_4TPP]X_2$ (**51**) or $[H_4OEP]X_2$ (**52**). This proceeds *via* a monocation, *e.g.*, **49** or **50**, which can only rarely be isolated. B: illustration of pyrrole out-of-plane distortion in porphyrins/porphyrin core acids. C: porphyrin acid salts, *e.g.*, $[H_2\mathbf{53}]X_2$ are H-bonding complexes where various conformations, such as (1) and (2) are conceivable. X^- = acid anion.

Indeed, crystal structures of porphyrin diacid salts indicate severely nonplanar geometries of the macrocycles as a result of both steric interactions of the crowded core and electrostatic repulsion of the partially positive pyrrole nitrogen atoms.[89] In most cases, protonation results in the formation of saddle-distorted (*sad*-type) porphyrins with 1,3-alternating pyrrole tilts (↑↓↑↓, *e.g.*, in **54**).[90] However, individual cases of 1,2-alternating forms (↑↑↓↓) have also been observed; for example, in 2,3,7,8,12,13,17,18-octaalkylporphyrin diacid salts, such as **55** (Figure 14).[90a,91]

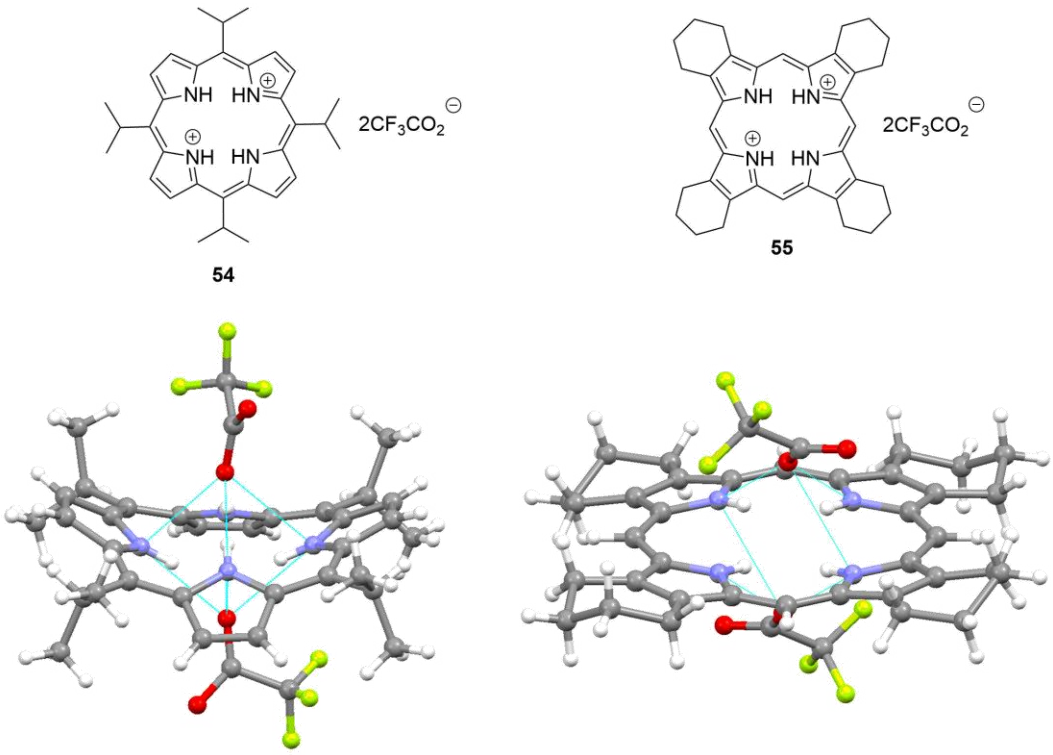

Figure 14. Top: view of the molecular structure of porphyrin salt **54** in the crystal (CCDC: KIBMEN).[58,90b] Bottom: view of the molecular structure of **55** in the crystal (YEVKAL).[58,91]

The question of how much the porphyrin macrocycle can be distorted by this means or whether there is a 'breaking point' has been thoroughly discussed and an understanding of this approach is vital for the design of sensors based on weak interactions with the core. Accordingly, it was elaborated that peripheral (*vide infra*) and core steric strain[88] (*i.e.* protonation and *N*-substitution)[91,92] are some of the most important 'adjusting screws' to exert

conformational control.[1] One case study provided that the ditrifluoroacetate salt of **56**, **57**, is one of the most nonplanar porphyrins described so far.[91] A comparison with the analogous salt of **47**, **58** that is less distorted, clearly points at the additional distorting effects of peripheral substituents. These are involved in repulsive *peri*-interactions, which cause a highly substituted porphyrin like **56** to be 'pre-distorted' even without protonation. Thus, by comparing dodecasubstituted free base porphyrins (*e.g.*, **56**) with their dications (*e.g.*, **57**), an increase in nonplanarity of only 13–25% depending on the individual substituents was noted. At the same time, this effect is significantly stronger in sterically unhindered systems (*e.g.*, **47**) where protonation can result in distortion of up to 300% (**47**→**58**), suggesting that there is a maximum level of nonplanarity for porphyrins (Figure 15).

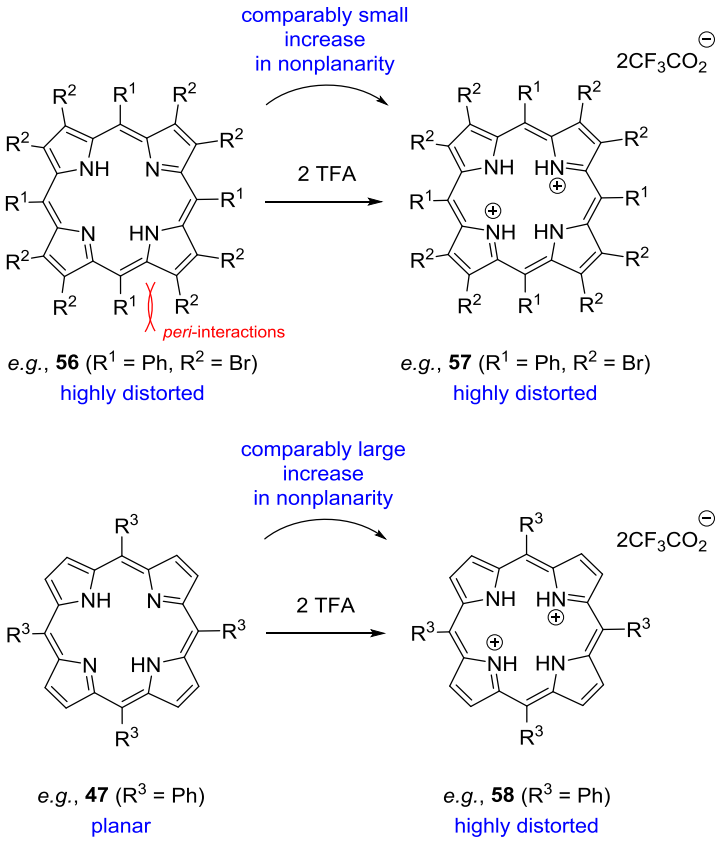

Figure 15. A dodecasubstituted porphyrin like **56** is 'pre-distorted' due to repulsive *peri*-interactions of the meso- and β-substituents. As such, core protonation results in a comparably small increase in nonplanarity in **57**. At the same time, sterically unhindered **47** undergoes a significantly large increase in distortion upon formation of **58**.

Webb and Bampos investigated the dynamics and the complexation behavior of porphyrin diacids in solution and offered insight into the mechanisms of both porphyrin protonation and acid-accelerated metallation.[93] They also showed the effects of varying both the acid and the porphyrin on proton transfer and anion recognition and put an emphasis on the role of macrocyclic conformational control in intramolecular proton transfer. In addition, the effects of saddling, meso-phenyl tilting, and different hydrogen-bonded counterions on the optical properties of $[H_4TPP]X_2$ (where $X^- = F^-$, Cl^-, Br^-, I^-) were elaborated theoretically *via* DFT and time-dependent density functional theory (TDDFT) by Rosa *et al*.[94]

Next to this fundamental research, a broad landscape of applications emphasizing the H-bonding and anion binding properties of porphyrin dications exists: The diprotonated form of octaalkylporphyrin **59** acted as a bromide-selective sensor in the system **59**–Et_4NBr–$HClO_4$–MeCN (Figure 16, top).[95] Under these conditions, the stable H-bonding complexes **60** and **61** formed preferably, which was considered as a step towards halide-selective molecular anion receptors of good detectability. A later study investigated the binding of various halides and alkali metal cations by diprotonated porphyrin hosts **59** and **62**.[96] Upon titration of a **59**–$HClO_4$–MeCN system with various halide salts, stable 1:1 and 2:1 hydrogen-bonding complexes with the halides formed. While the complexation constants decreased in the order $Cl^- > Br^- > I^-$, strong fluorescence quenching occurred in the presence of iodide. On the other hand, alkali metal ions could be trapped with monoarylporphyrin dication **62** containing a complexing polyether fragment that was both peripherally attached and hydrogen-bonded to the core through a pyridyl moiety (Figure 16, bottom). Note, that a high binding selectivity of **62** for K^+ over Li^+ and Na^+ was observed.

Other efforts focused on nonplanar porphyrin diacids in supramolecular assemblies.[97] In one report, Honda *et al*. constructed a series of hydrogen-bonded supramolecular complexes of saddle-distorted diprotonated **64** and electron donors with carboxylic acids.[98] These were then investigated in terms of photo-induced electron transfer dynamics. In such studies, the role of the H-bound counterions is often crucial. For example, the dihydrochloride

salt of 5,10,15,20-tetrakis(4-sulfonatothienyl)porphyrin showed chloride-specific aggregation in aqueous solution.[99]

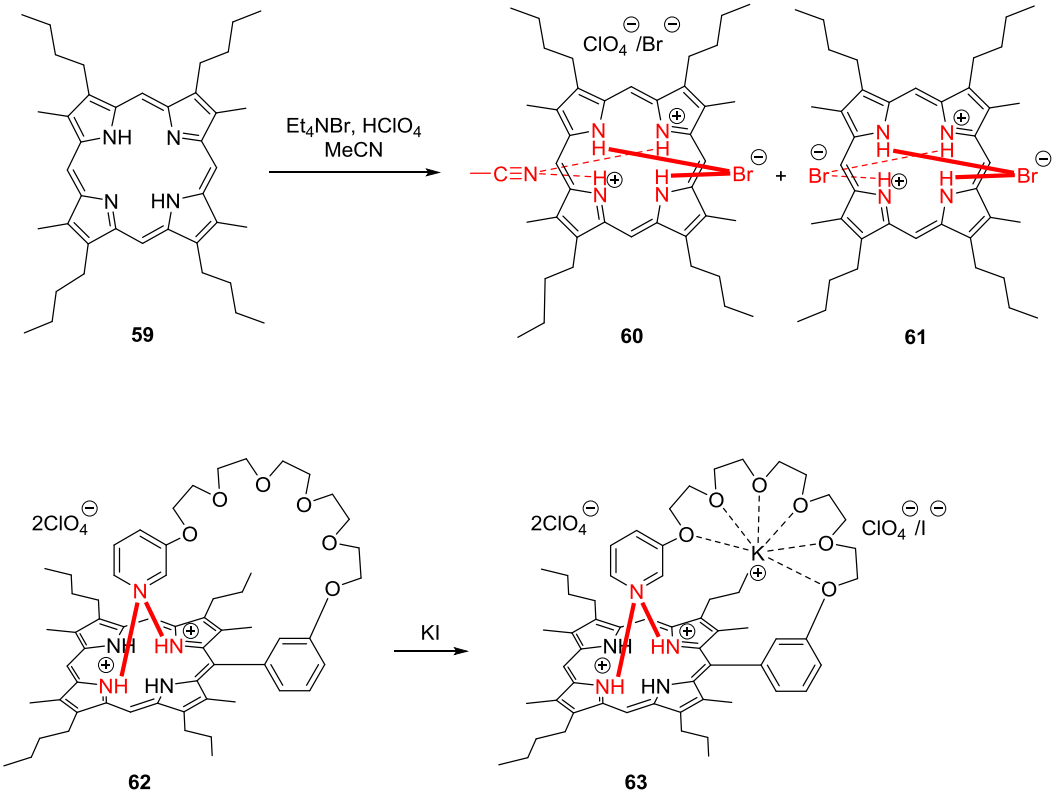

Figure 16. Top: selective formation of hydrogen-bonding complexes **60** and **61** *in situ* from the system **59**–Et_4NBr–$HClO_4$–MeCN.[95] Bottom: dicationic hydrogen-bonding complex **62** for complexation of potassium, yielding **63**.[96]

The presence of Cl^- induced H-aggregation followed by conversion into J-aggregates with increasing chloride concentration. Nakanishi *et al*. investigated the photoconductivity of nanochannels composed of *sad*-type porphyrin dications and electron donors.[100] Specifically, the dihydrochloride salt of **64**, $[H_4DPP]Cl_2$, gave supramolecular architectures by self-assembly based on intermolecular π–π-interactions that could host tetrathiafulvalene and *p*-aminophenol. Additionally, porphyrin diacid–polyelectrolyte supramolecules formed *via* electrostatic self-assembly in aqueous solution were used as effective photocatalytic systems for iodide oxidation.[101] Herein, the cationic porphyrin architectures showed a significantly higher catalytic activity than aggregates under neutral conditions. Porphyrin

dications have also generated some interest, for example, in nonlinear optics (NLO) where laser-induced protonation of free base porphyrin in chloroform gave a positive nonlinear absorption (NLA) due to conformational distortion.[102]

Often, the more elusive porphyrin monocations are also saddle-distorted, although tendentially less than the corresponding diacids,[103] and stand as a 'missing species' in porphyrin chemistry since they are generally difficult to produce, characterize, and isolate. Porphyrin monoacids are usually less stable than their diprotonated counterparts. It is likely that a large saddle distortion destabilizes the monoacids because their out-of-plane distortion significantly reduces the steric crowding of the remaining unprotonated nitrogen atom. This leads to the uptake of a second proton being more energetically favorable than the first.[89] As a result, most observations of these species are limited to theoretical methods and spectroscopic sightings, often in equilibria with the respective dication.[104] Nevertheless, the crystal structure of the H-bonded complex $[H_3TPP]I_3$ has been solved[105] and in another study, Kojima and Fukuzumi obtained the stable monocation complexes **66** and **68** of saddle-distorted **64** by reaction with anthracene sulfonic acids **65** and **67**.[106] This was possible presumably due to the only weakly hydrogen binding character of the conjugate anthracene bases (Figure 17A). H_2DPP (**64**) also formed a stable monoacid complex **69** in the presence of methanol and TFA in DCM.[107] The crucial role of methanol is highlighted as stabilizing the monoacid through hydrogen bonding with an out-of-plane N–H group and an imine moiety at the same time, preventing the second acid–base reaction of the macrocycle (Figure 17B). Furthermore, Almarsson *et al*. were the first to observe a monoprotonated 5,10,15,20-tetraphenylporphyrin, which was capped on one face so that access of a trifluoroacetate anion to the second protonation site was restricted.[108] In another notable study, the group of Kojima formed supramolecular hetero-triads of diprotonated **64**, *e.g*., **70**.[109] In this context, formation of $[H_3DPP]X$ (where X = *e.g*., tosylate) species was correlated with destabilization of $[H_4DPP]X_2$ due to decreasing pK_a values of the protonating acids used. This

occurred as stronger acids provided weaker corresponding bases that were weaker H-bond acceptors (Figure 17C).

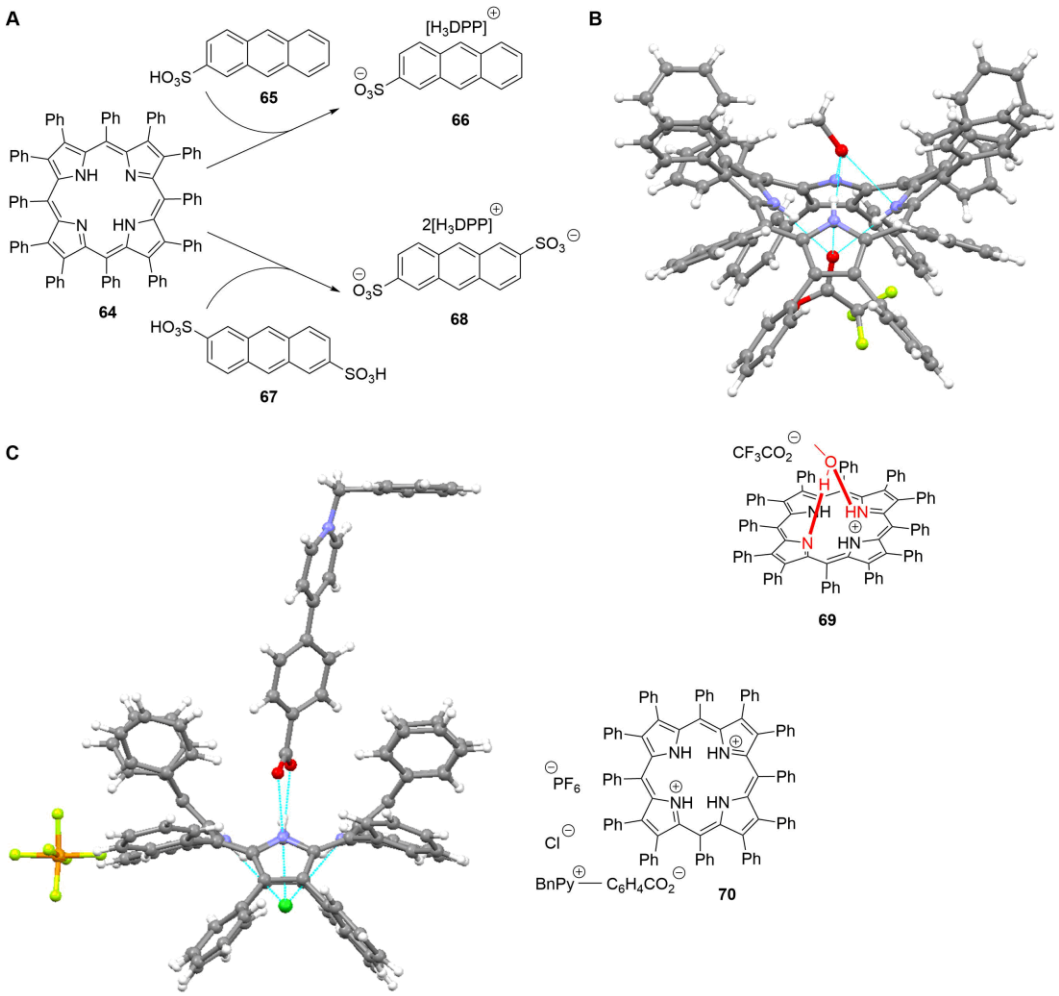

Figure 17. A: stable $[H_3DPP]^+$ H-bonding complexes **66** and **68** made from H_2DPP (**64**) in the presence of anthracene sulfonic acids **65** and **67**, respectively.[106] B: structure of **69** in the crystal (CCDC: RATXOC) where the monoacid $[H_3DPP]^+$ is stabilized by hydrogen bonding with methanol.[58,107] C: supramolecular hetero-triad **70** and its structure in the crystal (RARQEJ).[58,109]

Still, while anion binding, material science, and other applications of such salts are of contemporary interest, neutral free base porphyrins have a potential to be used as receptors and organocatalysts. As illustrated in **5** and Figure 13B, this requires nonplanar macrocycle conformations with accessible N–H and imine donors/receptors. As such, methods to achieve

significant distortion while retaining the tetrapyrrole's characteristics will be introduced in the following.

Nature's Way: Chelatases. Here, as so often, nature provides inspiration when taking a closer look at how conformational control in tetrapyrroles is achieved by chelatases. As was surmised for a long time, these natural enzymes incorporate a range of metals, such as iron, magnesium, nickel, and cobalt into porphyrins by a distortion-mediated mechanism. This commences by deforming the macrocycle, thus rendering the core more accessible, followed by metal insertion and relaxation of the system.[110] The product, a metalloporphyrin, is then released from the protein to fulfill its biological function (Figure 18).

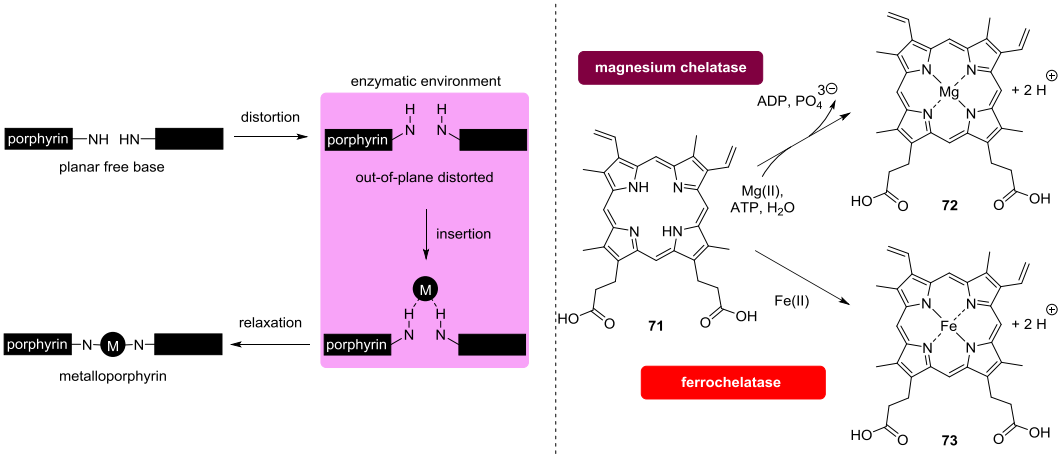

Figure 18. Left: schematic illustration of metal insertion into porphyrins by chelatases. Right: net reactions of the biocatalyzed Mg(II) and Fe(II) complexation by PPIX (**71**) to produce (protoporphyrinato IX)magnesium (**72**) and (protoporphyrinato IX)iron(II) (heme b, **73**), respectively. ADP = adenosine diphosphate; ATP = adenosine triphosphate.

This mechanism was initially proposed based on kinetic studies, chemical modifications, and the enzyme's strong inhibition by *N*-alkylporphyrins[111] and supported by the finding that antibodies elicited to a distorted *N*-methylporphyrin (= analogue of ferrochelatase–substrate transition state) could catalyze metal ion chelation.[112] Further indications were obtained through spectroscopic analyses[103,113] and crystal structural studies yielded final proof.[110]

In the case of ferrochelatase, the terminal enzyme in heme biosynthesis that inserts Fe(II) into the macrocycle **71**, the energetics of the accompanying ring distortion process have been calculated by DFT and a quantum mechanics/molecular modelling (QM/MM) approach.[114] On the base of this, it was argued that once the metal is inserted, the porphyrin becomes stiffer and flatter, resulting in a lower binding affinity to a site designated to bind its nonplanar form. This would ultimately result in release of the metalloporphyrin **73** from the enzyme. It was also suggested that the protein may increase the basicity of the pyrrole nitrogen atoms by macrocyclic deformation. Furthermore, the structure of the PPIX substrate bound to ferrochelatase was estimated: all pyrrole rings were tilted out of the mean-plane, most towards the putative binding site of the metal ion.

This brief overview illustrates how nature uses an efficiently 'designed' method to achieve what is tedious, maybe even unimitable in a synthetic setting. Such being the case, researchers have yet to find a synthetic methodology that mimics all the conveniences of these natural enzymes in less time than nature used through evolution.

Highly Substituted, Nonplanar Porphyrins. Uncharged nonplanar porphyrins (as opposed to core dications) are essential for biological functions and frequently found in photobiological systems[115,116] and other proteins.[21a] However, the first experimental proof of such nonplanar conformations was provided in the early 1960s, namely with the tetragonal forms of H_2TPP (**47**) and Cu(II)TPP.[117] The historical development and classic cases of tetrapyrrole nonplanarity have been discussed elsewhere[88] and nowadays, the family of dodecasubstituted porphyrins stands as a typical workhorse for studies in this area as they are often accessible by rational syntheses towards conformationally designed targets.[55,118] Therefore, it is important to give a brief introduction to the basic characteristics (*e.g.*, conformation–properties relationships) of such compounds.

The various nonplanar distortion modes for highly substituted porphyrins were defined and categorized by Medforth *et al*. (Figure 19, left).[119] In

H_2OETPP (**74**) and its derivatives, a well-understood and frequently used class of saddle-distorted free base porphyrins that are structural hybrids of H_2TPP (**47**) and H_2OEP (**48**), the central N–H donors are severely forced out-of-plane. More precisely, a main structural consequence of the repulsive *peri*-interactions between neighboring meso- and β-substituents is an alternating 'up and down' tilt of the individual pyrrole rings in **74**, which are tilted *ca*. 30° out of the mean-plane.[120] At the same time, meso-aryl groups in nonplanar porphyrins show increasing in-plane rotation. Note, that such a structural reconfiguration continues to exist even after oxidation of the π-electronic system.[121] Altogether, the *sad*-type conformation of OETPPs and other 2,3,7,8,12,13,17,18-octaalkyl-5,10,15,20-tetraarylporphyrins causes the amine functions to be oriented significantly towards the sphere of the tetrapyrrole rather than in-plane and increases the chances to interact with surrounding H-bond acceptors. On the other hand, a similar effect may be expected for the imine groups in the form of both increased basicity and H-bond acceptor potential (Figure 19, right).

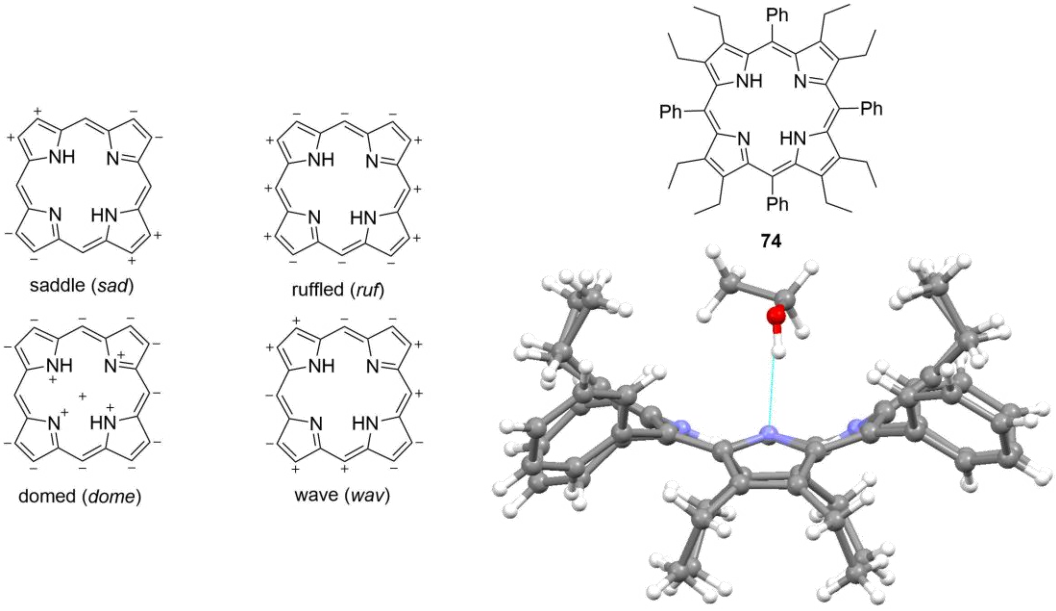

Figure 19. Left: representation of the four most common distortion modes for porphyrins. Only the most significant displacements are shown (+ and − indicate displacements above and below the 24-atom mean-plane (Δ24), respectively). Right: H_2OETPP (**74**)·EtOH and its structure in the crystal (CCDC: SATQOU).[58,120b]

Nonplanarity results in a range of measurable physicochemical effects besides changes in the electronic absorption spectra (*i.e.* a bathochromic shift).[122] Their increased basicity was noted during the initial synthesis of 2,3,7,8,12,13,17,18-octamethyl-5,10,15,20-tetraphenylporphyrin (H_2OMTPP, **75**) by Dolphin.[123] The product was protonated even by water and also showed broad absorption bands, which were attributed to steric interactions between the meso-aryl and β-methyl functions. Metallation experiences a significant rate enhancement in nonplanar tetrapyrroles, an effect that is likely to benefit the distortion-mediated metal insertion by chelatases.[124] These and more effects of macrocyclic deformation have been summrized by Shelnutt *et al*. with an emphasis on new functional properties and their significance in biological system.[21a] Another early observation was that nonplanar porphyrins have altered oxidation and reduction potentials compared to flat analogues and that this effect can be as powerful to the extent that electronic substituent effects are surpassed.[37,40,125]

Various other studies have evaluated the nature and effects of nonplanarity in tetrapyrroles, including investigations into (dynamic) photophysical and excited state properties,[120b,126] the oxidation to π-cation radicals,[127] spectroelectrochemistry,[128] and conformational flexibility[129] of 'stereotypical' representatives, such as 2,3,7,8,12,13,17,18-octaalkyl-5,10,15,20-tetraarylporphyrins **76**, 5,10,15,20-tetraaryl-2,3,7,8,12,13,17,18-octahalogenoporphyrins **77**, ruffled 5,10,15,20-tetraalkylporphyrins **78**, 2,3,5,7,8,10,12,13,15,17,18,20-dodecaarylporphyrins **79**, and their metal complexes (Figure 20). Notably, almost all photophysical parameters are directly affected by macrocycle distortion: nonplanar porphyrins have significantly lower fluorescence yields, large Stokes shifts, and shorter lifetimes of the lowest excited state due to faster intersystem crossing and internal conversion.[1,130]

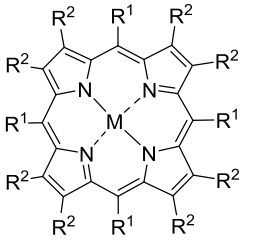

75 R^1 = Ph, R^2 = Me, M = 2H
76 R^1 = aryl, R^2 = alkyl, M = 2H, metal
77 R^1 = aryl, R^2 = halogen, M = 2H, metal
78 R^1 = alkyl, R^2 = H, M = 2H, metal
79 R^1 = R^2 = aryl, M = 2H, metal
80 R^1 = Ph, R^2 = Et, M = Cu(II)

Figure 20. Selected porphyrins and their metal complexes discussed in various studies on distorted systems.

An illustrative example of how substituent bulk and their interactions may be utilized for conformational control on the macrocycles is the series of cycloalkenyl-substituted porphyrins **81**–**83** 'enclosing' the β-positions prepared by Medforth *et al.*[118b] These macrocycles became increasingly nonplanar with larger peripheral cycloalkenyl rings by forcing the methylene groups into closer contact with the meso-phenyl substituents (Figure 21A). In line with that are X-ray studies of conformationally designed nonplanar Ni(II) porphyrins by Barkigia *et al*.[131] and a comparative study on the synthesis and ste reochemical properties of **47**, **74**, and tetraphenylporphyrins with graded degrees of β-ethyl substitution **84**–**87** (H_2Et_xTPPs where x = 0, 2, 4, 6, 8) plus their metal complexes.[132]

Macrocycle distortions lead to the formation of cavities on both sides of the tetrapyrroles where small molecules can bind. As a result, solvents can often be found incorporated within the crystal lattice of nonplanar porphyrins. For example, saddle-shaped tetrapyrroles often produce tunnel-like structures in the solid state, which are commonly filled with solvate molecules as in the case of Cu(II)OETPP (**80**)·2DCM (Figure 22).[133] However, at present it remains a challenge to find a universal and straightforward method to prove such weak interactions for the solution state by standard analytic methods.

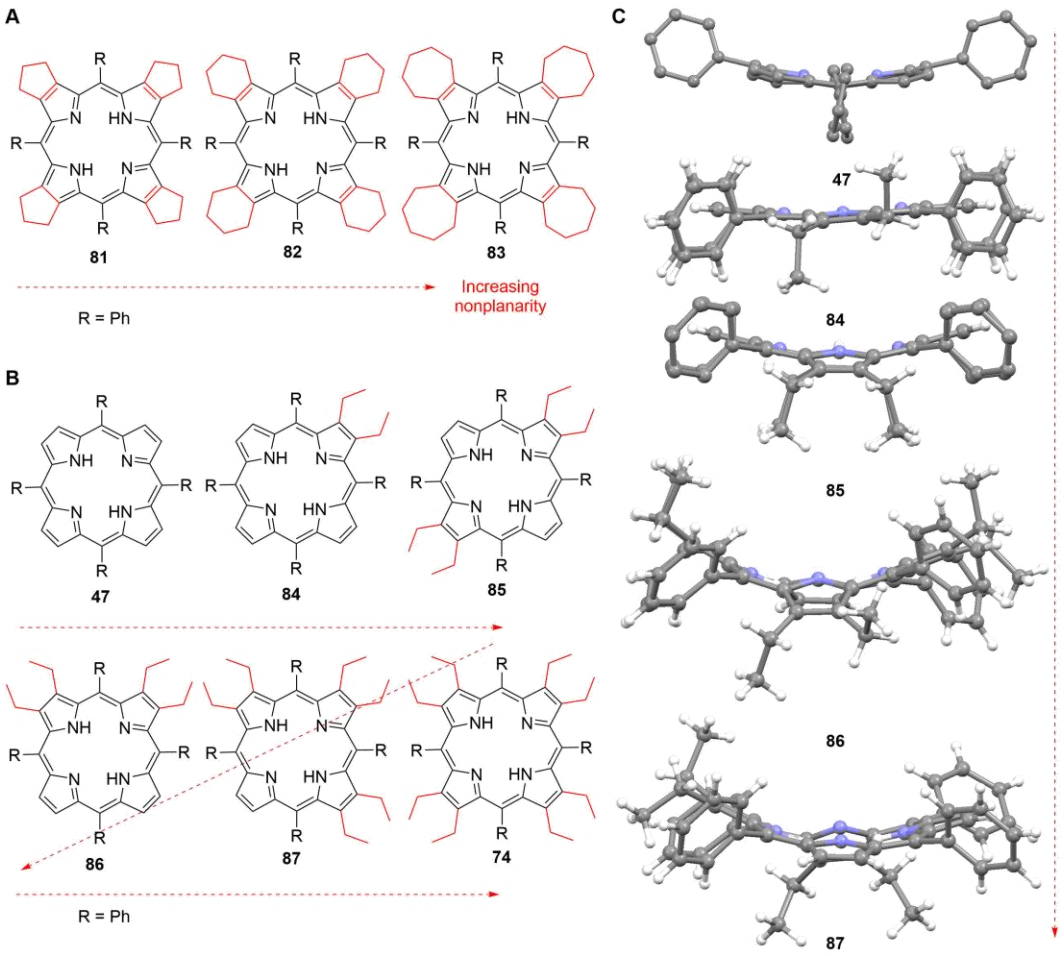

Figure 21. A: gradually distorted cycloalkenyl-substituted porphyrins **81**–**83**.[118a] B: distorted H_2Et_xTPPs **84**–**87** as well as **47** and **74** with graded degrees of β-ethyl substitution and incrementally increasing nonplanarity.[132] C: structures[58] of **47** (CCDC: TPHPOR10)[117a] and **84**–**87** (TATPOT01, TATPUZ01, TATQAG01, TATQEK01) in the crystal.[132] For comparison, see Figure 19 for a crystal structure of **74**.

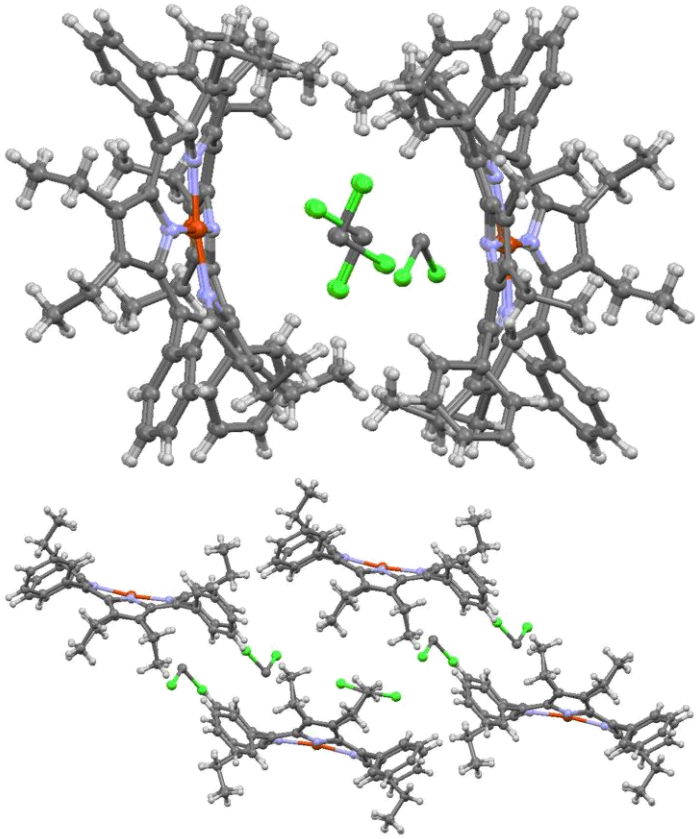

Figure 22. Cu(II)OETPP (**80**)·2DCM and excerpts of its crystal structure lattice diagram at different visual angles (CCDC: WADROI).[58,133]

Although conformationally close to OETPPs, the structural chemistry of DPPs that are often *sad*-type, including weak interactions with guests, appears to be more variable. This is best illustrated by **64** itself, which can undergo macrocycle inversion in solution as shown by variable temperature (VT) NMR.[55] The broad conformational landscape of DPPs is also represented by its various crystal structures: First reported was that of the free base **64** in an orthorhombic modification,[119] then another orthorhombic form (albeit in a different space group) with a more symmetric saddle distortion than previously seen and three water molecules incorporated within the unit cell.[134,135] Similarly to **64**, ethanol has also been found within the crystal structure of **74** where it was coordinating to the central nitrogen atoms (Figure 19).[120b] It should also be noted that multiple conformations in a single dodecaarylporphyrin have been observed, including *sad*, *ruf*, *wav*

modes, and mixtures thereof, which is once again ample evidence for their remarkable flexibility, if not adaptability and points at utilization as selective H-bonding sensors.[119]

It should be highlighted that due to the wealth of literature on distorted porphyrins, any synoptic view can only be a snapshot of this fast-developing and diverse landscape, with their applications spanning from medicinal, optical, and technical uses to as far as crystal engineering, methods development,[136] catalysis,[137] and sensing.[138] As was shown, only the introduction of saddling results in significant N–H exposure and as such, this approach stands at the base of a number of new and up-and-coming functional modes for nonplanar porphyrins based on the binding and activation of small molecules.

1.1.5 Applications: Porphyrins for Anion Binding, Explosive Detection, 'Chemical Nose'

When applied as sensors, the properties of the porphyrin macrocycle change upon interaction (*e.g.*, metal coordination, H-bonding, π–π-interactions, irreversible chemical reactions) with a substrate, resulting in a detectable response, such as a color change, fluorescence quenching/'turn off' or 'turn on', or an electric signal, which mirrors the presence of the analyte (Figure 23).

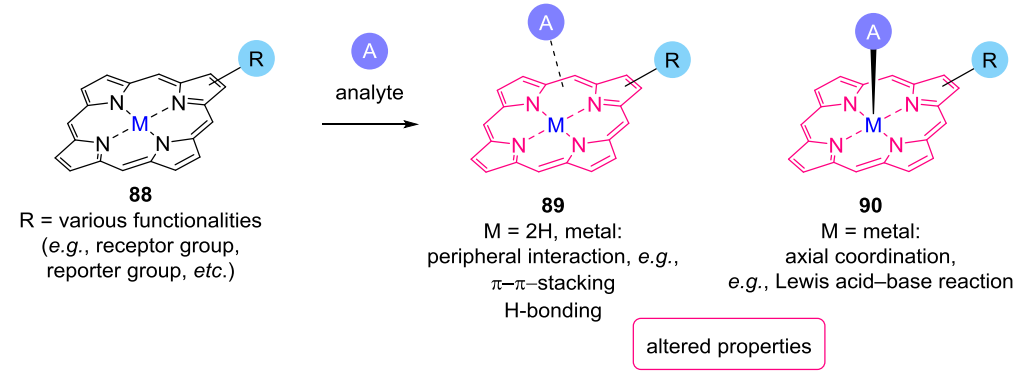

Figure 23. Porphyrins **88** for use as sensors and schematic representation of peripheral (as in **89**) and axial binding (as in **90**).

The development of such molecular probes benefits from the distinct relationship between the porphyrins' physicochemical features and structure, which provides diverse opportunities to design sensors with tailored characteristics. Such methods involve covalent synthetic modification (*i.e*. the introduction of additional functions, including receptor and reporter groups), metal insertion, or altering the molecular skeleton itself, to name but a few. As outlined above, macrocycle conformation and size can be tuned to a great extent by the number and nature of peripheral substituents,[1,3] thus modulating ion selectivity and sensitivity. What qualifies porphyrin–substrate complexes in particular for straightforward optical and fluorescence-based detection are their excellent photophysical properties, for instance, intense absorption of the Soret and Q bands and red to near-infrared emission. On a different note, they often mimic biological functions, such as reversible binding of gaseous compounds or catalytic activation as methods of action.[139]

(Metallo)porphyrins can facilitate multiple interactions and allow for tailoring of their physicochemical properties through alteration of the macrocycle, the complexed metal, and the functional groups. Similarly, free base porphyrins equipped with particular functional moieties acting as peripheral reporter groups or binding sites are important classes of receptors already at hand. As such, typical (metallo)porphyrin- and porphyrinoid-based chemical sensors can spot gaseous substrates, such as NO_2, CO_2, and volatile organic compounds (VOCs) as well as analytes in liquid phase. For instance, many common anions, NO in cells, H_2O_2, dopamine and other neurotransmitters, explosives, pollutants, pharmaceutical analytes, ammonia and amines, metal ions, protons, ascorbic acid, glucose, ion pairs, and reactive oxygen species (ROS).[4a,4b,6d,139,140] Moreover, porphyrins are of interest for military and security-related applications and can counteract explosives (as in the case of **91**–**94**) and hazardous biological, chemical, and radiological/nuclear materials (Figure 24).[138,141–144] However, currently this rarely involves the core of free base porphyrins but rather peripheral acceptor groups and often interactions other than H-bonding, leaving plenty

of room for new developments and to exploit the high potential of the N–H···X binding motif for probing.

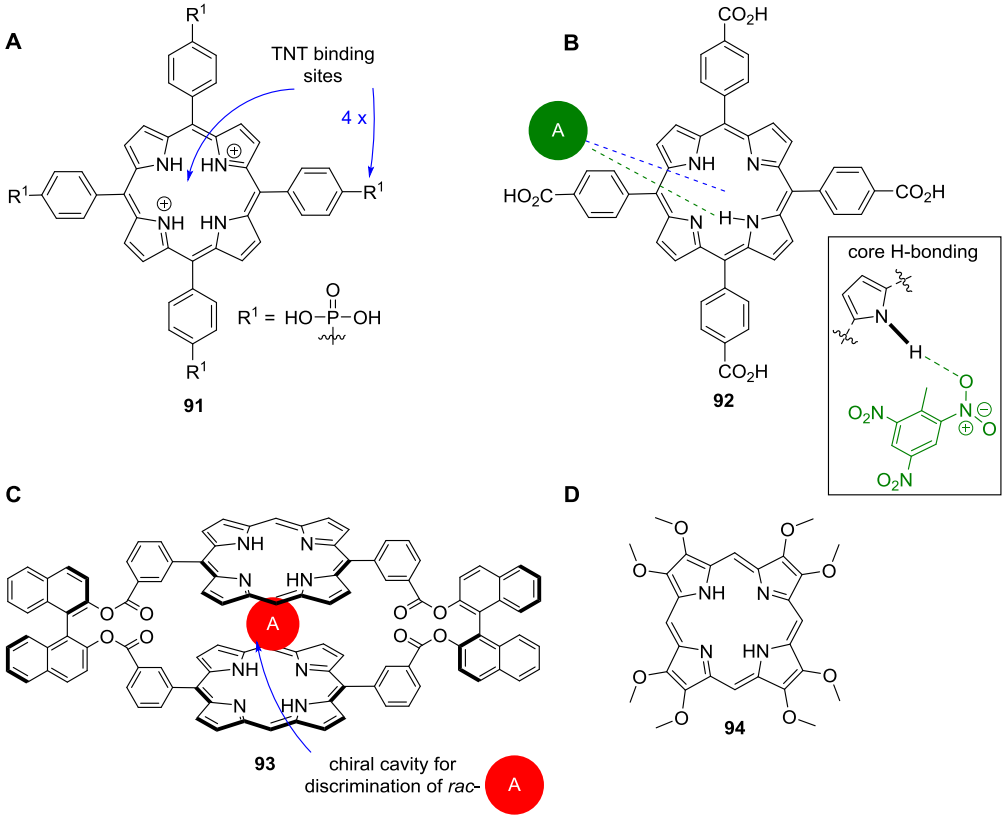

Figure 24. Selected porphyrin-based sensors for nitroaromatic compounds. A: porphyrin diacid **91** for efficient recognition of ≥ 5 ppb 2,4,6-trinitrotoluene (TNT) through emission 'turn off' following intermolecular hydrogen bonding and π–π-stacking.[141] B: complex of **92** and TNT (green dashed line = N–H···X-type hydrogen bond, blue dashed line = π–π-stacking).[144] C: chiral dimer **93** for naked-eye recognition of 1,3,5-trinitrobenzene and chiral discrimination of racemic mixtures of nitroaromatics by guest intercalation into a structural cavity *via* cooperative π–π-stacking.[143] D: macrocycle **94** for detection of, *e.g.*, TNT, 2,3-dimethyl-2,3-dinitrobutane (DMNB), 1,3,5,7-tetranitro-1,3,5,7-tetrazocane (HMX), and 1,3,5-trinitro-1,3,5-triazinane (RDX).[142]

Selective chemical sensors that sense gaseous and liquid analytes based on molecular interactions can be compared to the receptors of the olfactory and gustatory systems. This insight inspired research into artificial sensory organs,[145] with the result that today, a range of 'chemical noses' and 'tongues' are at hand,[139,146] often based on porphyrins. The current trends

in such tetrapyrrole-based applications have been reviewed by Paolesse *et al*. who engaged in studies on 'chemical noses',[138] spanning from basic research[147] to applications as far as breath testing and food analysis.[148] However, many of these systems are metalloporphyrins, free base porphyrins that contain peripheral receptor units, or porphyrinoids, where interactions with the inner core system are largely irrelevant for the respective recognition processes.

At the same time, others have merged various intramolecular interactions with intelligent novel analytical methods, resulting, for example, in 'optoelectronic noses' based on chemoresponsive dyes or fluorophores. Introduced by Suslick *et al*., 'optoelectronic noses' can utilize (metallo)porphyrins as platforms for odor visualization[149] and since then, their scope has broadened continually[140a] to recognize explosives,[150] pathogens,[151] toxic industrial chemicals,[152] and even to monitor foods freshness.[153] For this purpose, simplest, a colorimetric sensor assay (CSA) is digitally imaged before and during contact with a substrate to produce a difference map *via* digital subtraction, *i.e*. pixel by pixel of the image of the array before and after contact with regards to red, green, and blue (RGB) values (Figure 25).[154] An overview on Suslick's and other groups' work in this area, including phthalocyanine/porphyrin metal complexes[155] and doped materials[155a] for 'smell seeing' applications[149b] was given in 2013.[140a]

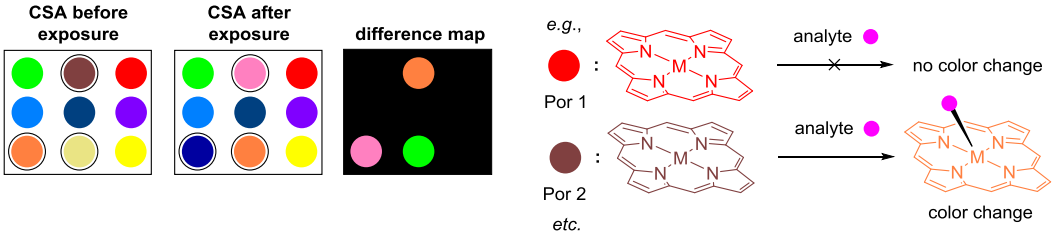

Figure 25. Illustration of a CSA where each spot represents a different chemoresponsive dye (*e.g.*, (metallo)porphyrins) before and after analyte exposure. Following testing, a difference map was generated. Some ligands show a color change upon contact with the substrate.[154]

1.2 Nucleophilic Aromatic Substitution (S_NAr) Chemistry on Highly Substituted Porphyrins

Modifications of the porphyrin macrocycle allow tailoring the tetrapyrrole scaffold for a plethora of applications. As was mentioned above, highly substituted porphyrins stand at the base of new functions in supramolecular chemistry, sensing, catalysis, *etc*. Consequently, novel and versatile synthetic methods, including functional group interconversions, *e.g*., substitution reactions are highly sought after. An outstanding example of great synthetic relevance is the 'Senge' reaction of free meso-positions using organolithium reagents.[118c,156] Other meso-substitutions have been developed, for instance, for the synthesis of meso-azidoporphyrins from the corresponding brominated precursors for use as potential synthons for 'Click Chemistry'.[157] Similar strategies may be used on highly substituted porphyrins, such as 2,3,7,8,12,13,17,18-octaethyl-5,10,15,20-tetranitroporphyrin (**95**) to access new derivatives with interesting and unique chemical and photophysical properties *via* elementary transformations. The H_2OETNP (**95**) framework in particular has previously found frequent use in studies on nonplanar porphyrins, π-aggregation, and supramolecular chemistry and remains a subject of contemporary interest.[21b,158] As such, focusing on the properties and chemistry of 2,3,7,8,12,13,17,18-octaethylporphyrins with 1–4 meso-nitro-groups may allow to deduce the effects of advancing nonplanarity as a result of increasing peripheral substitution. On the other hand, this series would also stand at the base of a case study on how the nitro moietites can be targeted for incremental functional group interconversions with the aim to produce new distorted porphyrins with mixed substituents.

In practical terms, compound **95** is obtained in a sequence of Zn(II) insertion, meso-nitration, and demetallation of the parent compound H_2OEP (**48**). A method established by Watanabe *et al.*, in which **48** is treated with zinc nitrate gives {2,3,7,8,12,13,17,18-octaethyl-5,10,15,20-tetranitroporphyrinato}zinc(II) (Zn(II)OETNP) in moderate yield.[159] However, this strategy cannot be utilized to access the mono-, di-, or

trinitrated products in high yield, which instead is possible by the reaction of Zn(II)OETNP with various equivalents of a stock solution of NO_2 in DCM.[160] Thus, the Zn(II) complexes of stepwise meso-substitution are formed in good yields. Demetallation can then easily be achieved under acidic conditions.[159]

Effects of the introduction of the powerfully electron-withdrawing nitro groups are a decreased electron density in the aromatic π-system and therefore more difficult oxidation of the porphyrin as well as facilitation of ring reductions.[160] Furthermore, it has been shown that each additional nitro group in **48** results in a bathochromic shift of the spectral bands of the absorption spectra for both the nitrated Zn(II)OEP complexes and the corresponding free bases as compared to **48**, which was accounted to steric effects (*i.e.*, *peri*-interactions). In accordance with that, crystal structure analysis of **95** indicates significant nonplanarity of the macrocycle[158a,c] whereas **48** is found to be planar.[161]

A good example of the S_NAr reactivity of the free base **95** is the meso-substitution with halides as reported by Gong and Dolphin (Figure 26).[162]

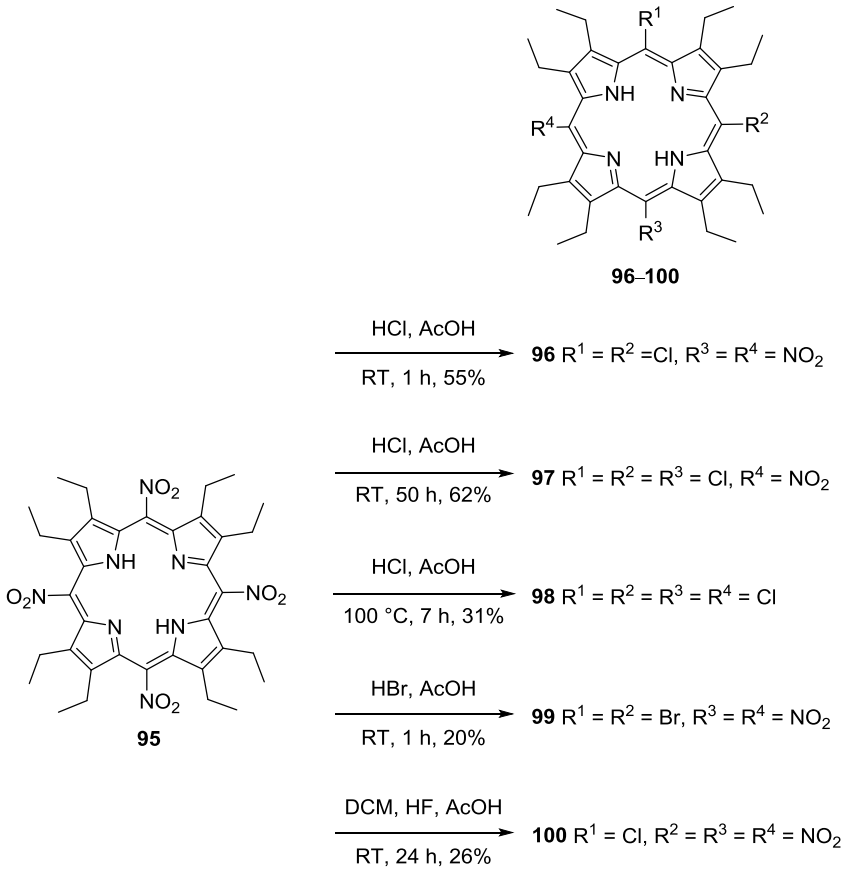

Figure 26 Overview on the literature known S_NAr reactivity of **95** in the presence of halides.[162] In the case of **100**, the chloride ion presumably stems from DCM.

Compound **95** undergoes stepwise nitro-substitution in the presence of chloride resulting in the formation of **96**–**98** and **100**. The outcome of each reaction depends to a large extent on the reaction temperature and time in the case of chloride substitution whereas in the case of bromide substitution, only the 5,15-dibromo-substituted product **99** was observed. Mechanistically, it is presumed that the highly activated H_2OETNP (**95**) system undergoes an addition–elimination mechanism, in which a Jackson–Meisenheimer complex (**101**) is formed.[163,164] The stability of the delocalized anion **102** is the driving force of the reaction and the elimination of the leaving group *in summa* represents a nucleophilic substitution (Figure 27).

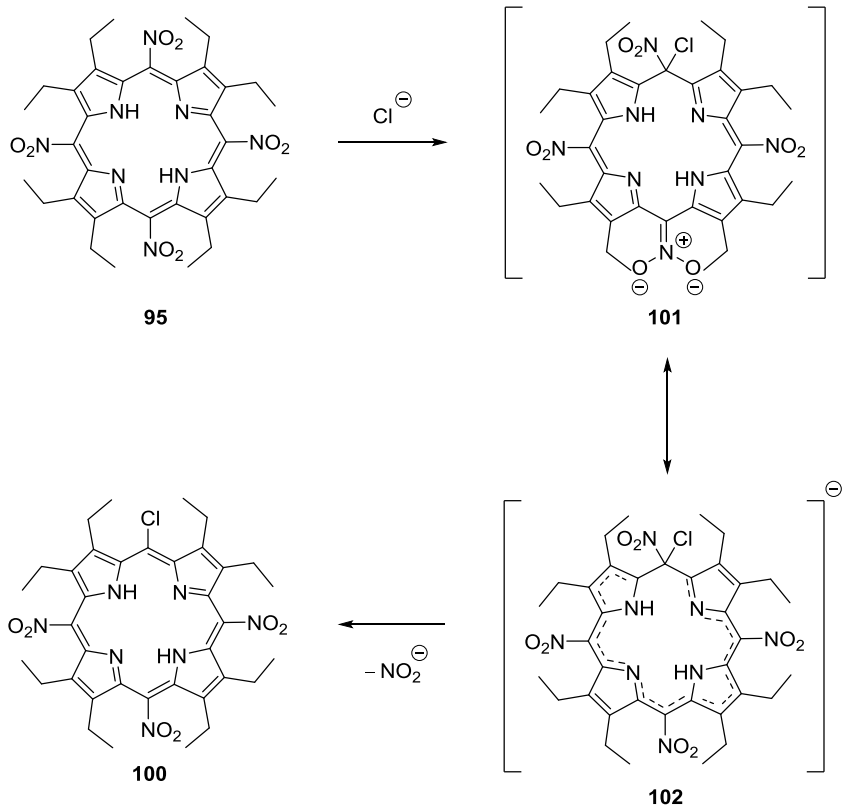

Figure 27 Presumed mechanism of the formation of **100** *via* a Jackson–Meisenheimer complex **101**/**102**.[162–164]

Another example is the reaction of {5-nitro-15,20-diphenyl-10-(4-tolyl)porphyrinato}nickel(II) (**103**) with sodium azide and various amines in the presence of potassium hydroxide. Compound **103** readily reacts with various primary and secondary alkyl-, aryl-, and cyclic amines bearing electron-withdrawing and electron-donating groups to yield a plethora of compounds, which includes meso-amino-substituted products **104a–f** as well as N–H-bridged porphyrin dimers **104g** and **104h** (Figure 28).[165]

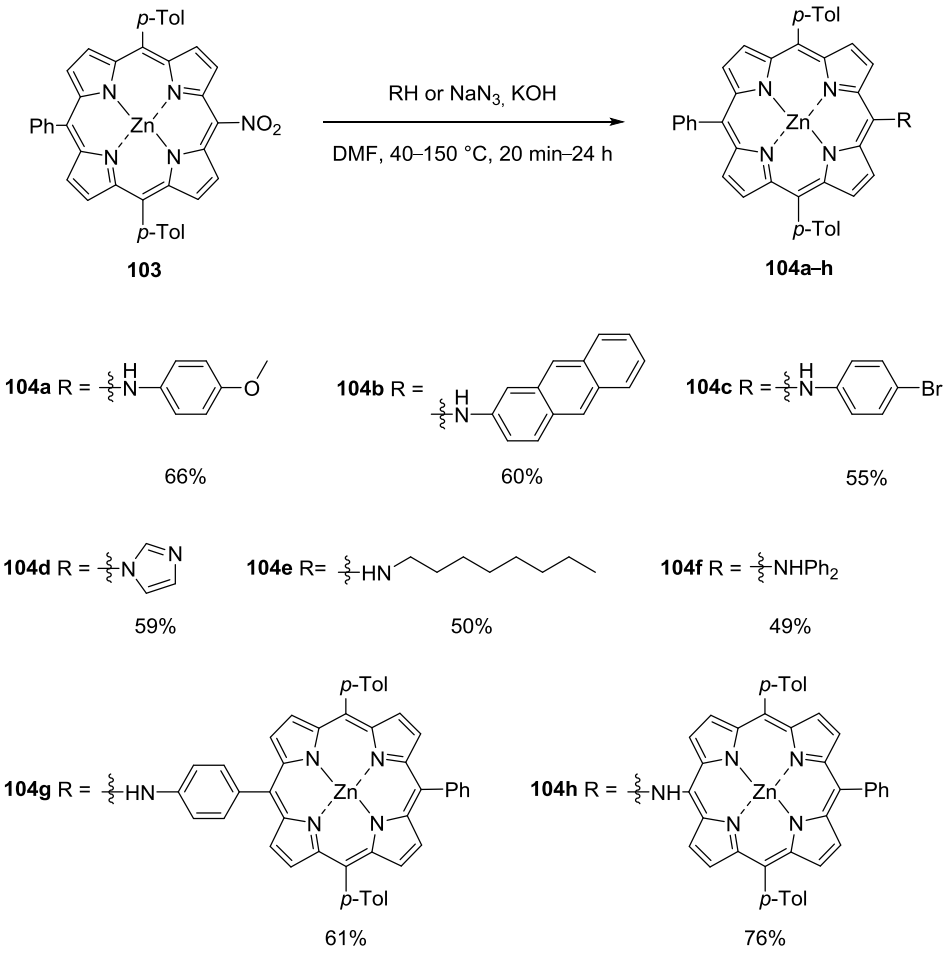

Figure 28. S_NAr reactivity of **103** with various amines.[165]

The same reaction type was utilized for the synthesis of sulfur-linked porphyrin dimers **106a**–**e** in good yields using porphyrin thiol 'surrogates'. The nucleophilic attack was carried out by the corresponding thiolates **107a**–**e**, which were formed after basic deprotection. Substitution of the thioether group of yet unprotected substrate **105a**–**e** then completed the sequence (Figure 29).[166] This is unique in a sense that the S_NAr proceeds under very mild conditions and with excellent yields using a seemingly unactivated system where the isooctyl-3-mercaptopropionate substituent acts as a good leaving group.

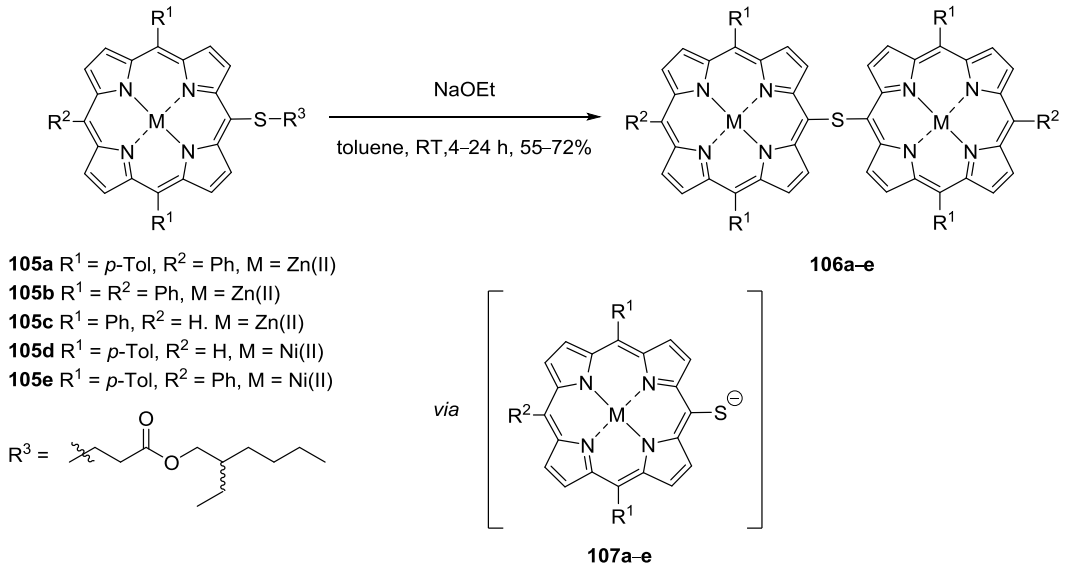

Figure 29. Synthesis of sulfur-linked porphyrin dimers **106a–e**.[166]

Additionally, a range of porphyrin thioethers underwent displacement reactions in the presence of base and alkyl halides or nucleophilic reagents. This yielded the products **108a–c** where the isooctyl-3-mercaptopropionate moiety acted as a leaving group and the porphyrins **109a–c** where a sequence of thiolate generation and nucleophilic attack on the alkyl halide had taken place (Figure 30).[166]

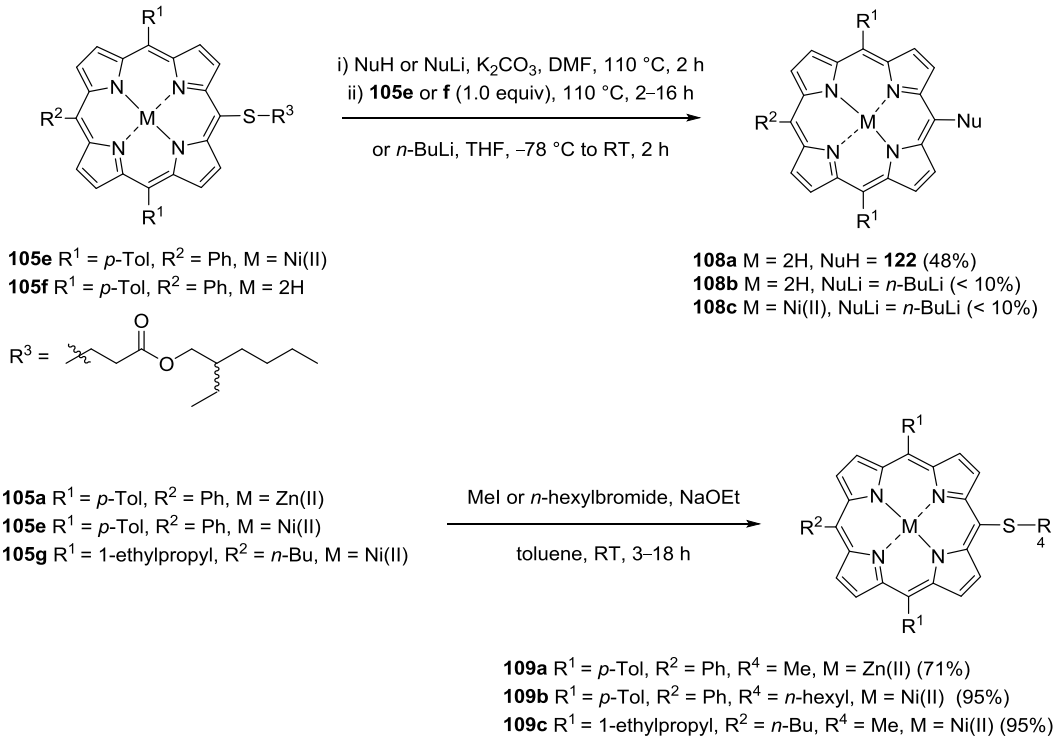

Figure 30. Displacement reactions of the porphyrin thioethers **105a** and **105e–g**.[166]

2. Objectives

A striking common feature of all natural and synthetic catalytically active tetrapyrroles is the presence of a central metal ion, with the macrocyclic scaffold serving merely as a fine-tuning molecular frame.[3a] Accordingly, the catalytic activity of porphyrins almost exclusively arises from the central metal ion. At the same time, it is surprising that distortion as a method to achieve nonplanar tetrapyrrole conformations for use as organocatalysts and sensors has remained mostly unexplored. This leaves the high potential of the inner nitrogen atoms, the primary structural motif of all free base porphyrins, to bind and recognize analytes and to activate small molecules unexploited. Therefore, one goal is to explore the opportunities that conformational design provides as a novel tool to access porphyrins with an exposed core. However, applying free base porphyrins in this capacity remains a tedious task, particularly when the bifunctional properties of the core itself (*i.e*. basic imine functions for deprotonation, which in turn, once protonated, become H-bond donors, and acidic pyrroles for hydrogen bond donation) are to be exploited for probing and catalysis. As mentioned several times, this is because the inner nitrogen atoms are 'hidden' for steric reasons and cannot usually be contacted by suitable reaction components (Figure 31). Hence, it can be proposed that the availability of the central amine and imine motifs is critical for novel applications of free base nonplanar porphyrins. Consequently, one aim of this work is to provide a first case on the importance of N–H···X-type hydrogen bonding for distorted porphyrin catalysts/sensors.

In terms of catalysis, the goal is to apply nonplanar porphyrins as organocatalysts in fundamental reactions, such as Michael additions, Diels–Alder reactions, aldol reactions, *etc*. This would yield the first example of metal-free porphyrin catalysis and illustrate the utility of conformational design to prepare tailor-made porphyrins with specific binding and receptor functions (Figure 32).

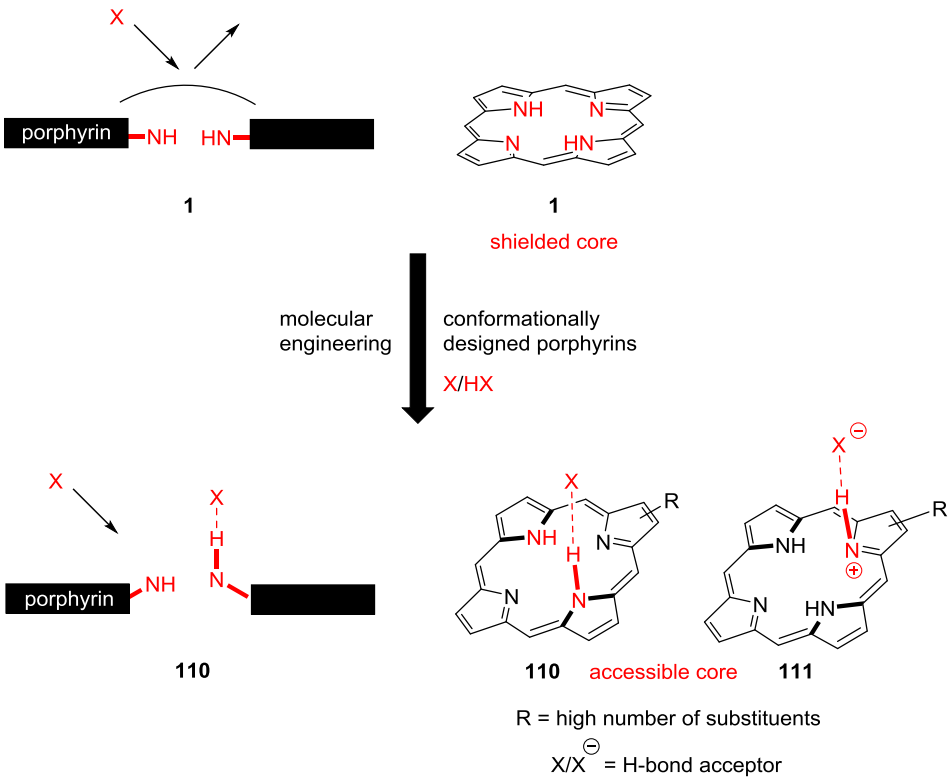

Figure 31. Concept of molecular engineering to produce nonplanar free base porphyrins. Due to an exposed core, binding of substrates may take place in saddled tetrapyrroles. Anticipated interactions are, for example, hydrogen bonding as in **110** and deprotonation followed by hydrogen bonding as in **111**.

Next to steric aspects, it will also be attempted to enhance the reactivity of the macrocycles via electronic modulation of the β- and meso-substituents. An extensive comparative screening of a number of nonplanar porphyrins as well as reaction conditions

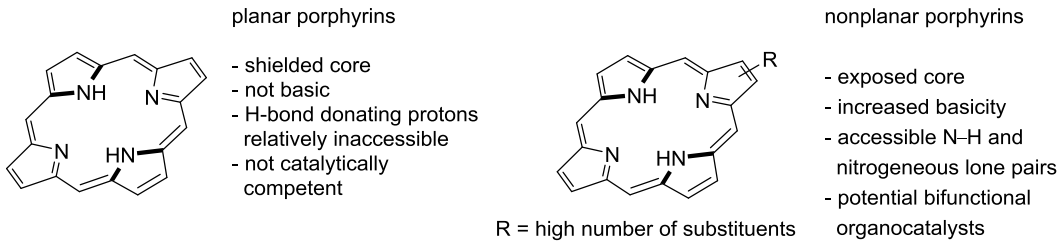

Figure 32. Summary: planar *vs*. nonplanar porphyrins and proposed catalytic properties of the latter.

is expected to evaluate their catalytic properties and if successful, to give a major contribution to the pool of synthetic methods available. Ultimately, this research may also impact the understanding of the role of catalytically active nonplanar porphyrins and their metal complexes found in nature.

In order to produce such tailored tetrapyrroles and as part of an ongoing methods development program, general and flexible syntheses will have to be developed. As a starting point, where possible, new highly substituted, multi-functionalized macrocycles will be synthesized based on methods previously established for planar porphyrins. The tetrapyrroles prepared in this way will then be screened for applications, such as organocatalysis, sensing, optics, *etc*. Additionally, X-ray crystallographic studies will identify their distortion modes and allow to deduce interrelationships between substituent pattern, specific conformations, and utility in new applications.

3. Results and Discussion

3.1 Synthesis of Electron Deficient Nonplanar Porphyrins and Initial Catalyst Screening

(Thio)ureas[167] and squaramides[168] incorporating basic functionalities have been shown to catalyze a host of reactions through the activation of both the nucleophilic and electrophilic reaction components. Such reactions can occur *via* either a general catalysis-like mechanism or a specific catalysis-like process (Figure 33).[169,170]

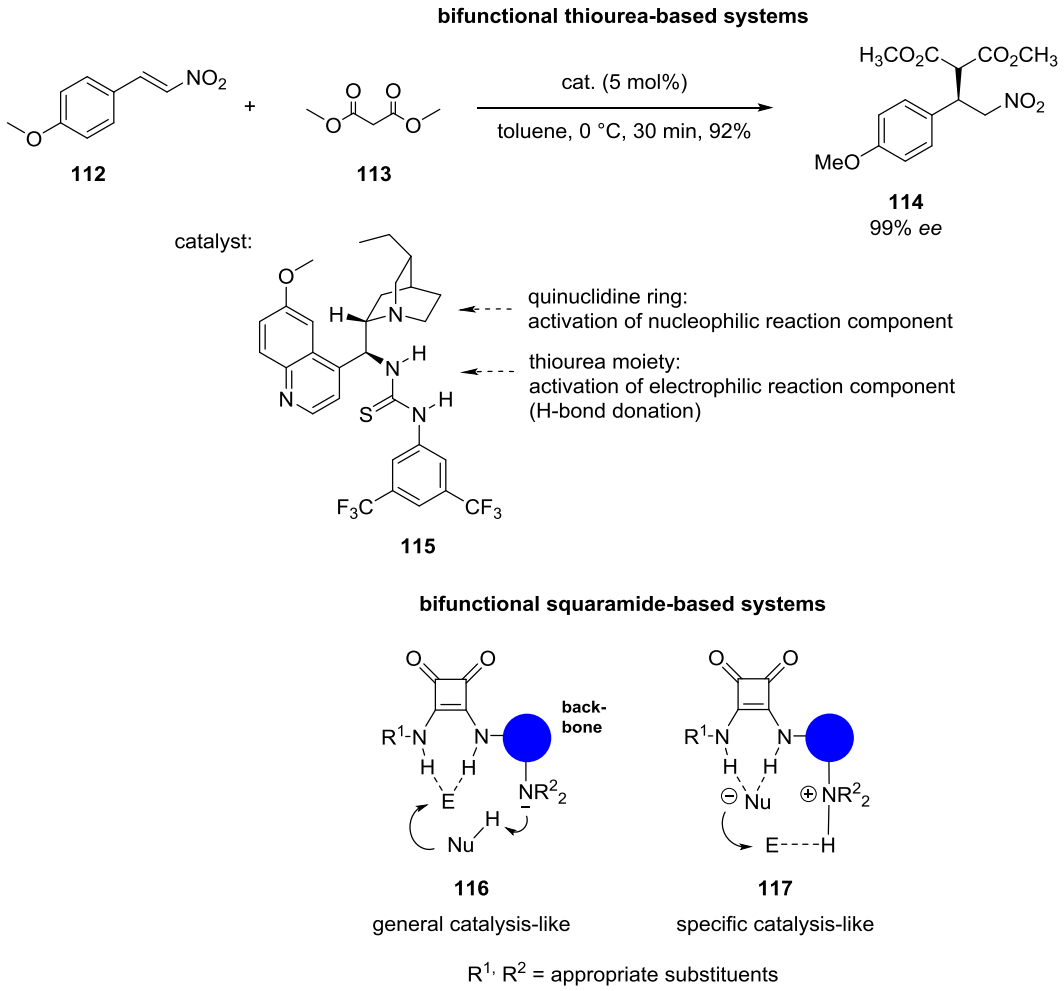

Figure 33. Top: enantioselective Michael addition of dimethyl malonate (**113**) to *trans*-β-nitrostyrene derivative **112** in the presence of **115**. The chiral product **114** can be obtained with high *ee*.[167e] Bottom: catalysis using squaramide-based sytems. General- (as in **116**) *vs*. specific catalysis-like (as in **117**) mechanism.[169,170]

To test whether a similar reactivity could be obtained using nonplanar porphyrins, as they have a bifunctional (Lewis acidic and basic) inner core system that can be compared to catalytically competent (thio)ureas and squaramides, a first series of potential porphyrin organocatalysts was prepared. Therein, focus was on distorted macrocycles carrying electron-withdrawing units as it was envisioned that these substituents would result in an increased Lewis acidity of the core N–H groups and therefore good hydrogen bonding potential. At the same time, nonplanarity should enhance the accessibility and basicity of the central imine moieties. Michael additions were selected as first test reactions because they can be susceptible to bifunctional activation.[167e] Moreover, the catalysts used therein, for example, **115** have acidic and basic groups reminiscent of distorted free base porphyrins (see Figure 33). As such, it was surmised that this reaction type may also be susceptible to activation by porphyrin organocatalysts and provide a good starting point.

The highly substituted, electron deficient tetrapyrroles 2,3,7,8,12,13,17,18-octabromo-5,10,15,20-tetraphenylporphyrin (H_2TPPBr$_8$, **56**)[171,172] and 2,3,7,8,12,13,17,18-octabromo-5,10,15,20-tetrakis(2,3,4,5,6-pentafluorophenyl)porphyrin (H_2TFPPBr$_8$, **121**)[173] were synthesized similar to published methods from easily accessible precursors (Figures 34 and 35). The tetrapyrroles H_2OETNP (**95**)[159] and H_2TPP (**47**)[174,175] were prepared according to the literature.

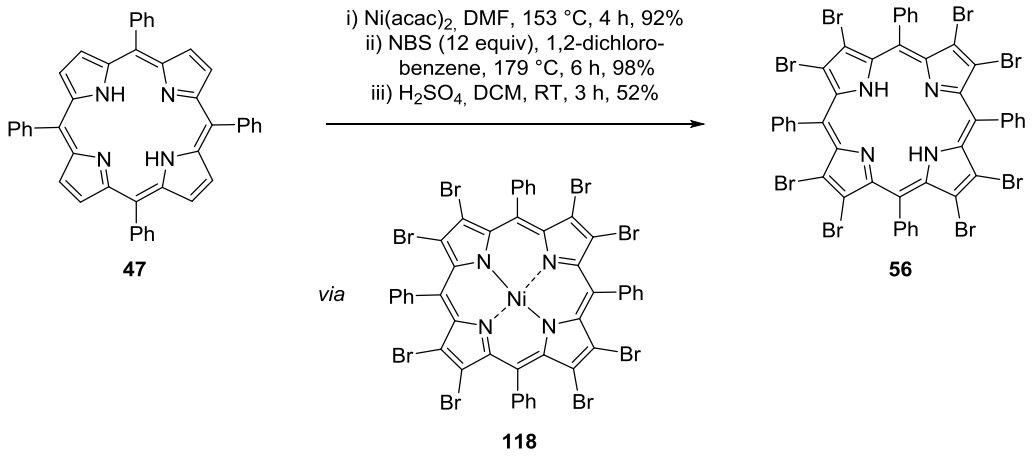

Figure 34. Synthesis of **56** from **47** via **118** in a sequence of metallation, bromination, and demetallation.[172]

Compound **121** was synthesized as an even more electron deficient alternative to **56**, which was expected to display yet stronger Lewis acidic properties.

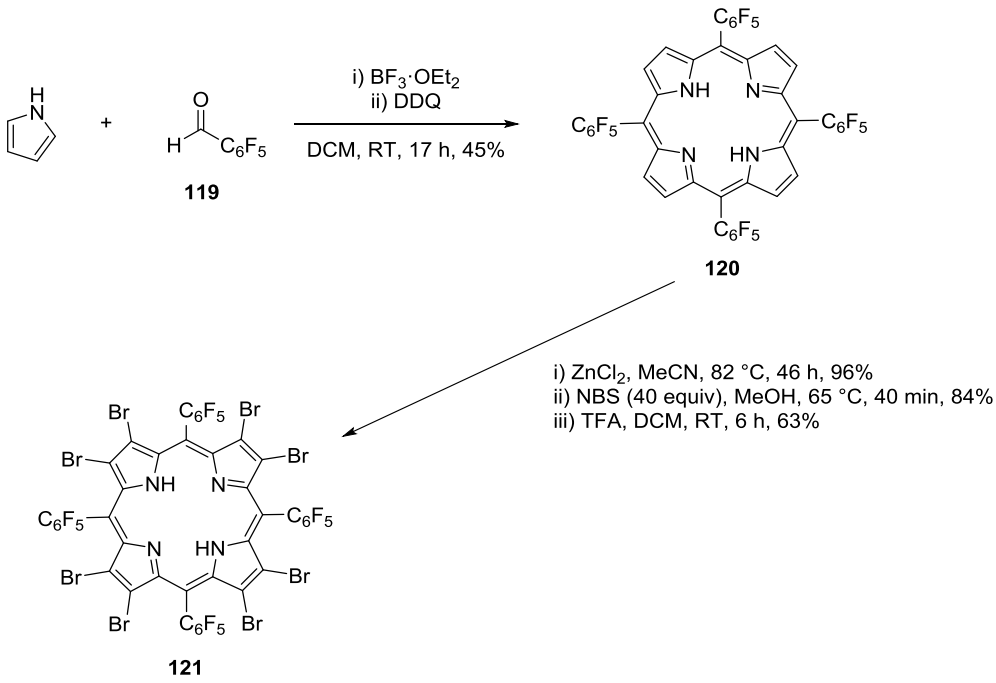

Figure 35. Condensation of pyrrole and 2,3,4,5,6-pentafluorobenzaldehyde (**119**) to form 5,10,15,20-tetrakis(2,3,4,5,6-pentafluorophenyl)porphyrin **120**, then metallation, bromination, and demetallation to yield **121**.[173] For an exemplary mechanism of a porphyrin condensation see Appendix, Figure A1.

With the porphyrins **56**, **95**, and **121** at hand, a variety of reaction conditions to find a porphyrin-catalyzed model reaction were screened. This included the use of different electrophilic and nucleophilic substrates, variation of catalyst loadings and concentration of reagents, reaction time as well as temperature. Initially, the catalytic activity of **95** was investigated (Table 1).

Table 1. Catalyst screening of **95**.[a,b,c]

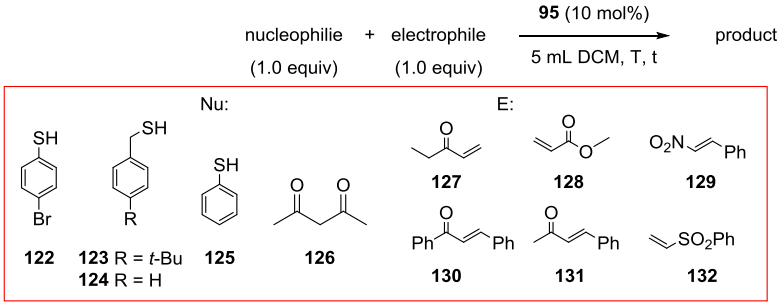

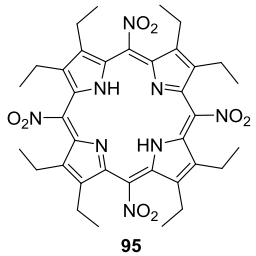

entry	Nu	E	T	t	conv., %
1	**122**	**127**	RT	24 h	blank: up to 87 cat.: up to 89
2	**122**	**128**	RT	24 h	0
3	**122**	**129**	RT	4 d	0
4	**122**	**130**	RT	4 d	0
5	**122**	**131**	RT	4 d	0
6	**123**	**127**	RT	7 d	blank: 37 cat.: 8
7	**123**	**128**	RT	6 d	0
8	**123**	**129**	RT	24 h	0
9	**123**	**130**	RT	24 h	0
10	**123**	**131**	RT	3 d	0
11	**124**	**132**	66 °C (in THF)	8 d	blank: traces cat. (10 and 20 mol%): traces
12[d]	**125**	**132**	RT (in THF)	5 h	blank: traces TEA (10 mol%): 93
13	**125**	**132**	RT (in THF)	19 h	blank: traces cat. (10/20 mol%): traces

Table 1 (continued)

14[e]	**126**	**129**	RT		5 d	0

[a] See Experimental for a general procedure. [b] Conversions were determined by ^{1}H NMR spectroscopy using 4-iodoanisole or 2,4-dinitrotoluene as internal standard. [c] [**95**] = $2.5 \cdot 10^{-2}$ M (10 mol%); 5.0 10^{-2} M (20 mol%) if not otherwise stated. [d] [TEA] = $2.5 \cdot 10^{-2}$ M. [e] [**95**] = $3.5 \cdot 10^{-3}$ M.

The screening of **95** in model (sulfa-)Michael reactions between the nucleophilic substrates **122–126** and the electrophilic substrates **127–132** did not reveal any catalytic activity. Instead, comparison of the entries 12 and 13 suggests that the catalytic activity of the porphyrin was insufficient for substrate activation. While the addition proceeded in good yield using TEA, no conversion was observed in the presence of **95**. Entries 1 and 6 indicate that the addition of **122** to **127** and, to a lesser extent, that of **123** to **127** took place regardless of the presence of porphyrin. The reaction between **122** and **127** was repeated multiple times under the same conditions and the amount of product formed varied significantly from experiment to experiment. This was attributed to a side reaction between **95** and **122**. Subsequent TLC analysis confirmed that an irreversible background reaction between **95** and the thiols **122–125** took place during each screening. Presumably, this involved the meso-nitro groups (see Chapter 3.4), qualifying **95** as intolerant to many substrates. This and the poor performance of the porphyrin in general led to **56** being screened hereafter (Table 2).

Despite the investigation of a broad range of nucleophilic substrates **113**, **124**, **126**, and **133** and electrophilic reagents **127–129**, **131**, **132**, and **134–139**, the screening of porphyrin **56** did not reveal any catalytic reactivity either. One possible explanation is insufficient basicity of the tetrapyrrole due to the presence of electron-withdrawing substituents. At the same time, activation of the electrophilic substrates may require stronger Lewis acidic properties of the catalyst, which is why the highly electron deficient porphyrin **121** was evaluated subsequently (Table 3).

Table 2. Screening of the catalytic activity of **56**.[a,b,c]

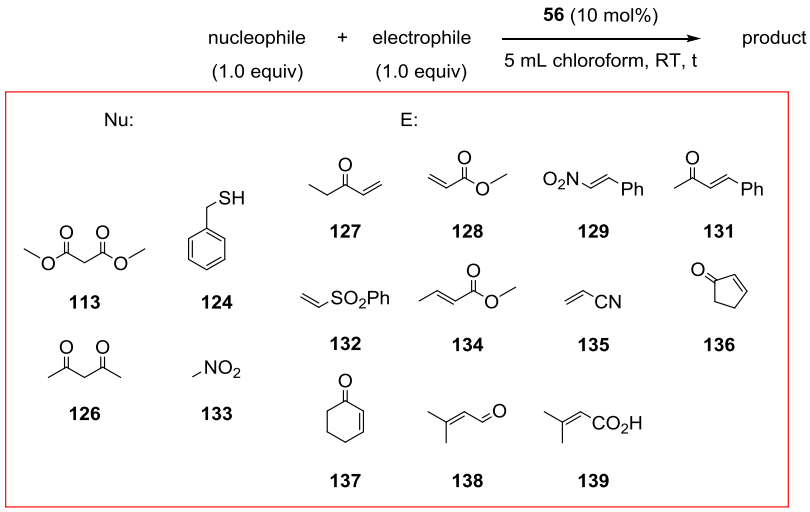

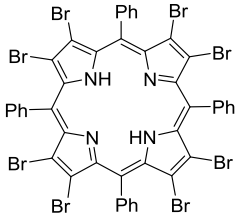

entry	Nu	E	t	conv., %
1	**113**	**127**	5 d	0
2	**113**	**134**	5 d	0
3	**113**	**135**	5 d	0
4	**113**	**136**	4 d	0
5	**113**	**137**	4 d	0
6	**113**	**138**	2 d	0
7	**113**	**139**	2 d	0
8	**124**	**128**	3 d	0
9[d]	**124**	**132**	7 d	0
10[e]	**124**	**134**	2 d	0
11	**126**	**129**	5 d	0
12	**133**	**127**	2 d	0
13	**133**	**128**	2 d	0
14	**133**	**131**	3 d	0
15	**133**	**134**	2 d	0
16	**133**	**135**	2 d	0
17	**133**	**136**	4 d	0
18	**133**	**137**	4 d	0

[a] See Experimental for a general procedure. [b] Conversions were determined by ^{1}H NMR spectroscopy using 4-iodoanisole or 2,4-dinitrotoluene as internal standard. [c] [**56**] = 10^{-3} M if not otherwise stated. [d] [**56**] = $1.5 \cdot 10^{-3}$ M. [e] [**56**] = $4.0 \cdot 10^{-3}$ M.

Table 3. Screening of the catalytic activity of **121**.[a,b,c]

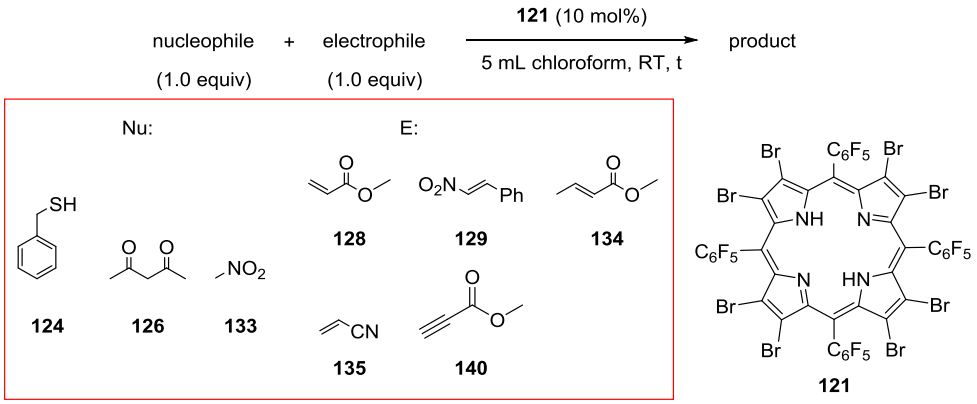

entry	Nu	E	t	conv., %
1	**124**	**128**	4 d	0
2	**124**	**134**	4 d	0
3	**126**	**129**	3 d	0
4	**133**	**128**	3 d	0
5	**133**	**129**	3 d	0
6	**133**	**134**	3 d	0
7	**133**	**135**	3 d	0
8	**133**	**140**	2 d	0

[a] See Experimental for a general procedure. [b] Conversions were determined by ^{1}H NMR spectroscopy using 4-iodoanisole or 2,4-dinitrotoluene as internal standard. [c] [**121**] = $2.0 \cdot 10^{-3}$ M.

Similar to the observations on compounds **56** and **95**, and porphyrin **121** did not show any catalytic activity under these conditions. Given the electron deficient character of all three macrocycles, it became evident that the introduction of electron-withdrawing groups may actually have been of disadvantage for their catalytic activity. Even though the Lewis acidity should in principle have been increased, introducing halogen substituents might have had the drawback of reducing the potential catalysts' inherent basicity below a threshold.

As mentioned, the targeted mode of substrate activation was bifunctional, that is, simultaneous interaction of the porphyrin with the electrophilic and nucleophilic reaction components. As such, it appeared justified to test a large variety of both components despite the absence of any Michael

reactivity from an early stage on. It was assumed that Lewis acidity and basicity of electrophile and nucleophile, respectively, would have to fall into a certain range to match the porphyrin's acid–base properties in order to be able to interact with the catalyst at the same time. On a different note, selecting Michael donors with distinctively low pK_a values would most likely have resulted in conversion without the need for a catalyst, as seen in Table 1. Hence, a broad range of subsrates was selected without thourough pre-evaluation of pK_a values. Utilizing the aforementioned electron poor macrocycles, it could have been a possibility that H-bonding of Michael acceptors occured readily while deprotonation of donors was absent, resulting in no conversion altogether. As such, all further investigations involved electron rich tetrapyrroles that should be more basic than **56**, **95**, and **121** while retaining their Lewis acidic amine moieties.

3.2 Catalyst Screening of Electron Rich Nonplanar Porphyrins under Revised Conditions

Revised conditions for porphyrin-catalyzed sulfa-Michael additions were found by M. Roucan, initially using saddle-shaped 21-methyl-5,10,15,20-tetraphenylporphyrin (**146**)[92c,176] as a benchmark compound (Figure 36).[137] Therein, **146** was applied as an electron rich alternative to **56**, **95**, and **121** where distortion had been achieved through facile *N*-methylation of readily available **47**. It was found that the addition of 4-*tert*-butylbenzyl mercaptan

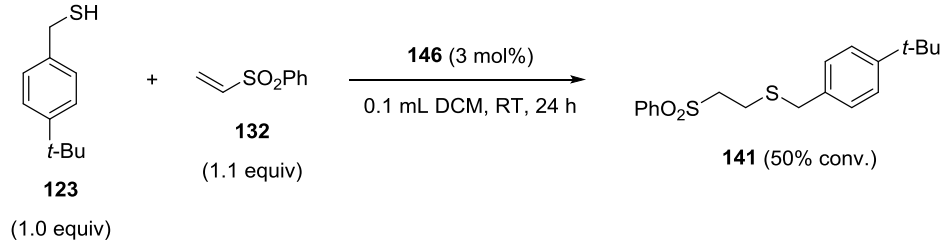

Figure 36. Optimized conditions (subsequently referred to as 'concentrated standard conditions') for the sulfa-Michael addition between **123** and **132**. Initially, **146** was used as a first benchmark organocatalyst.[137] [a] See Experimental for a general procedure. [b] Conversions were determined by ^{1}H NMR spectroscopy using dibromomethane as internal standard. [c] [**146**] = $7.1 \cdot 10^{-2}$ M.

(**123**) to phenyl vinyl sulfone (**132**) was susceptible to catalytic activation upon variation of the catalyst to electron rich **146** and increasing the concentration of all components. Furthermore, catalyst loading could be kept as low as 3 mol% to achieve a threshold value of 50% conversion.

Applying these improved conditions, screening of a library of porphyrins commenced in parallel with M. Roucan. For that, a suite of potential catalysts was evaluated, in which the degree of distortion from planarity, the electronic properties of the macrocycle, and the potential H-bond-donating proclivities had been gradually varied. Again, the addition of **123** and **132** was used as a test case as the reaction was likely susceptible to bifunctional catalysis (Table 4). In the absence of catalyst, no background reaction was observed at ambient temperature (entry 1) and the *de facto* planar 5,10,15,20-tetraphenyl- and 2,3,7,8,12,13,17,18-octaethylporphryin **47** and **48**[178,179] possessed no catalytic activity under the conditions employed (entries 2 and 3). Gratifyingly, a chimera of both these materials (*i.e.* the highly distorted porphyrin **74**)[118a,120a] promoted the reaction to full conversion (entry 4). Under diluted standard conditions, 80% conversion was noted. Notably, this catalyst system exhibited extraordinary sensitivity to variation of its electronic properties: the brominated analogue **142**[92c] was inactive (entry 8) while the tolyl analogue **143**[181] displayed a level of activity on a par with **74** itself (entry 9). While a 4-bromo substituent may not be regarded as a particularly powerful electron-withdrawing group, it was posited that bringing four such substituents to bear on the conjugated macrocycle core brings about the observed modulation of catalyst basicity, leading to inefficient deprotonation of the nucleophilic substrate.

Table 4. Porphyrin catalyst screening under optimized conditions.[a,b,c]

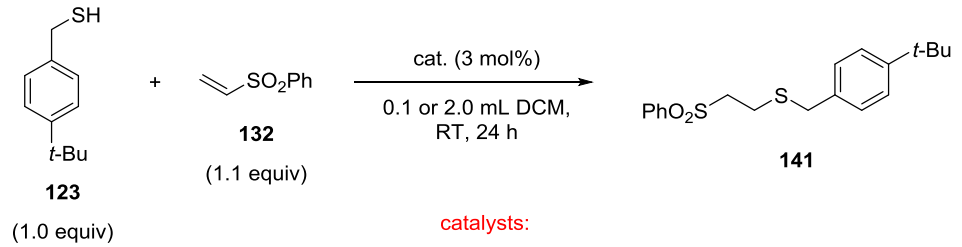

catalysts:

non-alkylated

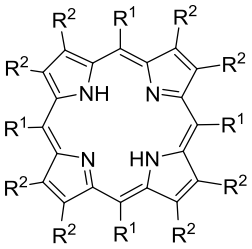

47 R^1 = Ph, R^2 = H
48 R^1 = H, R^2 = Et
56 R^1 = Ph, R^2 = Br
74 R^1 = Ph, R^2 = Et
95 R^1 = NO_2, R^2 = Et

121 R^1 = C_6F_5, R^2 = Br
142 R^1 = 4-Br-C_6H_4, R^2 = Et
143 R^1 = *p*-Tol, R^2 = Et
144 R^1 = *t*-Bu, R^2 = H

neutral alkylated

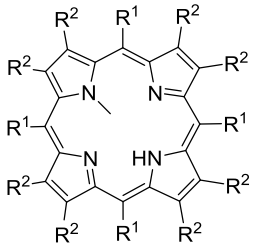

145 R^1 = H, R^2 = Et
146 R^1 = Ph, R^2 = H
147 R^1 = Ph, R^2 = Et
148 R^1 = 4-Cl-C_6H_5, R^2 = H
149 R^1 = 4-MeO-C_6H_5, R^2 = H

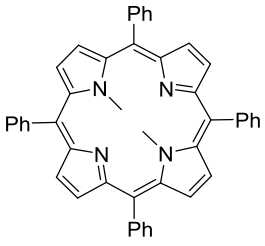

150

cationic alkylated

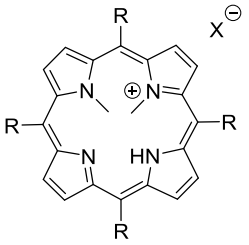

151 R = 4-Cl-C_6H_4, X = $CF_3SO_3^-$

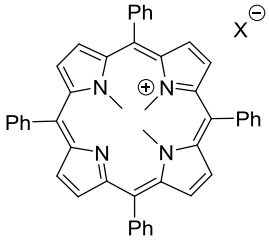

152 X = $CF_3SO_3^-$

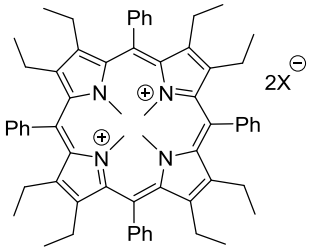

153 X = $CF_3SO_3^-$

entry	catalyst	Δ24, Å[d]	λ_{max}, nm[e]	#N–H	yield, %
1	-	-	-	-	0
2	**47**[174,175]	0.05,[177] 0.19[117a]	417	2	0
3	**48**[178,179]	0.02[161]	399	2	0
4	**74**[118a,120a]	0.54[120b]	456	2	quant. (80[f])
5	**95**[159]	0.40[158c]	422	2	0
6	**56**[171,172]	0.62[124b]	468	2	0
7	**121**[173]	0.56[180]	495	2	0

Table 4 (continued)

8	**142**[92c]	–	459	2	0
9	**143**[181]	–	457	2	quant. (75[f])
10	**144**[87]	–	446	2	0
11	**145**[182]	–	410	1	< 5
12	**146**[176]	0.26/0.30[92c]	433	1	50
13	**147**[92b]	–	477	1	quant. (< 5[f])
14	**148**[92a,137]	–	435	1	3
15	**149**[92a,137]	0.37[92c]	437	1	62
16	**150**[92c,183]	0.61/0.71[92c]	457	0	5
17	**151**[137]	–	461	1	quant. (20[f])
18	**152**[92b]	0.44[184]	463	0	0
19	**153**[92b,185]	0.61[92b]	506	0	0

[a] See Experimental for a general procedure. [b] Conversions were determined by ^{1}H NMR spectroscopy using dibromomethane as internal standard. [c] [cat.] = $7.1 \cdot 10^{-2}$ M if not otherwise stated. [d] Average deviation from the 24-atom mean-plane as a measure of the overall degree of nonplanarity in the solid state. [e] λ_{max} = Soret absorption band in DCM (+ 1% TEA) as a measure of the overall macrocycle distortion in solution.[1,3a,119] [f] [cat.] = $3.6 \cdot 10^{-3}$ M (subsequently referred to as 'diluted standard conditions').

In line with these observations, the highly *sad*-distorted free base porphyrins **56**, **95**, and **121** equipped with multiple electron-withdrawing substituents at the meso- and/or β-positions again failed to accelerate the reaction even under these revisited conditions (entries 5–7). Ensuing the investigation of *sad*-distorted porphyrins, the *ruf*-distorted tetrapyrrole **144** was explored.[87] Though highly distorted, no promotion of the reaction was observed due to the N–H groups still being concealed in the porphyrin plane (entry 10).

Next, *N*-methylporphyrins were investigated as potential catalysts. They are classic inhibitors of ferrochelatase,[92a,186] where the *N*-substitution and the consequential macrocycle distortion is known to result in increased porphyrin basicity.[104e] Thus, while these porphyrins contain one less H-bond-donating pyrrolic N–H unit, they should possess more accessible and reactive inner core functionalities. While *N*-methylation of **48** to afford **145**[182] led to only a marginal increase in catalyst efficacy (entry 11), the *N*-methyl analogue of the similarly inactive catalyst **47** (*i.e.* **146**)[176] resulted in a

significant improvement to 50% conversion (entry 12). Disappointingly, the alkylated variant of the efficient catalyst **74** (*i.e*. **147**)[92b] was able to catalyze the quantitative formation of **141** under concentrated standard conditions (entry 13) but not when diluted. Catalysts **148**[92a,137] and **149**,[92a,137] which possess *N*-methyl and meso-aryl groups but are devoid of octaethyl substitution did not serve as highly active promoters of the reaction, yet they did exhibit the electronic sensitivity observed in the archetypal free base systems (entries 14 and 15). The *N,N'*-dimethylporphyrin **150**[92c,183] proved a poor catalyst, although it is noteworthy that it is more efficient than **47** (entries 2 and 16). Thus, it is clear that electron-donating meso-aryl groups, octaethyl substitution, and *N*-alkylation can be used to improve catalytic activity. However, the effects of all three modifications are not entirely additive, and the former two are best utilized in concert from a catalyst design standpoint.

Finally, the performance of cationic porphyrins was screened. Compound **151**[137] has a '*cis'*-like 21,22-dimethylation pattern with a higher degree of distortion than in '*trans'*-like 21,23-dimethylated macrocycles.[92c] Despite the presence of electron-withdrawing aromatic groups, cationic **151** displayed promising activity under concentrated standard conditions but was a poor promoter under diluted standard conditions (entry 17). Interestingly, the analogue **152**,[92b] in which the remaining N–H unit was methylated and the electronegative chlorine atom absent could not catalyze the addition (entry 18). A dicationic *N*,*N'*,*N"*,*N'"*-tetramethylated version of the most efficacious catalyst **74** (*i.e.* **153**)[92b] was also inactive (entry 19).

Assessment of the performance of cationic porphyrins seems complex at first. Methylation at both the N21 and N22 positions brings about high levels of distortion, which were shown to be beneficial to catalytic activity. However, this also generates a positive charge, and it was also shown that rendering the porphyrin less electron rich leads to decreased catalytic performance (*vide supra*). But it is conceivable that delocalization of the charge throughout the large aromatic system lessens its impact. In addition, it may be relevant that the charge likely increases the Lewis acidity of the remaining pyrrole N–H function. In any case, since **151** is active despite the presence

of electron-withdrawing meso-substituents, it is clear that the contribution of distortion is dominant in determining the competence of the cationic catalyst. Of considerable interest is the failure of **152** as a promoter, which supports the hypothesis that hydrogen bonding by two porphyrin N–H units (*i.e.* one 'original' pyrrole N–H group and an iminium ion generated after protonation by the substrate (as in **155**, Figure 37)) is also a key facet of catalysis by these systems (*i.e.* suggesting a bifunctional mode of operation). This correlates well with the fact that **146** (possessing only one pyrrole N–H unit) is a mediocre promoter while its analogue **150** with none left is incapable of catalysis under these conditions. However, it will have to be confirmed in more detail, *e.g.*, by calculations to what extent this model is appropriate. Specifically, one question that remains is if the electrophile can indeed H-bond to one N–H unit that points to the other face of the porphyrin plane relative to the electrophile. If this is not the case, the current model will have to be revisited and other binding modes (for example, a different H-bonding pattern and electrostatic interactions between substrates and protonated catalyst) will have to be considered. Another issue is how the binding illustrated in **155** will have to be modified to account for the catalytic activity of *N*-substituted porphyrins like **146**.

In order to set the catalytic activity of these distorted porphyrins in context, the performance of the superior system **74** was compared to a range of amines of disparate basicity under diluted conditions (Table 5).

Table 5. Comparison of the catalytic activity of **74** with amine bases under diluted standard conditions.[a,b,c]

entry	catalyst	pK_{AH}[d,187]	conv., %
1	aniline	4.6	0
2	pyridine	5.2	0
3	DMAP	9.7	43
4	TEA	10.9	76
5	**74**	not determined	80[e]
6	DBU	*ca*. 13	quant.

[a] See Experimental for a general procedure. [b] Conversions were determined by ^{1}H NMR spectroscopy using dibromomethane as internal standard. [c] [cat.] = $3.6 \cdot 10^{-3}$ M. [d] Refers to the conjugate acid of the base listed (H_2O, 25 °C). [e] Data from Table 4.

The use of weak amine bases failed to lead to product formation (entries 1 and 2). DMAP promoted the reaction with moderate efficiency (entry 3) while both TEA, which is an order of magnitude more basic than DMAP and **74** could catalyze the reaction to *ca*. 80% conversion (entries 4 and 5).

To confirm that distorted porphyrins, particularly **74**, are more basic than some 'standard' amines, a 1:1 mixture of **74** and DMAP·HCl in $CDCl_3$ was prepared. Rapid and quantitative deprotonation of the DMAP conjugate acid was observed using ^{1}H NMR and UV-vis spectroscopic methods, indicating a substantial difference in basicity between the two catalysts (see Appendix, Figures A2 and A3).

Given the formation of the diprotonated analogue of **74** in the experiment outlined above, it was investigated if it would be possible to form such a species under the reaction conditions outlined in Table 4. Accordingly, substrate thiol **123** was added to **74** and the interaction was monitored using ^{1}H NMR spectroscopy (see Appendix, Figure A4). At an equimolar ratio, only traces of porphyrin protonation were detected. However, in the presence of a tenfold excess of **123**, the starting material **74** had been consumed and N–H resonances tentatively assigned to both mono- and diprotonated **74** could be observed, with monoprotonation being dominant. Increasing the excess of thiol to the molar ratio that was present at the outset of the catalytic

reaction between **74**, **123**, and **132** (porphyrin:thiol, 1:33) gave rise to significantly more diprotonated material with monoprotonated porphyrin still being prevailing. Ultimately, the dication became the major product at a catalyst:substrate molar ratio of 1:100 and the sole discernible porphyrin species present at a molar ratio of 1:200.

Rather than general catalysis (as in **154**, Figure 37, top), this strongly supports a specific catalysis-like mechanism (as in **155**, Figure 37, bottom), in which a porphyrin–thiolate ion pair is catalytically relevant. Given that all free base porphyrin catalysts evaluated required at least one N–H unit to be active, it also seems likely that activation by electrophile H-bond donation *via* at least two N–H units (one formed *via* protonation of the porphyrin by substrate thiol **123**) is a feature of the catalysis, *i.e*. the system is bifunctional. However, at the moment the queries addressed above remain and it is unclear at this juncture whether the mono- or diprotonated porphyrin species (or both) are catalytically competent. In any case, based on NMR data it appears likely that the monoprotonated species is the dominant catalyst in solution.

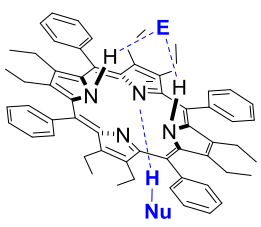

154

general catalysis-like

- H-bond-mediated electrophile activation
- aromatic system stabilizes positive charge upon protonation
- 'anti'-relationship between the catalyst's functional units appears stereoelectronically problematic

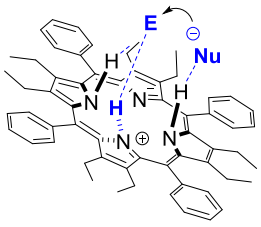

155

specific catalysis-like

- pronucleophile is deprotonated before rate-limiting step and H-bound by the catalyst
- protonated iminium ion stabilizes developing negative charge in the electrophile
- requires significant increase in basicity relative to nonplanar porphyrins
- no stereoelectronic issues due to vector of N–H bonds

Figure 37. Specific catalysis as the likely mode of porphyrin organocatalysts in nucleophilic additions (as in **155**) and comparison with general catalysis (as in **154**).

Revisiting the scope of Michael donors, a range of nucleophilic substrates other than **123** was subjected to concentrated standard conditions using **74** as a catalyst (Figure 38).

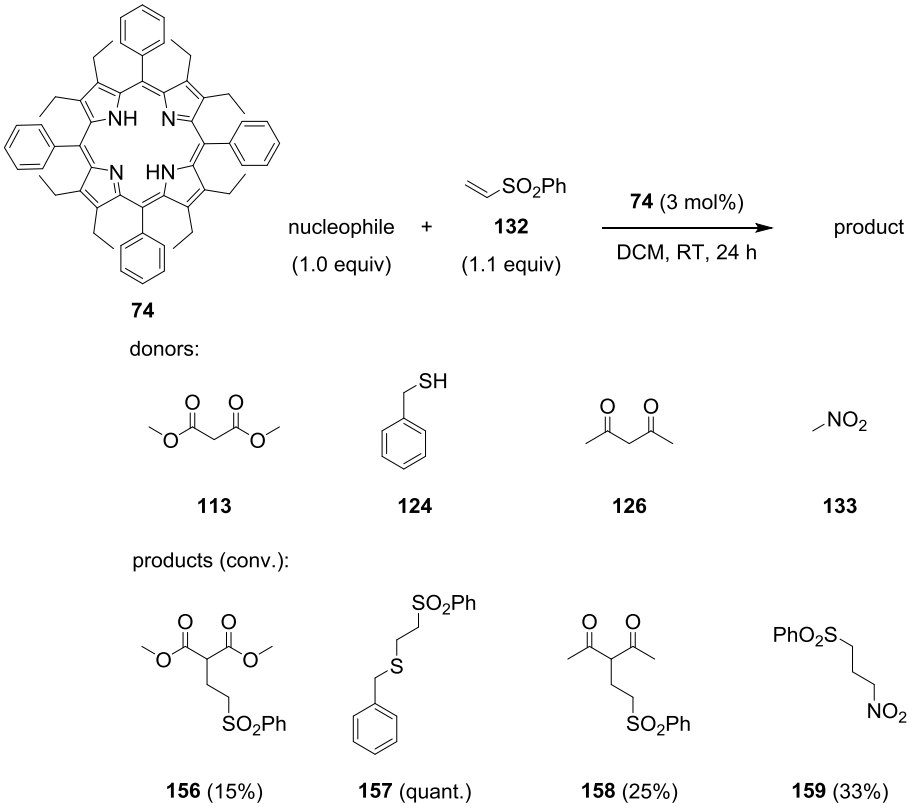

Figure 38. Catalyst screening of **74** using different Michael donors to yield addition products **156**–**159**. [a] See Experimental for a general procedure. [b] Conversions were determined by ^{1}H NMR spectroscopy using dibromomethane as internal standard. [c] [**74**] = $7.1 \cdot 10^{-2}$ M.

The results show that the reaction is tolerant to variation of the nucleophilic substrate. It is also of special note that C–C bond formations, which have a pronounced synthetic value, are possible, too, as in the case of the formation of **156**, **158**, and **159**, albeit with lower conversions. Studies on the tolerance to variation of the electrophilic substrate are currently in process.

A series of follow-up experiments under concentrated standard conditions revealed that the Michael reaction of **123** and **132** was also promoted efficiently at significantly reduced catalyst loadings. Hence, 92% and 73% conversion were achieved using 0.1 mol% and 35 mol‰ of **74**, respectively. This points at nonplanar porphyrins as efficient *and* mole economic catalytic

systems, and additional investigations on turnover numbers (TONs) and other kinetic parameters are intended to get a better understanding of concentration-dependent effects (*e.g.*, aggregation).

After this, porphyrins **162** and **164** were prepared in order to see whether larger aromatic ring systems at the meso-positions would benefit their catalytic activity (*i.e.* by an increased saddle distortion as compared to, *e.g.*, **74**). Both could be obtained through acid-catalyzed 'Lindsey' condensation[188] of the appropriate aldehyde **161** or **163** and 3,4-diethylpyrrole[179,189] (**160**, Figure 39).

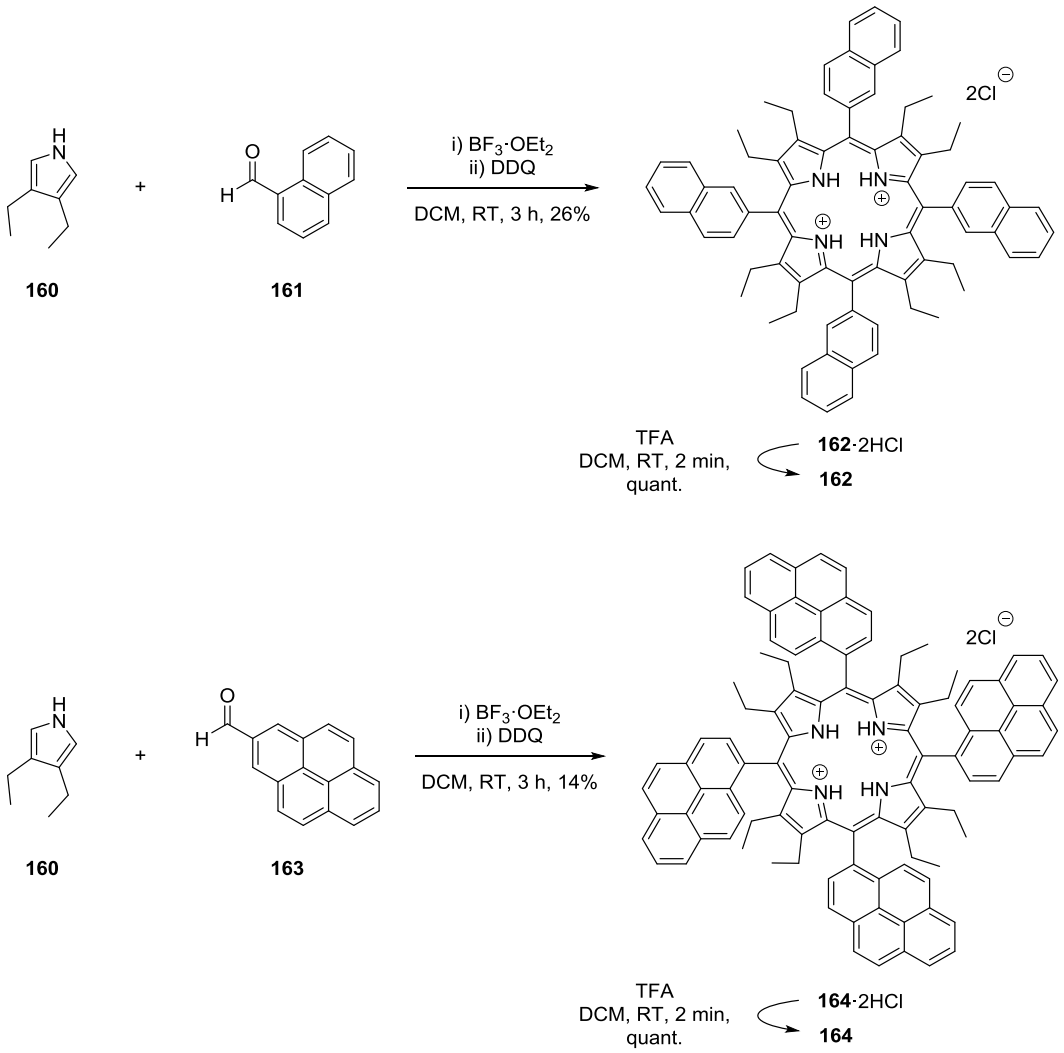

Figure 39. Synthesis of **162** and **164**.

UV-vis analysis indicated that the macrocycles **162** and **164** were isolated as dications, most likely as dihydrochloride salts due to protonation by residual hydrochloric acid present in the solvent. While both compounds could initially be neutralized through the addition of DCM:TFA (100:1, v/v), redissolving **164** in DCM for a catalyst screening resulted in anew protonation and no catalytic activity being observed (entry 3, Table 6). Unfortunately, this could not be prevented even when the solvent was predried and neutralized over K_2CO_3 and filtered through silica before use. In the future, utilization of molecular sieves and drying over CaH_2 followed by distillation may be considered for the most basic systems. However, catalyst screening of **162** under concentrated standard conditions resulted in quantitative conversion and 63% under diluted standard conditions (entry 2). But overall, while likely more distorted than **74** as suggested by bathochromic shifts of the spectral bands of the absorption spectrum, the performance of **162** was below that of **74** (entries 1 and 2).

Table 6. Comparison of the catalytic activity of **74** and various nonplanar porphyrins under standard conditions, using substrates **123** and **132**.[a,b,c]

entry	catalyst	conv., %
1	**74**	80[d]
2	**162**	63 (quant.[e])
3	**164**	0
4	**166**	0
5	**64**	3
6	**195**	6[e]
7	**197**	9[e]
8	**174**	89
9	**175**	quant.

[a] See Experimental for a general procedure. [b] Conversions were determined by ^{1}H NMR spectroscopy using dibromomethane as internal standard. [c] [cat.] = $3.6 \cdot 10^{-3}$ M if not otherwise stated. [d] Data from Table 4. [e] [cat.] = $7.1 \cdot 10^{-2}$ M.

One reason might be partial deactivation of **162** through intermolecular π–π-stacking and aggregation due to the relatively large π-aromatic

naphthalenyl systems. In part, this could also have contributed to the broad signals observed in the UV-vis spectra of both **162** and **164**. This could have been further evidenced through ^{1}H NMR studies of the porphyrin at different concentrations. On the other hand, the fact that **162** was protonated during its synthesis while **74** was not, points at an increased basicity. However, while this should generally be favorable for substrate activation, it may also lead to **162** being partly deactivated by residual hydrochloride during the catalyst screening and *de facto* incomplete promotion of the test reaction. In that case, once the catalysts' basicity exceeds a threshold, strictly aprotic conditions will have to be maintained. For example, DCM would have to be considered as a solvent with a labile H^+ function under these circumstances. Note, that this was likely the reason why **164** could not be used as a catalyst here.

Up to this point, all active porphyrin organocatalysts carried aliphatic β-ethyl substituents. Hence, the effects of installing various electron rich β-substituents was investigated in the following. As first examples, **166**[190] and **64**[55] were synthesized from **165**[191,192] and **56**,[171,172] respectively.[193,194] This proceeded *via* palladium-catalyzed Suzuki reactions from readily available precursors and notably, tetraarylation of **165** took two days and 12 equivalents of boronic acid for completion while octaarylation of **24** took eight days and 20 equivalents of boronic acid for completion (Figure 40).

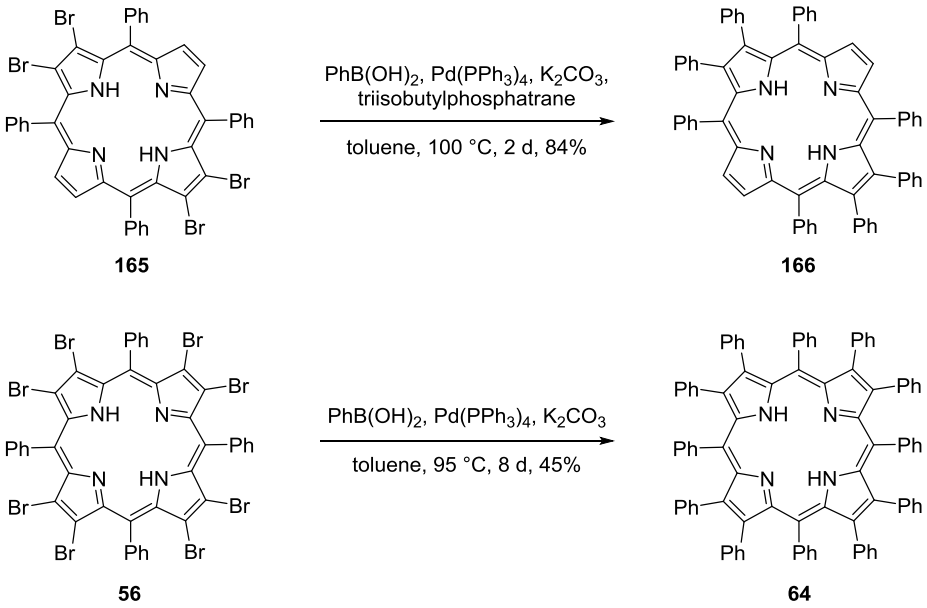

Figure 40. Synthesis of **166** and **64**.[193,194]

Catalyst screening of **166** and **64** under diluted standard conditions (entries 4 and 5, Table 6) revealed that both were unfit as organocatalysis under these conditions. Previous crystal structure analysis of **166** revealed an almost planar macrocycle,[190] with the degree of distortion likely being too low for the inner core system to engage in intermolecular interactions whereas highly nonplanar **64** can undergo macrocycle inversion in solution and is conformationally flexible.[55,119,134,135] It can only be assumed that this or a detrimental electronic effect due to the presence of twelve phenyl groups (*e.g.*, π–π-stacking, which was also indicated by broad spectral bands of the absorption spectrum and could have been further evidenced by ^{1}H NMR studies at different concentrations) might lower the molecule's catalytic activity.

Applying porphyrin thioethers **195** and **197** that had sulfur spacers connected to all meso-positions (see Chapter 3.4) revealed that they were equally ineffective (entries 6 and 7, Table 6).

While β-aryl groups and installing meso-substituents other than directly attached, (functionalized) phenyl rings proved unfeasible, it was surmisable that careful electronic modulation of the meso-groups and increasing the steric demand of the β-alkyl units would ultimately lead to free base

porphyrins with a catalytic activity greater than that of **74**. Therefore, first, 3,4-diisobutylpyrrole (**173**) was synthesized according to the literature[195–197] as a sterically demanding tetrapyrrole building block and condensed with benzaldehyde and 4-methoxybenzaldehyde, respectively (Figure 41).[121]

The preparation of **173** proceeded *via* α-bromination of 3-methylbutan-2-one (**167**)[195] followed by substitution on **168** with triphenylphosphane to yield **169**.[196] This underwent a Wittig reaction in the presence of isobutyraldehyde (**170**), giving **171**, and then pyrrole **172** formation through a Van Leusen reaction.[197] Subsequently, precursor **172** was reduced to **173** by lithium aluminium hydride and condensed with various aldehydes.

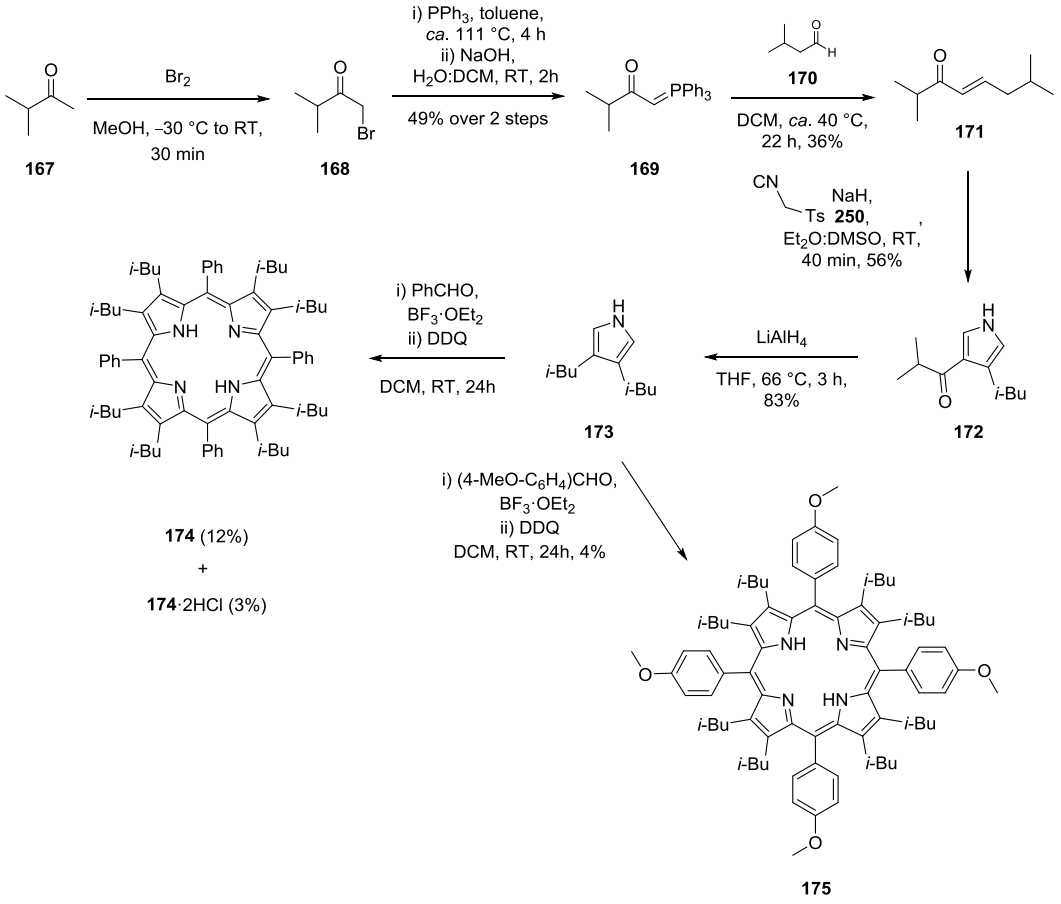

Figure 41. Synthesis of **173** and acid-catalyzed condensation with aldehydes.[121,195–197]

Macrocycle 2,3,7,8,12,13,17,18-octaisobutyl-5,10,15,20-tetraphenylporphyrin (**174**)[121] and its dihydrochloride salt **174**·2HCl,

presumably formed by reaction of the free base with residual HCl present in the solvent, was isolated following the condensation of **173** and benzaldehyde. While having physicochemical traits similar to neutral **174**, diprotonation in **174**·2HCl was conveniently indicated by UV-vis analysis since the absorption spectrum featured only two Q bands as compared to four in its free base form. Dihydrochloride salt generation during condensation may again be seen as indicative of the increased basicity of **174**, as was previously observed for **162** and **164**. By condensation of 4-methoxybenzaldehyde and pyrrole **173** under similar conditions, free base 2,3,7,8,12,13,17,18-octaisobutyl-5,10,15,20-tetrakis(4-methoxyphenyl)porphyrin (**175**) was produced.

Catalyst screening of **174** and **175** under diluted standard conditions gave 89% and quantitative conversion, respectively, thus qualifying both as superior to **74** (entries 8 and 9, Table 6). Certainly, the increased steric bulk at the β-positions through isobutyl substitution results in more distorted macrocycles and the high degree of nonplanarity in **174** and **175** was indicated both by bathochromically shifted absorption spectra and single crystal X-ray structural analysis of the former (see Appendix. Figure A5). In the case of **175**, the catalyst profited from the effects of both increased distortion and favorable electron-donating properties of the 4-methoxyphenyl substituents. Conclusively, the observed high conversion confirms the initial hypothesis that careful modulation of both the β- and meso-functionalities can be exploited to produce organocatalysts with a performance surpassing that of **74** and eventually that of common organic bases.

After that, the preparation of 3,4-diisopropylpyrrole (**180**), an even bulkier building block than 3,4-diisobutylpyrrole (**173**), was attempted (Figure **42**).

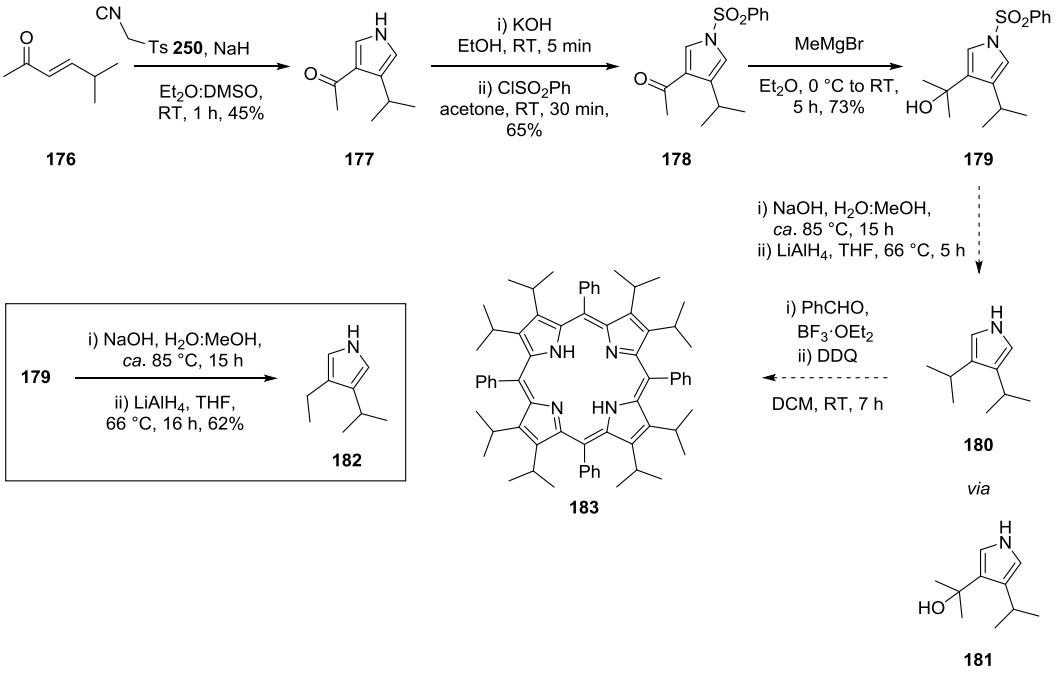

Figure 42. Attempted synthesis of **180**.[198]

According to the literature,[198] α,β-unsaturated ketone **176** was subjected to a Van Leusen reaction, yielding pyrrole **177**, which was protected subsequently. *N*-Substituted pyrrole **178** was then reduced to give **179** and deprotection and reduction of *in situ* generated **181** through lithium aluminium hydride was attempted. But instead of the target pyrrole **180**, only the unexpected formation of 3-ethyl-4-isopropylpyrrole (**182**) occurred. At this stage, reduction of **179** at revised conditions and ultimately, synthesis of **183** was not attempted due to time restrictions, but it is probable that a shorter reaction time and/or lower temperature, in accordance with the literature, will ultimately yield **180**.

After establishing nonplanar free base porphyrins as efficient organocatalysts in (sulfa-)Michael additions, another type of nucleophilic reaction was investigated briefly, namely the Henry reaction (Figure 43).

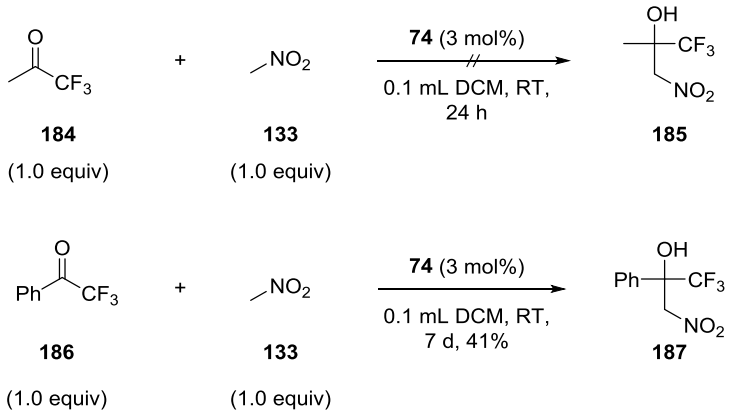

Figure 43. Initial attempts to identify a free base porphyrin-catalyzed nitroaldol reaction. [a] See Experimental for a general procedure. [b] Conversions were determined by ^{1}H NMR spectroscopy using dibromomethane as internal standard. [c] [**74**] = $7.1 \cdot 10^{-2}$ M.

In the case of the reaction of **184**, an instant color change of the solution from brown to green occurred, indicating porphyrin protonation. After 24 h, almost complete consumption of **184**, but not **41**, was noted, indicating that the former underwent a side reaction rather than the expected 1,2-addition, *e.g.*, trimerization[199] or base-catalyzed reaction with itself. In the blank sample, both reagents were almost unreacted. When using non-enolizable ketone **186**, no reaction was observed in the blank sample while the expected β-nitro alcohol **187** formed in 41% in the presence of **74**. This provides initial evidence that porphyrins may be applied to a wider scope of nucleophilic addition reactions and further optimizations will have to be carried out in order to produce more examples.

3.3 Incremental Introduction of Organocatalytic Activity into Conformationally Engineered Porphyrins

The DFT calculations presented in this chapter were performed by Dr. N. Grover.

As mentioned above, saddle-shaped H_2OETPP (**74**) is severely nonplanar and its organocatalytic activity was revealed in Chapter 3.2. Moreover, a mostly structural, comparative study by Senge and Kalisch focused on the H_2Et_xTPP series that includes **47**, **74**, and the related compounds **84–87**.[132]

Therein, the steric consequences of incremental peripheral substitution on the macrocycles and the effects on physicochemical properties were elaborated. H_2Et_xTPPs are structural hybrids of H_2TPP (**47**) and H_2OEP (**48**), which become increasingly nonplanar in the order: H_2TPP (**47**) < 7,8-diethyl-5,10,15,20-tetraphenylporphyrin (H_2DETPP, **84**) < 7,8,17,18-tetraethyl-5,10,15,20-tetraphenylporphyrin ($H_2tTETPP$, **85**) < 2,3,7,8-tetraethyl-5,10,15,20-tetraphenylporphyrin ($H_2cTETPP$, **86**) < 2,3,7,8,17,18-hexaethyl-5,10,15,20-tetraphenylporphyrin (H_2HETPP, **87**) < H_2OETPP (**74**) because the central N–H donors are severely forced out-of-plane as β-substitution increases (Figures 21B and 44). With their structural landscape established and in light of the promising organocatalytic activity of **74**, the aim was to study the effects of out-of-plane conformations on binding properties and catalytic activation more in-depth.[200,201] In order to obtain a better understanding and additional proof for the likely bifunctional mode of activation, a case study was designed where conversion was correlated with the stepwise accessibility of both Lewis acidic amine and Lewis basic imine moieties. That is because an understanding of these correlations will ultimately allow design of porphyrins that surpass the performance of standard bases due to their greater tunability and superior potential for functionalization.

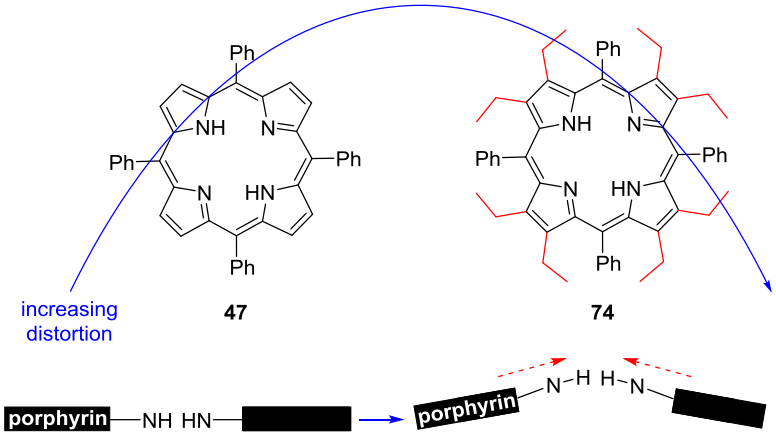

Figure 44. H_2Et_xTPPs **47** and **74:** incrementally increasing nonplanarity due to substituent effects.[132]

In a few words, the structural assessment of all H_2Et_xTPPs **47**, **74**, and **84**–**87** points at an inner core system (*i.e*. N/N–H groups) that becomes more and more exposed to the sphere of the porphyrin as one progresses from **47** to **74**.[132] This was proven by a structural evaluation (*e.g*., Δ24 values, pyrrole tilts) and also indicated through diagnostic spectroscopic parameters (*e.g*., bathochromic shifts of the Soret and Q bands of the electronic absorption spectra,[122] deshielded N–H protons as seen in ^{1}H NMR spectra) (Table 7).

Table 7. Selected structural and spectroscopic parameters of H_2Et_xTPPs **47**, **74**, and **84**–**87**.[132]

entry	catalyst	Δ24, Å[a]	av. pyrrole tilt, deg.	λ_{max}, nm[b]	δ, ppm[c]
1	**47**[177]	0.05	4.0	417	−2.77
2	**84**	0.10	4.3	420	−3.04/−2.45
3	**85**	0.29	15.0	426	−2.60
4	**86**	0.38	20.4	433	−2.38
5	**87**	0.46	24.0	444	−2.23
6	**74**[120b]	0.54	31.2	456	−2.04

[a] Average deviation from the 24-atom mean-plane. [b] Soret absorption band in DCM (+ 1% TEA). [c] ^{1}H NMR chemical shifts of the inner core protons in $CDCl_3$.

Increasing Δ24 values and pyrrole tilts indicate that the potentially catalytically active N/N–H sites are displaced above and below the mean-plane, respectively, and tilted so that the N–H donors point out of the macrocycle. At the same time, drastic red-shifts of the Soret and Q bands of the absorption spectra along with increasing chemical shifts serve as a measure of severe macrocyclic distortion in solution. This formally resembles a stepwise molecular reshaping process and is a prerequisite for the ability to activate reaction components, as exemplified by **74** in Chapter 3.2. However, taking the complete library **47**, **74**, and **84**–**87** into account allowed to trace the process of inducing catalytic activity into the tetrapyrroles end-to-end. Herein, by closing the gap between **47** (inactive)

and **74** (highly active), it became possible to seamlessly proof the key role of nonplanar conformations in organocatalysis.

Reviewing the sulfa-Michael reaction of **123** and **132** from the initial studies on catalytically active distorted porphyrins (see Table 4), it was assumed that this system may also prove to be susceptible to activation by **84**–**87**. And indeed, comparative screening of tetrapyrroles **47**, **74**, and **84**–**87** under standard conditions revealed a close correlation between conversion and distortion (Table 8).

Table 8. Results of the catalytic screening of H_2Et_xTPPs **47**, **74**, and **84**–**87**, using **123** and **132** as substrates.[a,b,c]

entry	catalyst	conv., %
1	**47**	0[d]
2	**84**	0
3	**85**	3
4	**86**	51
5	**87**	97 (8[e])
6	**74**	quant.[d] (80[e])

[a] See Experimental for a general procedure. [b] Conversions were determined by ^{1}H NMR spectroscopy using dibromomethane as internal standard. [c] [cat.] = $7.1 \cdot 10^{-2}$ M if not otherwise stated [d] Data from Table 4. [e] [cat.] = $3.6 \cdot 10^{-3}$ M.

Almost planar H_2TPP (**47**) and H_2DETPP (**84**) failed to promote the reaction (entries 1 and 2). When H_2*t*TETPP (**85**) was applied, which has a noticeable degree of saddle distortion, catalytic activation started to become measurable, resulting in 3% conversion (entry 3). While having the same number of β-ethyl groups, the pyrrole units in H_2*c*TETPP (**86**) point significantly more out of the mean-plane than in **85**, which gave 51% product (entry 4). Initial screening of H_2HETPP (**87**) and **74** under these conditions showed almost identical, nearly quantitative conversions (entries 5 and 6). In order to distinguish the competence of **87** *vs*. **74**, diluted standard conditions were applied. As expected, it was now possible to discriminate their activity, as significantly different conversions of 8% and 80% became evident for **87** and the most distorted species **74**, respectively (entries 5 and

6). The outcome of this comparative screening is clearly in favor of the initial hypothesis: as distortion increases, the inner core system becomes more available to activate substrates. Based on the previous proposal, this may be ascribed to an escalating propensity of the more nonplanar macrocycles to form hydrogen bonds with **132** and to deprotonate **123**, as illustrated in Figure 37.

The availability of the inner core N/N–H entities for intermolecular contacts in nonplanar porphyrins is certainly a result of the induction of an out-of-plane vector. However, while this correlation is rather coherent, it was also of interest to monitor how saddle distortion and formal β-ethylation would affect their electronic properties. As such, the aim was to analyze whether enhanced imine basicity and amine acidity in the order **47**→**74** would be mirrored by trends in the charge densities assigned to the N/N–H functional groups.

In order to gather insight into the compounds' electronic properties, DFT calculations were performed on **47**, **74**, and **84**–**87** by Dr. N. Grover using a B3LYP functional and a 6-31G(d,p) basis set (see Experimental).[202] Coordinates for geometry optimizations were taken from previously known crystal structures (CCDC:[58c] PHPOR10 (**47**),[177] TATPOT01 (**84**),[132] TATPUZ01 (**85**),[132] TATQAG01 (**86**),[132] TATQEK01 (**87**),[132] and SATQOU (**74**)[120b]). Figure 45 compiles the calculated Mulliken charges assigned to the $N^{a/b}$/N–$H^{a/b}$ atoms of these porphyrins in detail and it was found that the charge densities at the inner core amine and imine moieties varied only slightly depending on the number of peripheral ethyl groups. For better comparison, the individual values for $N^{a/b}$ and N–$H^{a/b}$ were also averaged.

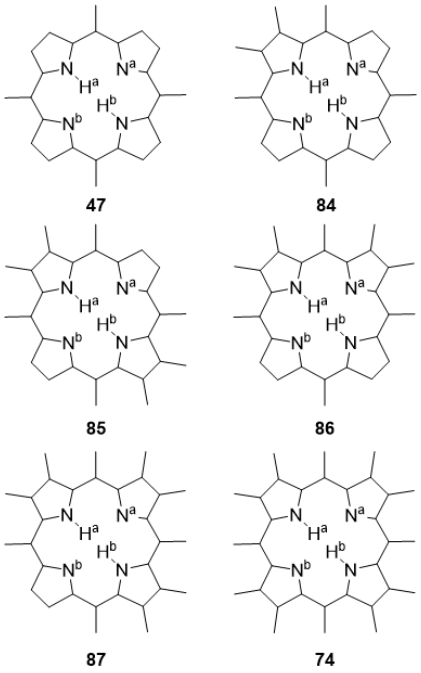

catalyst	N–H^{a}	N–H^{b}	av.	N^{a}	N^{b}	av.
47	0.402	0.402	0.402	−0.565	−0.565	−0.565
84	0.399	0.403	0.401	−0.563	−0.561	−0.562
85	0.394	0.394	0.394	−0.552	−0.552	−0.552
86	0.381	0.394	0.388	−0.544	−0.559	−0.552
87	0.384	0.385	0.385	−0.537	−0.557	−0.547
74	0.374	0.375	0.375	−0.537	−0.537	−0.537

Figure 45. Calculated charge densities assigned to the N$^{a/b}$/N–H$^{a/b}$ atoms of porphyrins **47**, **74**, and **84**–**87**.

Two trends became evident upon incremental β-ethyl substitution: (1) decreasing charge densities at the amine hydrogen atoms and (2) increasing charge densities at the imine moieties. For example, the average partial positive charges of inner core N–H$^{a/b}$ hydrogen atoms in **74** are lower than in **47** (0.374 *vs*. 0.402). In contrast, **47** has a more pronounced average partial negative charge at the core imine functions than **74** (−0.565 *vs*. −0.537). Therefore, an isolated assessment of only these electronic parameters would in principal suggest that **47** should have more favorable acid/base properties than **74**. However, in general, there are two main aspects to the catalytic activity of nonplanar porphyrins: a steric factor (tied to the core accessibility to substrates) and an electronic factor (tied to the acid/base properties of the inner core system). Catalytic screening revealed

that *de facto*, **74** exhibits the best performance (entry 6, Table 8). As such, the charge densities provided by the DFT model fail to mirror the trends observed in catalytic activity. One reason might be that the changes in partial charges are rather small. Hence, they may simply be outperformed by the increasing core availability. This would suggest that in the H_2Et_xTPP series, a nonplanar geometry may be of more significance than favorable electronic properties of the N/N–H atoms. However, it was previously shown that electron rich macrocycles are better organocatalysts than electron deficient species (see Chapter 3.2). Again, this shows that differentiating the influence of steric and electronic factors in nonplanar porphyrins is nontrivial and both cannot be treated as separate entities.[203] Moreover, additional factors may contribute to the observed changes in partial charges of the inner core, such as destabilization of the aromatic system due to macrocyclic deviation from an ideal planar shape. As a consequence, the results of the DFT calculations appear to be unable to reflect all aspects that contribute to an increased organocatalytic activity. One issue that remains is the difficulty of finding porphyrin compounds that have the same conformation but clearly differentiated electronic structures or *vice versa*.

3.4 Investigations on the Reaction of 2,3,7,8,12,13,17,18-Octaethyl-5,10,15,20-tetranitroporphyrin with Nucleophilic Thiols

The crystallographic data presented in this chapter was collected and solved by Dr. K. J. Flanagan. Dr. K. J. Flanagan also performed the NSD calculations for this chapter.

Substitutions involving sulfur nucleophiles usually require a number of prerequisites, such as activating groups, high temperatures, or metal catalysts.[204] As a result, catalyst-free S_NAr reactions at the meso-positions of tetrapyrroles are scarce,[118c,156,157,163,166,205] but it was briefly reported that thiolate anions substitute nitro groups on porphyrins[206] and recently, sulfur-linked porphyrin dimers involving S_NAr reactions of porphyrin thiolates under mild conditions where seemingly unactivated systems gave excellent yields, were reported.[166] This appears to be in accordance with the transformations

observed when compound **95** was reacted with 4-bromobenzenethiol (**122**/**HSAr^1**) during catalyst screenings (entry 1, Table 1). As such, it was aimed to investigate and exploit this unusual reactivity with the ultimate goal to synthesize a family of porphyrin thioethers carrying a high number of meso-arylthio substituents as a new class of highly substituted porphyrins. These compounds might be suitable for biological and medicinal applications due to the presence of sulfur,[207] applicable as SAMs on gold surfaces,[208] or even as nonplanar organocatalysts and sensors (*vide supra*). Note, that interest in such systems is now expanding to other porphyrinoids as well.[209]

3.4.1 Synthesis of Highly Substituted Porphyrin Thioethers

To establish a standard protocol for the synthesis of highly substituted arylthioporphyrins from the parent compound **95** and to generate a library of such molecules, the reactivity of a large number of aromatic thiolates was investigated. Initial screening experiments were performed with 4-bromobenzenethiol (**HSAr^1**). Thus, when compound **95** was reacted with an excess of **HSAr^1** in boiling chloroform in the absence of a base, the products **188**–**191** were formed (Figure 46). Presumably, the thiolate needed for the reaction originated from a thiol–thiolate equilibrium in solution.

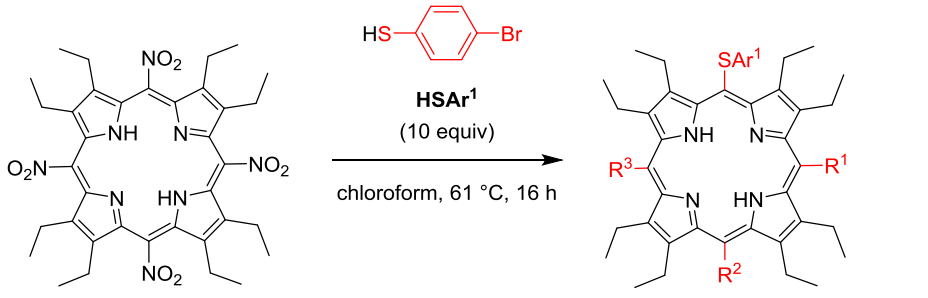

Figure 46. Reaction of **95** with **HSAr^1** in the absence of a base. [a] An inseparable 3:2 mixture of compounds **190** and **191** was isolated.

Next, screening of a range of thiolate nucleophiles was conducted and the use of TEA for thiol deprotonation allowed for shorter reaction times and

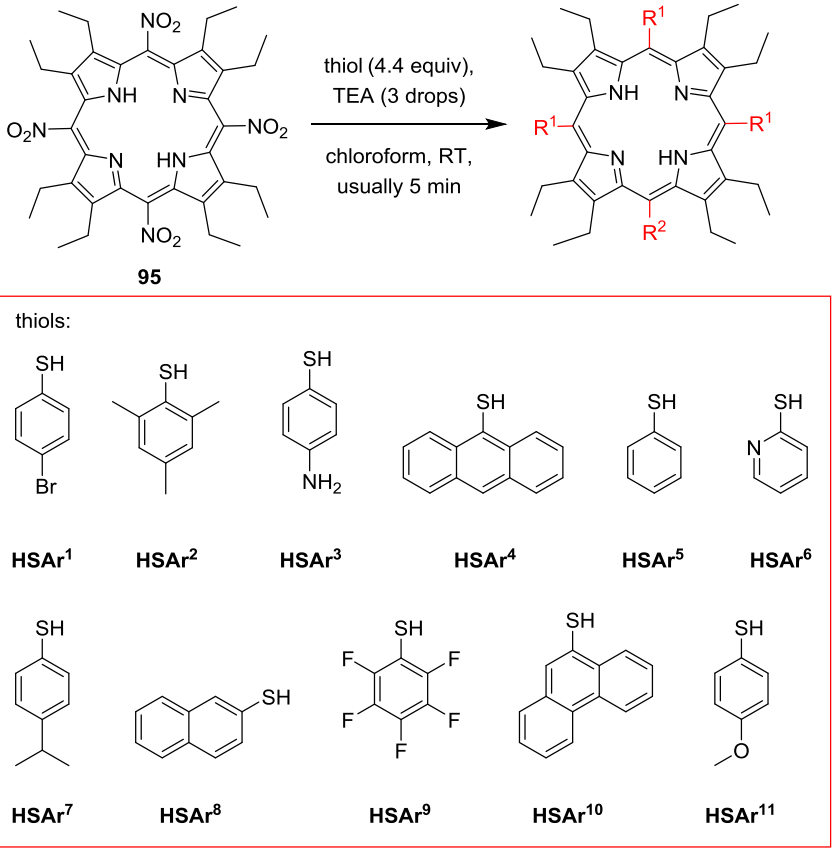

entry	R^1	R^2	product	yield, %
1	SAr^1	SAr^1	**188**	73
2	SAr^2	H	**192**	40
3[a]	SAr^3	H	**193**	40
4[b]	SAr^4	H	**194**	35
5	SAr^5	SAr^5	**195**	86
6	SAr^6	SAr^6	**196**	65
7	SAr^7	SAr^7	**197**	63
8	SAr^8	SAr^8	**198**	46
9	SAr^9	SAr^9	**199**	43
10	SAr^{10}	SAr^{10}	**200**	17
11	SAr^{11}	H	**201**	< 5[c]
12	SAr^{11}	SAr^{11}	**202**	< 5[c]

Figure 47. S_NAr on **95** using nucleophilic sulfur substrates **$HSAr^1$–$HSAr^{11}$**. [a] 7.8 equiv of **$HSAr^3$** were used. [b] 8.8 equiv of **$HSAr^4$** were used. [c] Obtained as a mixture of **201** and **202** and identified by HRMS only due to the small amount of material obtained.

lower temperatures, with most reactions being complete within minutes (Figure 47). Furthermore, the number of equivalents of thiol used could be reduced in many cases. A good example is the synthesis of porphyrin **188**: While the dodecasubstituted product was formed in 52% yield along with 30% of the undecasubstituted porphyrin **189** in the absence of a base under harsh conditions (Figure 46), the same product was obtained in 73% yield under basic conditions along with less than 10% of **189**.

A series of follow-up experiments, in which **95** and **HSAr^{1}** were reacted in the presence of varying amounts of TEA revealed that rapid (< 5 min) and complete conversion of the porphyrin was achieved once a threshold of 50 mol% TEA (relative to the thiol) was reached (see Appendix, Table A1). Hence, three drops of TEA (*ca*. 0.27 mmol) were used in each substitution reaction from that point for synthetic ease.

Subsequent conversions of **95** with a number of electron deficient and electron rich aromatic thiols (**HSAr^{2}**–**HSAr^{11}**) resulted in the formation of the highly substituted products **192**–**202** with yields of up to 86% for the phenylthio-substituted species **195** (Figure 47) and an addition–elimination mechanism, in which a Jackson–Meisenheimer complex is formed is proposed.[162–164] In order to optimize the outcome of each reaction, the number of equivalents of thiol used and reaction time had to be increased in some cases. Formation of the compounds **189**–**194** and **201** revealed the ambivalence of some thiolates to both substitute and reduce the meso-positions in nitroporphyrin **95**: differences in the reactivity and probably steric demand of the sulfur reagents determined that in some cases only the triarylthio-substituted product was isolated.

To study the effects of the central metal, nickel complex **203** was reacted with **HSAr^{6}** in a test reaction (Figure 48). As a result, **204** and **205** were obtained as products from the same reaction along with unreacted starting material. Interestingly, substitution was less prominent compared to the free base and denitration prevailed. Electrochemical data suggest that Ni(II)porphyrins are generally more difficult to reduce[171,210] and better electrophiles.[165] Remarkably, the unsymmetric undecasubstituted tetrapyrrole **205** was formed in only one step from **203** *via*

desymmetrization.[211]

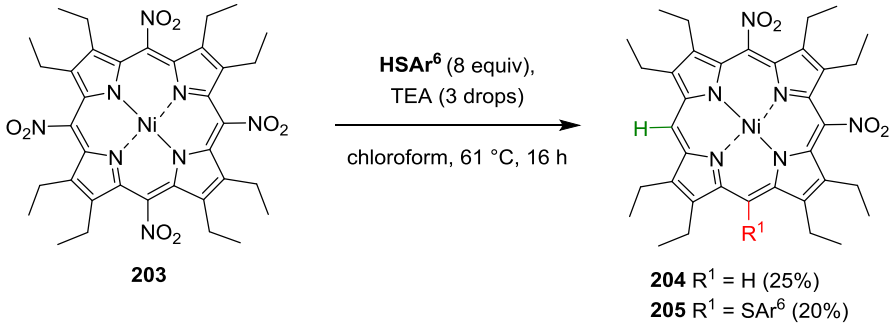

Figure 48. Reaction of Ni(II)porphyrin **203** with 2-mercaptopyridine (**HSAr^6**).

3.4.2 Stepwise Denitration of 2,3,7,8,12,13,17,18-Octaethyl-5,10,15,20-tetranitro-porphyrin

The frequent formation of desubstituted meso-positions in a number of reactions under involvement of the organosulfur reagents was investigated further during attempts to substitute **95** with the thiols **HSA^1**–**HSA^3** (Figure 49). Rather than substitution, a tendency towards desubstitution was observed and conditions for stepwise reduction were elaborated and optimized. In order to access the individual denitration products in good yields, it was necessary to increase the number of equivalents of thiol used and in the case of **HSAr^2** and **HSA^3**, the temperature. Treatment of **95** with 1,2-ethanedithiol (**HSA^1**) at room temperature gave dinitroporphyrins **206** and **207** and longer reaction times lead to an increased formation of **208** and eventually traces of **48** while the reaction using 2-mercaptoethanol (**HSA^2**) in boiling DCM resulted in the formation of mononitroporphyrin **208** as the main product with traces of **48** being formed at longer reaction times. Ultimately, **95** was reduced to **48** in the presence of **HAS^3**. Since formation of **48** occurred slowly as opposed to **206**–**208**, the reaction time had to be increased significantly. Despite all effort, such as decreasing the number of equivalents of thiolate used to one or less, no trinitro-substituted product **209** was observed, presumably due to immediate additional denitration steps once the species is formed. Instead of **209**, mostly unreacted starting

material along with small amounts of **206** and **207** were typically observed and further comparative studies on thiol reactivity were disregarded at this point.

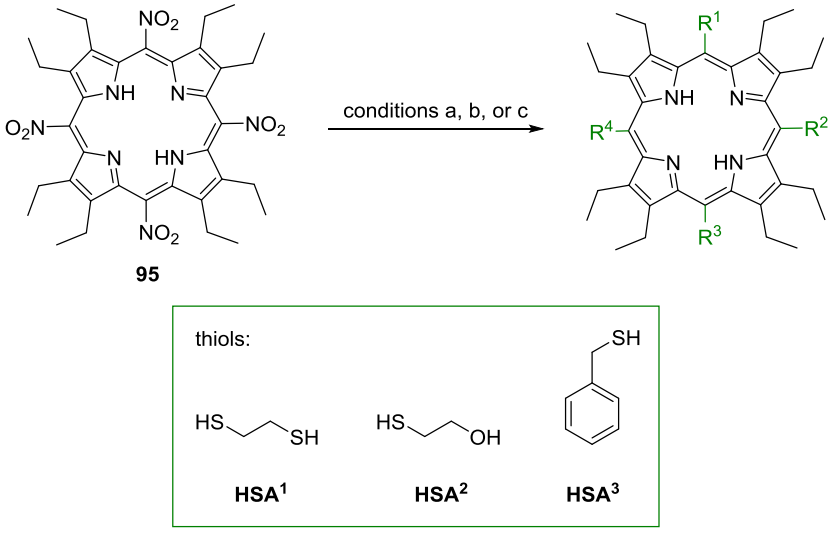

entry	R^1	R^2	R^3	R^4	product	yield, %
1[a]	NO_2	H	H	NO_2	**206**	24
2[a]	NO_2	H	NO_2	H	**207**	21
3[b]	NO_2	H	H	H	**208**	49
4[c]	H	H	H	H	**48**	49
5	NO_2	NO_2	NO_2	H	**209**	-

Figure 49. Denitration of **95** with thiols **HSA^1–HSA^3**. [a] Conditions a: **HSA^1** (7 equiv), TEA (3 drops), chloroform, RT, 40 min. [b] Conditions b: **HSA^2** (12 equiv), TEA (3 drops), DCM, 40 °C, 15 min. [c] Conditions c: **HSA^3** (41 equiv), TEA (0.1 mL), DCM, 40 °C, 72 h.

These reactions proceeded rapidly, presumably due to the lower oxidation potential of alkyl thiols compared to aromatic thiols, which facilitated the reduction of **95** to an extent that no substitution products could be isolated, even though alkyl thiolates are more nucleophilic. Note, that **206**–**208** are potential precursors for the preparation of nonplanar porphyrins with mixed substituents, which could be of relevance for fundamental studies on the conformational flexibility of porphyrins. It was also considered that in these cases, the basicity of TEA was insufficient to effectively deprotonate the sulfur reagents and initial studies on the reaction of **95** with **HSA^1**–**HSA^3** utilizing DBU and KO*t*-Bu were conducted. However, these attempts were

discontinued due to the formation of complex mixtures of inseparable products, potentially resulting from breakdown of the macrocycle.

A comparison of the substitution and denitration reactions indicates that both pathways are two independent reactions that contribute to the overall outcome of a conversion of **95** and a thiolate. The tendency to undergo either substitution or reductive desubstitution strongly depends on the reactivity of the sulfur reagents and how fast S_NAr proceeds compared to the competing reduction process.

Significant formation of denitration products in the presence of **HSA^1**–**HSA^3** was only observed upon addition of TEA as indicated by TLC analysis. In comparison, almost no conversion was noted after several hours in the absence of TEA, which suggests a process initiated by thiolate. Furthermore, substantial disulfide formation was occurring, too. Therefore, a mechanism in accordance with initial studies by Crossley, Gosper, and Wilson,[212] which includes single electron transfer (SET) from thiolate to porphyrin **210** may be proposed (Figure 50). The delocalized radical anion **211** is reduced in a sequence of elimination of nitrite to give radical **212** and abstraction of a hydrogen radical from yet unreacted thiol so that product **213** is formed. Simultaneously, thiyl radical recombination yields the corresponding disulfide. However, more in-depth investigations of the mechanism will have to be progressed.

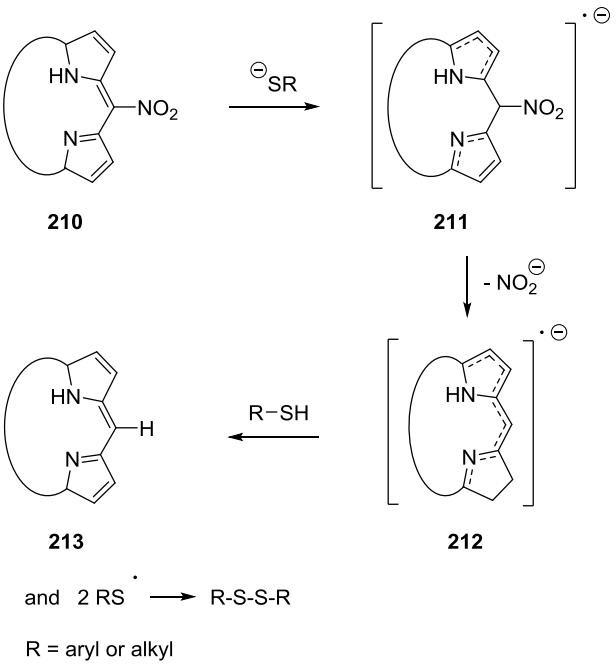

Figure 50. Proposed mechanism of the reduction of a nitroporphyrin **210** in the presence of thiolate and a base.

3.4.3 Crystallographic Studies

Highly Substituted Porphyrin Thioethers. The meso-thioether-substituted porphyrins described above are representatives of a new class of highly substituted tetrapyrroles. Historically, these are defined as porphyrins where *peri*-interactions of peripheral substituents result in steric strain and consequently nonplanar macrocycle conformations (*vide supra*). Single crystals suitable for X-ray crystallography were obtained for several of said dodecasubstituted tetrapyrroles, which allowed for a thorough analysis of their conformational features. Likewise, crystallography confirmed formation of the 5,10,15,20-tetrasubstituted compounds **188**, **195**, and **196** (Figure 51).

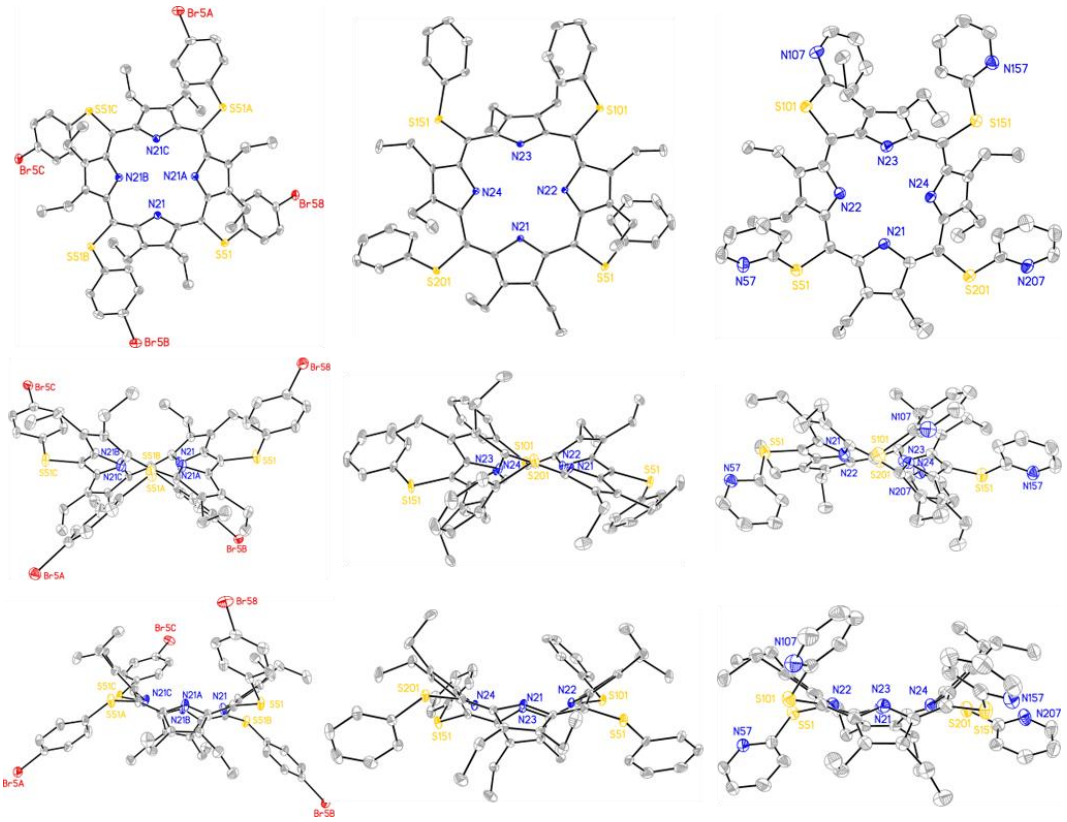

Figure 51. Top and two side views of the crystal structures of **188** (left), **195** (middle), and **196** (right). Hydrogen atoms and minor disorder have been omitted for clarity. Thermal ellipsoids indicate 50% probability.

Each of these macrocycles had a high degree of nonplanarity with almost exclusive saddle distortion. Table 9 provides a comparison of the geometry of these thioethers with the archetypical dodecasubsituted porphyrins **74**[120b] and **64**,[119] meso-oxygen-substituted tetrapyrrole **214**,[213] and the planar porphyrins **48**[161] and **47**.[177]

The deviations of macrocyclic atoms from the 24-atom mean-plane of the meso-arylthio-substituted representatives range between 0.78–0.79 Å and are comparable to **74** and **64** (0.71 and 0.62 Å). As seen from a normal structural decomposition (NSD) analysis,[36b,214] compounds **188**, **195**, and **196** show typical high saddle distortion (B_{2u} mode), a feature not shared with the planar counterparts **47** and **48** (Figure 52).

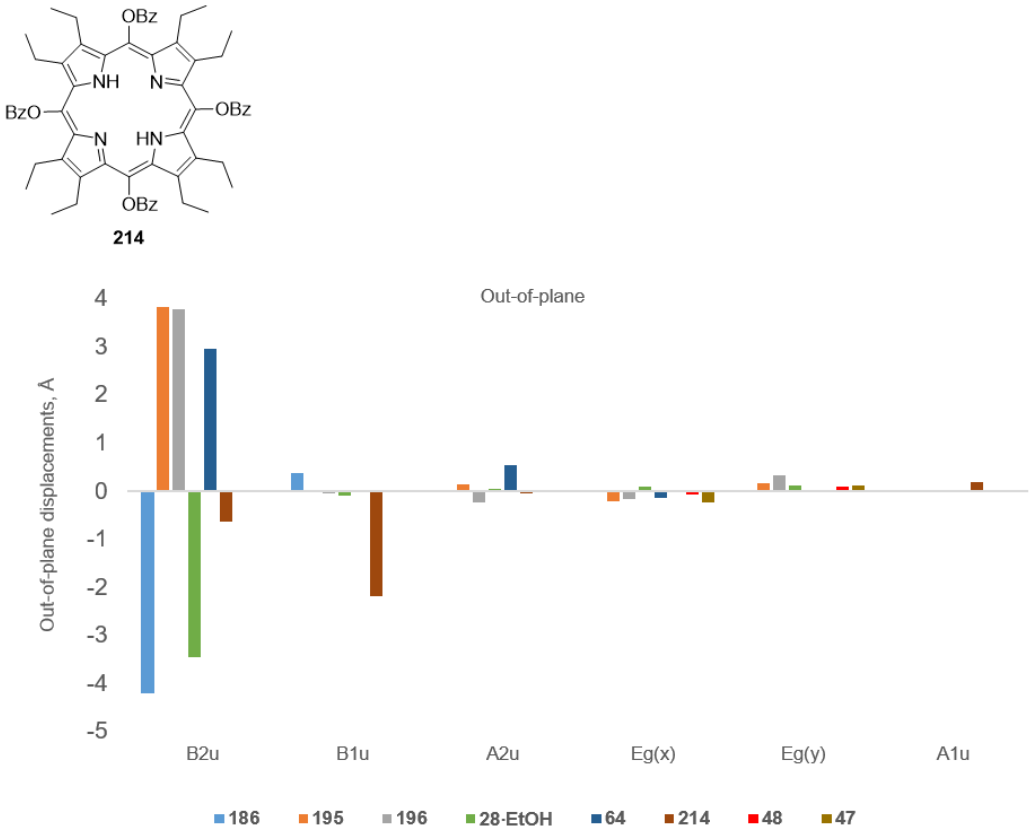

Figure 52. NSD analysis of the crystal structures of **188**, **195**, and **196** and comparative tetrapyrrole examples.

The overall simulated total in-plane distortion and total out-of-plane distortion (Δ_{ip} and Δ_{oop}) of **188**, **195**, and **196** are significantly larger than for compounds **47**, **48**, **64**, **74**, and **214**. There is an overall increase in the deviation of both the C_α and C_β atoms from the 24-atom mean-plane. Most notably, **186** shows the largest ΔC_α and ΔC_β values as well as average ΔC_m, $\Delta 24$, and ΔN values with only a small decrease in core size as compared to most of the other tetrapyrroles listed in Table 9. At the same time, the pyrrole tilts of compounds **186**, **195**, and **196** indicate much larger deviations from the 24-atom mean-plane (34.9–39.3°) when compared to **74** and **64** (30.5 and 22.1°, respectively). This seems to be a direct result of the multifold meso-arylthio substitution. The sulfur atom forces the meso-substituent out-of-plane by a C_m–S–R angle of 103.6–104.8° and previously studied meso-sulfur-substituted porphyrins exhibit comparable C_m–S–R angles of 102–

104.8°.[166,215] Note, that no correlation was observed in the degree of pyrrole tilt *vs*. C_m–S–R angles. Compound **186** features the highest pyrrole tilt of 39.3°; however, it also contains the smallest C_m–S–R angles at 103.6°. This increase in pyrrole tilt is most likely due to a heavy atom effect of the bromine atom present in its molecular structure. When compared to **214**, the C_m–O–R angle of 114.8° is larger than the C_m–S–R angle in compounds **188**, **195**, and **196**. The pyrrole tilts in tetrapyrrole **214** (25.7°) are characterized by a deviation from the 24-atom mean-plane that is similar to those in the macrocycles **74** and **64** but much smaller than in **188**, **195**, and **196**. There is a significant decrease of the pyrrole tilts in the planar species **48** and **47** (1.6 and 4.0°) when compared to tetrapyrroles **188**, **195**, and **196**. Overall, there are only small differences in the N–C_α–C_β, C_α–N–C_α, C_α–C_β–C_α, and C_α–C_β–C_β angles of the new porphyrin thioethers **188**, **195**, and **196** if compared to those of the dodecasubstituted porphyrins **74** and **64**. On the other hand, the N–C_α–C_m angles shows a decreased size of 119.9–120.6° for **188**, **195**, and **196** as compared to 122.5 and 124.1° for **74** and **64** while the C_m–C_α–C_β angles display a minor increase of 130.3–130.9° compared to 129.0 and 127.1°, respectively. In conclusion, the macrocycles **188**, **195**, and **196** have traits similar to archetypical dodecasubstituted tetrapyrroles, such as **74** and **64** with regard to distortion mode, pyrrole tilt, atom deviations from the 24-atom mean-plane, N–C_a–C_b angles, and N–C_a bond lengths. However, specific features are clearly reminiscent of previously studied sulfur porphyrins, such as the C_m–S–R angles.

Table 9. Averaged geometrical parameters for bond lengths and angles, core conformations, and atom displacements of **186**, **195**, and **196** as well as comparative tetrapyrrole examples.

	186	**195**	**196**	**74**·EtOH[120b]	**64**[119]	**214**[213]	**48**[161]	**47**[177]
bond lengths, Å								
N–C_α	1.364(4)	1.368(3)	1.370(7)	1.369	1.366	1.369	1.366	1.369
C_α–C_β	1.447(4)	1.453(3)	1.453(7)	1.457	1.457	1.444	1.450	1.442
C_α–C_m	1.413(4)	1.411(3)	1.411(7)	1.411	1.412	1.364	1.392	1.399
C_β–C_β	1.381(5)	1.371(3)	1.375(7)	1.367	1.387	1.354	1.363	1.351
bond angles, deg.								
N–C_α–C_m	119.9(3)	120.6(2)	120.6(5)	122.5	124.1	121.2	125.0	126.2
N–C_α–C_β	108.9(3)	108.8(2)	108.7(4)	108.26	108.7	110.1	109.3	108.8
C_α–N–C_α	108.4(3)	108.2(2)	108.5(4)	108.84	109.0	106.1	107.7	107.7
C_α–C_m–C_α	123.1(3)	124.1(2)	124.2(5)	124.0	123.0	125.9	127.6	125.6
C_α–C_β–C_β	106.6(3)	106.9(2)	106.9(5)	107.1	106.8	106.8	106.9	107.5
C_m–C_α–C_β	130.9(3)	130.3(2)	130.3(5)	129.0	127.1	127.9	125.7	125.1
C_m–S/O–C_{Ph}	103.6(2)	103.8(1)	104.3(3)	-	-	114.8	-	-
pyrrole tilt	39.3(9)	34.9(6)	34.7(9)	30.5	22.1	25.7	1.634	4.032
further parameters, Å								
Δ_{ip}[a]	1.01	0.74	0.79	0.52	0.68	0.65	0.23	0.20
Δ_{oop}[b]	4.23	3.83	3.80	3.46	3.01	2.29	0.11	0.26
core size[c]	2.90	2.92	2.93	2.91	2.91	2.67	2.92	2.92
Δ24[d]	0.78	0.79	0.78	0.71	0.62	0.47	0.03	0.07
ΔN[e]	0.05	0.06	0.07	0.07	0.14	0.01	0.03	0.09

Table 9 (continued)

ΔC_m[f]	0.15	0.20	0.10	0.04	0.07	0.79	0.02	0.03
ΔC_α[g]	0.52	0.46	0.46	0.42	0.36	0.46	0.01	0.03
ΔC_β[h]	1.41	1.26	1.27	1.16	0.99	0.39	0.03	0.06

[a] Simulated total in-plane distortion. [b] Simulated total out-of-plane distortion. [c] Average distance between adjacent pyrrole nitrogen atoms. [d] Average deviation from the 24-atom mean-plane. [e] Simulated displacement of the four internal nitrogen atoms from the 24-atom mean-plane. [f] Average deviation of the meso-carbon atoms from the 24-atom mean-plane. [g] Average deviation of the α-carbon atoms from the 24-atom mean-plane. [h] Average deviation of the β-carbon atoms from the 24-atom mean-plane.

meso-Nitro-substituted Octaethylporphyrins (OEPs). The denitration reactions described above gave access to several meso-nitro-substituted OEPs **206**–**208**, which, together with **209** and structures available from the literature,[158a–c] allowed for a comparative analysis of the structural features of OEPs having different numbers and arrangements of meso-nitro units. Previous studies featuring meso-nitro and β-nitro substituents include, for example, Barkigia *et al.*'s study on iron(III) porphyrin complexes with various degrees of distortion.[216] Furthermore, the structure of 7-nitro-5,10,15,20-tetraphenylporphyrin has been shown to exhibit an almost planar geometry.[217] However, there is currently no example of a comparative structural study focusing on the effects of a varying degrees and spatial arrangements of meso-nitro substitution.

Comparison of the saddle distortion of the meso-nitro-OEPs **206**–**209** and **95** with **48** reveals that the latter has no visible nonplanarity while **208** shows only a small deformation that indicates minor saddling (Figure 53).

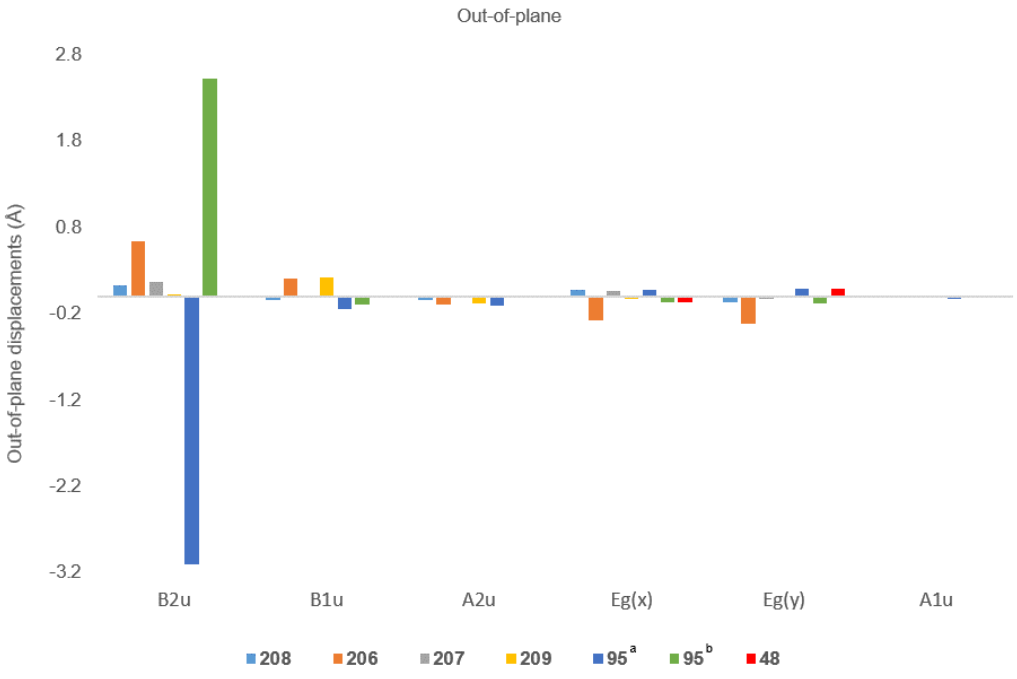

Figure 53. NSD analysis of the crystal structures of meso-nitro-OEPs **206**–**209** and **95** as well as **48** for comparison.[158a–c] [a] Data collection at 283–303 K. [b] Data collection at 130 K.

However, a notable increase in the B_{2u} mode of compound **206** suggests

that multifold nitro substitution results in increased distortion. When this is compared to its regioisomer **207**, the influence of the spatial distribution of the nitro groups proves to be of importance, as a 'flattening' of the porphyrin ring is noted. Compound **209** displays the most notable change as there is no more contribution to the B_{2u} mode, with the largest contribution being in the ruffled distortion mode (B_{1u}) instead. Ultimately, it can be seen that compound **95**, carrying four nitro moieties, shows the largest contribution to the B_{2u} mode, again suggesting that higher meso-nitro substitution distorts the porphyrin ring to a large degree. This is clearly shown in Figure 54 where compound **206** has a larger visual deformation than **207** and **209**, which are notably more planar.

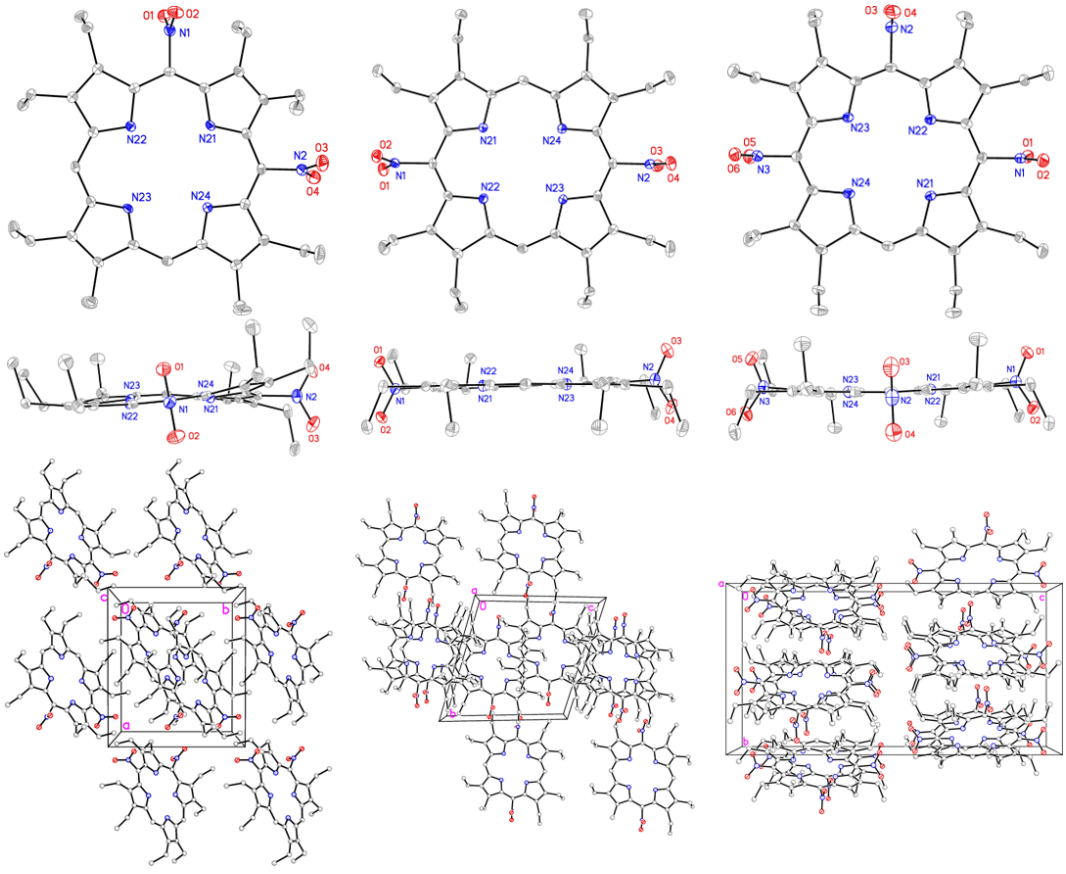

Figure 54. Top, side and crystal lattice views of the crystal structures of **206** (left), **207** (middle), and **209** (right). Hydrogen atoms have been omitted for clarity. Thermal ellipsoids indicate 50% probability.

Table 10 provides a comparison of the geometry of nitroporphyrins **206**–**209** and **95** with the virtually planar macrocycle **48**.

Table 10. Averaged geometrical parameters for bond lengths and angles, core conformations, and atom displacements of meso-nitro-OEPs **206**–**209** and **95** as well as **48** for comparison.

	208[158b]	**206**	**207**	**209**	**95**_1[a,158a]	**95**_2[b,158c]	**48**
bond lengths, Å							
N–C_α	1.364	1.366(5)	1.367(9)	1.368(3)	1.362	1.363	1.378(4)
C_α–C_β	1.449	1.454(5)	1.451(7)	1.456(3)	1.450	1.458	1.450(5)
C_α–C_m	1.396	1.394(5)	1.393(7)	1.394(3)	1.399	1.397	1.380(4)
C_β–C_β	1.364	1.365(5)	1.365(7)	1.366(3)	1.375	1.368	1.361(5)
bond angles, deg.							
N–C_α–C_m	124.2	123.6(2)	123.6(3)	123.0(2)	120.5	121.0	122.9(2)
N–C_α–C_β	109.7	109.5(2)	109.5(4)	109.5(2)	109.4	109.6	111.1(2)
C_α–N–C_α	107.3	107.5(3)	107.5(3)	107.5(2)	107.9	107.4	104.7(3)
C_α–C_m–C_α	128.8	129.5(2)	130.1(4)	131.5(2)	128.9	130.5	125.8(1)
C_α–C_β–C_β	106.7	106.7(2)	106.8(4)	106.8(2)	106.6	106.5	106.4(2)
C_m–C_α–C_β	126.1	126.8(1)	126.9(4)	127.5(2)	129.8	129.2	125.6(1)
pyrrole tilt	1.7	7.1(5)	1.7(9)	2.7(7)	25.5	20.5	17.3(8)
further parameters, Å							
Δ_{ip}[c]	0.34	0.30	0.50	0.46	0.39	0.13	0.23
Δ_{oop}[d]	0.17	0.80	0.19	0.24	3.11	2.52	0.11
core size[e]	2.93	2.94	2.94	2.95	2.91	2.93	2.75
Δ24[f]	0.04	0.16	0.04	0.05	0.64	0.52	0.31
ΔN[g]	0.02	0.07	0.01	0.03	0.10	0.08	0.02

Table 10 (continued)

ΔC_m[h]	0.03	0.11	0.02	0.08	0.05	0.03	0.53
ΔC_α[i]	0.02	0.09	0.02	0.04	0.40	0.32	0.31
ΔC_β[j]	0.04	0.21	0.06	0.03	1.02	0.83	0.22

[a] Data collection at 283–303 K. [b] Data collection at 130 K. [c] Simulated total in-plane distortion. [d] Simulated total out-of-plane distortion. [e] Average distance between adjacent pyrrole nitrogen atoms. [f] Average deviation from the 24-atom mean-plane. [g] Simulated displacement of the four internal nitrogen atoms from the 24-atom mean-plane. [h] Average deviation of the meso-carbon atoms from the 24-atom mean-plane. [i] Average deviation of the α-carbon atoms from the 24-atom mean-plane. [j] Average deviation of the β-carbon atoms from the 24-atom mean-plane.

Comparing the Δ_{oop} values of compounds **95** and **206**–**209** reveals that porphyrins **95** and **206** have the highest figures while their Δ_{ip} values are the smallest. Furthermore, there is a small but notable elongation of the N–C_α bond in the order **95**_1 < **95**_2 < **208** < **206** < **207** < **209**. The C_β–C_β and C_α–C_β bonds both show moderate increase in length in the orders **208** < **206** = **207** < **209** < **95**_2 < **95**_1 and **208** < **95**_1 < **207** < **206** < **209** < **95**_2, respectively while the C_α–C_m bond elongates in the sequence **207** < **206** = **209** < **208** < **95**_2 < **95**_1. Analysis of the bond angles reveals a set of similar trends: While the N–C_α–C_β, C_α–N–C_α, and C_α–C_β–C_β angles undergo only small changes, the N–C_α–C_m angles show an overall increase of about 4° in the order **95**_1 < **95**_2 < **209** < **206** = **207** < **208**. The C_α–C_m–C_α bond angles ascend in the sequence **208** < **95**_1 < **206** < **207** < **95**_2 < **209** and the C_m–C_α–C_β angles show an increase of **208** < **206** < **207** < **209** < **95**_2 < **95**_1, with the pyrrole tilts rising in the order **207** = **208** < **209** < **206** < **95**_2 < **95**_1. This trend is similar to the ones found in the Δ24 and ΔC_α values. However, ΔN, ΔC_m, and ΔC_β values increase in the successions **207** < **208** < **209** < **206** < **95**_2 < **95**_1, **207** < **208** = **95**_2 < **95**_1 < **209** < **206**, and **209** < **208** < **207** < **206** < **95**_2 < **95**_1, respectively. Ultimately, the core size shows a slight elongation of **95**_1 < **208** = **95**_2 < **206** = **207**< **209**. In conclusion, the macrocyclic distortion and the corresponding geometries of meso-nitro-OEPs significantly depend on the extent and pattern of nitro substitution. As such, (meso-)nitro introduction may be seen as a versatile tool to induce specific conformations in tetrapyrroles for future use in a molecular engineering context.

Previous studies on nitro-substituted OEP metal complexes have elucidated the structures of several examples of pentacoordinated iron(III) porphyrins (Figure 55).

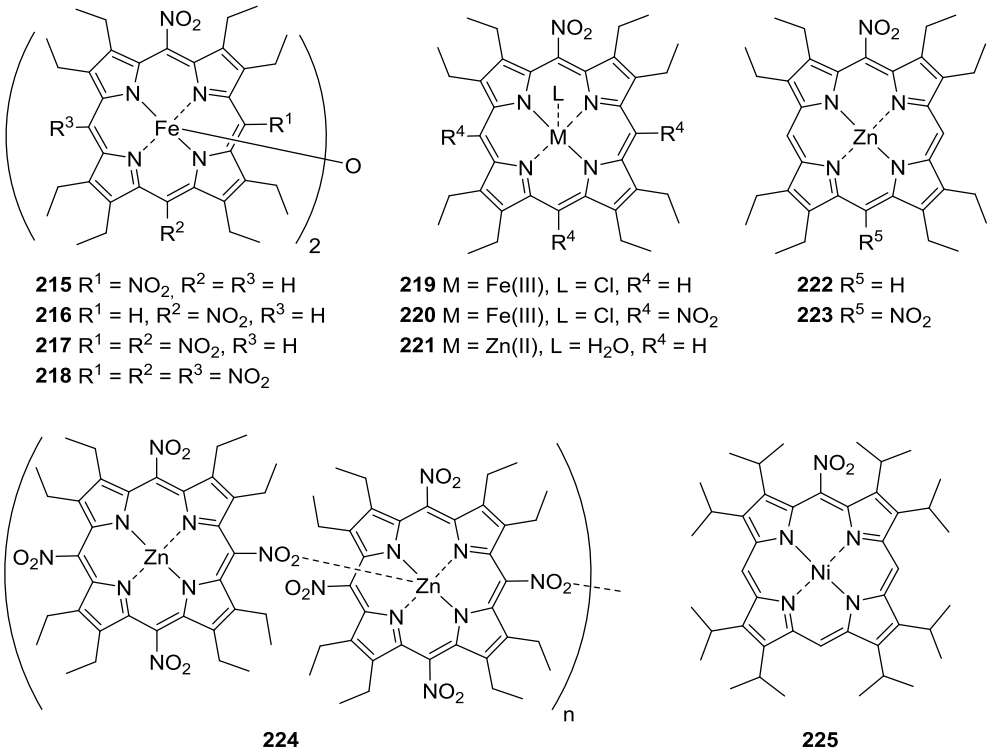

215 $R^1 = NO_2$, $R^2 = R^3 = H$
216 $R^1 = H$, $R^2 = NO_2$, $R^3 = H$
217 $R^1 = R^2 = NO_2$, $R^3 = H$
218 $R^1 = R^2 = R^3 = NO_2$

219 M = Fe(III), L = Cl, $R^4 = H$
220 M = Fe(III), L = Cl, $R^4 = NO_2$
221 M = Zn(II), L = H_2O, $R^4 = H$

222 $R^5 = H$
223 $R^5 = NO_2$

224 **225**

Figure 55. Selection of previously studied nitro-substituted porphyrin complexes with reported crystal structures.

Fe(III) porphyrin **219**[218] exhibits similar displacements as the corresponding free base **208** (see Table 10) with the Fe(III) center located above the 24-atom mean-plane. Complexes **215**,[158g] **216**,[219] **217**,[158g] and **218**[158g] have been reported as planar dimers with both rings joined by metal–oxo bridges. Tetrapyrrole **220**[220] shows a significant saddle distortion similar to its free base counterpart **95** (see Table 10).[158a,c] Additionally, the structures of several tetra- and pentacoordinated Zn(II) complexes have been determined. Compounds **221**,[158b] **222**,[158b] and **223**[158a] are planar, similar to the corresponding free bases **206** and **207** (see Table 10). Interestingly, the structure of **224**[158d] demonstrates to be polymeric with highly disordered porphyrin moieties bending and rotating to accommodate a nitro group, which coordinates to the Zn(II) center of an adjacent macrocycle, thus forming a continuous chain.

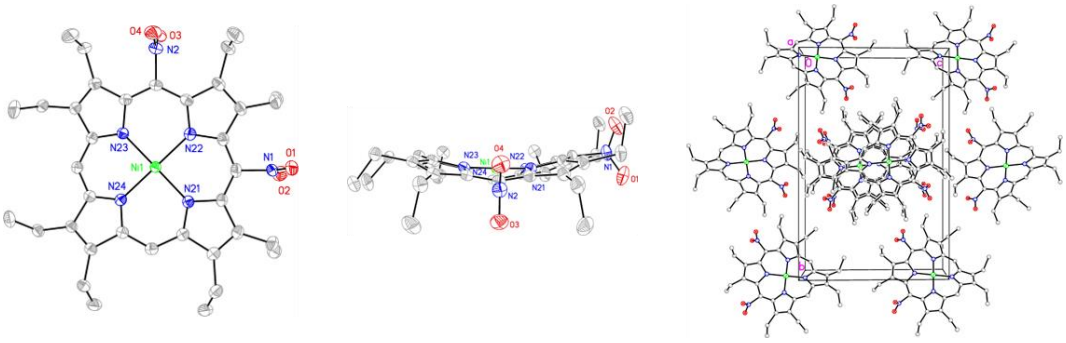

Figure 56. Views of the crystal structures of **204**. Hydrogen atoms have been omitted for clarity. Thermal ellipsoids indicate 50% probability.

In this work, the structure of the Ni(II) complex **204** was determined (Figure 56). When compared to free base **206** (see Table 10), there is an elongation of the N─C_α bond and a contraction of the C_α─C_m bond. An increase is also noticed in the N─C_α─C_β bond angles along with notably decreased C_α─N─C_α and C_α─C_m─C_α bond angles. Furthermore, higher displacement values (Δ24, ΔC_m, and ΔC_α) coupled with a large pyrrole tilt indicate a ruffled distortion. In comparison, the two tetracoordinated complexes **203**[158c] and a corresponding isopropyl-substituted Ni(II) porphyrin **225**[221] display similar C_α─C_m─C_α angles of 125.0 and 126.4°, respectively, which also applies to their C_α─N─C_α angles. Another observation is the decrease in core size from **204** (2.746 (7)°) to **203** (2.717°). This trend is similar to that found in the free base **95** and **206** (see Table 10) and confirms related studies on the conformational effects in meso-substituted porphyrin regioisomers.[222]

3.5 Synthesis of Highly Substituted Type I Porphyrins

The crystallographic data presented in this chapter was collected and solved by Dr. K. J. Flanagan.

The nomenclature relating to porphyrin ('type'[223]) isomers was initially introduced by Fischer as a way to define the nature of the substituent array in certain porphyrins and reviewed in all its facets by Taniguchi and Lindsey (Figure 57).[224]

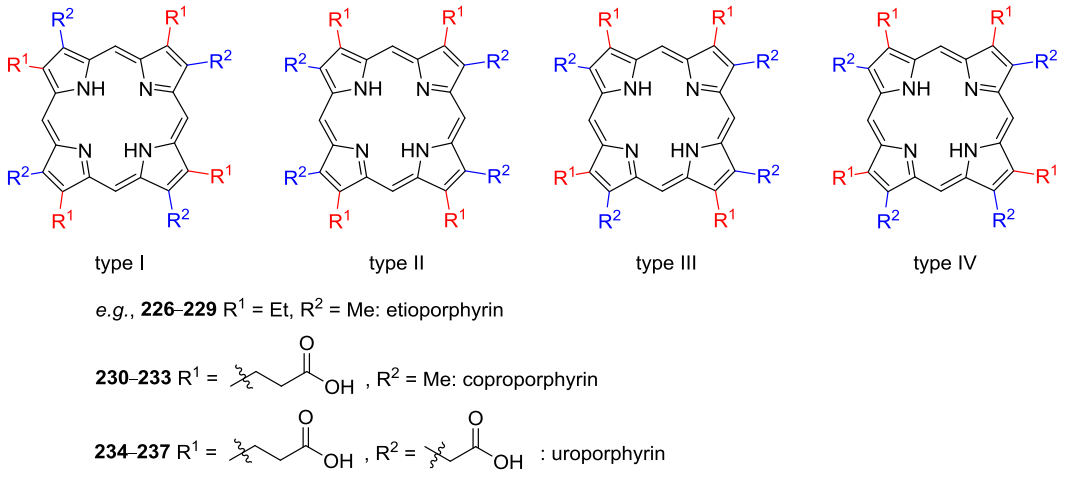

Figure 57. Examples of porphyrin type isomers: etioporphyrin I–IV (**226–229**) as well as biologically relevant copro- and uroporphyrins I–IV (**230–233** and **234–247**, respectively).

The synthesis of regioisomerically enriched or pure porphyrin type isomers usually depends on the preparation of special pyrrolic precursors or the design of particular condensation strategies. That is because conventional condensation reactions of, *e.g.*, 3,4-disubstituted pyrroles would result in the formation of statistical mixtures of all possible type isomers. Moreover, due to their very similar physicochemical properties, it is not trivial to separate these on a preparative scale. Thus, for example, etioporphyrin I (**226**) and coproporphyrin I tetramethyl ester are accessible by tetramerization of α-functionalized pyrroles[225] and so-called *opp*-porphyrins, in which like pyrrole rings are regiochemically situated opposite to each other were prepared in a similar fashion.[226] On the other hand, dipyrromethenes have been utilized in the syntheses of **226** and coproporphyrin I (**230**) as well as to prepare regioisomerically pure etiobiliverdin IVγ, which is a bile pigment.[227] This methodology was later extended to the use of dipyrromethenes for the preparation of isomers other than type I.[228] At the same time, where separation of type isomers from statistical mixtures is attempted, time consuming or small-scale purification methods are required, such as HPLC. Naturally this is more challenging the more type isomers are present in a given sample. Type I and III isomers of penta-, hexa-, and heptacarboxyporphyrin as well as those of uro- (**234** and **236**), copro- (**230** and **232**), and

isocoproporphyrin were separated *via* HPLC.[229] The authors stated that this method would be suitable for their preparative isolation and for the detailed analysis of such isomers in clinical materials, *e.g*., urine and feces of patients. More recently, HPLC was also applied to separate coproporphyrin I and III (**230** and **232**) where tetrapyrroles were extracted from various types of yeast and bacteria and then analyzed by MS–MS.[230]

Porphyrin type isomers have been subject of a range of medicinal and synthetic studies: Tetrapyrroles excreted by patients with different types of porphyria were analyzed.[231] Therein, the type isomer composition was disclosed with regards to, for example, type I and III uro- (**234** and **236**) and coproporphyrin (**230** and **232**) presence depending on the type of porphyria. On a different note, the synthetic value of all β-tetra(*tert*-butyl)porphyrin type isomers has been proven when they were used as precursors for porphyrin ('porphine', **1**). Similar to 5,10,15,20-tetra(*tert*-butyl)porphyrin (**144**),[232] they can be tetra-dealkylated to give porphrin ('porphine') (**1**) in good yield.[233] Macrocycle **1** is the parent structure of all porphyrins found in nature and therefore a synthetic target of immense importance for fundamental research.

This shows that methods for the facile synthesis of regioisomerically pure porphyrin type isomers are scarce. Moreover, the synthetic approaches shown above are usually not broadly applicable and as such, a relatively small library of such tetrapyrroles is at hand. Thus, the unexpected formation of 3-ethyl-4-isopropylpyrrole (**182**) during the attempted synthesis of 3,4-diisopropylpyrrole (**180**) was taken as an occasion to elaborate a concept where simple condensation reactions would lead to the preferential formation of type I porphyrins (Figure 58).

In this proposal, the pyrrolic precursors are designed in a way that a distinct difference in steric demand between the groups carried at the 3- vs. the 4-position is generated (*e.g*., as in **182**). Upon acid-catalyzed condensation with bulky aldehydes, type I porphyrins would be obtained as the major products due to minimized *peri*-interactions and overall steric strain.

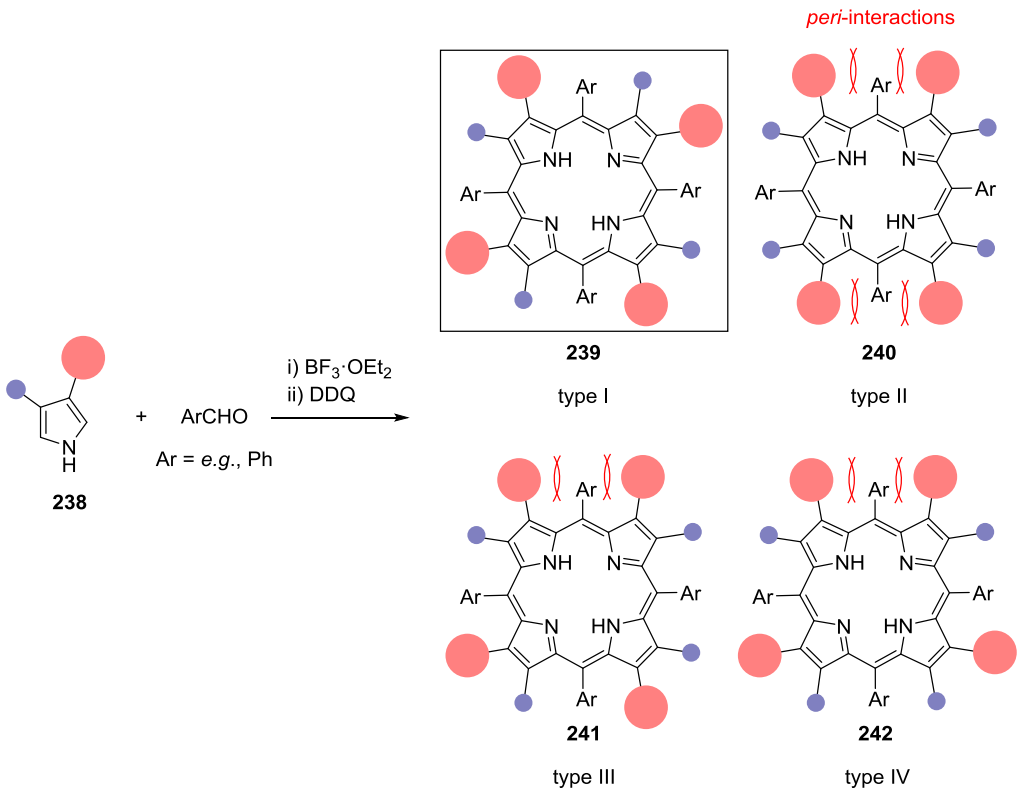

Figure **58**. Concept of the synthesis of type I porphyrins (**239**) rather than a statistical mixture of **239**−**242** from unsymmetrical 3,4-difunctionalized pyrroles **238** and sterically demanding aldehydes.

First, a stock of **182** to be used in such condensation reactions was prepared by reduction of **177** with lithium aluminium hydride. And indeed, the following reaction of this pyrrole with benzaldehyde yielded **243**·2HCl as the only detectable porphyrin species (Figure 59). Once again, similar to **162** and **164**, the porphyrin was isolated as its dihydrochloride salt **243**·2HCl due to protonation by residual hydrochloric acid present in the solvent (see Chapter 3.1).

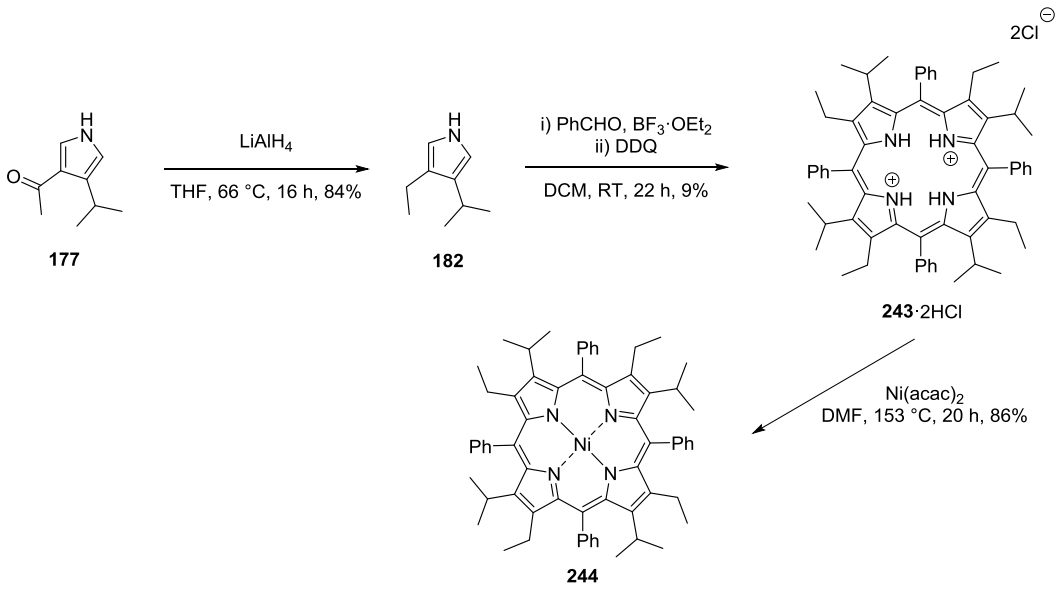

Figure 59. Synthesis of type I porphyrin isomers **243**·2HCl and **244** through condensation and metallation.

Additionally, formation of the type I isomer was confirmed by single crystal X-ray analysis of both **243**·2HCl and its Ni(II) complex **244** (see Experimental for details on crystal growth), which revealed severe saddle distortion of both macrocycles (Figure 60, top and middle). The crystal structure lattice diagram of **244** also showed a tunnel-like structure where DCM was incorporated (Figure 60, bottom). This is reminiscent of Cu(II)OETPP (**80**)·2DCM (see Figure 22) and points at possible receptor applications due to the availability of solvent-accessible binding pockets.[133]

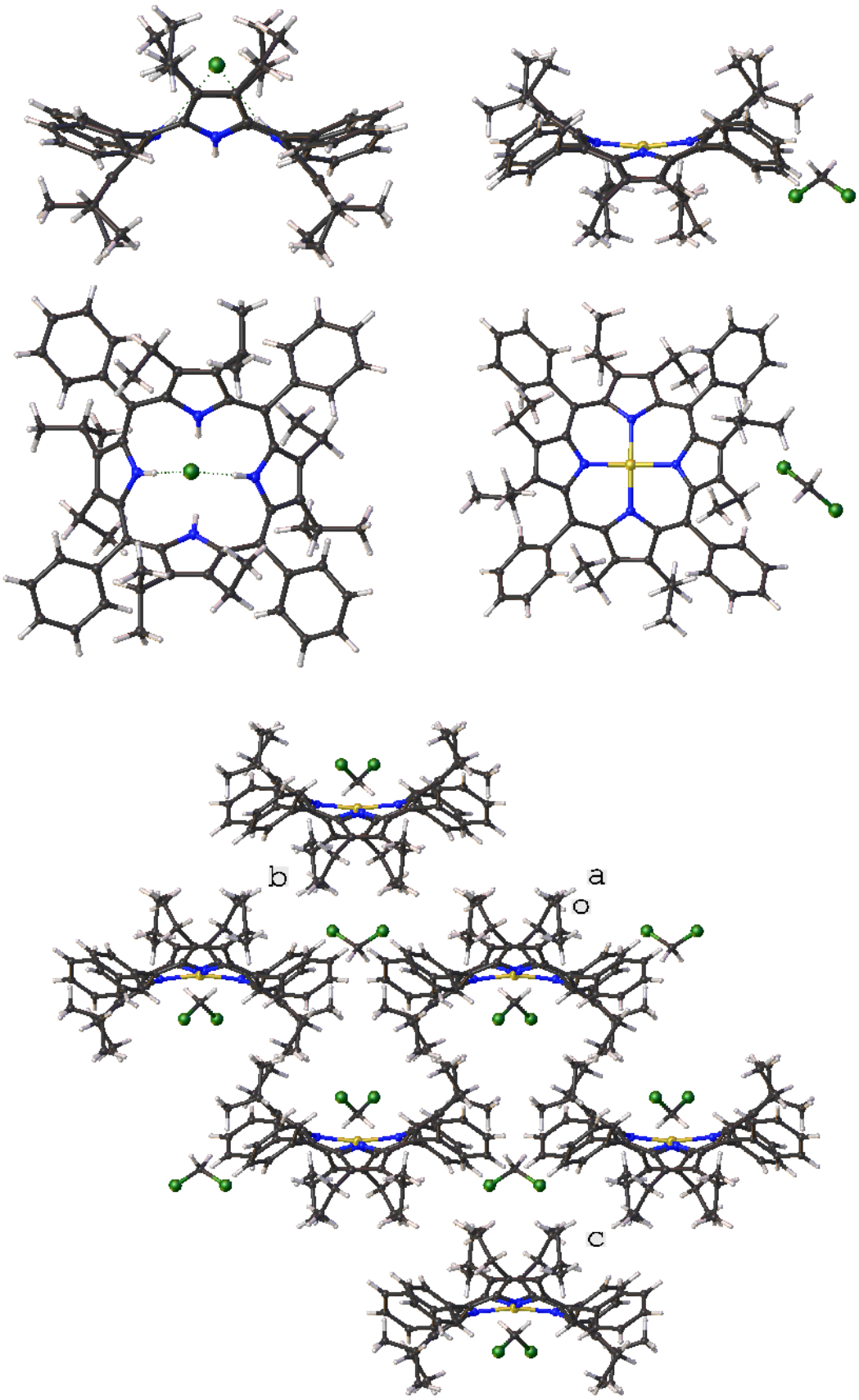

Figure 60. Top left and middle left: side and top views of **243**·2HCl. Top right and middle right: side and top views of **244**·DCM. Bottom: excerpt of the crystal structure lattice diagram of **244**·DCM.[58a]

Selective formation of **243**·2HCl confirmed the initial hypothesis that rational choice of the pyrrole and aldehyde components would open an avenue to regioisomerically pure type I porphyrin isomers *via* simple condensation pathways. In order to establish a library of highly substituted type I porphyrins, **182** was also reacted with 4-methoxybenzaldehyde and 2,6-dichlorobenzaldehyde with similar outcomes (Figure 61).

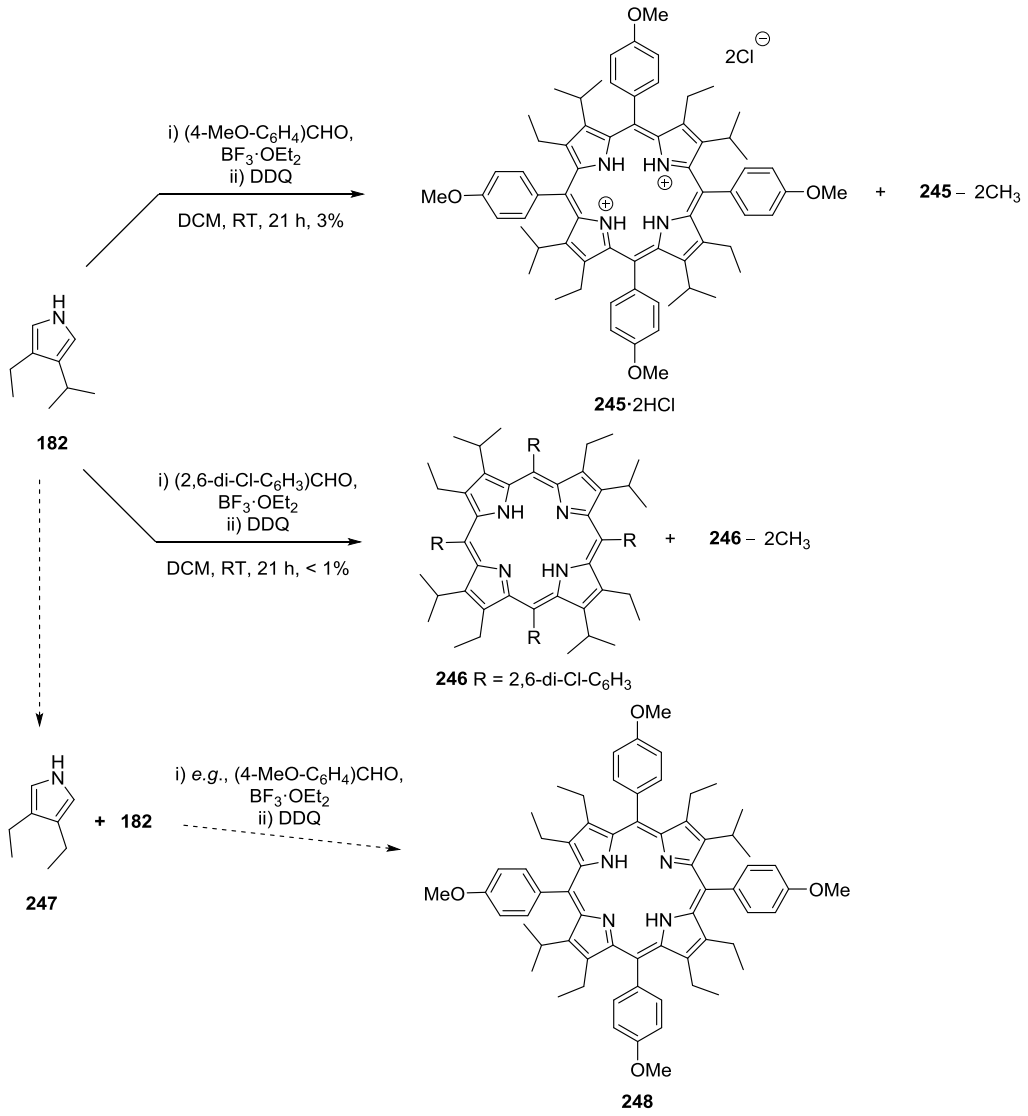

Figure **61**. Synthesis of type I porphyrins **245**·2HCl and **246** through condensation reactions.

While the only observed and isolated porphyrin type isomers were **245**·2HCl and **246**, respectively, the presence of another porphyrin after each condensation reaction was noted. In both cases, this tetrapyrrole

could be isolated but no structure was assigned with ultimate certainty. However, NMR and HRMS analysis indicated that these porphyrins were devoid of two CH_3 fragments when compared to **245**·2HCl and **246**, respectively. Probably a fraction of **182** underwent a type of dealkylation prior to condensation to form **247**, which could then have reacted with unaltered **182** and aldehyde, *e.g.*, 4-methoxybenzaldehyde to form a tetrapyrrole like **248** or corresponding regioisomers. In any case, these side products could be separated from **245**·2HCl and **248**, respectively, through conventional column chromatography and unambiguous assignment of the structures is currently under investigation.

In the following, it was attempted to extend this method to different types of pyrroles. Heterocycle **252** was selected as a first target in order to test whether it would be possible to introduce aromatic functions into the β-positions of type I porphyrins. In practical terms, 3-methyl-4-phenylpyrrole (**252**) was synthesized from **249** and **250** in a sequence of a Van Leusen reaction under similar conditions to the preparation of **172**[197] and **177**[198] followed by reduction of the methyl ester function in **251** (Figure 62).

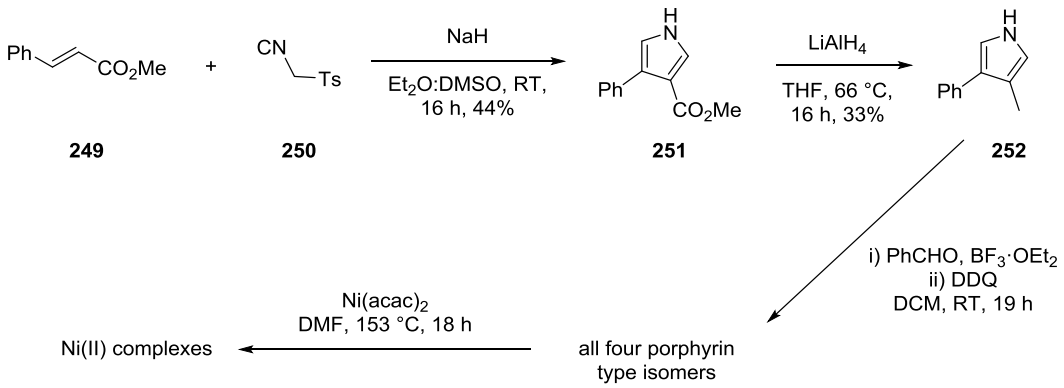

Figure 62. Synthesis of 3-methyl-4-phenylpyrrole (**252**), acid-catalyzed condensation with benzaldehyde, and metallation.

Unfortunately, the condensation of **252** with benzaldehyde resulted in the formation of an inseparable statistical mixture of all four porphyrin isomers. This was reflected by a high number of methyl signals in the ^{1}H NMR spectra of the free base products and its Ni(II) complexes (see Appendix, Figures A6–A9). Apparently, the difference in steric bulk

between the methyl and phenyl group in **252** was not distinct enough for selective type I porphyrin formation based on the considerations outlined in Figure 58. While the phenyl substituent may be considered as larger than any moiety in **252**, its flat geometry (as opposed to a three-dimensional isopropyl group) may account for this result. However, while this example does not eliminate the option that in the future, 3,4-disubstituted pyrroles with more sterically demanding aromatic substituents may eventually lead to type I porphyrin formation, it was at this stage decided to synthesize 3-substituted pyrroles for use in a similar capacity.

In principle, the difference in substituent bulk in appropriate 3-substituted pyrroles should be maximized (such as in **255**: 3-*tert*-butyl *vs*. 4-hydrogen). For that, pyrrole was protected[234] and **253** *tert*-butylated in an electrophilic substitution reaction to yield **254**.[235,236] Deprotection under basic conditions then yielded the first target compound **255**.[236,237] Likewise, **253** was converted to **256** and **257** under Friedel–Crafts conditions, giving a mixture of both the 2- and 3-substituted products, albeit it was reported that only the 3-benzoyl-substituted pyrrole should form under these conditions.[238] Both pyrroles were reacted with methyl magnesium bromide and separation of **258** and **259** by column chromatography was successfully performed thereafter. While the idea was to transform **258** to bulky 3-substituted **261** *via* **260** in a sequence of deprotection and reduction, the compound unexpectedly underwent dehydration to yield **262** in the presence of potassium hydroxide at an elevated temperature. Therefore, instead, **262** was used as an alternative in the acid-catalyzed condensation with benzaldehyde. But when either **256** or **262** were reacted under Lindsey conditions, no porphyrin formation became evident at all (Figure 63).

One possible explanation for the failed condensation reactions using **255** and **262** could be that the repulsive *peri*-interactions between the original 3-groups and neighboring phenyl units in fully formed porphyrins would be too adverse for the macrocycles **263** and **264** or any of their regioisomers to form. Alternatively, it may not have been possible to oxidize/aromatize the intermediary hydroporphyrins. In any case, at this stage it was considered that 3-substituted pyrroles (as opposed to 3,4-

disubstituted pyrroles and unsubstituted pyrrole) were generally unfit for condensation reactions. This might also have been due to an electronic substituent effect: an electron rich 3-substituent (as in **255** and **262**) directs the next electrophilic substitution to the neighboring α-position and therefore, the macrocycles may not have formed in the first place.

To conclude, while initial evidence was produced that highly substituted type I porphy-

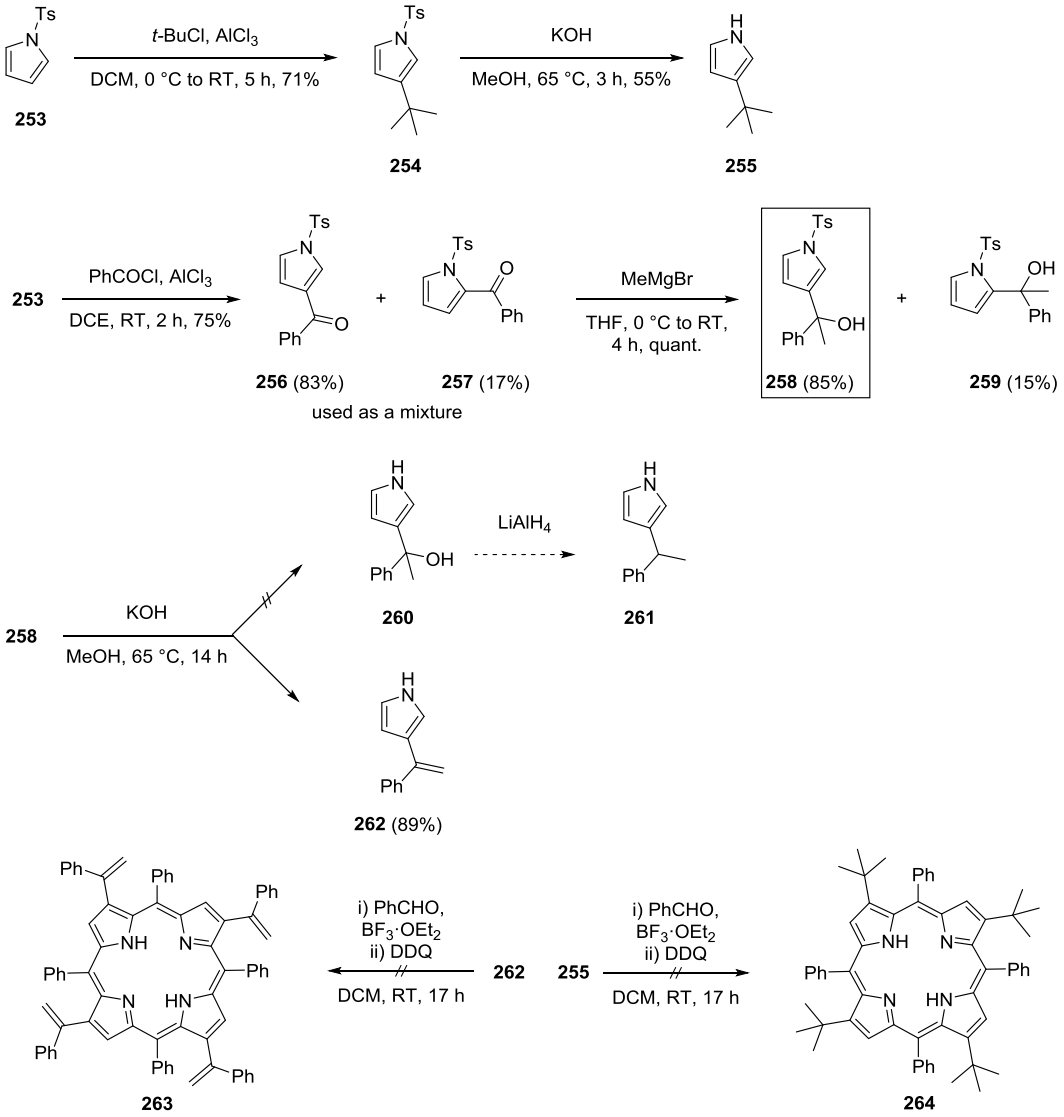

Figure 63. Synthesis of 3-substituted pyrroles **255** and attempted preparation of **261**. Subsequent condensation attempts are shown, too.

rins can be accessible through straightforward condensation reactions, the expansion of this method to using pyrroles other than **182** has been

met with difficulties. Therefore, additional work will have to be invested in order to derive a general-purpose method for the preparation of such tetrapyrroles. Since the best results were achieved when a 3,4-dialkylpyrrole was employed, further studies should initially focus on the use of similar pyrroles, for example, 3-isopropyl-4-methylpyrrole to gain more insight into the substrate scope before proceeding to more diverse systems.

4. Summary and Outlook

Porphyrins as Organocatalysts.[137,201] For the first time, free base and *N*-methylated porphyrins have been utilized as bifunctional organocatalysts in Michael additions and, tentatively, in Henry reactions. Based on these experiments, it was found that distortion of the macrocycles is a vital prerequisite for their catalytic activity. Therefore, conformational design has been used to tailor the properties of nonplanar porphyrins with regards to availability of the N–H units for hydrogen bonding (distortion-dependent hydrogen bonding) and the basicity of the heterocyclic groups. Moreover, NMR spectroscopy and catalyst screening studies provided insight into the likely mode of catalyst action. This unprecedented use of free base and *N*-substituted tetrapyrroles as organocatalysts opens a new functional role for porphyrins with plenty of opportunities and potential for further investigations. To obtain more information and to be able to make additional conclusion on the catalysts' performance, kinetic studies will have to be performed in the future. As a result, it would be possible to determine, for example, reaction rates and TONs. These additional data points would allow for a better comparison of the investigated porphyrins between themselves and with other, established systems.

In-depth structure–activity correlations were derived upon applying a series of six β-substituted, incrementally distorted H_2Et_xTPPs **84**–**87** as well as **47** and **74** as potential organocatalysts in sulfa-Michael reactions. The study allowed to trace the incremental introduction of catalytic activity into the porphyrins as was shown in a catalyst screening where increasing conversions were noted. This behavior was ascribed to an escalating saddle-type distortion of the compounds as a form of

molecular engineering. It is well documented that saddle-type nonplanarity increases the vector of all inner core N/N–H entities outwards (*vide supra*) and as seen through DFT calculations, results in some degree of modification of the groups' electronic properties. While the applied DFT model falls short of supporting the observed increase in catalytic activity, conformational analysis of the title compounds strongly supports the findings. Nevertheless, both electronic and steric factors in nonplanar porphyrins are usually tied inseparably and it is evident that both are prerequisites for the design of future porphyrin organocatalysts. Conclusively, a combination of modulating electronic properties and conformations in tetrapyrroles stands at the base of a new generation of bifunctional organocatalysts with great potential for tunability. Altogether, this will provide new avenues in organocatalysis using conformational design to prepare tailor-made porphyrins. Therein, specific binding and receptor functions play a key role, opening unprecedented functional roles. Further studies on the concept of activation and mechanism as well as applications in other catalytic reactions, *e.g*., halogen bond catalysis with halogenated porphyrins are currently under way. Note, that nonplanar porphyrins occur frequently in nature. Hence, a number of catalytically active porphyrin-containing enzymes will be revisited with regards to indications of comparable organocatalytic activity.

• For the first time, porphyrins were tailored and used as organocatalysts.

• Mechanistic studies indicated a bifunctional mode of substrate activation where the presence of an accessible inner core system was paramount.

• The correlations between degree of nonplanarity and catalytic activity was studied in detail using a series of H_2Et_xTPPs.

• The relationships between electronic factors and catalyst performance was analyzed.

Investigations on the Reaction of 2,3,7,8,12,13,17,18-Octaethyl-5,10,15,20-tetranitroporphyrin with Nucleophilic Thiols.[136] A range of highly substituted, nonplanar porphyrin thioethers were synthesized

from one precursor (**95**) in moderate to good yield, which also proved to be insensitive to air and moisture, thus allowing for convenient syntheses without protective atmosphere. The reactions involved a S_NAr method that was applied using both electron rich and poor as well as bulky aromatic thiolate nucleophiles. In the future, this method may be used as a versatile tool for the linkage of functional groups or chromophores to porphyrin scaffolds with minimal synthetic effort. Additionally, a methodology for the stepwise desubstitution of **95** was developed, which may be expanded to other nitroaromatic compounds in the future. This was intriguing as comparable desubstitutions of meso-positions are limited to only few examples.[206,212] One major obstacle was to take control of the competing substitution *vs*. reduction reactions that the meso-nitro groups could undergo. This was successfully achieved by establishing reaction conditions that would favor either possibility (Figure 64).

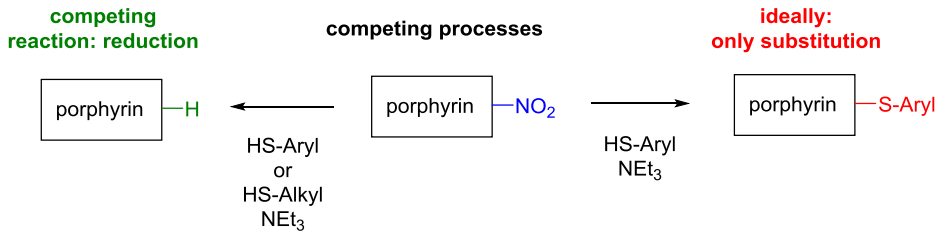

Figure 64. Reaction of nitroporphyrins with thiolates: substitution *vs*. reduction.

In addition, the structures of three new meso-arylthio-substituted tetrapyrroles **186**, **195**, and **196** as the first examples of a new class of highly substituted porphyrins were evaluated. These compounds exhibit specific features reminiscent of previously studied porphyrin thioethers, such as the C_m–S–R angles. However, they also possess the structural features of highly substituted porphyrins, such as increased pyrrole tilts and atom deviations from the 24-atom mean-plane. Additionally, the first complete study on the effects of an incremental increase of meso-nitro-substitution on highly substituted porphyrins was reported, elucidating macrocyclic deviations based on the number and pattern of nitro substituents. This was accompanied by thorough structural analysis of **204** and comparison to similar complexes and its free base counterpart.

• A series of highly substituted porphyrin thioethers was synthesized from H_2OETNP.

• The new S_NAr method allows to access a large variety of meso-substituted porphyrins form the same precursor.

• Stepwise denitration of H_2OETNP was investigated, yielding a series of nitro-substituted porphyrins.

• Comparative crystal structural analyses of porphyrin thioethers and nitroporphyrins, respectively, was performed, confirming a distinct dependance between substitution pattern and degree of nonplanarity.

Synthesis of Highly Substituted Type I Porphyrins. A concept was proposed where highly substituted type I porphyrin isomers would selectively form in condensation reactions through rational choice of the pyrrole and aldehyde components (see Figure 58). This could initially be confirmed through the isolation of **243**·2HCl, **245**·2HCl, and **246**, with crystal structures of the former and its Ni(II) complex at hand. However, the anticipated general-purpose nature of this method could not yet be sufficiently evidenced, as 3-alkyl-4-arylpyrroles and 3-substituted pyrroles did not show similar outcomes. Still, it may be expected that screening of a range of appropriate unsymmetrical 3,4-difunctionalized pyrroles will yield more examples of exclusive type I porphyrin formation and prove the relevance of this approach.

• Initial studies on selective type I porphyrin formation in condensdation reactions were performed.

• Selective type I porphyrin formation could be confirmed in a number of cases and crystal structural analysis affirmed the type I substitution pattern.

Outlook: Nonplanar Porphyrins as Sensors.[138,200] Due to the limited timeframe, this work did not yield a first case study on nonplanar free base porphyrin sensors based on N–H···X-type core interactions *per se*. However, the findings on porphyrin organocatalysis allow for a promising outlook and point at a number of proposals towards such new sensors

that would also tackle some of the obstacles encountered when using established porphyrin chemosensors already at hand: Previously, it has been reviewed how (metallo)porphyrins are particularly suited for sensing applications[4a,4b,138,139,140] and their catalytic activity has been proved in numerous contributions.[137] But since these reports depend on metallation of the core, this has the drawbacks of (1) decreased conformational flexibility of the macrocycle (core) and (2) essentially rendering the central nitrogen atoms inert towards the formation of intermolecular hydrogen bonds. And while free base porphyrins, thanks to their various (optical) properties that change upon alteration of the microenvironment of the tetrapyrroles, were indeed used as probes for, *e.g.*, sensing of VOCs,[239] water and ethanol,[240] gases, *etc*.,[241] and furthermore, as was recently summarized,[140d] ions and ion pairs, ROS, chiral discrimination, and as thermosensitive probes, specific tailoring of the free base macrocycle skeleton as a form of molecular engineering towards improved substrate binding/recognition, and probing appears underrepresented, leaving in turn plenty of room for innovation.

Comparable to the likely mode of activation in bifunctional porphyrin organocatalysis, during sensing the substrates may bind to the tetrapyrrole's active center *via* N–H···X-type hydrogen bonds. In line with this is a study on aryl phosphonate- and phosphonic acid-functionalized porphyrins for molecular recognition of ≥5 ppb TNT where macrocyclic distortion upon protonation increased selectivity towards the explosive at nanomolar levels.[141] Additionally, quantitative complexation of TNT (0.46 ppm) by a complex of a carboxylporphyrin **92** and a metal–organic framework (MOF) occurred in aqueous media and involved hydrogen binding with the porphyrin's central N–H groups.[144] Thus, with 'nonplanar sensing' being a feasible application, molecular engineering of the porphyrin macrocycle could principally be used to increase selectivity and sensitivity of the recognition process.

In practical terms, since there are often scenarios where multiple analytes compete, it will be crucial to engineer receptor platforms of high selectivity that specifically emphasize desired interactions while neglecting interferers. This is where the broad and tunable landscape of macrocyclic conformations may take a critical position: as was elaborated above,

porphyrins that have similar substitution patterns can have significantly different conformations. As such, next to say, modulation of the peripherally attached groups and electronic effects, three-dimensional distortion could benefit the specificity of a recognition process. That is because, in a sense, nonplanarity may be seen as an additional 'adjusting screw': synthesizing a family of deformed porphyrins based on differing stereochemical parameters (*e.g.*, specific volume and diameter of the binding pocket, chirality) would result in a diverse toolbox of conformationally designed porphyrins to serve as a close fit to specific substrates while disregarding others (Figure 65). This could also be achieved in liaison with surface science as it has been evidenced that porphyrins undergo structural transformations when anchored to a surface.[242] One approach by the group of Aida that relied on such molecular geometry-based considerations for sensing fabricated a D_2-symmetric, dodecasubstituted, *sad*-type porphyrin where the absolute configuration of chiral acids could be recognized and 'memorized' through formation of asymmetric core hydrogen-bonding complexes and circular dichroism (CD) as an analytical tool.[243] The 'chirality memory' could also be 'released' and 'retrieved' in response to stimuli, such as heat and light.

As an alternative approach to an accessible inner core system, the introduction of doming into tetrapyrroles could be investigated. This mode should produce out-of-plane N–H units, too. However, the challenge will be to utilize free bases in this capacity as doming typically only occurs in certain metalloporphyrins.[244]

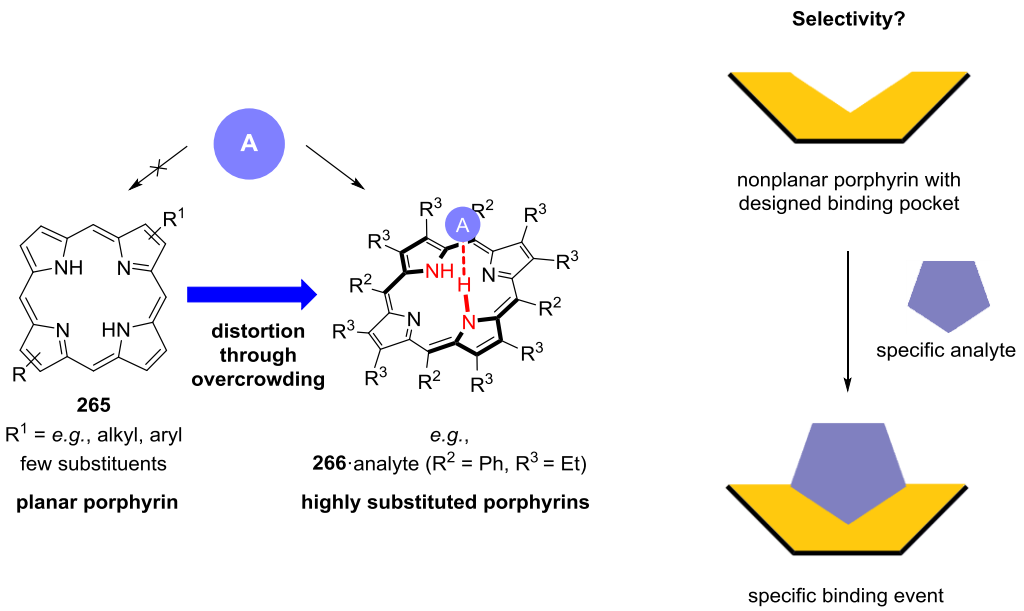

Figure 65. Left: concept of distortion-dependent porphyrin sensors. The core of planar porphyrins **265** is unable to complex an analyte while highly substituted, distorted analogues (*e.g.*, **266**) are able to do so. Right: one conceptual example of new sensors based on engineered nonplanar porphyrins.

To conclude, it can be proposed that N–H···X binding in tetrapyrrole ligands can be exploited to a previously unknown extent by means of conformational control to produce improved catalysts, receptors, sensors, or maybe even drugs, advanced (supramolecular) materials, *etc*. Hopefully, this will open new functional roles and lead to a rethinking, if not renaissance, of the use of natural and synthetic porphyrins ('the pigments of life'), particularly their metal-free derivatives, with a plenitude of new and up-and-coming applications on offer.

5. Experimental

Analytical Techniques. Analytical TLC was performed using sheets precoated with silica gel to a depth of 0.2 mm or aluminum oxide plates, both impregnated with fluorescence indicator F_{254}. Visualization was accomplished with UV lamp. Flash column chromatography was carried out using silica gel 60 (230–400 mesh) or aluminum oxide (neutral, activated with 6% H_2O, Brockman Grade III). Mass spectrometry analysis was performed with a Q-Tof Premier Waters MALDI quadrupole time-of-flight (Q-TOF) mass spectrometer equipped with Z-spray electrospray ionization (ESI) and matrix-assisted laser desorption ionization (MALDI) sources either in a positive or negative mode with DCTB (*trans*-2-[3-(4-*tert*-butylphenyl)-2-methyl-2-propenylidene]malononitrile) as the matrix. APCI experiments were performed on a Bruker microTOF-Q III spectrometer interfaced to a Dionex UltiMate 3000 LC. UV-vis absorption measurements were performed in DCM, DCM + 1% TEA, or toluene as solvent using a Shimadzu MultiSpec-1501. Melting points are uncorrected and were measured with a Stuart SMP-50 melting point apparatus. ^{1}H, ^{13}C $\{^{1}H\}$ and ^{19}F NMR spectra were recorded at 400.13 MHz, 100.61 MHz and 376.59 MHz using Bruker DPX400, Bruker AV 600, and Bruker AV 400 devices, respectively. All NMR experiments were performed at 25 °C. Resonances δ are given in ppm units and referenced to the deuterium peak in the NMR solvent $CDCl_3$ (δ_H = 7.26 ppm, δ_C = 77.2 ppm). Signal multiplicities are abbreviated as follows: singlet = s, doublet = d, quartet = q, septet = sept, multiplet = m. Photophysical measurements were carried out in DCM or toluene as solvent. IR spectra were recorded on a PerkinElmer Spectrum 100 FTIR spectrometer utilizing the ATR sampling technique.

General Information. To protect air and moisture sensitive compounds, the corresponding reactions were carried out under ‘Schlenk’ conditions using argon as inert gas. Air and residual moisture were removed from the instruments by a hot air gun under high vacuum and the flasks were purged with argon subsequently. This cycle was repeated up to three times as necessary. Air sensitive thiols were stored under argon at RT to prevent oxidation.

In some NMR spectra of the new 2,3,7,8,12,13,17,18-octaethyl-5,10,15,20-tetrasubstituted porphyrin thioethers and other highly substituted porphyrins, the signals corresponding to the β-ethyl groups are broad. This is in accordance with conformational studies by Medforth *et al.* on decaalkylporphyrins.[245] Presumably, the highly substituted products exist as a mixture of atropisomers in solution, particularly in the case of unsymmetrical meso-substituents, as in **198**, causing signal broadening due to different interactions between β-ethyl groups and meso-substituents. Opposed to this, the introduction of bulky substituents such as anthracenyl and mesityl groups resulted in a 'locking' of the conformation and clearer signals for the β-ethyl groups. However, VT NMR experiments could not be performed due to the low solubility of the compounds in appropriate solvents, such as DMSO-d_6, or THF-d_8. Missing signals corresponding to the inner protons as observed in most ^{1}H NMR spectra have been reported previously, too.[159]

Materials. Most commercially available reagents were used as received unless otherwise noted. For example, THF, Et_2O, toluene, and DCM were obtained by passing the degassed solvents through an activated alumina column. Alternatively, DCM for porphyrin syntheses was obtained *via* drying over phosphorus pentoxide and distillation. Where precursors and targets have been prepared following the literature, the individual references were cited in the corresponding chapters. For example, porphyrins **47**,[175} **48**,[179] **56**[172], **64**,[194] **74**,[120a] **95**,[159] **120**,[188] **121**,[173]] **143**,[181] **144**,[87], **145**,[182] **146**,[176], **147**,[92b] **152**,[92b] **153**,[185] **165**,[192], **166**,[193] **174**,[121] **203**,[158c] and **209**[159] as well as the H_2Et_xTPP series (**47**, **74**, and **84–87**)[132] and pyrroles **160**,[179,189] **173**,[195−197] **251**,[246] **252**,[247] **253**,[234] **254**,[236] **255**,[236] and **258**[248] have been synthesized according to the literature and gave satisfactory analytical data. The same applies to DMAP·HCl[249] and 9-anthracenethiol (**HSAr^4**).[250] 9-Phenanthrenthiol (**HSAr^{10}**)[251] was prepared similar to **HSAr^4**.[250] The synthesis of **204** has been reported previously but full characterization was unavailable.[252]
In several cases, the preparation of porphyrins, especially for use in Chapter 3.2 has been performed in collaboration with M. Roucan. Further, compounds **141**,[137] **142**,[92c] **148**,[137] **149**,[137] **150**,[92c,183] and

151[137] were previously unkown or incompletely characterized and have been prepared by M. Roucan, with full experimental details available elsewhere.[92c,137]

Synthesis and Characterization

2,3,7,8,12,13,17,18-Octaethyl-5,10,15,20-tetra(naphthalen-2-yl)porphyrin 162: 3,4-Diethylpyrrole (**160**, 0.18 g, 1.46 mmol, 1 equiv) and 2-naphthylaldehyde (**161**, 0.23 g, 1.46 mmol, 1 equiv) were dissolved in dry DCM (150 mL) and boron trifluoride diethyl etherate (18 μL, 146 μmol, 10 mol%) was added. This was stirred for 3 h at RT followed by the addition of DDQ (1.6 g, 7.05 mmol, 4.8 equiv). The red solution became deep red and opaque and was left to stir for further 16 h. The solvent was removed under reduced pressure, the residue dissolved in chloroform and pushed through a plug of silica using chloroform and mixtures of chloroform and methanol (up to 10% methanol) to achieve partial separation of the products. A deep green band was identified as the main fraction and evaporated *in vacuo*. The deep green residue was chromatographed (SiO_2, DCM, then DCM + 10% ethyl acetate) twice, collecting a major green band after removal of impurities (brown band). Evaporation of the solvents yielded **162**·2HCl as a green solid (105 mg, 0.41 mmol, 28%) where protonation was indicated by UV-vis analysis. Upon dissolving **162**·2HCl in a mixture of DCM and TEA (100:1, v/v), the color changed from light green to deep green. This was washed with a saturated $NaHCO_3$ solution, dried over $MgSO_4$, filtered, and evaporated to dryness at reduced pressure to yield **162** as a green solid (95 mg, 0.40 mmol, 97% from **162**·2HCl). mp: > 300 °C. R_f: 0.56 (SiO_2, ethyl acetate). ^{1}H NMR (400.13 MHz, $CDCl_3$, δ): 0.17–0.59 (m, 24H), 2.00–2.52 (m, 16H), 7.76–7.88 (m, 8H), 8.18–8.29 (m, 4H), 8.31–8.48 (m, 8H), 8.72–8.93 (m, 4H), 8.94–8.98 (m, 2H), 8.98–9.19 ppm (m, 2H). ^{13}C {^{1}H} NMR (100.61 MHz, $CDCl_3$, δ): 15.7 (× 2), 15.8 (× 2), 15.9, 16.0 (× 2), 16.1 (× 2), 18.9 (× 2), 19.1, 117.8, 118.3, 118.8, 127.3, 127.8, 128.0, 128.2, 129.4, 133.1, 133.2 (× 2), 133.6, 134.0, 134.1, 134.2, 134.3, 134.4, 135.7, 135.8 (× 3), 135.9, 137.1, 137.2, 137.3, 137.4, 137.5, 137.6, 137.7, 138.0, 138.1 (× 3), 138.3, 138.4, 138.7 (× 2), 138.8, 144.4, 144.5 (× 2), 144.6, 145.2 (× 3), 145.3 ppm. UV-vis (DCM + 1% TEA) λ_{max} (log

ε): 463 (5.00), 559 (3.82), 609 (3.74), 715 nm (3.27). HRMS–MALDI (*m/z*): $[M + H]^+$ calcd. for $C_{76}H_{71}N_4$, 1039.5679; found, 1039.5675. MS–MALDI *m/z* (% relative intensity, ion): 1039.47 (100, M + H), 995.51 (90, M – C_2H_5 – CH_3 + H), 981.49 (51, M – $2C_2H_5$ + H), 966.42 (30, M – $2C_2H_5$ – CH_3 + H), 951.40 (28, M – $3C_2H_5$), 937.39 (19, M – $3C_2H_5$ – CH_3 + H).

2,3,7,8,12,13,17,18-Octaethyl-5,10,15,20-tetra(pyren-1-yl)porphyrin 164: 3,4-Diethylpyrrole (**160**, 1.23 g, 10 mmol, 1 equiv) and 1-pyrenecarboxaldehyde (**163**, 2.30 g, 10 mmol, 1 equiv) were dissolved in dry DCM (1 L) and boron trifluoride diethyl etherate (0.12 mL, 1 mmol, 10 mol%) was added. This was reacted for 3 h at RT followed by the addition of DDQ (10.9 g, 48 mmol, 4.8 equiv). The purple solution became deep purple and opaque and was left to stir for further 16 h. The solvent was removed under reduced pressure, the residue dissolved in DCM and pushed through a plug of silica using DCM to remove non-porphyrin material, then chloroform + 10% methanol to collect a major deep red band containing the product. The solvent was removed and **164**·2HCl was obtained as a green solid (500 mg, 1.40 mmol, 14%) without further purification after evaporation of the solvent at reduced pressure. Neutralization was done similar to **164**·2HCl and **164** was obtained as a green solid (450 mg, 1.33 mmol, 95% from **164**·2HCl) after evaporation of the solvent. mp: > 300 °C. R_f: 0.55 (SiO_2, hexane:DCM, 2:1, v/v). ^{1}H NMR (400.13 MHz, $CDCl_3$, δ): −0.27–0.11 (m, 24H), 1.12–2.36 (m, 16H), 8.18–8.28 (m, 4H), 8.36–8.48 (m, 14H), 8.48–8.55 (m, 4H), 8.56–8.63 (m, 2H), 8.64–8.74 (m, 4H), 8.85–8.92 (m, 1H), 8.99–9.11 (m, 2H), 9.19–9.27 (m, 1H), 9.29–9.44 ppm (m, 4H). ^{13}C {^{1}H} NMR (100.61 MHz, $CDCl_3$, δ): 11.6, 14.3, 14.5, 15.4, 15.5, 15.6 (× 3), 16.3, 16.4 (× 2), 16.5, 17.7, 17.8, 17.9, 18.0, 18.1, 18.6, 18.7, 18.8, 18.9 (× 2), 20.6, 20.9, 22.8, 25.5, 27.1, 29.2, 31.8, 34.7, 34.8, 36.3, 41.5, 116.5, 116.8, 116.9, 117.1 (× 2), 124.5, 124.6, 124.7, 124.8, 124.9, 126.0 (× 2), 126.1, 126.2, 126.3 (× 3), 126.4, 126.5 (× 2), 126.9, 127.8, 127.9 (× 2), 129.6, 129.7, 129.8, 129.9, 130.1, 131.5, 131.6, 131.8, 132.3, 132.4 (× 2), 132.5 (× 2), 132.6, 133.2, 133.3, 134.3 (× 2), 134.4 (× 2), 134.5, 135.4, 135.5, 135.6 (× 2), 135.7, 135.9, 136.0, 136.1, 136.2, 137.5, 137.8 (× 2), 138.5, 138.6, 138.7, 139.1 (× 2), 139.2, 139.3, 139.8 (× 2), 139.9, 143.6. 144.1, 144.2, 144.4, 144.5,

144.7, 144.8, 145.0, 145.2, 145.8, 145.9, 146.0, 146.1, 166.5, 166.7, 171.4 (× 2), 173.3, 173.6, 173.7 ppm. UV-vis (DCM + 1% TEA) λ_{max} (log ε): 324 (5.06), 337 (5.12), 481 (5.46), 568 (4.42), 619 (4.40), 723 nm (3.83). HRMS–MALDI (*m/z*): $[M + H]^+$ calcd. for $C_{100}H_{79}N_4$, 1335.6305; found, 1335.6312. MS–MALDI *m/z* (% relative intensity, ion): 1336.48 (100, M + 2H), 1307.52 (36, M – C_2H_5 + 2H), 1291.51 (12, M – C_2H_5 – CH_3 + 2H), 1278.53 (4, M – $2C_2H_5$ + 2H), 1120.51 (4, M – $C_{16}H_9$ – CH_3 + 2H).

2,3,7,8,12,13,17,18-Octaisobutyl-5,10,15,20-tetrakis(4-methoxyphenyl)porphyrin 175: 3,4-Diisobutylpyrrole (**173**, 0.79 g, 4.41 mmol, 1.0 equiv) and 4-methoxybenzaldehyde (0.6 g, 4.41 mmol, 1.0 equiv) were dissolved in 800 mL of dry DCM. Then, $BF_3{\cdot}OEt_2$ (55 µL, 0.42 mmol, 10 mol%) was added and the solution turned red within 23 h. After the addition of DDQ (4.4 g, 19.4 mmol, 4.4 equiv) the color changed to brown within another 23 h. The solvent was removed *in vacuo* and the crude product purified by filtration through a plug of Al_2O_3 (Brockman grade III). Using DCM as eluent gave a red–brown fraction first. When ethyl acetate was used, a green–brown fraction and an orange fraction were obtained. After that, methanol was applied, and a reddish fraction could be isolated. All fractions were analyzed through TLC and the relevant porphyrin-containing solutions combined and dried *in vacuo*. This was then subjected to column chromatography (Al_2O_3, Brockman grade III) utilizing DCM:ethyl acetate, 9:1, v/v as eluent to remove less polar side products and DCM:ethyl acetate, 3:2, v/v to obtain a major green fraction. The green fraction was evaporated *in vacuo* to yield an impure green oil. Another filtration through a plug of Al_2O_3 (Brockman grade III) gave a light green fraction first with DCM as eluent and then a dark green solution using DCM:ethyl acetate, 1:1, v/v. The latter was found to contain a dark green solid after evaporation of the solvent at reduced pressure, which was subjected to another column chromatography (Al_2O_3, Brockman grade III, DCM:ethyl acetate, 9:1−1:2, v/v). A major green fraction could be isolated, giving the title compound as a green solid (46 mg, 0.18 mmol, 4%) after evaporation of the solvent *in vacuo* and drying on high vacuum for 3 h. mp: > 300 °C. R_f: 0.40 (Al_2O_3,

DCM:ethyl acetate, 9:1, v/v). ^{1}H NMR (400.13 MHz, $CDCl_3$, δ): −1.06 (s, 2H), −0.18–0.24 (m, 24H), 0.24–0.64 (m, 24H), 1.06–1.26 (m, 8H), 1.82–2.13 (m, 8H), 2.13–2.39 (m, 8H), 4.06 (s, 12H), 7.20–7.32 (m, 8H), 8.12–8.35 ppm (m, 8H). ^{13}C {^{1}H} NMR (100.61 MHz, $CDCl_3$, δ): 22.5, 30.4, 35.4, 55.9, 113.0, 118.1, 133.3, 137.6, 138.3, 160.1 ppm. UV-vis (DCM) λ_{max} (log ε): 485 (5.39), 714 nm (4.52). HRMS–MALDI (*m/z*): $[M + H]^+$ calcd. for $C_{80}H_{103}N_4O_4$, 1183.7979; found, 1183.7960.

Substitution Reactions

Reaction of H_2OETNP with 4-bromobenzenethiol in absence of TEA. In a 50 mL round bottom flask fitted with a reflux condenser, compound **95** (75 mg, 0.11 mmol, 1 equiv) and 4-bromobenzenethiol (**HSAr[1]**, 1.05 mmol, 198 mg, 10 equiv) were dissolved in 10 mL of chloroform and heated to 61 °C for 19 h. Upon consumption of the starting material, as indicated by TLC analysis, the solvent was removed *in vacuo* and column chromatography was performed. The second fraction of the first column chromatography (SiO_2, hexane:DCM, 2:1, v/v) yielded an inseparable mixture of the isomers **190** and **191** as a purple solid (15 mg, 17.6 µmol of a 3:2 mixture, combined yield 16% (see Appendix, Figure A10)) after elution of less polar side products, removal of the solvent and recrystallization by slow diffusion from DCM and methanol. The column was flushed with ethyl acetate, the solvent was removed and two more chromatographic purification steps of this fraction were performed: The first chromatography (SiO_2, hexane + 1% TEA) gave **188** (60 mg, 58.3 µmol, 53%) as the first major fraction upon removal of the solvent. Subsequently, the column was flushed with ethyl acetate, the solvent was removed and this fraction was purified by chromatography (Al_2O_3, Brockman grade III, hexane:DCM, 50:1–1:1, v/v) to give **189** (40 mg, 33.0 µmol, 30%) as the major component upon removal of the solvent. Compound **188** was obtained as green crystals after being recrystallized by slow evaporation (acetone:water, 10:1, v/v).

5,10,15,20-Tetrakis[(4-bromophenyl)thio]-2,3,7,8,12,13,17,18-octaethylporphyrin 188: mp: 115–120 °C dec. R_f: 0.78 (SiO_2, hexane:ethyl acetate, 10:1, v/v). ^{1}H NMR (400.13 MHz, $CDCl_3$, δ): 0.96–

1.90 (m, 24H), 2.60–3.67 (m, 16H), 6.74–6.95 (m, 8H), 7.10–7.25 ppm (m, 8H). ^{13}C {^{1}H} NMR (100.61 MHz, $CDCl_3$, δ): 16.7, 20.3, 119.2, 127.5, 132.1, 141.9 ppm. UV-vis (DCM) λ_{max} (log ε): 488 (5.01), 581 (3.84), 639 (3.83), 743 nm (3.75). HRMS–MALDI (*m/z*): M^+ calcd for $C_{60}H_{58}Br_4N_4S_4$, 1278.0278; found, 1278.0283. MS–MALDI *m/z* (% relative intensity, ion): 907 (100), 531 (43, M − 4SAr + H), 685 (30, M − 3SAr).

5,10,15-Tris[(4-bromophenyl)thio]-2,3,7,8,12,13,17,18-octaethylporphyrin 189: mp: 87–90 °C dec. R_f: 0.64 (Al_2O_3, hexane:DCM, 2:1, v/v). ^{1}H NMR (400.13 MHz, $CDCl_3$, δ): 0.97–1.19 (m, 12H), 1.42–1.53 (m, 12H), 2.70–3.53 (m, 8H), 2.54–3.63 (m, 4H), 3.64–4.04 (m, 4H), 6.65–6.75 (m, 4H), 6.79–6.98 (m, 2H), 7.04–7.10 (m, 2H), 7.12–7.18 (m, 4H), 8.92 ppm (s, 1H). ^{13}C {^{1}H} NMR (100.61 MHz, $CDCl_3$. δ): 17.0, 17.3, 17.7, 19.4, 20.3, 20.4, 22.1, 29.6, 118.8, 119.3, 127.5, 132.0, 132.1, 142.5 ppm. UV-vis (DCM) λ_{max} (log ε): 469 (5.01), 567 (3.92), 617 (3.94), 700 nm (3.57). HRMS–MALDI (*m/z*): $[M + H]^+$ calcd for $C_{54}H_{56}Br_3N_4S_3$, 1093.1212; found, 1093.1216. MS–MALDI *m/z* (% relative intensity, ion): 503 (100), 531 (93, M − 3SAr), 719 (53, M − 2SAr + H).

5,10-Bis[(4-bromophenyl)thio]-2,3,7,8,12,13,17,18-octaethylporphyrin 190 and 5,15-bis[(4-bromophenyl)thio]-2,3,7,8,12,13,17,18-octaethylporphyrin 191: HRMS–ESI (*m/z*): $[M + H]^+$ calcd for $C_{48}H_{53}Br_2N_4S_4$, 909.2058; found, 909.2055.

Reaction of H_2OETNP with 4-bromobenzenethiol in absence of TEA. In a sample tube, porphyrin **95** (30 mg, 42 μmol, 1 equiv) and 4-bromobenzenethiol (**HSAR[1]**, 35 mg, 0.18 mmol, 4.4 equiv) were dissolved in chloroform (2 mL) and TEA (3 drops) was added. The color changed to dark red within 10 min and the crude product was chromatographed on silica (hexane:ethyl acetate, 40:1–10:1, v/v). A green band was collected to give the green solid **189** (< 10%) upon removal of the solvent while the second fraction (dark red band) yielded **188** (39 mg, 30.7 μmol, 73%) as a green solid after evaporation of the solvent.

2,3,7,8,12,13,17,18-Octaethyl-5,10,15-tris(1,3,5-trimethylbenzenethio)porphyrin 192: Compound **95** (25 mg, 35 μmol, 1 equiv), 2,4,6-trimethylthiophenol (**HSAr²**, 24 mg, 0.15 mmol, 4.4 equiv) and TEA (3 drops) were reacted at 25 °C in chloroform (5 mL) until completion, as indicated by TLC analysis. The solvent was removed *in vacuo* and column chromatography (SiO_2, hexane:ethyl acetate, 75:1–0:1, v/v) was performed. After the removal of less polar side products, **192** was obtained as a green solid (16 mg, 14.0 μmol, 40%) upon evaporation of the solvent. mp: 54–57 °C dec. R_f: 0.21 (SiO_2, hexane:ethyl acetate, 4:1, v/v). ^{1}H NMR (400.13 MHz, $CDCl_3$, δ): 0.68–0.72 (m, 6H), 1.47–1.50 (m, 6H), 1.60–1.63 (m, 12H), 1.95–1.98 (m, 18H), 2.25–2.28 (m, 9H), 2.81–2.82 (m, 4H), 3.01–3.15 (m, 4H), 3.32–3.34 (m, 4H), 3.64–3.66 (m, 4H), 6.70 (s, 6H), 7.88 ppm (s, 1H). ^{13}C {^{1}H} NMR (100.61 MHz, $CDCl_3$, δ): 16.2, 16.5, 16.8, 17.3, 18.7, 19.0, 19.1, 21.0, 21.2, 21.4, 21.7, 22.0, 29.6, 32.1, 90.4, 129.8 (× 2), 133.4, 134.0, 136.3, 136.8, 138.7, 138.2, 143.5, 143.7 ppm. UV-vis (DCM) λ_{max} (log ε): 470 (5.07), 592 (4.01), 632 (4.25), 718 nm (3.87). HRMS–MALDI (*m/z*): $[M + H]^+$ calcd for $C_{63}H_{77}N_4S_3$, 985.5310; found, 985.5313.

5,10,15-Tris(anilin-4-ylthio)-2,3,7,8,12,13,17,18-octaethylporphyrin 193: Compound **95** (30 mg, 42 μmol, 1 equiv) and 4-aminobenzenethiol (**HSAr³**, 41 mg, 0.33 mmol, 7.8 equiv) were dissolved in 6 mL of chloroform and TEA (3 drops) was added. The resulting solution was stirred at 25 °C for 20 min. After removal of the solvent at reduced pressure, the residue was purified by column chromatography (SiO_2, hexane:ethyl acetate, 75:1–0:1, v/v) and compound **193** was obtained as a green solid (15 mg, 16.8 μmol, 40%) upon removal of the solvent. mp: 98–102 °C dec. R_f: 0.13 (SiO_2, ethyl acetate). ^{1}H NMR (400.13 MHz, $CDCl_3$, δ): 0.96–1.01 (m, 12H), 1.47–1.55 (m, 12H), 3.00–4.00 (m, 22H), 6.29-6.36 (m, 2H), 6.36–6.44 (m, 2H), 6.52–6.65 (m, 2H), 6.70–6.85 (m, 2H), 8.63 ppm (s, 1H). ^{13}C {^{1}H} NMR (100.61 MHz, $CDCl_3$, δ): 16.1, 17.1, 17.4, 17.6, 19.3, 22.1, 27.1, 115.1, 116.1 (× 2), 128.4, 128.7, 134.1, 144.2, 144.6 ppm. UV-vis (DCM) λ_{max} (log ε): 478 (4.23), 626 (3.32), 755 nm (3.30). HRMS–MALDI (*m/z*): $[M + H]^+$ calcd for $C_{54}H_{62}N_7S_3$, 904.4229; found, 904.4254.

5,10,15-Tris(anthracen-9-ylthio)-2,3,7,8,12,13,17,18-octaethylporphyrin 194: Compound **95** (40 mg, 56 μmol, 1 equiv), 9-anthracenethiol (**HSAr[4]**, 103 mg, 0.49 mmol, 8.8 equiv) and TEA (3 drops) were reacted at 25 °C in chloroform (8 mL) until completion, as indicated by TLC analysis. After removal of the solvent *in vacuo*, column chromatography was performed (SiO_2, hexane:ethyl acetate, 75:1–0:1, v/v) to remove less polar side products. The first major fraction was collected, the solvent was removed and recrystallization by slow diffusion from DCM and petroleum ether gave **194** as a green solid (23 mg, 19.6 μmol, 35%). mp: 138–142 °C dec. R_f: 0.39 (SiO_2, ethyl acetate). ^{1}H NMR (400.13 MHz, $CDCl_3$, δ): 0.56–0.74 (m, 12H), 1.20–1.35 (m, 6H), 1.36–1.53 (m, 6H), 2.41–2.57 (m, 4H), 2.71–2.87 (m, 4H), 2.99–3.13 (m, 4H), 3.19–3.38 (m, 4H), 6.70–6.93 (m, 2H), 6.99–7.11 (m, 4H), 7.26–7.35 (m, 6H), 7.60 (s, 1H), 7.87–8.01 (m, 8H), 8.01–8.12 (m, 2H), 8.28–8.43 ppm (m, 7H). ^{13}C {^{1}H} NMR (100.61 MHz, $CDCl_3$, δ): 16.4, 16.6 (× 2), 17.0, 18.9, 19.2, 21.1, 22.6, 53.6, 91.7, 125.2, 125.6, 126.1, 126.3, 128.0, 128.7, 128.9, 130.3, 130.9, 131.6 (× 2), 131.8, 132.0, 132.2, 142.6 ppm. UV-vis (toluene) λ_{max} (log ε): 417 (4.77), 489 (4.67), 678 (3.96), 753 nm (3.88). HRMS–MALDI (*m/z*): $[M + H]^+$ calcd for $C_{78}H_{71}N_4S_3$, 1159.4841; found, 1159.4828. MS–MALDI *m/z* (% relative intensity, ion): 503 (100), 531 (81, M − 3SAr), 741 (65, M − 2SAr + H), 950 (12, M − SAr).

2,3,7,8,12,13,17,18-Octaethyl-5,10,15,20-tetrakis(phenylthio)porphyrin 195: A sample tube was charged with H_2OETNP (**95**, 30 mg, 42 μmol, 1 equiv) and 6 mL of chloroform. Upon addition of thiophenol (**HSAr[5]**, 20 mg, 0.19 mmol, 4.4 equiv) and TEA (3 drops), the mixture was allowed to react at 25 °C for 5 min. The solvent was removed *in vacuo* and the crude product was purified by column chromatography (SiO_2, hexane:ethyl acetate, 75:1–0:1, v/v). After elution of less polar side products, the title compound was obtained as a green solid (35 mg, 36.1 μmol, 86%) upon evaporation of the solvent. Recrystallization by slow evaporation (hexane:ethyl acetate, 10:1, v/v) yielded green crystals. mp: 209–212 °C dec. R_f: 0.48 (SiO_2, hexane:ethyl acetate, 2:1, v/v). ^{1}H NMR (400.13 MHz, $CDCl_3$, δ): 0.93–1.32 (m, 24H), 2.85–3.53 (m, 16H), 6.89–7.16 ppm (m, 20H). ^{13}C {^{1}H} NMR (100.61

MHz, $CDCl_3$, δ): 16.8, 20.2, 125.3, 126.0, 129.1, 142.4 ppm. UV-vis (DCM) λ_{max} (log ε): 487 (4.82), 584 (3.63), 639 (3.66), 748 nm (3.54). HRMS–MALDI (*m/z*): $[M + H]^+$ calcd for $C_{60}H_{63}N_4S_4$, 967.3936; found, 967.3948. MS–MALDI *m/z* (% relative intensity, ion): 611 (100), 857 (10, M − SAr).

2,3,7,8,12,13,17,18-Octaethyl-5,10,15,20-tetrakis(pyridine-2-ylthio)porphyrin 196: Tetrapyrrole **95** (10 mg, 14 μmol, 1 equiv), 2-mercaptopyridine (**HSAr^6**, 7.2 mg, 65 μmol, 4.4 equiv) and TEA (3 drops) were reacted at 25 °C in chloroform until completion, as indicated by TLC analysis. The solvent was removed *in vacuo* and column chromatography (SiO_2, ethyl acetate) was performed to remove less polar side products. The title compound was obtained as a green solid (9.5 mg, 9.1 μmol, 65%) after recrystallization by slow evaporation (acetone:water, 10:1, v/v). mp: 205–210 °C dec. R_f: 0.13 (SiO_2, ethyl acetate). ^{1}H NMR (400.13 MHz, $CDCl_3$, δ): 0.94–1.21 (m, 12H), 1.35–1.76 (m, 12H), 2.72–3.67 (m, 16H), 6.02–6.67 (m, 4H), 6.94–7.17 (m, 8H), 8.43–8.58 ppm (m, 4H). ^{13}C {^{1}H} NMR (100.61 MHz, $CDCl_3$, δ): 16.5, 20.2, 120.0, 120.8, 136.8, 142.6, 149.6, 165.7 ppm. UV-vis (DCM) λ_{max} (log ε): 482 (5.06), 579 (3.90), 635 (3.83), 744 nm (3.52). HRMS–MALDI (*m/z*): $[M + H]^+$ calcd for $C_{56}H_{59}N_8S_4$, 971.3740; found, 971.3713. MS–MALDI *m/z* (% relative intensity, ion): 529 (100, M − 4SAr – H), 530 (86, M − 4SAr), 640 (38, M − 3SAr), 751 (4, M − 2SAr + H).

2,3,7,8,12,13,17,18-Octaethyl-5,10,15,20-tetrakis[(4-isopropylphenyl)thio]porphyrin 197: 4-Isopropylbenzenethiol (**HSAr^7**, 28 mg, 0.19 mmol, 4.4 equiv) was added to a solution of porphyrin **95** (30 mg, 42 μmol, 1 equiv) in 4 mL of chloroform and TEA (3 drops) was added. The reaction mixture was stirred at 25 °C for 5 min, the color changed from brown to dark red and the crude product was purified by column chromatography (SiO_2, hexane:ethyl acetate, 75:1–2:1, v/v). After separation of less polar side products, **197** was obtained as a green solid (30 mg, 26.5 μmol, 63%) upon removal of the solvent. mp: 107–110 °C dec. R_f: 0.31 (SiO_2, hexane:ethyl acetate, 8:1, v/v). ^{1}H NMR (400.13 MHz, $CDCl_3$, δ): 0.93–1.25 (m, 24H), 1.14–1.20 (m, 24H), 2.72–2.85 (m,

4H), 2.72–3.46 (m, 16H), 6.81–6.98 ppm (m, 16H). ^{13}C {^{1}H} NMR (100.61 MHz, $CDCl_3$, δ): 16.8, 20.1, 24.1, 33.7, 126.4, 126.8, 127.1,133.4, 136.8, 139.2, 145.9 ppm. UV-vis (DCM) λ_{max} (log ε): 490 (5.64), 586 (4.49), 641 (4.52), 750 nm (4.27). HRMS–MALDI (*m/z*): $[M + H]^+$ calcd for $C_{72}H_{87}N_4S_4$, 1135.5814; found, 1135.5806. MS–MALDI *m/z* (% relative intensity, ion): 956 (100), 834 (84, M − 2SAr + H), 681 (78, M − 3SAr), 984 (56, M − SAr), 531 (23, M − 4SAr + H).

2,3,7,8,12,13,17,18-Octaethyl-5,10,15,20-tetrakis(naphthalen-2-ylthio)porphyrin 198: Porphyrin **95** (50 mg, 70 μmol, 1 equiv), 2-naphthalenethiol (**HSAr[8]**, 47 mg, 0.29 mmol, 4 equiv) and TEA (3 drops) were reacted in chloroform (10 mL) at 25 °C for 5 min in which the color changed from brown to dark red. The solvent was removed *in vacuo* and column chromatography (SiO_2, hexane:ethyl acetate, 75:1–0:1, v/v) was performed. After elution of less polar side products, porphyrin **198** was obtained as a green solid upon removal of the solvent. Recrystallization by slow evaporation (hexane:ethyl acetate, 10:1, v/v) gave **198** as green crystals (40 mg, 32.2 μmol, 46%). mp: 168–170 °C dec. R_f: 0.37 (SiO_2, hexane:ethyl acetate, 2:1, v/v). ^{1}H NMR (400.13 MHz, $CDCl_3$, δ): 0.93–1.15 (m, 12H), 1.39–1.64 (m, 12H), 2.50–3.57 (m, 16H), 6.83–7.14 (m, 8H), 7.28–7.41 (m, 8H), 7.41–7.49 (m, 4H), 7.50–7.63 ppm (m, 8H). ^{13}C {^{1}H} NMR (100.61 MHz, $CDCl_3$, δ): 16.8, 20.1, 23.5, 24.8, 28.5, 36.7, 123.9, 124.7, 125.4, 126.6, 127.3, 127.9, 128.7, 131.6, 134.0, 140.0 ppm. UV-vis (DCM) λ_{max} (log ε): 493 (5.32), 586 (4.18), 640 (4.20), 751 nm (4.05). HRMS–MALDI (*m/z*): $[M + H]^+$ calcd for $C_{76}H_{71}N_4S_4$, 1167.4562; found, 1167.4557. MS–MALDI *m/z* (% relative intensity, ion): 689 (100, M − 3SAr), 849 (84, M − 2SAr + H), 1008 (72, M – SAr + H), 531 (24, M − 4SAr + H).

2,3,7,8,12,13,17,18-Octaethyl-5,10,15,20-tetrakis[(2,3,4,5,6-pentafluorophenyl)thio]porphyrin 199: In a sample tube, H_2OETNP (**95**, 20 mg, 28 μmol, 1 equiv) was dissolved in chloroform (3 mL). Then, perfluorobenzenethiol (**HSAr[9]**, 25 mg, 0.12 mmol, 4.4 equiv) and TEA (3 drops) were added and the solution was stirred at 25 °C for 5 min. To prevent consecutive decomposition of **199** with reactive species, the

reaction mixture was washed with 3 × 10 mL of aqueous sodium hydroxide solution (2 M). The organic phase was dried using $MgSO_4$, filtered and the solvent was removed *in vacuo*. Column chromatography (SiO_2, hexane:ethyl acetate, 75:1–5:1, v/v) gave **199** as a green solid (15.9 mg, 12.0 μmol, 43%) after separation of less polar side products. mp: 86–87 °C dec. R_f: 0.90 (SiO_2, hexane:ethyl acetate, 8:1, v/v). ^{1}H NMR (400.13 MHz, $CDCl_3$, δ): 1.07–1.18 (m, 24H), 2.97–3.42 ppm (m, 16H). ^{13}C {^{1}H} NMR (100.61 MHz, $CDCl_3$, δ): 16.1, 19.3, 34.9, 36.8, 46.4, 53.1, 108.2, 111.3, 111.5, 111.6, 117.8, 136.4, 138.9, 139.7, 142.2, 145.1, 147.6 ppm. ^{19}F NMR (376.59 MHz, $CDCl_3$, δ): −160.9 (s, 8F), −153.4 (s, 4F), −135.6 ppm (s, 8F). UV-vis (DCM) λ_{max} (log ε): 471 (4.68), 577 (3.69), 621 nm (3.76). HRMS–MALDI (*m/z*): $[M + H]^+$ calcd for $C_{60}H_{43}N_4S_4F_{20}$, 1327.2051; found, 1327.2039. MS–MALDI *m/z* (% relative intensity, ion): 150 (100), 729 (43, M − 3SAr), 929 (35, M − 2SAr + H), 531 (32, M − 4SAr + H), 1127 (31, M − SAr).

2,3,7,8,12,13,17,18-Octaethyl-5,10,15,20-tetrakis(phenanthren-9-ylthio)porphyrin 200: Porphyrin **95** (30 mg, 42 μmol, 1 equiv) and 9-phenanthrenethiol (**HSAr[10]**, 39 mg, 0.19 mmol, 4.4 equiv) were dissolved in chloroform (4 mL) and TEA (3 drops) was added. The mixture was then stirred at 25 °C until completion, as indicated by TLC analysis. After removal of the solvent at reduced pressure, the residue was chromatographed (SiO_2, hexane:ethyl acetate, 75:1–2:1, v/v) and the main fraction gave 10 mg (7.1 μmol, 17%) of the green solid **200** after elution of less polar side products. mp: 194–195 °C dec. R_f: 0.40 (SiO_2, hexane:ethyl acetate, 3:1, v/v). ^{1}H NMR (400.13 MHz, $CDCl_3$, δ): 0.82–1.24 (m, 24H), 2.56–3.49 (m, 16H), 6.78–7.21 (m, 8H), 7.29–7.72 (m, 8H), 7.73–7.88 (m, 8H), 8.49–8.89 ppm (m, 12H). ^{13}C {^{1}H} NMR (100.61 MHz, $CDCl_3$, δ): 16.8, 20.3, 24.8, 29.5, 31.1, 36.8, 53.9, 122.5, 123.4, 124.1, 126.1, 127.0, 127.3, 128.0, 128.8, 129.7, 130.7, 132.3, 138.8, 143.1 ppm. UV-vis (DCM) λ_{max} (log ε): 490 (3.81), 495 (4.81), 642 nm (3.85). HRMS–MALDI (*m/z*): M^+ calcd for $C_{92}H_{78}N_4S_4$, 1366.5109; found, 1366.5090. MS–MALDI *m/z* (% relative intensity, ion): 950 (100), 1159 (92, M − SAr). 739 (73, M − 3SAr), 949 (41, M − SAr + H), 531.35 (17, M − 4SAr + H).

2,3,7,8,12,13,17,18-Octaethyl-5,10,15-tris[(4-methoxyphenyl)thio]porphyrin 201 and 2,3,7,8,12,13,17,18-octaethyl-5,10,15,20-tetrakis[(4-methoxyphenyl)thio]porphyrin 202: Porphyrin **95** (10 mg, 14 μmol, 1 equiv), 4-methoxybenzenethiol (**HSAr[11]**, 8.4 mg, 60 μmol, 4 equiv) and TEA (3 drops) were reacted in chloroform (2 mL) for 5 min at 25 °C During that time, the color changed from brown to red. Purification by preparative TLC (SiO_2, ethyl acetate) yielded an impure and inseparable mixture of the title compounds (combined yield < 5%), as indicated by HRMS. **201**: HRMS–MALDI (*m/z*): $[M + H]^+$ calcd for $C_{57}H_{65}N_4O_3S_3$, 949.4213; found, 949.4241. **202**: HRMS–MALDI (*m/z*): M^+ calcd for $C_{64}H_{71}N_4O_4S_4$, 1087.4358; found, 1087.4333.

{2,3,7,8,12,13,17,18-Octaethyl-5,10-dinitroporphyrinato}nickel(II) 204 and (2,3,7,8,12,13,17,18-octaethyl-10,15-dinitro-5-(pyridin-2-ylthio)porphyrinato}nickel(II) 205: Compound **95** (29 mg, 41 μmol, 1 equiv), 2-mercaptopyridine (**HSAr[6]**, 18 mg, 0.16 mmol, 4 equiv) and TEA (3 drops) were reacted in chloroform (5 mL) for 15 h at 25 °C after which another 4 equiv of **HSAr[6]** were added. Completion of the reaction was then achieved after 15 minutes, as indicated by TLC analysis. The solvent was removed *in vacuo* and column chromatography (SiO_2, hexane:DCM, 2:1, v/v) was performed. After elution of less polar side products and unconsumed **95**, collection of the first major fraction gave the pink solid **204** (7.0 mg, 10.3 μmol, 25%) upon removal of the solvent and recrystallization by slow evaporation (hexane:DCM, 10:1, v/v). A second column chromatography (SiO_2, hexane:ethyl acetate, 75:1, v/v) was performed with a mixture of the more polar fractions which yielded **205** (6.1 mg, 8.2 μmol, 20%) after elution of impurities and removal of the solvent. **204**: mp: > 300 °C. R_f: 0.60 (SiO_2, hexane:DCM, 2:1, v/v). ^1H NMR (400.13 MHz, $CDCl_3$, δ): 1.36–1.47 (m, 12H), 1.67–1.77 (m, 12H), 3.40–3.51 (m, 8H), 3.73–3.84 (m, 8H), 9.53 ppm (s, 2H). ^{13}C $\{^1H\}$ NMR (100.61 MHz, $CDCl_3$, δ): 17.8, 17.9, 18.1, 18.2, 19.7, 20.2, 20.6, 98.5, 129.8, 131.7, 132.6, 141.7, 142.6, 142.8, 144.0, 145.3, 147.4 ppm. UV-vis (DCM) λ_{max} (log ε): 400.13 (4.84), 531 (3.77), 567 nm (4.04). HRMS–MALDI (*m/z*): M^+ calcd for $C_{36}H_{42}N_6NiO_4$, 680.2621; found, 680.2627. **205**: mp: 151–153 °C dec. R_f: 0.13 (SiO_2, hexane:DCM, 2:1, v/v). ^1H NMR

(400.13 MHz, $CDCl_3$, δ): 1.12–1.16 (m, 3H), 1.37–1.49 (m, 9H), 1.61–1.67 (m, 12H), 3.21–4.20 (m, 16H), 6.53–6.55 (m, 1H), 6.61–6.62 (m, 1H), 7.28 (s, 1H), 8.16–8.19 (m, 1H), 9.20 ppm (s, 1H). ^{13}C {^1H} NMR (100.61 MHz, $CDCl_3$, δ): 17.2, 17.6 (× 2), 17.7, 17.8, 17.9, 18.0, 19.4, 19.5, 20.0, 20.1, 20.2, 20.5, 22.1, 22.9, 98.6, 103.0, 119.3, 119.9, 129.7, 130.6 (× 2), 131.4, 132.0, 132.6, 136.8, 140.7, 142.1, 143.2, 145.1, 145.7, 145.8, 146.1, 148.0, 148.6, 149.3, 149.6, 150.2, 163.1 ppm. UV-vis (DCM) λ_{max} (log ε): 430 (4.40), 560 (3.43), 600 nm (3.57). HRMS–MALDI (*m/z*): M^+ calcd for $C_{41}H_{45}N_7NiO_4S$, 789.2607; found, 789.2629.

Denitration Reactions

2,3,7,8,12,13,17,18-Octaethyl-5,20-dinitroporphyrin 206[253] **and 2,3,7,8,12,13,17,18-octaethyl-5,15-dinitroporphyrin 207:**[253] 1,2-Ethanedithiol (**HSAr^{12}**, 19 mg, 0.20 mmol, 7 equiv) and TEA (3 drops) were added to a solution of **95** (20 mg, 28 μmol, 1 equiv) in chloroform (1.5 mL). After 40 min, the solvent was removed at reduced pressure and the crude product was purified *via* column chromatography (SiO_2, hexane:DCM, 2:1, v/v). The first fraction yielded **207** as a purple solid (3.7 mg, 5.9 μmol, 21%), mp: 282–284 °C (lit.[253] mp: 280–282 °C), after removal of the solvent while the second fraction gave the purple solid **206** (4.2 mg, 6.7 μmol, 24%), mp: 227–230°C (lit.[253] mp: 224–226 °C), upon evaporation of the solvent. A third fraction yielded tetrapyrrole **208** as a side product (< 10%).

2,3,7,8,12,13,17,18-Octaethyl-5-nitroporphyrin 208:[253] Tetrapyrrole **95** (10 mg, 14 μmol, 1 equiv) and 2-mercaptoethanol (**HSAr^{13}**, 13 mg, 0.17 mmol, 12 equiv) were dissolved in DCM (2 mL) and TEA (3 drops) was added. After 15 min at 40 °C, the solvent was removed at reduced pressure and the crude product was purified by column chromatography (SiO_2, hexane:DCM, 2:1, v/v). This yielded the purple solid **208** (4.1 mg, 6.9 μmol, 49%) upon removal of the solvent: mp: 255–258 °C (lit.[253] mp: 251–252 °C).

2,3,7,8,12,13,17,18-Octaethylporphyrin 48:[254] Porphyrin **95** (15 mg, 21 μmol, 1 equiv) and benzyl mercaptan (**HSAr^{14}**, 107 mg, 0.86 mmol,

41 equiv) were dissolved in 1.5 mL of DCM and TEA (0.1 mL) was added. This was allowed to react at 40 °C until completion, as indicated by TLC analysis (72 h). After removal of the solvent *in vacuo*, the crude product was purified *via* column chromatography (SiO_2, hexane:DCM, 2:1–1:1, v/v). A red band was collected to give tetrapyrrole **48** (5.5 mg, 10.3 μmol, 49%): mp: > 300 °C (lit.[254] mp: 324–325 °C).

Synthesis of Type I Porphyrins

3-Ethyl-4-isopropylpyrrole 182: Pyrrole **177** (4.0 g, 26.50 mmol, 1 equiv) in 70 mL THF was added dropwise to a suspension of $LiAlH_4$ (3.14 g, 82.70 mmol, 3.1 equiv) in 20 mL THF at 0 °C. After that, the reaction mixture was left to stir for 1 h at RT and heated to 66 °C for 17 h. Upon careful hydrolysis with *ca*. 150 mL of a 2 M sodium hydroxide solution at 0 °C, Et_2O was added and the layers were separated. The aqueous phase was extracted with Et_2O and the combined organic layers were washed with water, dried using $MgSO_4$, filtered, and the solvent was removed *in vacuo*. The title compound was obtained as a yellow oil (3.05 g, 22.26 mmol, 84%). R_f: 0.55 (SiO_2, hexane). ^{1}H NMR (400.13 MHz, $CDCl_3$, δ): 1.36–1.42 (m, 9H), 2.68 (q, J = 7.5 Hz, 2H), 3.02 (sept, J = 6.8 Hz, 1H), 6.65 (d, J = 2.7 Hz, 2H), 7.91 ppm (s, 1H). ^{13}C {^{1}H} NMR (100.61 MHz, $CDCl_3$, δ): 14.6, 18.5, 24.0, 25.2, 113.3, 114.6, 124.0, 129.8 ppm. HRMS−APCI (*m/z*): $[M + H]^+$ calcd. for $C_9H_{16}N$, 138.1277; found, 138.1281. MS–APCI *m/z* (% relative intensity, ion): 96.07 (100, M – C_3H_7 (likely *i*-Pr) + 2H). IR (ATR): $\tilde{\nu}$ = 2959, 2931, 2870, 1670, 1640, 1462, 1379, 1076, 896, 776 cm^{-1}.

3-(1-Phenylvinyl)pyrrole 262: Pyrrole **258** (2.63 g, 7.70 mmol, 1 equiv) and potassium hydroxide (16.34 g, 0.29 mol, 42 equiv) were dissolved in 20 mL methanol and the suspension was heated to *ca*. 65 °C for 14 h. After removal of the solvent *in vacuo*, water and DCM were added to the residue and the layers were separated. The aqueous phase was extracted with DCM and the combined organic layers were washed with water, dried using $MgSO_4$, filtered, and the solvent was removed at reduced pressure to yield the title compound as a dark oil (1.16 g, 6.85 mmol, 89%). R_f: 0.25 (SiO_2, hexane). ^{1}H NMR (400.13 MHz, $CDCl_3$, δ):

5.09 (d, *J* = 1.5 Hz, 1H), 5.43 (d, *J* = 1.5 Hz, 1H), 6.38–6.42 (m, 1H), 6.66–6.70 (m, 1H), 6.77–6.81 (m, 1H), 7.30–7.38 (m, 3H), 7.45–7.50 (m, 2H), 8.15 ppm (s, 1H). ^{13}C {^{1}H} NMR (100.61 MHz, $CDCl_3$, δ): 107.6, 109.8, 117.6, 118.6, 125.3, 127.6, 128.1, 128.4, 142.6, 144.1 ppm. HRMS−APCI (*m/z*): [M + H]$^+$ calcd. for $C_{12}H_{12}N$, 170.0964; found, 170.0968. MS–APCI *m/z* (% relative intensity, ion): 103.04 (100), 170.09 (20). IR (ATR): $\tilde{\nu}$ = 3211, 3056, 2930, 1678, 1610, 1549, 1492, 1444, 1423, 1374, 1332, 1251, 1231, 1182, 1181, 1156, 1118, 1096, 1079, 1027, 947, 882, 801, 773, 718, 698, 674, 645, 570 cm^{-1}.

2,7,12,17-Tetraethyl-3,8,13,18-tetraisopropyl-5,10,15,20-tetraphenyl-22*H*,24*H*-porphyrindiium dihydrochloride 243·2HCl: 3-Ethyl-4-isopropylpyrrole (**182**, 1.0 g, 7.29 mmol, 1 equiv) and benzaldehyde (0.77 g, 7.29 mmol, 1 equiv) were dissolved in dry DCM (1 L) and boron trifluoride diethyl etherate (90 μL, 0.73 mmol, 10 mol%) was added. This was reacted for 22 h at RT followed by the addition of DDQ (7.28 g, 32.1 mmol, 4.4 equiv). The solution became purple and was left to stir for another hour. The solvent was removed at reduced pressure, the residue dissolved in DCM and pushed through a plug of Al_2O_3, Brockman grade III, using DCM, mixtures of DCM and ethyl acetate, and eventually mixtures of ethyl acetate and methanol in order to partly separate the relevant green fractions. These were evaporated to dryness and chromatographed on Al_2O_3, Brockman grade III, using DCM:ethyl acetate, 2:1, v/v. A major green band was isolated, which contained the title compound. After drying *in vacuo*, **243**·2HCl was obtained as a green solid (172 mg, 0.66 mmol, 9%). mp: > 300 °C. R_f: 0.34 (Al_2O_3, DCM:ethyl acetate, 10:1, v/v). ^{1}H NMR (400.13 MHz, $CDCl_3$, δ): −0.34 (s, 4H), −0.17–0.58 (m, 24H), 1.38–1.55 (m, 12H), 2.12–2.33 (m, 4H), 2.41–2.74 (m, 8H), 7.73–7.98 (m, 12H), 8.39–8.72 ppm (m, 8H). ^{13}C {^{1}H} NMR (100.61 MHz, $CDCl_3$, δ): 14.7, 15.9, 16.4, 16.5, 16.6, 16.7 (× 3), 19.6 (× 2), 19.8, 23.0, 23.1, 23.2 (× 2), 23.3 (× 2), 27.4, 27.5, 32.2, 118.1, 118.2, 118.5, 118.7 (× 2), 118.8, 119.1, 128.7, 128.8, 128.9 (× 2), 129.0 (× 2), 129.1, 130.0 (× 2), 130.1, 130.7, 134.3, 137.3, 137.4 (× 2), 137.6, 137.7, 137.8 (× 2), 137.9 (× 2), 138.4, 138.7, 138.9, 139.1 (× 2), 139.2, 139.3, 139.5, 139.7, 139.9, 140.2, 140.8, 140.9, 141.1, 141.2 (× 2), 141.5,

144.9, 145.0 (× 2), 145.1, 145.2, 145.4, 145.5, 145.6, 145.7 (× 2), 145.8, 145.9, 146.0, 146.2 ppm. UV-vis (DCM) λ_{max} (log ε): 484 (5.57), 646 (4.09), 703 nm (4.69). HRMS−MALDI (*m/z*): $[M - H - 2Cl]^+$ calcd. for $C_{64}H_{71}N_4$, 895.5673; found, 895.5670.

{2,7,12,17-Tetraethyl-3,8,13,18-tetraisopropyl-5,10,15,20-tetraphenylporphyrinato}nickel(II) 244: Porphyrin **243**·2HCl (60.3 mg, 62 µmol, 1 equiv) and $Ni(acac)_2$ (159 mg, 0.62 mmol, 10 equiv) were dissolved in 0.6 mL DMF and heated to 153 °C for 20 h during which the reaction mixture turned from green to purple. After cooling to RT, water and DCM were added and the layers were separated. The aqueous phase was extracted with DCM and the combined organic layers were washed with water, dried using $MgSO_4$, filtered, and the solvent was evaporated *in vacuo*. The purple crude product was purified by column chromatography (Al_2O_3, Brockman grade III, using DCM:petroleum ether, 1:10, v/v). The first fraction, a purple band, was isolated and upon evaporation of the solvent, the title compound was obtained as a purple solid (51 mg, 53.3 µmol, 86%). mp: > 300 °C. R_f: 0.61 (SiO_2, hexane:DCM, 5:1, v/v). ^{1}H NMR (400.13 MHz, $CDCl_3$, δ): 0.33–0.49 (m, 12H), 0.54–0.77 (m, 12H), 1.26–1.45 (m, 12H), 1.79–2.09 (m, 4H), 2.52–2.83 (m, 8H), 7.53–7.70 (m, 12H), 7.94–8.21 ppm (m, 8H). ^{13}C {^{1}H} NMR (100.61 MHz, $CDCl_3$, δ): 17.6, 20.4, 23.2, 26.7, 26.8, 26.9, 127.0, 127.3, 127.6, 127.8, 127.9, 128.1, 134.2, 134.7, 135.3, 140.7, 146.3, 146.5, 148.7, 148.9 ppm. UV-vis (DCM) λ_{max} (log ε): 444 (5.33), 593 (4.15), 599 nm (4.01). HRMS−MALDI (*m/z*): $[M - H - 2Cl]^+$ calcd. for $C_{64}H_{68}N_4Ni$, 950.4797; found, 950.4785.

2,7,12,17-Tetraethyl-3,8,13,18-tetraisopropyl-5,10,15,20-tetrakis(4-methoxyphenyl)-22*H*,24*H*-porphyrindiium dihydrochloride 245·2HCl:

Similar to the synthesis of **243**·2HCl, 3-ethyl-4-isopropylpyrrole (**182**, 500 mg, 3.60 mmol, 1.1 equiv) and 4-methoxybenzaldehyde (0.40 mL, 3.30 mmol, 1.0 equiv) were dissolved in 500 mL dry DCM and $BF_3{\cdot}OEt_2$ (43 µL, 0.33 mmol, 10 mol%) was added. This was reacted at RT for 21 h during which the reaction mixture turned red, followed by DDQ addition (3.30 g, 14.52 mmol, 4.4 eq.). After stirring for another 2 h, the solvent

was removed *in vacuo* and the residue dissolved in DCM and filtered through Al_2O_3, Brockman grade IIII, using DCM and DCM:ethyl acetate mixtures up to pure ethyl acetate to remove DDQ derivatives and other non-porphyrin material. Then, DCM:methanol, 1:1, v/v was applied to isolate a green–brown fraction. The relevant fractions, which had brown or green–brown colors were combined upon TLC analysis and the solvent was evaporated. The crude product was then subjected to column chromatography. Column chromatography (Al_2O_3, Brockman grade IIII) was performed using DCM to remove brown impurities, then DCM:ethyl acetate, 10:1, v/v to isolate a light green fraction of **245**·2HCl, giving a green solid (27 mg, 0.10 mmol, 3%) upon evaporation of the solvent. Second, a porphyrin that was devoid of two CH_3 fragments when compared to **245**, as indicated by HRMS analysis was eluted as a dark green band, yielding a green solid (5 mg, < 1%) after evaporation of the solvent. mp: = 286–290 °C (dec.) R_f: 0.67 (Al_2O_3, DCM:ethyl acetate, 10:1, v/v). ^{1}H NMR (400.13 MHz, $CDCl_3$, δ): 0.02–0.24 (m, 12H), 0.25–0.38 (m, 12H), 1.44–1.54 (m, 12H), 2.21–2.39 (m, 4H), 2.44–2.71 (m, 8H), 4.09 (s, 3H), 4.11 (s, 6H), 4.12 (s, 3H), 7.35–7.44 (m, 8H) 8.31–8.55 ppm (m, 8H). ^{13}C {^{1}H} NMR (100.61 MHz, $CDCl_3$, δ): 15.7, 15.8, 15.9 (× 2), 16.0, 19.1, 26.6, 26.7, 113.7, 114.1 (× 2), 116.6, 116.8, 117.2, 117.4, 117.7, 118.0, 130.4, 131.5, 131.8, 132.7, 133.0, 137.5, 137.8, 137.9, 138.0, 138.1, 138.4, 138.5 (× 2), 138.6, 139.6, 139.7, 140.0, 140.5, 144.8, 144.9, 145.0, 145.3, 145.4, 145.6, 145.7, 145.8, 146.0, 146.3, 146.5, 161.0, 161.1 ppm. UV-vis (DCM) λ_{max} (log ε): 486 (5.63), 722 nm (4.87). HRMS−MALDI (*m/z*): $[M - H - 2Cl]^+$ calcd. for $C_{68}H_{79}N_4O_4$, 1015.6101; found, 1015.6074.

2,7,12,17-Tetraethyl-3,8,13,18-tetraisopropyl-5,10,15,20-tetrakis(2,6-dichlorophenyl)porphyrin 246: Similar to the synthesis of **243**·2HCl, 3-ethyl-4-isopropylpyrrole (**182**, 1.0 g, 7.30 mmol, 1.1 equiv) and 2,6-dichlorobenzaldehyde (1.16 g, 6.60 mmol, 1.0 equiv) were dissolved in 1 L of dry DCM. Upon addition of $BF_3{\cdot}OEt_2$ (50 µL, 0.38 mmol, 6 mol%) this was left to stir for 21 h during which the solution turned purple. Then, DDQ (6.59 g, 29.04 mmol, 4.4 equiv) was added and the reaction mixture was stirred for another 2 h. The deep purple solution was filtered through

Al_2O_3, Brockman grade III, using DCM to remove impurities and then ethyl acetate followed by methanol to separate fractions that contained porphyrin. The relevant fractions were combined and purified *via* column chromatography (Al_2O_3, Brockman grade III) using DCM, mixtures of DCM and ethyl acetate, and ultimately ethyl acetate and ethyl acetate + 10% methanol. Elution of porphyrin was indicated by a green color. The impure porphyrin solutions were combined and subjected to a second and a third chromatography (Al_2O_3, Brockman grade III) using DCM and ethyl acetate where the amount of ethyl acetate was slowly increased. This yielded 9 mg (7.8 µmol, < 1%) of **246** as a green solid after evaporation of the solvent and drying *in vacuo* for 12 h. The presence of a porphyrin that was devoid of two CH_3 fragments when compared to **246** was indicated by HRMS analysis of the crude product before the third column chromatography. mp: > 300 °C. R_f: 0.30 (Al_2O_3, ethyl acetate). ^{1}H NMR (400.13 MHz, $CDCl_3$, δ): −1.07 (s, 2H), 0.47–0.68 (m, 12H), 0.75–0.92 (m, 12H), 1.32–1.47 (m, 12H), 2.04–2.36 (m, 4H), 2.59–3.06 (m, 8H), 7.35–7.84 (m, 12H). ^{13}C {^{1}H} NMR (100.61 MHz, $CDCl_3$, δ): 15.9, 16.0, 20.3, 22.2, 22.3, 22.5, 22.7, 23.0, 26.3, 26.7, 111.5, 127.8, 128.0, 128.4, 128.6, 129.1, 129.7, 130.0, 130.2, 130.4, 131.6, 133.6, 136.3, 138.2, 139.6, 140.2, 140.5, 141.0, 141.3 ppm. UV-vis (DCM) λ_{max} (log ε): 477 (4.95), 587 (3.72), 651 (3.80), 707 nm (3.44). HRMS−MALDI (*m/z*): $[M + H]^+$ calcd. for $C_{64}H_{63}N_4Cl_8$, 1167.2561; found, 1167.2582.

Catalyst Screening. For small amounts of material, microliter syringes and an analytical balance were used. All reactions were carried out in 1 mL screw-cap vials ([cat.] = $7.1\cdot10^{-2}$ M), 5 mL round-bottom flasks ([cat.] = $3.6\cdot10^{-3}$ M), or 10 mL round bottom flasks ([cat.] = $2.5\cdot10^{-2}$ M, $3.5\cdot10^{-2}$ M, $5.0\cdot10^{-2}$ M, and $1.0\cdot10^{-3}$ M, $1.5\cdot10^{-3}$ M, $4.0\cdot10^{-3}$ M) under a protective argon atmosphere. All solvents used were purified before use as appropriate. All reactions were set up in pairs of two and for each reaction pair, a blank sample without catalyst was set up, too.

For example, corresponding to entry 1, Table 8: The nucleophile (43.8 µL; $7.05\cdot10^{-2}$ mmol; 1 equiv), catalyst (5.92 mg; $7.05\cdot10^{-3}$ mmol; 3 mol%), and Michael acceptor (43.5 mg for; $7.76\cdot10^{-2}$ mmol; 1.1 equiv) were dissolved in DCM (0.1 or 2 mL according to Table 8) and the mixture

was stirred in the dark at RT for 24 h. At the end of each reaction, the internal standard (CH_2Br_2, 8.25 µL; $3.53 \cdot 10^{-2}$ mmol; 0.5 equiv) was added into the reaction mixture and a ^1H NMR spectrum was recorded. The conversion was determined *via* quantitative ^1H NMR by comparison of the product integrals with the integrals of the internal standard.

Crystallography

Crystallographic data was collected and solved by Dr. K. J. Flanagan.

Crystal Structure Determinations. Crystals were grown following the protocol developed by Hope, by dissolving the compounds in DCM, layering with methanol or hexane and allowing for slow diffusion over time. In some cases, this was aided by slow evaporation once the layers had mixed completely.[255] Diffraction data for all compounds were collected on a Bruker APEX 2 DUO CCD diffractometer by using graphite-monochromated MoK_α radiation (λ = 0.71073 Å) and Incoatec IμS CuK_α radiation (λ = 1.54178 Å). Crystals were mounted on a MiTeGen MicroMount and collected at 100(2) K by using an Oxford Cryosystems Cobra low-temperature device. Data were collected by using omega and phi scans and were corrected for Lorentz and polarization effects by using the APEX software suite.[256] The structures were solved with Direct Methods and refined against $|F^2|$ with with XL using least squares minimization.[257] Non-hydrogen atoms were refined with anisotopical thermal parameters. Hydrogen atoms were generally placed into geometrically calculated positions and refined using a riding model. The N–H hydrogen atoms were located using different maps and refined using the standard riding model. All images were prepared by using Mercury CSD 2.0[58b] or Olex2.[258]

Crystal data for 2,3,7,8,12,13,17,18-octaisobutyl-5,10,15,20-tetraphenylporphyrin 174: $C_{38}H_{47}N_2$, M = 531.77, monoclinic, $C2/c$, a = 13.767(2) Å, b = 23.613(2) Å, c = 22.626(2) Å, β = 93.535(3)°, V = 7341.4(14) Å^3, T = 100.0 K, Z = 8, μ(MoK_α) = 0.055, 113643 reflections measured, 6658 unique (R_{int} = 0.0575) which were used in all calculations. The final wR_2 was 0.2031 (all data) and R_1 was 0.0681 (I >

$2\sigma(I)$).

Crystal data for 5,10,15,20-tetrakis[(4-bromophenyl)thio]-2,3,7,8,12,13,17,18-octaethylporphyrin 188: $C_{60}H_{58}Br_4N_4S_4$, M = 1282.98, tetragonal, $P\bar{4}2_1c$, a = 19.0974(9) Å, b = 19.0974(9) Å, c = 8.3204(4) Å, $\alpha = \beta = \gamma = 90°$, V = 3034.5(3) Å^3, T = 100.02 K, Z = 2, Z' = 0.25, $\mu(MoK_\alpha)$ = 2.830, 27514 reflections measured, 3487 unique (R_{int} = 0.0308) which were used in all calculations. The final wR_2 was 0.0630 (all data) and R_1 was 0.0278 ($I > 2\sigma(I)$). The structure was resolved as an inversion twin with one quarter molecule appearing in the asymmetric unit. The bromine unit was modelled over two parts using restraints (SADI, ISOR) in a 75–25% occupancy.

Crystal data for 2,3,7,8,12,13,17,18-octaethyl-5,10,15,20-tetrakis(phenylthio)porphyrin 195: $C_{60}H_{62}N_4S_4$, M = 967.37, monoclinic, $P2_1/n$, a = 8.9470(5) Å, b = 55.603(3) Å, c = 20.6784(10) Å, β = 91.7016(15)°, $\alpha = \gamma$ = 90 , V = 10282.6(9) Å^3, T = 100 K, Z = 8, Z' = 2, $\mu(MoK_\alpha)$ = 0.228, 101172 reflections measured, 21189 unique (R_{int} = 0.0506) which were used in all calculations. The final wR_2 was 0.1050 (all data) and R_1 was 0.0488 ($I > 2\sigma(I)$).

Crystal data for 2,3,7,8,12,13,17,18-octaethyl-5,10,15,20-tetrakis(pyridine-2-ylthio)porphyrin 196: $C_{56}H_{58}N_8S_4$, M = 971.34, orthorhombic, $P2_12_12_1$, a = 8.7585(5) Å, b = 23.2617(14) Å, c = 24.6838(14) Å, $\alpha = \beta = \gamma = 90°$, V = 5029.0(5) Å^3, T = 100(2) K, Z = 4, Z' = 1, $\mu(CuK_\alpha)$ = 2.095, 60358 reflections measured, 9224 unique (R_{int} = 0.1181) which were used in all calculations. The final wR_2 was 0.1773 (all data) and R_1 was 0.0656 ($I > 2\sigma(I)$).

Crystal data for 2,3,7,8,12,13,17,18-octaethyl-5,20-dinitroporphyrin 206: $C_{36}H_{44}N_6O_4$, M = 624.77, monoclinic, $P2_1/c$, a = 12.7085(6) Å, b = 10.9353(5) Å, c = 23.2462(11) Å, β = 92.6748(15)°, $\alpha = \gamma = 90°$, V = 3227.0(3) Å^3, T = 100 K, Z = 4, Z' = 1, $\mu(MoK_\alpha)$ = 0.085, 33510 reflections measured, 6660 unique (R_{int} = 0.0641) which were used in all calculations. The final wR_2 was 0.1158 (all data) and R_1 was 0.0471 ($I > 2\sigma(I)$).

Crystal data for 2,3,7,8,12,13,17,18-octaethyl-5,15-dinitroporphyrin 207: $C_{36}H_{44}N_6O_4$, M = 624.77, triclinic, $P\bar{1}$, a = 9.6015(5) Å, b = 13.6688(8) Å, c = 13.7637(8) Å, α = 101.568(3)°, β = 106.044(2)°, γ = 104.705(2)°, V = 1606.37(16) Å^3, T = 100 K, Z = 2, Z' = 1, μ(MoKα) = 0.086, 26989 reflections measured, 6283 unique (R_{int} = 0.0814) which were used in all calculations. The final wR_2 was 0.1167 (all data) and R_1 was 0.0480 (I > 2σ(I)).

Crystal data for 2,3,7,8,12,13,17,18-octaethyl-5,10,15-trinitroporphyrin 209: $C_{36}H_{43}N_7O_6$, M = 669.77, orthorhombic, $P2_12_12_1$, a = 8.6656(11) Å, b = 13.9561(17) Å, c = 27.365(3) Å, $\alpha = \beta = \gamma$ = 90°, V = 3309.5(7) Å^3, T = 100 K, Z = 4, Z' = 1, μ(MoKα) = 0.093, 45306 reflections measured, 7236 unique (R_{int} = 0.0572) which were used in all calculations. The final wR_2 was 0.1000 (all data) and R_1 was 0.0411 (I > 2σ(I)).

Crystal data for {2,3,7,8,12,13,17,18-octaethyl-5,10-dinitroporphyrinato}nickel(II) 204: $C_{36}H_{42}N_6NiO_4$, M = 681.46, monoclinic, $P2_1/c$, a = 9.5646(4) Å, b = 23.0982(9) Å, c = 14.9997(6) Å, β = 93.453(2)°, $\alpha = \gamma$ = 90°, V = 3307.8(2) Å^3, T = 100 K, Z = 4, Z' = 1, μ(CuKα) = 1.243, 61642 reflections measured, 6026 unique (R_{int} = 0.0883) which were used in all calculations. The final wR_2 was 0.1240 (all data) and R_1 was 0.0451 (I > 2σ(I)). The nitro group at the C5 position was modelled over two positions with 58–42% occupancy.

Crystal data for 2,7,12,17-tetraethyl-3,8,13,18-tetraisopropyl-5,10,15,20-tetraphenyl-22*H*,24*H*-porphyrindiium dihydrochloride 243·2HCl: $C_{64}H_{72}Cl_2N_4$, M = 968.15, cubic, I-43d, a = 27.139(5) Å, V = 19988(11) Å^3, T = 99.98 K, Z = 12, , μ(CuKα) = 1.139, 95734 reflections measured, 2057 unique (R_{int} = 0.1571) which were used in all calculations. The final wR_2 was 0.2003 (all data) and R_1 was 0.0658 (I > 2σ(I)).

Crystal data for {2,7,12,17-Tetraethyl-3,8,13,18-tetraisopropyl-5,10,15,20-tetraphenylporphyrinato}nickel(II) 244: $C_{65}H_{70}Cl_2N_4Ni$, M = 1036.86, tetragonal, $P4_2/n$, a = 14.6097(5) Å, c = 15.4733(5) Å, V =

3302.7(2) Å^3, T = 99.95 K, Z = 2, μ(CuKα) = 1.443, 71558 reflections measured, 2931 unique (R_{int} = 0.0495) which were used in all calculations. The final wR_2 was 0.2712 (all data) and R_1 was 0.0893 (I > 2σ(I)).

DFT Calculations

DFT calculations were performed by Dr. N. Grover.

Theoretical calculations were performed using DFT[259] with Becke's three-parameter hybrid exchange functional (B3)[260] and the Lee-Yang-Parr correlation functional (LYP),[261] collectively abbreviated as B3LYP. Pople's split-valence double-zeta basis set, *i.e*. 6-31G (d,p) was used for the macrocyclic core atoms (C, H, N) in all cases.[262] To confirm the potential energy minima, analytical frequency calculations were carried out for the optimized geometries. Gaussian 09 was used to execute the DFT calculations.[263] The polarizable continuum model (PCM) was used to elucidate the solvent effects for DCM.[264] DFT calculations[259] were carried out without any symmetry restrictions. Mulliken charge analysis was performed using above-mentioned functional and basis set in DCM.[265]

NSD Analysis

NSD calculations were performed by Dr. K. J. Flanagan.

The theoretical background and development of this method have been described by Shelnutt *et al*.[3a,36b,214] NSD is a conceptually simple method that employs the decomposition of the conformation of the macrocycle by a basis set composed of its various normal modes of vibration, affording clear separation of the contributing distortions to the macrocycle conformation in a quantitative fashion. For calculations, the NSD engine program established by Shelnutt was used.[266]

References

[1] M. O. Senge, *Chem. Commun*. **2006**, 243–256.

[2] R. Huber, *Eur. J. Biochem*. **1990**, *187*, 283–305.

[3] a) M. O. Senge, S. A. MacGowan, J. M. O'Brien, *Chem. Commun*. **2015**, *51*, 17031–17063; b) M. O. Senge, *ECS Trans*. **2015**, *66*, 1–10.

[4] a) Y. Ding, W.-H. Zhu, Y. Xie, *Chem. Rev*. **2017**, *117*, 2203–2256; b) M. Biesaga, K. Pyrzynska, M. Trojanowicz, *Talanta* **2000**, *51*, 209–224; c) Z. Zhang, D. S. Kim, C.-Y. Lin, H. Zhang, A. D. Lammer, V. M. Lynch, I. Popov, O. Š. Miljanić, E. V. Anslyn, J. L. Sessler, *J. Am. Chem. Soc*. **2015**, *137*, 7769–7774; d) S. Minegishi, A. Yumura, H. Miyoshi, S. Negi, S. Taketani, R. Motterlini, R. Foresti, K. Kano, H. Kitagishi, *J. Am. Chem. Soc*. **2017**, *139*, 5984–5991.

[5] a) T. Hayashi, H. Ogoshi, *Chem. Soc. Rev*. **1997**, *26*, 355–364; b) M. Zawadzka, J. Wang, W. J. Blau, M. O. Senge, *J. Phys. Chem. A* **2013**, *117*, 15–26; c) M. Harsha Vardhan Reddy, R. M. Al-Shammari, N. Al-Attar, E. Kennedy, L. Rogers, S. Lopez, M. O. Senge, T. E. Keyes, J. H. Rice, *Phys. Chem. Chem. Phys*. **2014**, *16*, 4386–4393; d) J. Liu, W. Zhou, J. Liu, I. Howard, G. Kilibarda, S. Schlabach, D. Coupry, M. Addicoat, S. Yoneda, Y. Tsutsui, T. Sakurai, S. Seki, Z. Wang, P. Lindemann, E. Redel, T. Heine, C. Wöll, *Angew. Chem*. **2015**, *127*, 7549–7553; *Angew. Chem. Int. Ed*. **2015**, *54*, 7441–7445; e) S. Haupt, I. Lazar, H. Weitman, M. O. Senge, B. Ehrenberg, *Phys. Chem. Chem. Phys*. **2015**, *17*, 11412–11422; f) S. Richert, G. Bullard, J. Rawson, P. J. Angiolillo, M. J. Therien, C. R. Timmel, *J. Am. Chem. Soc*. **2017**, *139*, 5301–5304.

[6] a) M. Ethirajan, Y. Chen, P. Joshi, R. K. Pandey, *Chem. Soc. Rev*. **2011**, *40*, 340–362; b) C. Moylan, E. M. Scanlan, M. O. Senge, *Curr. Med. Chem*. **2015**, *22*, 2238–2348, c) Q. Zou, M. Abbas, L. Zhao, S. Li, G. Shen, X. Yan, *J. Am. Chem. Soc*. **2017**, *139*, 1921–1927; d) S. Callaghan, M. O. Senge, *Photochem. Photobiol. Sci.* **2018**, 17, 1490–1514.

[7] a) M. O. Senge, M. Fazekas, E. G. A. Notaras, W. J. Blau, M. Zawadzka, O. B. Locos, E. M. Ni Mhuircheartaigh, *Adv. Mater*. **2007**, *19*, 2737–2774; b) J. Rawson, A. C. Stuart, W. You, M. J. Therien, *J. Am. Chem. Soc*. **2014**, *136*, 17561–17569; c) M. Zawadzka, J. Wang, W. J. Blau, M. O. Senge, *Photochem. Photobiol. Sci*. ***2013**, 12*, 996–1007.

[8] a) V. V. Roznyatovskiy, C.-H. Lee, J. L. Sessler, *Chem. Soc. Rev*. **2013**, *42*, 1921–1933; b) S. Shimizu, *Chem. Rev*. **2017**, *117*, 2730–2784; c) T. Sarma, P. K. Panda, *Chem. Rev*. **2017**, *117*, 2785–2838; d) B. Szyszko, M. J. Białek, E. Pacholska-Dudziak, L. Latos-Grażyński, *Chem. Rev*. **2017**, *117*, 2839–2909; e) J. Mack, *Chem. Rev*. **2017**, *117*, 3444–3478.

[9] a) M. O. Senge, *Chem. Commun*. **2011**, *47*, 1943–1960; b) J. S. Lindsey, *Acc. Chem. Res*. **2010**, *43*, 300–311; c) S. Hiroto, Y. Miyake, H. Shinokubo, *Chem. Rev*. **2017**, *117*, 2910–3043.

[10] a) N. Aratani, A. Osuka, Y. H. Kim, D. H. Jeong, D. Kim, *Angew. Chem*. **2000**, *112*, 1517–1521; *Angew. Chem. Int. Ed*. **2000**, *39*, 1458–1462; b) H. S. Cho, D. H. Jeong, S. Cho, D. Kim, Y. Matsuzaki, K. Tanaka, A. Tsuda, A. Osuka, *J. Am. Chem. Soc*. **2002**, *124*, 14642–14654; c) H. Shinokubo, A. Osuka, *Chem. Commun*. **2009**, 1011–1021; d) H.-W. Jiang, T. Tanaka, H. Mori, K. H. Park, D. Kim, A. Osuka, *J. Am. Chem. Soc*. **2015**, *137*, 2219–2222; e) M. C. O'Sullivan, J. K. Sprafke, D. V. Kondratuk, C. Rinfray, T. D. W. Claridge, A. Saywell, M. O. Blunt, J. N. O'Shea, P. H. Beton, M. Malfois, H. L. Anderson, *Nature* **2011**, *469*, 72–75; f) P. Liu, Y. Hisamune, M. D. Peeks, B. Odell, J. Q. Gong, L. M. Herz, H. L. Anderson, *Angew. Chem*. **2016**, *128*, 8498–8502; *Angew. Chem. Int. Ed*. **2016**, *55*, 8358–8362.

[11] a) W. Auwärter, D. Écija, F. Klappenberger, J. V. Barth, *Nat. Chem*. **2015**, *7*, 105–120; b) J. M. Gottfried, *Surf. Sci. Rep*. **2015**, *70*, 259–379.

[12] W. R. Scheidt, Y. J. Lee, *Struct. Bonding* **1987**, *64*, 1–70.

[13] a) W. J. Song, M. S. Seo, S. D. George, T. Ohta, R. Song, M.-J. Kang, T. Tosha, T. Kitagawa, E. I. Solomon, W. Nam, *J. Am. Chem. Soc*. **2007**, *129*, 1268–1277; b) R. L. Khade, Y. Zhang, *J.*

Am. Chem. Soc. **2015**, *137*, 7560–7563; c) P. F. Kuijpers, M. J. Tiekink, W. B. Breukelaar, D. L. J. Broere, N. P. van Leest, J. I. van der Vlugt, J. N. H. Reek, B. de Bruin, *Chem. Eur. J*. **2017**, *23*, 7945–7952; d) Y. Liu, W. Xu, J. Zhang, W. Fuller, C. E. Schulz, J. Li, *J. Am. Chem. Soc*. **2017**, *139*, 5023–5026.

[14] *Tetrapyrroles: Birth, Life and Death* (Eds.: M. J. Warren, A. G. Smith), Landes Bioscience, Austin, Texas, **2009**.

[15] M. O. Senge, A. A. Ryan, K. A. Letchford, S. A MacGowan, T. Mielke, *Symmetry* **2014**, *6*, 781–843.

[16] B. Kräutler, *Biochem. Soc. Trans*. **2005**, *33*, 806–810.

[17] I. Beletskaya, V. S. Tyurin, A. Y. Tsivadze, R. Guilard, C. Stern, *Chem. Rev*. **2009**, *109*, 1659–1713.

[18] a) B. Wehrle, H.-H. Limbach, M. Köcher, O. Ermer, E. Vogel, *Angew. Chem*. **1987**, *99*, 914–917; *Angew. Chem. Int. Ed. Engl*. **1987**, *26*, 934–936; b) P. Wacker, K. Dahms, M. O. Senge, E. Kleinpeter, *J. Org. Chem*. **2008**, *73*, 2182–2190; c) S. Gawinkowski, G. Orzanowska, K. Izdebska, M. O. Senge, J. Waluk, *Chem. Eur. J*. **2011**, *17*, 10039–10049; d) K. E. Thomas, L. J. McCormick, H. Vazquez-Lima, A. Ghosh, *Angew. Chem*. **2017**, *129*, 10222–10226; *Angew. Chem. Int. Ed*. **2017**, *56*, 10088–10092.

[19] International Union of Pure and Applied Chemistry (IUPAC), 2014, Compendium of Chemical Terminology, Gold Book, p. 835, retrieved from http://goldbook.iupac.org/pdf/goldbook.pdf, accessed January 2019.

[20] T. Steiner, *Angew. Chem*. **2002**, *114*, 50–80; *Angew. Chem. Int. Ed*. **2002**, *41*, 48–76.

[21] a) J. A. Shelnutt, X.-Z. Song, J.-G. Ma, S.-L. Jia, W. Jentzen, C. J. Medforth, *Chem. Soc. Rev*. **1998**, *27*, 31–42; b) K. M. Barkigia, M. W. Renner, M. O. Senge, J. Fajer, *J. Phys. Chem. B* **2004**, *108*, 2173–2180.

[22] G. R. Desiraju, *Angew. Chem*. **1995**, *107*, 2541–2558; *Angew. Chem. Int. Ed. Engl*. **1995**, *34*, 2311–2327.

[23] V. Villari, P. Mineo, E. Scamporrino, N. Micali, *RSC Adv*. **2012**, *2*, 12989–12998.

[24] P. Bhyrappa, S. R. Wilson, K. S. Suslick, *J. Am. Chem. Soc*. **1997**, *119*, 8492–8502.

[25] a) S. B. Lei, C. Wang, S. X. Yin, H. N. Wang, F. Xi, H. W. Liu, B. Xu, L. J. Wan, C. L. Bai, *J. Phys. Chem. B* **2001**, *105*, 10838–10841; b) Z. Zhang, T. Imae, *Nano Lett*. **2001**, *1*, 241–243.

[26] I. Radivojevic, I. Likhtina, X. Shi, S. Singh, C. M. Drain, *Chem. Commun*. **2010**, *46*, 1643–1645.

[27] T. Ishizuka, M. Sankar, Y. Yamada, S. Fukuzumi, T. Kojima, *Chem. Commun*. **2012**, *48*, 6481–6483.

[28] A. Garcia-Lekue, R. González-Moreno, S. Garcia-Gil, D. F. Pickup, L. Floreano, A. Verdini, A. Cossaro, J. A. Martín-Gago, A. Arnau, C. Rogero, *J. Phys. Chem. C* **2012**, *116*, 15378–15384.

[29] a) S. Pagola, P. W. Stephens, D. S. Bohle, A. D. Kosar, S. K. Madsen, *Nature* **2000**, *404*, 307–310; b) M. O. Senge, S. Hatscher, *ChemBioChem* **2000**, *1*, 247–249.

[30] G. T. Oostergetel, H. van Amerongen, E. J. Boekema, *Photosynth. Res*. **2010**, *104*, 245–255.

[31] W. Yang, B. Li, H. Wang, O. Alduhaish, K. Alfooty, M. A. Zayed, P. Li, H. D. Arman, B. Chen, *Cryst. Growth Des*. **2015**, *15*, 2000–2004.

[32] L. Zeininger, F. Lodermeyer, R. D. Costa, D. M. Guldi, A. Hirsch, *Chem. Commun.* **2016**, *52*, 8842–8845.

[33] M. Paoli, J. Marles-Wright, A. Smith, *DNA Cell Biol*. **2002**, *21*, 271–280.

[34] S.-R. Yeh, S. Han, D. L. Rousseau, *Acc. Chem. Res*. **1998**, *31*, 727–736.

[35] S. E. J. Bowman, K. L. Bren, *Nat. Prod. Rep*. **2008**, *25*, 1118–1130.

[36] a) A. M. Berghuis, G. D. Brayer, *J. Mol. Biol*. **1992**, *223*, 959–976; b) W. Jentzen, X.-Z. Song, J. A. Shelnutt, *J. Phys. Chem. B* **1997**, *101*, 1684–1699.

[37] J. A. Hodge, M. G. Hill, H. B. Gray, *Inorg. Chem*. **1995**, *34*, 809–812.

[38] a) P. A. Arnold, D. R. Benson, D. J. Brink, M. P. Hendrich, G. S. Jas, M. L. Kennedy, D. T. Petasis, M. Wang, *Inorg. Chem*. **1997**,

36, 5306–5315; b) A. B. Cowley, M. L. Kennedy, S. Silchenko, G. S. Lukat-Rodgers, K. R. Rodgers, D. R. Benson, *Inorg. Chem*. **2006**, *45*, 9985–10001.

[39] a) J.-G. Ma, M. Laberge, X.-Z. Song, W. Jentzen, S.-L. Jia, J. Zhang, J. M. Vanderkooi, J. A. Shelnutt, *Biochemistry* **1998**, *37*, 5118–5128; b) J.-G. Ma, J. M. Vanderkooi, J. Zhang, S.-L. Jia, J. A. Shelnutt, *Biochemistry* **1999**, *38*, 2787–2795.

[40] M. O. Senge, M. W. Renner, W. W. Kalisch, J. Fajer, *J. Chem. Soc., Dalton Trans*. **2000**, 381–385.

[41] a) M. F. Perutz, *Nature* **1979**, *228*, 726–734; b) R. van Grondelle, J. P. Dekker, T. Gillbro, V. Sundstrom, *Biochim. Biophys. Acta* **1994**, *1187*, 1–65.

[42] A. Freer, S. Prince, K. Sauer, M. Papiz, A. Hawthornthwaite-Lawless, G. McDermott, R. Cogdell, N. W. Isaacs, *Structure* **1996**, *4*, 449–462.

[43] a) J. C. Kendrew, R. E. Dickerson, B. E. Strandberg, R. G. Hart, D. R. Davies, D. C. Phillips, V. C. Shore, *Nature* **1960**, *185*, 422–427; b) R. E. Fenna, B. W. Matthews, *Nature* **1975**, *258*, 573–577; c) B. W. Matthews, R. E. Fenna, *Acc. Chem. Res*. **1980**, *13*, 309–317; d) D. E. Tronrud, M. F. Schmid, B. W. Matthews, *J. Mol. Biol*. **1986**, *188*, 443–454.

[44] a) R. C. Ladner, E. J. Heidner, M. F. Perutz, *J. Mol. Biol*. **1977**, *114*, 385–413; b) J. F. Deatherage, R. S. Loe, K. Moffat, *J. Mol. Biol*. **1976**, *104*, 723–728.

[45] a) M. O. Senge, K. M. Smith, *Photochem. Photobiol*. **1991**, *54*, 841–846; b) M. O. Senge, N. W. Smith, K. M. Smith, *Inorg. Chem*. **1993**, *32*, 1259–1265; c) S. A. McGowan, M. O. Senge, *Inorg. Chem*. **2013**, *52*, 1228–1237; d) S. A. MacGowan, M. O. Senge, *Chem. Commun*. **2011**, *47*, 11621–11623; e) S. A. MacGowan, M. O. Senge, *Biochim. Biophys. Acta* **2016**, *1857*, 427–442.

[46] a) P. D. Beer, P. A. Gale, *Angew. Chem*. **2001**, *113*, 502–532; *Angew. Chem. Int. Ed*. **2001**, *40*, 486–516; b) S. K. Kim, J. L. Sessler, *Chem. Soc. Rev*. **2010**, *39*, 3784–3809; c) N. Busschaert, C. Caltagirone, W. V. Rossom, P. A. Gale, *Chem. Rev*. **2015**, *115*,

8038–8155; d) G. I. Vargas-Zúñiga, J. L. Sessler, *Coord. Chem. Rev*. **2017**, *345*, 281–296.

[47] A. Baeyer, *Ber. Dtsch. Chem. Ges*. **1886**, *19*, 2184–2185.

[48] a) D. Jacoby, C. Floriani, A. Chiesi-Villa, C. Rizzoli, *J. Chem. Soc., Chem. Commun*. **1991**, 220–222; b) L. Bonomo, O. Dandin, E. Solari, C. Floriani, R. Scopelliti, *Angew. Chem*. **1999**, *111*, 963–966; *Angew. Chem. Int. Ed*. **1999**, *38*, 913–915; c) C. Floriani, R. Floriani-Moro, *Adv. Organomet. Chem*. **2001**, *47*, 167–233.

[49] J. L. Sessler, S. J. Weghorn, *Expanded, Contracted & Isomeric Porphyrins*, Pergamon Press, Oxford, **1997**.

[50] J. L. Sessler, S. Camiolo, P. A. Gale, *Coord. Chem. Rev*. **2003**, *240*, 17–55.

[51] a) P. A. Gale, J. L. Sessler, V. Král, V. Lynch, *J. Am. Chem. Soc*. **1996**, *118*, 5140–5141; b) P. A. Gale, J. L. Sessler, V. Král, *Chem. Commun*. **1998**, 1–8.

[52] H. Miyaji, P. Anzenbacher Jr., J. L. Sessler, E. R. Bleasdale, P. A. Gale, *Chem. Commun*. **1999**, 1723–1724.

[53] a) P. A. Gale, L. J. Twyman, C. I. Handlin, J. L. Sessler, *Chem. Commun*. **1999**, 1851–1852; b) S. Camiolo, P. A. Gale, *Chem. Commun*. **2000**, 1129–1130; c) C. J. Woods, S. Camiolo, M. E. Light, S. J. Coles, M. B. Hursthouse, M. A. King, P. A. Gale, J. W. Essex, *J. Am. Chem. Soc*. **2002**, *124*, 8644–8652; d) S. K. Kim, V. M. Lynch, J. L. Sessler, *Org. Lett*. **2014**, *16*, 6128–6131.

[54] M. Aleśković, I. Halasz, N. Basarić, K. Mlinarić-Majerski, *Tetrahedron* **2009**, *65*, 2051–2058.

[55] C. J. Medforth, K. M. Smith, *Tetrahedron Lett*. **1990**, *31*, 5583–5586.

[56] a) W. E. Allen, P. A. Gale, C. T. Brown, V. M. Lynch, J. L. Sessler, *J. Am. Chem. Soc*. **1996**, *118*, 12471–12472; b) Y. Furusho, T. Aida, *Chem. Commun*. **1997**, 2205–2206.

[57] L. Adriaenssens, P. Ballester, *Chem. Soc. Rev*. **2013**, *42*, 3161–3277.

[58] a) This figure was generated using Mercury CSD 2.0;[58b] b) C. F. Macrae, I. J. Bruno, J. A. Chisholm, P. R. Edgington, P. McCabe, E. Pidcock, L. Rodriguez-Monge, R. Taylor, J. van de Streek, P.

A. Wood, *J. Appl. Cryst*. **2008**, *41*, 466–470; c) The data was downloaded from the Cambridge Crystallographic Data Centre (CCDC) 2018[58d] using ConQuest version 1.23;[58e] d) C. R. Groom, I. J. Bruno, M. P. Lightfoot, S. C. Ward, *Acta Cryst*. **2016**, *B72*, 171–179; e) I. J. Bruno, J. C. Cole, P. R. Edgington, M. Kessler, C. F. Macrae, P. McCabe, J. Pearson, R. Taylor, *Acta Cryst*. **2002**, *B58*, 389–397.

[59] a) P. A. Gale, J. L. Sessler, W. E. Allen, N. A. Tvermoes, V. Lynch, *Chem. Commun*. **1997**, 665–666; b) P. Anzenbacher Jr., K. Jursíková, V. M. Lynch, P. A. Gale, J. L. Sessler, *J. Am. Chem. Soc*. **1999**, *121*, 11020–11021.

[60] L. Escobar, G. Aragay, P. Ballester, *Chem. Eur. J*. **2016**, *22*, 13682–13689.

[61] a) J. L. Sessler, P. Anzenbacher Jr., K. Jursíková, H. Miyaji, J. W. Genge, N. A. Tvermoes, W. E. Allen, J. A. Shriver, P. A. Gale, V. Král, *Pure Appl. Chem*. **1998**, *70*, 2401–2408; b) H. Miyaji, W. Sato, J. L. Sessler, V. M. Lynch, *Tetrahedron Lett*. **2000**, *41*, 1369–1373.

[62] a) P. A. Gale, J. W. Genge, V. Král, M. A. McKervey, J. L. Sessler, A. Walker, *Tetrahedron Lett*. **1997**, *38*, 8443–8444; b) L. Bonomo, E. Solari, G. Toraman, R. Scopelliti, M. Latronico, C. Floriani, *Chem. Commun*. **1999**, 2413–2414; c) W. Sato, H. Miyaji, J. L. Sessler, *Tetrahedron Lett*. **2000**, *41*, 6731–6736.

[63] L. Escobar, F. A. Arroyave, P. Ballester, *Eur. J. Org. Chem*. **2018**, 1097–1106.

[64] P. A. Gale, J. L. Sessler, V. Lynch, P. I. Sansom, *Tetrahedron Lett*. **1996**, *37*, 7881–7884.

[65] a) P. A. Gale, *Coord. Chem. Rev*. **2001**, *213*, 79–128; b) P. A. Gale, P. Anzenbacher Jr., J. L. Sessler, *Coord. Chem. Rev*. **2001**, *222*, 57–102.

[66] a) P. Anzenbacher Jr., K. Jursíková, J. L. Sessler, *J. Am. Chem. Soc*. **2000**, *122*, 9350–9351; b) K. D. Bhatt, D. J. Vyas, B. A. Makwana, S. M. Darjee, V. K. Jain, H. Shah, *Chin. Chem. Lett*. **2016**, *27*, 731–737.

[67] V. Král, J. L. Sessler, T. V. Shishkanova, P. A. Gale, R. Volf, *J. Am. Chem. Soc*. **1999**, *121*, 8771–8775.

[68] a) P. A. Gale, M. B. Hursthouse, M. E. Light, J. L. Sessler, C. N. Warriner, R. S. Zimmerman, *Tetrahedron Lett*. **2001**, *42*, 6759–6762; b) W. Yang, Z. Yin, C.-H. Wang, J. He, X. Zhu, J.-P. Cheng, *Tetrahedron* **2008**, *64*, 9244–9252.

[69] A. Aydogan, A. Koca, M. K. Şener, J. L. Sessler, *Org. Lett*. **2014**, *16*, 3764–3767.

[70] J. L. Sessler, P. A. Gale, J. W. Genge, *Chem. Eur. J*. **1998**, *4*, 1095–1099.

[71] a) G. Cafeo, M. De Rosa, F. H. Kohnke, P. Neri, A. Soriente, L. Valenti, *Tetrahedron Lett*. **2008**, *49*, 153–155; b) G. Cafeo, M. De Rosa, F. H. Kohnke, A. Soriente, C. Talotta, L. Valenti, *Molecules* **2009**, *14*, 2594–2601.

[72] G. Cafeo, F. H. Kohnke, L. Valenti, *Tetrahedron Lett*. **2009**, *50*, 4138-4140.

[73] D. S. Kim, J. L. Sessler, *Chem. Soc. Rev*. **2015**, *44*, 532–546.

[74] a) T. G. Levitskaia, M. Marquez, J. L. Sessler, J. A. Shriver, T. Vercouter, B. A. Moyer, *Chem. Commun*. **2003**, 2248–2249; b) S. K. Kim, J. L. Sessler, *Acc. Chem. Res*. **2014**, *47*, 2525–2536; c) S. K. Kim, J. Lee, N. J. Williams, V. M. Lynch, B. P. Hay, B. A. Moyer, J. L. Sessler, *J. Am. Chem. Soc*. **2014**, *136*, 15079–15085; d) S. K. Kim, V. M. Lynch, B. P. Hay, J. S. Kim, J. L. Sessler, *Chem. Sci*. **2015**, *6*, 1404–1413; e) Q. He, Z. Zhang, J. T. Brewster, V. M. Lynch, S. K. Kim, J. L. Sessler, *J. Am. Chem. Soc*. **2016**, *138*, 9779–9782; f) Y. Yeon, S. Leem, C. Wagen, V. M. Lynch, S. K. Kim, J. L. Sessler, *Org. Lett*. **2016**, *18*, 4396–4399; g) R. J. Ellis, B. Reinhart, N. J. Williams, B. A. Moyer, V. S. Bryantsev, *Chem. Commun*. **2017**, *53*, 5610–5613.

[75] J. L. Sessler, A. Andrievsky, P. A. Gale, V. Lynch, *Angew. Chem*. **1996**, *108*, 2954–2957; *Angew. Chem. Int. Ed. Engl*. **1996**, *35*, 2782–2785.

[76] G. Gil-Ramírez, M. Chas, P. Ballester, *J. Am. Chem. Soc*. **2010**, *132*, 2520–2521.

[77] a) J. S. Park, F. Le Derf, C. M. Bejger, V. M. Lynch, J. L. Sessler, K. A. Nielsen, C. Johnsen, J. O. Jeppesen, *Chem. Eur. J.* **2010**, *16*, 848–854; b) C. M. Davis, J. M. Lim, K. R. Larsen, D. S. Kim, Y. M. Sung, D. M. Lyons, V. M. Lynch, K. A. Nielsen, J. O. Jeppesen, D. Kim, J. S. Park, J. L. Sessler, *J. Am. Chem. Soc*. **2014**, *136*, 10410–10417.

[78] a) G. Cafeo, G. Carbotti, A. Cuzzola, M. Fabbi, S. Ferrini, F. H. Kohnke, G. Papanikolaou, M. R. Plutino, C. Rosano, A. J. P. White, *J. Am. Chem. Soc*. **2013**, *135*, 2544–2551; b) Q. He, M. Kelliher, S. Bähring, V. M. Lynch, J. L. Sessler, *J. Am. Chem. Soc*. **2017**, *139*, 7140–7143; c) S.-K. Ko, S. K. Kim, A. Share, V. M. Lynch, J. Park, W. Namkung, W. V. Rossom, N. Busschaert, P. A. Gale, J. L. Sessler, I. Shin, *Nat. Chem*. **2014**, *6*, 885–892.

[79] R. Lappano, C. Rosano, A. Pisano, M. F. Santolla, E. M. De Fracesco, P. De Marco, V. Dolce, M. Ponassi, L. Felli, G. Cafeo, F. H. Kohnke, S. Abonante, M. Maggiolini, *Dis. Models Mech*. **2015**, *8*, 1237–1246.

[80] M. Bernátková, H. Dvořáková, B. Andrioletti, V. Král, P. Bouř, *J. Phys. Chem. A* **2005**, *109*, 5518–5526.

[81] a) V. Král, J. L. Sessler, R. S. Zimmerman, D. Seidel, V. Lynch, B. Andrioletti, *Angew. Chem*. **2000**, *112*, 1097–1100; *Angew. Chem. Int. Ed*. **2000**, *39*, 1055–1058; b) C. Bucher, D. Seidel, V. Lynch, V. Král, J. L. Sessler, *Org. Lett*. **2000**, *2*, 3103–3106.

[82] J. W. Buchler, L. Puppe, *Liebigs Ann. Chem.* **1970**, *740*, 142–163.

[83] I. Bischoff, X. D. Feng, M. O. Senge, *Tetrahedron* **2001**, *57*, 5573–5583.

[84] W. Dehaen, *Top. Heterocycl. Chem*. **2010**, *24*, 75–102.

[85] C. Bucher, R. S. Zimmerman, V. Lynch, V. Král, J. L. Sessler, *J. Am. Chem. Soc*. **2001**, *123*, 2099–2100.

[86] a) J. L. Sessler, R. S. Zimmerman, C. Bucher, V. Král, B. Andrioletti, *Pure Appl. Chem*. **2001**, *73*, 1041–1057; b) E. M. Finnigan, S. Giordani, M. O. Senge, T. McCabe, *J. Phys. Chem. A* **2010**, *114*, 2464–2470; c) M. Bernátková, B. Andrioletti, V. Král, E. Rose, J. Vaissermann, *J. Org. Chem*. **2004**, *69*, 8140–8143; d)

J. W. Buchler, K. L. Lay, Y. J. Lee, W. R. Scheidt, *Angew. Chem*. **1982**, *94*, 456–457; *Angew. Chem. Int. Ed. Engl*. **1982**, *21*, 432.

[87] T. Ema, M. O. Senge, N. Y. Nelson, H. Ogoshi, K. M. Smith, *Angew. Chem*. **1994**, *106*, 1951–1953; *Angew. Chem. Int. Ed. Engl*. **1994**, *33*, 1879–1881.

[88] M. O. Senge in *The Porphyrin Handbook*, *Vol. 1* (Eds.: K. M. Kadish, K. M. Smith, R. Guilard), Academic Press, New York, **2000**, pp. 239–347.

[89] A. Stone, E. B. Fleischer, *J. Am. Chem. Soc*. **1968**, *90*, 2735–2748.

[90] a) M. O. Senge, W. W. Kalisch, *Z. Naturforsch*. **1999**, *54b*, 943–959; b) M. O. Senge, *Z. Naturforsch*. **2000**, *55b*, 336–344.

[91] M. O. Senge, T. P. Forsyth, L. T. Nguyen, K. M. Smith, *Angew. Chem*. **1994**, *106*, 2554–2557; *Angew. Chem. Int. Ed. Engl*. **1995**, *33*, 2485–2487.

[92] a) D. K. Lavallee, *The Chemistry and Biochemistry of N-Substituted Porphyrins*, VCH, Weinheim, **1987**; b) M. O. Senge, W. W. Kalisch, S. Runge, *Liebigs Ann./Recl.* **1997**, 1345–1352; c) M. Roucan, K. J. Flanagan, J. O'Brien, M. O. Senge, *Eur. J. Org. Chem*. **2019**, in press, DOI: 10.1002/ejoc.201800960.

[93] M. J. Webb, N. Bampos, *Chem. Sci*. **2012**, *3*, 2351–2366.

[94] A. Rosa, G. Ricciardi, E. J. Baerends, A. Romeo, L. M. Scolaro, *J. Phys. Chem. A* **2003**, *107*, 11468–11482.

[95] V. B. Sheinin, E. L. Ratkova, N. Z. Mamardashvili, *J. Porphyrins Phthalocyanines* **2008**, *12*, 1211–1219.

[96] M. M. Kruk, A. S. Starukhin, N. Z. Mamardashvili, G. M. Mamardashvili, Y. B. Ivanova, O. V. Maltseva, *J. Porphyrins Phthalocyanines* **2009**, *13*, 1148–1158.

[97] a) S. Yoshimoto, T. Sawaguchi, *J. Am. Chem. Soc*. **2008**, *130*, 15944–15949; b) Y. Arai, H. Segawa, *Chem. Commun*. **2010**, *46*, 4279–4281; c) M. A. Gradova, V. N. Kuryakov, A. V. Lobanov, *Macroheterocycles* **2015**, *8*, 244–251.

[98] T. Honda, T. Nakanishi, K. Ohkubo, T. Kojima, S. Fukuzumi, *J. Am. Chem. Soc*. **2010**, *132*, 10155–10163.

[99] Y. Arai, H. Segawa, *J. Phys. Chem. B* **2011**, *115*, 7773–7780.

[100] T. Nakanishi, T. Kojima, K. Ohkubo, T. Hasobe, K.-i. Nakayama, S. Fukuzumi, *Chem. Mater*. **2008**, *20*, 7492–7500.

[101] S. Frühbeißer, G. Mariani, F. Gröhn, *Polymers* **2016**, *8*, 180.

[102] M. Zawadzka, J. Wang, W. J. Blau, M. O. Senge, *J. Porphyrins Phthalocyanines* **2013**, *17*, 1129–1133.

[103] R. Franco, J.-G. Ma, Y. Lu, G. C. Ferreira, J. A. Shelnutt, *Biochemistry* **2000**, *39*, 2517–2529.

[104] a) G. De Luca, A. Romeo, L. M. Scolaro, G. Ricciardi, A. Rosa, *Inorg. Chem*. **2007**, *46*, 5979–5988; b) S. Thyagarajan, T. Leiding, S. P. Årsköld, A. V. Cheprakov, S. A. Vinogradov, *Inorg. Chem*. **2010**, *49*, 9909–9920; c) S. Aronoff, *J. Phys. Chem*. **1958**, *62*, 428–431; d) A. B. Rudine, B. D. DelFatti, C. C. Wamser, *J. Org. Chem*. **2013**, *78*, 6040–6049; e) A. Neuberger, F. R. S. Scott, J. J. Scott, *Proc. R. Soc. London, A* **1952**, *213*, 307–326; f) H. Ogoshi, E. Watanabe, Z. Yoshida, *Tetrahedron* **1973**, *29*, 3241–3245.

[105] N. Hirayama, A. Takenaka, Y. Sasada, *J. Chem. Soc., Chem. Commun*. **1974**, 330–331.

[106] T. Honda, T. Kojima, S. Fukuzumi, *Chem. Commun*. **2009**, 4994–4996.

[107] W. Suzuki, H. Kotani, T. Ishizuka, K. Ohkubo, Y. Shiota, K. Yoshizawa, S. Fukuzumi, T. Kojima, *Chem. Eur. J*. **2017**, *23*, 4669–4679.

[108] Ö. Almarsson, A. Blaskó, T. C. Bruice, *Tetrahedron* **1993**, *49*, 10239–10252.

[109] W. Suzuki, H. Kotani, T. Ishizuka, Y. Shiota, K. Yoshizawa, T. Kojima, *Chem. Commun*. **2017**, *53*, 6359–6362.

[110] a) S. Al-Karadaghi, R. Franco, M. Hansson, J. A. Shelnutt, G. Isaya, G. C. Ferreira, *Trends Biochem. Sci*. **2006**, *31*, 135–142; b) A. Medlock, L. Swartz, T. A. Dailey, H. A. Dailey, W. N. Lanzilotta, *Proc. Natl. Acad. Sci. U. S. A*. **2007**, *104*, 1789–1793.

[111] a) H. A. Dailey in *Biosynthesis of Heme and Chlorophylls* (Ed.: H. A. Dailey), McGraw-Hill, New York, **1990**, pp. 123–163; b) C. J. Walker, J. D. Weinstein, *Plant Physiol*. **1991**, *95*, 1189–1196; c) T. Karlberg, M. D. Hansson, R. K. Yengo, R. Johansson, H. O.

Thorvaldsen, G. C. Ferreira, M. Hansson, S. Al-Karadaghi, *J. Mol. Biol*. **2008**, *378*, 1074–1083.

[112] A. G. Cochran, P. G. Schultz, *Science* **1990**, *249*, 781–783.

[113] a) G. A. Karger, J. D. Reid, C. N. Hunter, *Biochemistry* **2001**, *40*, 9291–9299; b) Y. Lu, A. Sousa, R. Franco, A. Mangravita, G. C. Ferreira, I. Moura, J. A. Shelnutt, *Biochemistry* **2002**, *41*, 8253–8262; c) Z. Shi, R. Franco, R. Haddad, J. A. Shelnutt, G. C. Ferreira, *Biochemistry* **2006**, *45*, 2904–2912.

[114] E. Sigfridsson, U. Ryde, *J. Biol. Inorg. Chem*. **2003**, *8*, 273–282.

[115] M. Ravikanth, T. K. Chandrashekar, *Struct. Bonding* **1995**, *82*, 105–188.

[116] M. O. Senge, *J. Photochem. Photobiol., B: Biol.* **1992**, *16*, 3–36.

[117] a) M. J. Hamor, T. A. Hamor, J. L. Hoard, *J. Am. Chem. Soc*. **1964**, *86*, 1938–1942; b) E. B. Fleischer, *J. Am. Chem. Soc*. **1963**, *85*, 1353–1354; c) E. B. Fleischer, C. K. Miller, L. E. Webb, *J. Am. Chem. Soc*. **1964**, *86*, 2342–2347.

[118] a) B. Evans, K. M. Smith, J.-H. Fuhrhop, *Tetrahedron Lett*. **1977**, *18*, 443–446; b) C. J. Medforth, M. D. Berber, K. M. Smith, J. A. Shelnutt, *Tetrahedron Lett*. **1990**, *31*, 3719–3722; c) M. O. Senge, *Acc. Chem. Res*. **2005**, *38*, 733–743.

[119] C. J. Medforth, M. O. Senge, K. M. Smith, L. D. Sparks, J. A. Shelnutt, *J. Am. Chem. Soc*. **1992**, *114*, 9859–9869.

[120] a) K. M. Barkigia, M. D. Berber, J. Fajer, C. J. Medforth, M. W. Renner, K. M. Smith, *J. Am. Chem. Soc*. **1990**, *112*, 8851–8857; b) A. Regev, T. Galili, C. J. Medforth, K. M. Smith, K. M. Barkigia, J. Fajer, H. Levanon, *J. Phys. Chem*. **1994**, *98*, 2520–2526.

[121] Y. Yamamoto, A. Yamamoto, S.-y. Furuta, M. Horie, M. Kodama, W. Sato, K.-y. Akiba, S. Tsuzuki, T. Uchimaru, D. Hashizume, F. Iwasaki, *J. Am. Chem. Soc*. **2005**, *127*, 14540–14541.

[122] A. B. J. Parusel, T. Wondimagegn, A. Ghosh, *J. Am. Chem. Soc*. **2000**, *122*, 6371–6374.

[123] D. Dolphin, *J. Heterocycl. Chem*. **1970**, *7*, 275–283.

[124] a) J. Takeda, T. Ohya, M. Sato, *Inorg. Chem*. **1992**, *31*, 2877–2880; b) P. Bhyrappa, M. Nethaji, V. Krishnan, *Chem. Lett*. **1993**, *22*, 869–872.

[125] a) K. M. Kadish, E. V. Caemelbecke, F. D'Souza, C. J. Medforth, K. M. Smith, A. Tabard, R. Guilard, *Inorg. Chem*. **1995**, *34*, 2984–2989; b) P. Ochsenbein, K. Ayougou, D. Mandon, J. Fischer, R. Weiss, R. N. Austin, K. Jayaraj, A. Gold, J. Terner, J. Fajer, *Angew. Chem*. **1994**, *106*, 355–357; *Angew. Chem. Int. Ed*. **1994**, *33*, 348–350.

[126] a) S. Gentemann, C. J. Medforth, T. P. Forsyth, D. J. Nurco, K. M. Smith, J. Fajer, D. Holten, *J. Am. Chem. Soc*. **1994**, *116*, 7363–7368; b) S. Gentemann, C. J. Medforth, T. Ema, N. Y. Nelson, K. M. Smith, J, Fajer, D. Holten, *Chem. Phys. Lett*. **1995**, *245*, 441–447; c) C. M. Drain, C. Kirmaier, C. J. Medforth, D. J. Nurco, K. M. Smith, D. Holten, *J. Phys. Chem*. **1996**, *100*, 11984–11993; d) S. Gentemann, N. Y. Nelson, L. Jaquinod, D. J. Nurco, S. H. Leung, C. J. Medforth, K. M. Smith, J. Fajer, D. Holten, *J. Phys. Chem. B* **1997**, *101*, 1247–1254.

[127] M. W. Renner, K. M. Barkigia, Y. Zhang, C. J. Medforth, K. M. Smith, J. Fajer, *J. Am. Chem. Soc*. **1994**, *116*, 8582–8592.

[128] P. Tagliatesta, J. Li, M. Autret, E. V. Caemelbecke, A. Villard, F. D'Souza, K. M. Kadish, *Inorg. Chem*. **1996**, *35*, 5570–5576.

[129] D. J. Nurco, C. J. Medforth, T. P. Forsyth, M. M. Olmstead, K. M. Smith, *J. Am. Chem. Soc*. **1996**, *118*, 10918–10919.

[130] J. Fajer, *J. Pept. Res*. **2000**, *4*, 382–385.

[131] K. M. Barkigia, M. W. Renner, L. R. Furenlid, C. J. Medforth, K. M. Smith, J. Fajer, *J. Am. Chem. Soc*. **1993**, *115*, 3627–3635.

[132] a) W. W. Kalisch, M. O. Senge, *Tetrahedron Lett*. **1996**, *37*, 1183–1186; b) M. O. Senge, W. W. Kalisch, *Inorg. Chem*. **1997**, *36*, 6103–6116.

[133] L. D. Sparks, C. J. Medforth, M.-S. Park, J. R. Chamberlain, M. R. Ondrias, M. O. Senge, K. M. Smith, J. A. Shelnutt, *J. Am. Chem. Soc*. **1993**, *115*, 581–592.

[134] K. M. Barkigia, D. J. Nurco, M. W. Renner, D. Melamed, K. M. Smith, J. Fajer, J*. Phys. Chem. B* **1998**, *102*, 322–326.

[135] A putative triclinic modification, which upon closer inspection appears to be a core monoacid with a N–H-bonded ethoxide: M. O. Senge, *Z. Naturforsch*. **1999**, *54b*, 821–824.

[136] M. Kielmann, K. J. Flanagan, K. Norvaiša, D. Intrieri, M. O. Senge, *J. Org. Chem*. **2017**, *82*, 5122–5134.

[137] M. Roucan, M. Kielmann, S. J. Connon, S. S. R. Bernhard, M. O. Senge, *Chem. Commun*. **2018**, *54*, 26–29.

[138] M. Kielmann, C. Prior, M. O. Senge, *New J. Chem*. **2018**, *42*, 7529–7550.

[139] R. Paolesse, S. Nardis, D. Monti, M. Stefanelli, C. Di Natale, *Chem. Rev*. **2017**, *117*, 2517–2583.

[140] a) J. R. Askim, M. Mahmoudi, K. S. Suslick, *Chem. Soc. Rev*. **2013**, *43*, 8649–8682; b) L. Wang, H. Li, J. Deng, D. Cao, *Curr. Org. Chem*. **2013**, *17*, 3078–3091; c) S. Ishihara, J. Labuta, W. V. Rossom, D. Ishikawa, K. Minami, J. P. Hill, K. Ariga, *Phys. Chem. Chem. Phys*. **2014**, *16*, 9713–9746; d) H. Lee, K.-I. Hong, W.-D. Jang, *Coord. Chem. Rev*. **2018**, *354*, 46–73.

[141] N. Venkatramaiah, C. F. Pereira, R. F. Mendes, F. A. Almeida Paz, J. P. C. Tomé, *Anal. Chem*. **2015**, *87*, 4515–4522.

[142] A. Rana, P. K. Panda, *RSC Adv*. **2012**, *2*, 12164–12168.

[143] T. Ema, N. Ura, K. Eguchi, Y. Ise, T. Sakai, *Chem. Commun*. **2011**, *47*, 6090–6092.

[144] J. Yang, Z. Wang, K. Hu, Y. Li, J. Feng, J. Shi, J. Gu, *ACS Appl. Mater. Interfaces* **2015**, *7*, 11956–11964.

[145] *Neurosciences - From Molecule to Behavior: A University Textbook* (Eds.: C. G. Galizia, P.-M. Lledo), Springer-Verlag, Heidelberg, **2013**.

[146] a) K. Persaud, G. Dodd, *Nature* **1982**, *299*, 352–355; b) F. Röck, N. Barsan, U. Weimar, *Chem. Rev*. **2008**, *108*, 705–725; c) K. Suslick, *MRS Bull*. **2004**, *29*, 720–725; d) Y. Vlasov, A. Legin, A. Rudnitskaya, C. Di Natale, A. D'Amico, *Pure Appl. Chem*. **2005**, *77*, 1965–1983; e) Y. Tahara, K. Toko, *IEEE Sens. J*. **2013**, *13*, 3001–3011.

[147] A. Catini, R. Kumar, R. Capuano, E. Martinelli, R. Paolesse, C. Di Natale, *Sensors* **2016**, *16*, 1640; b) C. Di Natale, R. Paolesse, A. Macagnano, A. Mantini, P. Mari, A. D'Amico, *Sens. Actuators B Chem*. **2000**, *68*, 319–323; c) C. Di Natale, D. Salimbeni, R. Paolesse, A. Macagnano, A. D'Amico, *Sens. Actuators B Chem*.

2000, *65*, 220–226; d) A. D'Amico, C. Di Natale, R. Paolesse, A. Macagnano, A. Mantini, *Sens. Actuators B Chem*. **2000**, *65*, 209–215; e) C. Di Natale, R. Paolesse, A. Macagnano, V. I. Troitsky, T. S. Berzina, A. D'Amico, *Anal. Chim. Acta* **1999**, *384*, 249–259; f) C. Di Natale, R. Paolesse, A. Macagnano, A. Mantini, C. Goletti, A. D'Amico, *Sens. Actuators B Chem*. **1998**, *52*, 162–168.

[148] a) J. H. Leopold, L. D. J. Bos, P. J. Sterk, M. J. Schultz, N. Fens, I. Horvath, A. Bikov, P. Montuschi, C. Di Natale, D. H. Yates, A. Abu-Hanna, *J. Breath Res*. **2015**, *9*, 046002; b) C. Di Natale, A. Macagnano, F. Davide, A. D'Amico, R. Paolesse, T. Boschi, M. Faccio, G. Ferri, *Sens. Actuators B Chem*. **1997**, *44*, 521–526.

[149] a) N. A. Rakow, K. S. Suslick, *Nature* **2000**, *406*, 710–713; b) N. A. Rakow, K. S. Suslick in *Artificial Chemical Sensing: Olfaction and the Electronic Nose* (Eds.: J. R. Stetter, W. R. Penrose), The Electrochemical Society, Pennington, **2001**, pp. 8–13; c) K. S. Suslick, N. A. Rakow, A. Sen, *Tetrahedron* **2004**, *60*, 11133–11138.

[150] a) J. R. Askim, Z. Li, M. K. LaGasse, J. M. Rankin, K. S. Suslick, *Chem. Sci*. **2016**, *7*, 199–206; b) Z. Li, W. P. Bassett, J. R. Askim, K. S. Suslick, *Chem. Commun*. **2015**, *51*, 15312–15315.

[151] Y. Zhang, J. R. Askim, W. Zhong, P. Orlean, K. S. Suslick, *Analyst* **2014**, *139* 1922–1928.

[152] S. H. Lim, L. Feng, J. W. Kemling, C. J. Musto, K. S. Suslick, *Nat. Chem*. **2009**, *1*, 562–567.

[153] Z. Li, K. S. Suslick, *ACS Sens*. **2016**, *1*, 1330–1335.

[154] M. C. Janzen, J. B. Ponder, D. P. Bailey, C. K. Ingison, K. S. Suslick, *Anal. Chem*. **2006**, *78*, 3591–3600.

[155] a) Y. Zilberman, Y. Chen, S. R. Sonkusale, *Sens. Actuators B Chem*. **2014**, *202*, 976–983; b) J. P. Mensing, A. Wisitsoraat, A. Tuantranont, T. Kerdcharoen, *Sens. Actuators B Chem*. **2013**, *176*, 428–436; c) W. Yang, J. Xu, Y. Mao, Y. Yang, Y. Jiang, *Synth. React. Inorg. Met.-Org. Chem*. **2016**, *46*, 735–740.

[156] W. W. Kalisch, M. O. Senge, *Angew. Chem*. **1998**, *110*, 1156–1159; *Angew*. *Chem*. *Int*. *Ed*. **1998**, *37*, 1107–1109.

[157] K.-i. Yamashita, K. Kataoka, M. S. Asano, K.-i. Sugiura, *Org*. *Lett*. **2012**, *14*, 190–193.

[158] a) N.-J. Zhu, Y. Li, G.-Z. Wu, X.-G. Liang, *Acta Chim. Sin.* **1992**, *50*, 249–256; b) M. O. Senge, C. W. Eigenbrot, T. D. Brennan, J. Shusta, W. R. Scheidt, K. M. Smith, *Inorg. Chem.* **1993**, *32*, 3134–3142; c) M. O. Senge, *J. Chem. Soc., Dalton Trans.* **1993**, 3539–3549; d) M. O. Senge, K. M. Smith, *J. Chem. Soc., Chem. Commun.* **1994**, 923–924; e) M. O. Senge, *J. Porphyrins Phthalocyanines* **1998**, *2*, 107–121; f) S. K. Ghosh, R. Patra, S. P. Rath, *Inorg. Chem.* **2008**, *47*, 9848–9856; g) R. Patra, S. Bhowmik, S. K. Ghosh, S. P. Rath, *Dalton Trans.* **2010**, *39*, 5795–5806; h) S. Dey, S. A. Ikbal, S. P. Rath, *New J. Chem.* **2014**, *38*, 1458–1470; i) S. Pukhoskaya, Y. Ivanova, D. T. Nam, A. Vashurin, O. Golubchikov, *J. Porphyrins Phthalocyanines* **2015**, *19*, 858–864.

[159] E. Watanabe, S. Nishimura, H. Ogoshi, Z. Yoshida, *Tetrahedron* **1975**, *31*, 1385–1390.

[160] L.-C. Gong, D. Dolphin, *Can*. *J*. *Chem*. **1985**, *63*, 401–405.

[161] J. W. Lauher, J. A. Ibers, *J. Am. Chem. Soc*. **1973**, *95*, 5148–5152.

[162] L.-C. Gong, D. Dolphin, *Can*. *J*. *Chem*. **1985**, *63*, 406–411.

[163] X. D. Feng, M. O. Senge, *J. Org. Chem.* **2001**, *66*, 8693–8700.

[164] a) C. J. Jackson, F. H. Gazzolo, *J*. *Chem*. *Soc*. **1900**, *23*, 376–396; b) J. Meisenheimer, *Liebigs Ann*. *Chem*. **1902**, *323*, 205–246.

[165] C. H. Devillers, S. Hebié, D. Lucas, H. Cattey, S. Clément, S. Richeter, *J*. *Org*. *Chem*. **2014**, *79*, 6424–6434.

[166] A. A. Ryan, S. Plunkett, A. Casey, T. McCabe, M. O. Senge, *Chem*. *Commun*. **2014**, 353–355.

[167] a) T. Okino, Y. Hoashi, Y. Takemoto, *J. Am. Chem. Soc*. **2003**, *125*, 12672–12673; b) T. Okino, Y. Hoashi, T. Furukawa, X. Xu, Y. Takemoto, *J. Am. Chem. Soc*. **2005**, *127*, 119–125; c) B.-J. Li, L. Jiang, M. Liu, Y.-C. Chen, L.-S. Ding, Y. Wu, *Synlett.* **2005**, 603–606; d) B. Vakulya, S. Varga, A. Csámpai, T. Soós, *Org. Lett*. **2005**, *7*, 1967–1969; e) S. H. McCooey, S. J. Connon, *Angew. Chem.* **2005**, *117*, 6525–6528; *Angew. Chem. Int. Ed*. **2005**, *44*,

6367–6370; f) J. Ye, D. J. Dixon, P. S. Hynes, *Chem. Commun*. **2005**, 4481–4483.

[168] a) J. P. Malerich, K. Hagihara, V. H. Rawal, *J. Am. Chem. Soc*. **2008**, *130*, 14416–14417; b) J. Alemán, A. Parra, H. Jiang, K. A. Jørgensen, *Chem. Eur. J*. **2011**, *17*, 6890–6899.

[169] a) B. Kótai, G. Kardos, A. Hamza, V. Farkas, I. Pápai, T. Soós, *Chem. Eur. J.* **2014**, *20*, 5631–5639; b) S. Ričko, J. Svete, B. Štefane, A. Perdih, A. Golobič, A. Meden, U. Grošelj, *Adv. Synth. Catal*. **2016**, *358*, 3786–3796; c) C. Trujillo, I. Rozas, A. Botte, S. J. Connon, *Chem. Commun*. **2017**, *53*, 8874–8877.

[170] a) A. Hamza, G. Schubert, T. Soós, I. Pápai, *J. Am. Chem. Soc.* **2006**, *128*, 13151–13160; b) M. N. Grayson and K. N. Houk, *J. Am. Chem. Soc*. **2016**, *138*, 1170–1173; c) M. N. Grayson and K. N. Houk, *J. Am. Chem. Soc*. **2016**, *138*, 9041–9044.

[171] P. Bhyrappa, V. Krishnan, *Inorg. Chem*. **1991**, *30*, 239–245.

[172] S. Rayati, S. Zakavi, E. Bohloulbandi, M. Jafarian, M. R. avei, *Polyhedron* **2012**, *34*, 102–107.

[173] D. Mandon, P. Ochsenbein, J. Fischer, R. Weiss, K. Jayaraj, R. N. Austin, A. Gold, P. S. White, O. Brigaud, P. Battioni, D. Mansuy, *Inorg*. *Chem*. **1992**, *31*, 2044–2049.

[174] P. Rothemund, *J. Am. Chem. Soc*. **1936**, *58*, 625–627.

[175] A. D. Adler, F. R. Longo, J. D. Finarelli, J. Goldmacher, J. Assour, L. Korsakoff, *J. Org. Chem*. **1967**, *32* 476.

[176] a) D. K. Lavallee, A. E. Gebala, *Inorg. Chem*. **1974**, *13*, 2004–2008; b) H. M. G. Al-Hazimi, A. H. Jackson, A. W. Johnson, M. Winter, *J. Chem. Soc., Perkin Trans. 1* **1977**, 98–103.

[177] S. J. Silvers, A. Tulinsky, *J. Am. Chem. Soc*. **1967**, *89*, 3331–3337.

[178] U. Eisner, A. Lichtarowicz, R. P. Linstead, *J. Chem. Soc*. **1957**, 733–739.

[179] a) G. D. Hartman, L. M. Weinstock, *Org. Synth*. **1979**, *59*, 183–188; b) J. L. Sessler, A. Mozzafari, M. R. Johnson, *Org. Synth*. **1992**, *70*, 68–74.

[180] E. R. Birnbaum, J. A. Hodge, M. W. Grinstaff, W. P. Schaefer, L. Henling, J. A. Labinger, J. E. Bercaw, H. B. Gray, *Inorg. Chem*. **1995**, *34*, 3625–3632.

[181] R.-J. Cheng, Y.-H. Chen, C.-C. Chen, G.-H. Lee, S.-M. Peng and P. P.-Y. Chen, *Inorg. Chem*. **2014**, *53*, 8848–8850.

[182] a) M. J. Broadhurst, R. Grigg, G. Shelton, *J. Chem. Soc. D* **1970**, 231–233; b) R. Grigg, A. Sweeney, G. R. Dearden, A. H. Jackson, A. W. Johnson, *J. Chem. Soc. D* **1970**, 1273–1274.

[183] S. M. S. Chauhan, B. Vijayaraghavan, K. V. Rao, *Indian J. Chem., Sect. B: Org. Chem. Incl. Med. Chem*. **1987**, *26*, 122–124.

[184] M. O. Senge, *J. Porphyrins Phthalocyanines* **1999**, *3*, 216–223.

[185] T. E. Clement, L. T. Nguyen, R. G. Khoury, D. J. Nurco, K. M. Smith, *Heterocycles* **1997**, *45*, 651–658.

[186] P. R. Ortiz de Montellano, H. S. Beilan, K. L. Kunze, *Proct. Natl. Acad. Sci. U. S. A*. **1981**, *78*, 1490–1494.

[187] *Handbook of Chemistry and Physics* (Ed.: W. M. Haynes), CRC Press, Boca Raton, Florida, **2016**, pp. 5–89.

[188] J. S. Lindsey, H. C. Hsu, P. C. Kearney, A. M. Marguerettaz, *J. Org. Chem*. **1987**, *52*, 827–836.

[189] a) D. H. R. Barton, S. Z. Zard, *J. Chem. Soc., Chem. Commun*. **1985**, 1098–1100; b) S. D. Roth, T. Shkindel, D. A. Lightner, *Tetrahedron* **2007**, *63*, 11030–11039.

[190] K. S. Chan, X. Zhou, B.-s. Luo, T. C. W. Mak, *J. Chem. Soc., Chem. Commun*. **1994**, 271–272.

[191] H. J. Callot, *Bull. Chim. Soc. Fr*. 1974, 1492–1496.

[192] P. K. Kumar, P. Bhyrappa, B. Varghese, *Tetrahedron Lett*. **2003**, *44*, 4849–4851.

[193] P. Bhyrappa, M. Sankar, B. Varghese, *Inorg. Chem*. **2006**, *45*, 4136–4149.

[194] K. S. Chan, X. Zhou, M. T. Au, C. Y. Tam, *Tetrahedron* **1995**, *51*, 3129–3136.

[195] T. C. McMorris, R. G. Chavez, P. A. Patil, *J. Chem. Soc., Perkin Trans. 1* **1996**, 295–302.

[196] H. Wei, Y. Li, K. Xiao, B. Cheng, H. Wang, L. Hu, H. Zhai*, Org. Lett*. **2015**, *17*, 5974–5977.

[197] B. Franck, A. Nonn, K. Fuchs, M. Gosmann, *Liebigs Ann. Chem*. **1994**, 503–510.

[198] S. Sugawara, M. Kodama, Y. Hirata, S. Kojima, Y. Yamamoto, *J.*

Porphyrins Phthalocyanines **2011**, *15*, 1326–1334.

[199] P.-L. Saaidi, M. Guyonnet, E. Jeanneau, P. Fleurat-Lessard, J. Hasserodt, *J. Org. Chem*. **2008**, *73*, 1209–1216.

[200] M. Kielmann, M. O. Senge, *Angew. Chem*. **2019**, *131*, 424–448; *Angew. Chem. Int. Ed*. **2019**, *58*, 418–441.

[201] M. Kielmann, N. Grover, W. W. Kalisch, M. O. Senge, *Eur. J. Org. Chem*. **2019**, in press, DOI: 10.1002/ejoc.201801691.

[202] a) A. Ghosh, *Acc. Chem. Res*. **1998**, *31*, 189−198; b) A. Ghosh in *The Porphyrin Handbook, Vol. 7* (Eds.: K. M. Kadish, K. M. Smith, R. Guilard), Academic Press, New York, **2000**, pp. 1−38.

[203] O. S. Finikova, A. V. Cheprakov, P. J. Carroll, S. Dalosto, S. A. Vinogradov, *Inorg. Chem*. **2002**, *41*, 6944–6946.

[204] a) P. Cogolli, F. Maiolo, L. Testaferri, M. Tingolo, M. Tiecco, *J. Org. Chem*. **1979**, *44*, 2642−2646; b) S. Montanari, C. Paradisi, G. Scorrano, *J. Org. Chem*. **1993**, *58*, 5628−5631; c) J. F. Hartwig, *Nature* **2008**, *455*, 314−322; d) B. Sreedhar, P. S. Reddy, M. A. Reddy, *Synthesis* **2009**, 1732−1738; e) C. E. Hoyle, C. N. Bowman, *Angew. Chem*. **2010**, *122*, 1584−1617; *Angew. Chem. Int. Ed*. **2010**, *49*, 1540−1573; f) H.-J. Xu, Y.-Q. Zhao, T. Feng, Y.-S. Feng, *J. Org. Chem*. **2012**, *77*, 2878−2884.

[205] Q. Chen, Y.-Z. Zhu, Q. J. Fan, S.-C. Zhang, J.-Y. Zheng, *Org. Lett*. **2014**, *16*, 1590−1593.

[206] a) J. E. Baldwin, M. J. Crossley, J. DeBernardis, *Tetrahedron* **1982**, *38*, 685−692; b) M. J. Crossley, L. G. King, S. M. Pyke, C. W. Tansey, *J. Porphyrins Phthalocyanines* **2002**, *6*, 685−694.

[207] R. Radi, J. S. Beckman, K. M. Bush, B. A. Freeman, *J. Biol. Chem*. **1991**, *266*, 4244−4250.

[208] a) J. E. Hutchison, T. A. Postlethwaite, R. W. Murray, *Langmuir* **1993**, *9*, 3277−3283; b) K. Shimazu, M. Takechi, H. Fujii, M. Suzuki, H. Saiki, T. Yoshimura, K. Uosaki, *Thin Solid Films* **1996**, *273*, 250−253; c) C. Clausen, D. T. Gryko, R. B. Dabke, N. Dontha, D. F. Bocian, W. G. Kuhr, J. S. Lindsey, *J. Org. Chem*. **2000**, *65*, 7363−7370; d) C. Clausen, D. T. Gryko, A. A. Yasseri, J. R. Diers, D. F. Bocian, W. G. Kuhr, J. S. Lindsey, *J. Org. Chem*. **2000**, *65*, 7371−7378.

[209] G. Copley, D. Shimizu, J. Oh, J. Sung, K. Furukawa, D. Kim, A. Osuka, *Eur*. *J*. *Org*. *Chem*. **2016**, 1977−1981.

[210] A. M. Stolzenberg, M. T. Stershic, *J*. *Am*. *Chem*. *Soc*. **1988**, *110*, 6391−6402.

[211] L. Rogers, E. Burke-Murphy, M. O. Senge, *Eur. J. Org. Chem*. **2014**, 4283−4294.

[212] M. J. Crossley, J. J. Gosper, M. G. Wilson, *J*. *Chem*. *Soc*., *Chem*. *Commun*. **1985**, 1798−1799.

[213] K. M. Kadish, M. Lin, E. V. Caemelbecke, G. De Stefano, C. J. Medforth, D. J. Nurco, N. Y. Nelson, B. Krattinger, C. M. Muzzi, L. Jaquinod, Y. Xu, D. Shyr, K. M. Smith, J. A. Shelnutt, *Inorg*. *Chem*. **2002**, *41*, 6673−6687.

[214] a) W. Jentzen, M. C. Simpson, J. D. Hobbs, X. Song, T. Ema, N. Y. Nelson, C. J. Medforth, K. M. Smith, M. Veyrat, *J. Am*. *Chem*. *Soc*. **1995**, *117*, 11085−11097; b) W. Jentzen, J. Ma, J. A. Shelnutt, *Biophys*. *J*. **1998**, *74*, 753−763.

[215] P. S. Clezy, D. C. Craig, V. J. James, J. F. McConnell, A. D. Rae, *Cryst*. *Struct*. *Commun*. **1979**, *8*, 605.

[216] K. M. Barkigia, M. Palacio, Y. Sun, M. Nogues, M. W. Renner, F. Varret, P. Battioni, D. Mansuy, J. Fajer, *Inorg*. *Chem*. **2002**, *41*, 5647−5649.

[217] M. O. Senge, *Acta Cryst*. **1998**, C*54*, IUC9800022.

[218] M. O. Senge, CCDC: TOYSAB: Experimental Crystal Structure Determination, **1997**, DOI: 10.5517/cc3c9pf.

[219] W. P. Schaefer, P. E. Ellis, J. E. Lyons, S. N. Shaikh, *Acta Cryst*. **1995**, C*51*, 2252−2255.

[220] R. Patra, A. Chaudhary, S. K. Ghosh, S. P. Rath, *Inorg*. *Chem*. **2008**, *47*, 8324−8335.

[221] R. Haddad, Y. Lu, J. M. E. Quirke, P. Berget, L. Sun, J. C. Fettinger, K. Leung, Y. Qiu, N. E. Schore, F. van Swol, C. J. Medforth, J. A. Shelnutt, *J*. *Porphyrins Phthalocyanines* **2011**, *15*, 727−741.

[222] a) M. O. Senge, W. W. Kalisch, I. Bischoff, *Chem. Eur. J.*, **2000**, *6*, 2721−2738; b) M. O. Senge, I. Bischoff, *Eur. J. Org. Chem.*, **2001**, 1735−1751.

[223] Assuming equivalent nitrogen atoms and a planar macrocycle, then the four porphyrins, which contain two different substituents, one of each on every pyrrole ring, have the following point group symmetries: type I: C_{4h}, type II: D_{2h}, type III: C_s, and type IV: C_{2v}.

[224] M. Taniguchi, J. S. Lindsey in *Handbook of Porphyrin Science, Vol. 23* (Eds.: K. M. Kadish, K. M. Smith, R. Guilard), World Scientific, Singapore, **2012**, pp. 3−80.

[225] L. T. Nguyen, K. M. Smith, *Tetrahedron Lett*. **1996**, *37*, 7177−7180.

[226] L. T. Nguyen, M. O. Senge, K. M. Smith, *Tetrahedron Lett*. **1994**, *35*, 7581−7584.

[227] K. M. Smith, *J. Chem. Soc., Perkin Trans. 1* **1972**, 1471−1475.

[228] J. B. Paine III, C. K. Chang, D. Dolphin, Heterocycles **1997**, *7*, 831−838.

[229] C. K. Lim, J. M. Rideout, D. J. Wright, *Biochem. J*. **1983**, *211*, 435−438.

[230] J. Fyrestam, N. Bjurshammar, E. Paulsson, A. Johannsen, C. Östman, *Anal. Bioanal. Chem*. **2015**, *407*, 7013−7023.

[231] T. C. Chu, J.-H. Chu, *Clin. Chem*. **1967**, *13*, 371−387.

[232] S. Neya, N. Funasaki, *Tetrahedron Lett*. **2002**, *43*, 1057−1058.

[233] S. Neya, J. Quan, T. Hoshino, M. Hata, N. Funasaki, *Tetrahedron Lett*. **2004**, *45*, 8629−8630.

[234] C. Zonta, F. Fabris, O. De Lucchi, *Org. Lett*. **2005**, *7*, 1003−1006.

[235] U. T. Mueller-Westerhoff, G. F. Swiegers, *Synth. Commun*. **1994**, *24*, 1389−1393.

[236] H. J. Anderson, C. E. Loader, R. X. Xu, N. Lê, N. J. Gogan, R. McDonald, L. G. Edwards, *Can. J. Chem*. **1985**, *63*, 896−902.

[237] J. K. Groves, H. J. Anderson, H. Nagy, *Can. J. Chem*. **1971**, *49*, 2427−2432.

[238] J. W. Hoffman, V. J. Smith, L. A. Padgett, *Tetrahedron* **2008**, *64*, 2104−2112.

[239] S. A. Brittle, T. H. Richardson, A. D. F. Dunbar, S. M. Turega, C. A. Hunter, *J. Mater. Chem*. **2011**, *21*, 4882–4887.

[240] S. Carturan, M. Tonezzer, A. Quaranta, G. Maggioni, M. Buffa, R. Milan, *Sens. Actuators B Chem*. **2009**, *137*, 281–290.

[241] a) J. Roales, J. M. Pedrosa, M. G. Guillén, T. Lopes-Costa, P. Castillero, A. Barranco, A. R. González-Elipe, *Sensors* **2015**, *15*, 11118–11132; b) M. Evyapan, A. D. F. Dunbar, *Sens. Actuators B Chem*. **2015**, *206*, 74–83; c) D. Çaycı, S. G. Stanciu, İ. Çapan, M. Erdoğan, B. Güner, R. Hristu, G. A. Stanciu, *Sens. Actuators B Chem*. **2011**, *158*, 62–68; d) V. C. Smith, S. V. Batty, T. Richardson, K. A. Foster, R. A. W. Johnstone, A. J. F. N. Sobral, A. M. D. R. Gonsalves, *Thin Solid Films* **1996**, *284*, 911–914; e) K. Nakagawa, K. Kumon, C. Tsutsumi, K. Tabuchi, T. Kitagawa, Y. Sadaoka, *Sens. Actuators B Chem*. **2000**, *65*, 138–140; f) A. D. F. Dunbar, T. H. Richardson, J. Hutchinson, C. A. Hunter, *Sens. Actuators B Chem*. **2008**, *128*, 468–481; g) S. Z. Topal, M. Z. Ongun, E. Onal, K. Ertekin, C. Hirel, *Dyes Pigm*. **2017**, *144*, 102–109.

[242] Q. Zhang, X. Zheng, G. Kuang, W. Wang, L. Zhu, R. Pang, X. Shi, X. Shang, X. Huang, P. N. Liu, N. Lin, *J. Phys. Chem. Lett*. **2017**, *8*, 1241–1247.

[243] Y. Furusho, T. Kimura, Y. Mizuno, T. Aida, *J. Am. Chem. Soc*. **1997**, *119*, 5267–5268.

[244] T. G. Spiro, J. D. Stong, P. Stein, *J. Am. Chem. Soc*. **1979**, *101*, 2648–2655.

[245] C. J. Medforth, M O. Senge, T. P. Forsyth, J. D. Hobbs, J. A. Shelnutt, K. M. Smith, *Inorg. Chem*. **1994**, *33*, 3865–3872.

[246] A. M. Van Leusen, H. Siderius, B. E. Hoogenboom, D. Van Leusen, *Tetrahedron Lett*. **1972**, *13*, 5337–5340.

[247] D. Van Leusen, E. Van Echten, A. M. Van Leusen, *J. Org. Chem*. **1992**, *57*, 2245–2249.

[248] R. Settambolo, M. Mazzetti, D. Pini, S. Pucci, R. Lazzaroni, *Gazz. Chim. Ital*. **1994**, *124*, 173–176.

[249] a) F. J. Arnáiz, *J. Chem. Educ*. **1995**, *72*, 1139; b) Z. Liu, Q. Ma, Y. Liu, Q. Wang, *Org. Lett*. **2014**, *16*, 236–239.

[250] M. A. Giarrusso, M. K. Taylor, J. Ziogas, K. M. Brody, P. E. Macdougall, C. H. Schiesser, *Asian J. Chem*. **2012**, *1*, 274–279.

[251] K. Šindelář, J. Holubek, M. Ryska, I. Koruna, M. Protiva*, Collect. Czech. Chem. Comm*. **1986**, *51*, 2848–2868.

[252] a) H. Ali, J. E. van Lier, *Tetrahedron Lett*. **1991**, *32*, 5015–5018; b) J. D. Hobbs, S. A. Majumder, L. Luo, G. A. Sickelsmith, J. M. E. Quirke, C. J. Medforth, K. M. Smith, J. A. Shelnutt, *J. Am. Chem. Soc*. **1994**, *116*, 3261–3270.

[253] R. Bonnett, G. F. Stephenson, *J. Org. Chem*. **1965**, *30*, 2791–2798.

[254] H. W. Whitlock Jr., R. Hanauer, *J. Org. Chem*. **1968**, *33*, 2169–2171.

[255] H. Hope, *Prog. Inorg. Chem.* **2007**, 1–19.

[256] a) in *Saint*, Version 8.37a ed., Bruker AXS, Inc., Madison, WI, **2013**; b) in *SADABS*, version 2016/2 ed., Bruker AXS, Inc, Madison, WI,, **2014**; c) in *APEX3*, Version 2016.9-0 ed., Bruker AXS, Inc., Madison, WI,, **2016**.

[257] a) O. V. Dolomanov, L. J. Bourhis, R. J. Gildea, J. A. K. Howard, H. Puschmann, *J. Appl. Crystallogr.* **2009**, *42*, 339–341; b) G. Sheldrick, *Acta Cryst. Sect. A* **2015**, *71*, 3–8.

[258] O. V. Dolomanov, L. J. Bourhis, R. J. Gildea, J. A. K. Howard, H. Puschmann, *J. Appl. Crystallogr*. **2009**, *42*, 339–341.

[259] R. G. Parr, W. Yang, *Density Functional Theory of Atoms and Molecules*, Oxford University Press, Oxford, UK, **1989**.

[260] D. Becke, *J. Chem. Phys.* **1993**, *98*, 5648–5652.

[261] C. Lee, W. Yang, R. G. Parr, *Phys. Rev. B* **1988**, *37*, 785–789.

[262] a) A. J. Wallace, D. L. Crittenden *J. Phys. Chem. A* **2014**, *118*, 2138–2148; b) W. J. Hehre, R. Ditchfield, J. A. Pople, *J. Chem. Phys*. **1972**, *56*, 2257–2261.

[263] M. J. Frisch, G. W. Trucks, H. B. Schlegel, G. E. Scuseria, M. A. Robb, J. R. Cheeseman, G. Scalmani, V. Barone, B. Mennucci, G. A. Petersson, H. Nakatsuji, M. Caricato, X. Li, H. P. Hratchian, A. F. Izmaylov, J. Bloino, G. Zheng, J. L. Sonnenberg, M. Hada, M. Ehara, K. Toyota, R. Fukuda, J. Hasegawa, M. Ishida, T. Nakajima, Y. Honda, O. Kitao, H. Nakai, T. Vreven, J. A. Montgomery Jr., J. E. Peralta, F. Ogliaro, M. Bearpark, J. J. Heyd, E. Brothers, K. N. Kudin, V. N. Staroverov, R. Kobayashi, J. Normand, K. Raghavachari, A. Rendell, J. C. Burant, S. S. Iyengar, J. Tomasi, M. Cossi, N. Rega, J. M. Millam, M. Klene, J.

E. Knox, J. B. Cross, V. Bakken, C. Adamo, J. Jaramillo, R. Gomperts, R. E. Stratmann, O. Yazyev, A. J. Austin, R. Cammi, C. Pomelli, J. W. Ochterski, R. L. Martin, K. Morokuma, V. G. Zakrzewski, G. A. Voth, P. Salvador, J. J. Dannenberg, S. Dapprich, A. D. Daniels, O. Farkas, J. B. Foresman, J. V. Ortiz, J. Cioslowski, D. J. Fox, Gaussian 09, Revision A.02, Gaussian, Inc., Wallingford CT, **2009**.

[264] V. Barone, M. Cossi, *J. Phys. Chem. A* **1998**, *102*, 1995–2001.

[265] R. S. Mulliken, *J. Chem. Phys.* **1955**, *23*, 1833–1840.

[266] in *NSDGUI*, Version 1.3 alpha ed., Sandia National Laboratory: New Mexico, **2001**.

Appendix

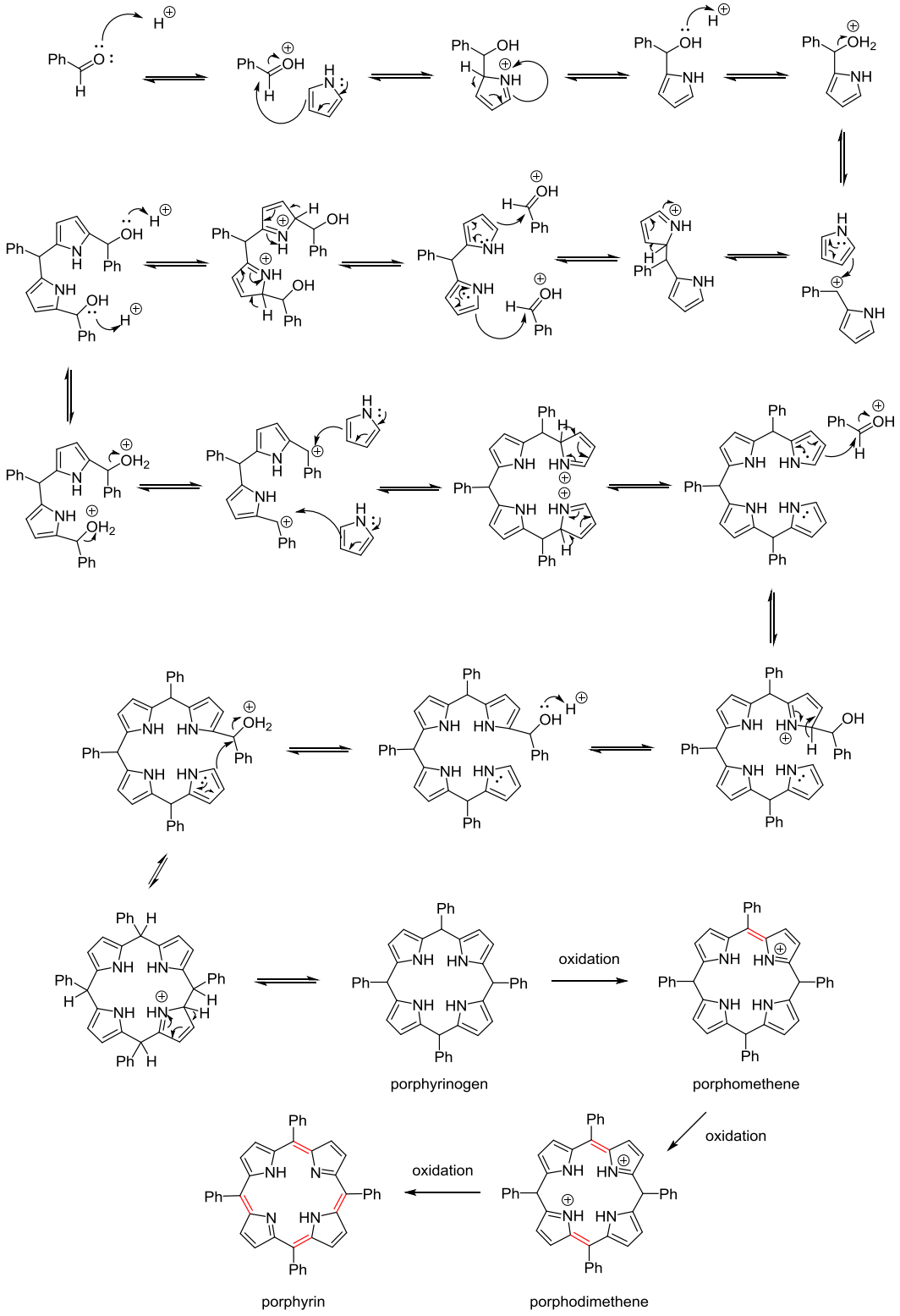

Figure A1. Exemplary reaction mechanism for the formation of a porphyrin through acid-catalyzed condensation of pyrrole and aldehyde.

Deprotonation of DMAP·HCl by 2,3,7,8,12,13,17,18-Octaethyl-5,10,15,20-tetraphenylporphyrin

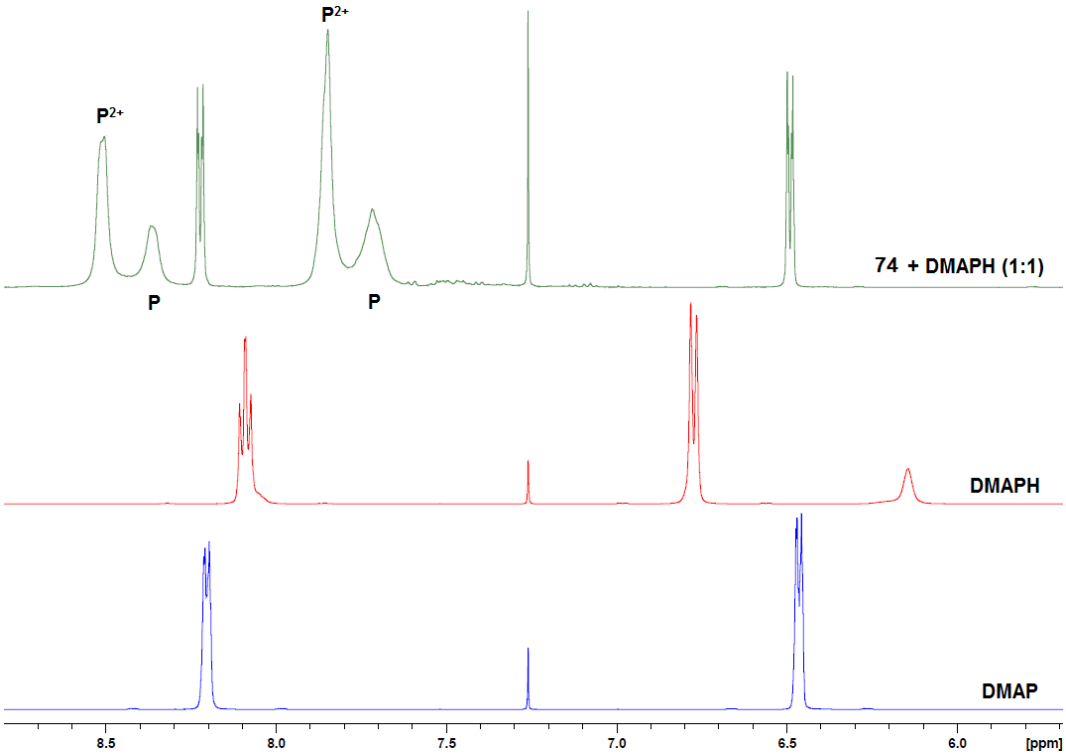

Figure A2. NMR studies on the deprotonation of DMAP·HCl by **74**.

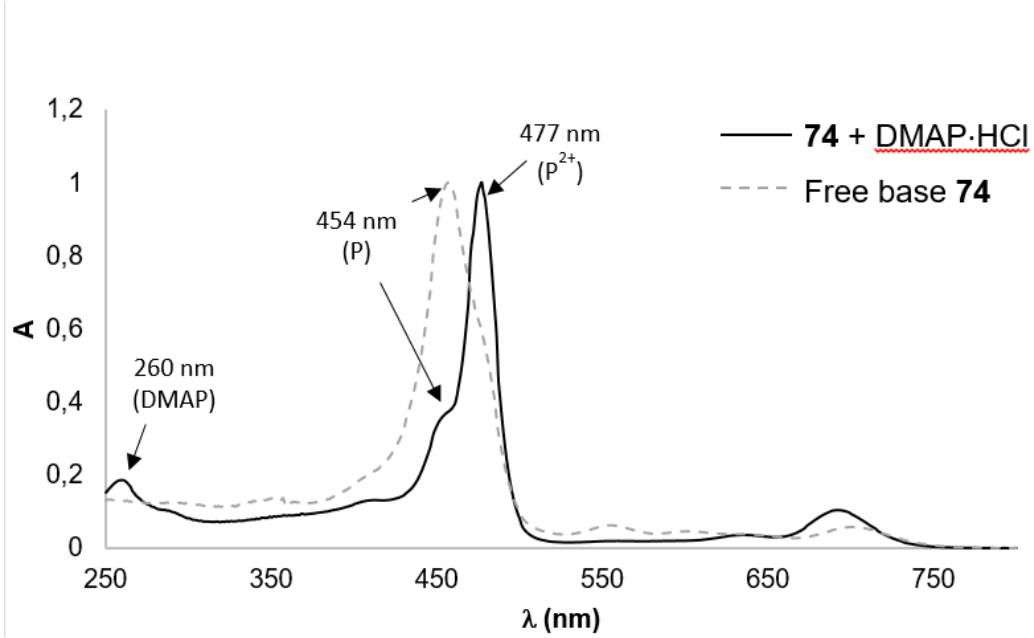

Figure A3. UV-vis studies on the deprotonation of DMAP·HCl by **74**.

Protonation of 2,3,7,8,12,13,17,18-Octaethyl-5,10,15,20-tetraphenylporphyrin by (4-(*tert*-Butyl)benzyl)(2-(phenylsulfonyl)ethyl)sulfane

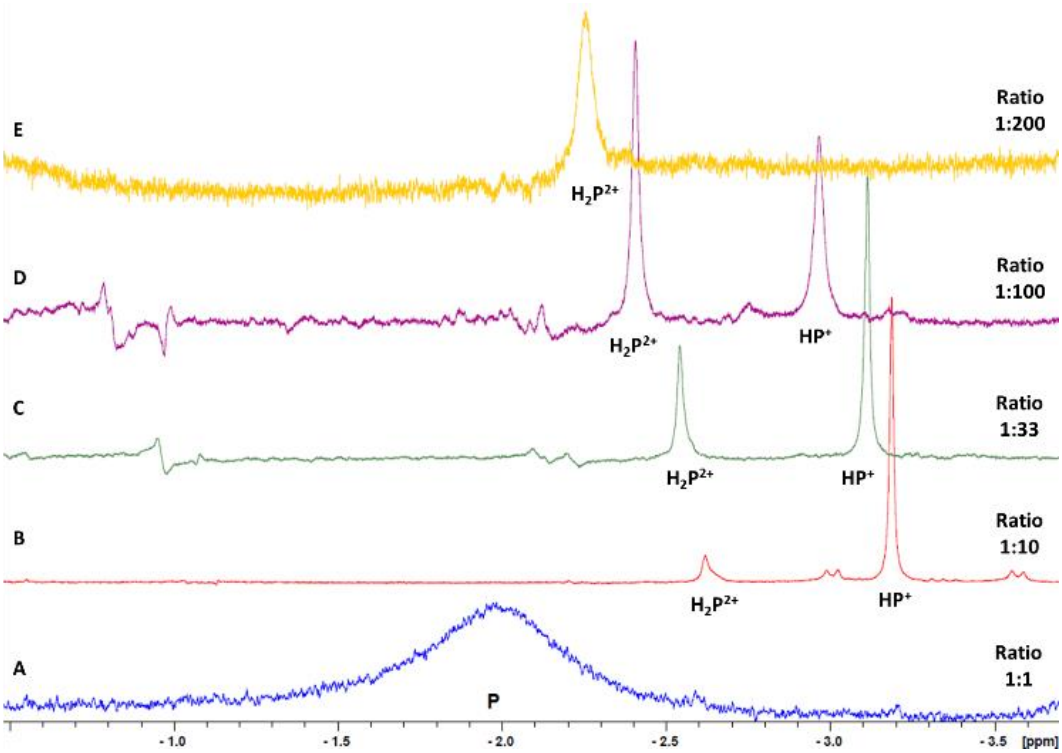

Figure A4. Protonation of **74** by **123** at different molar catalyst:substrate ratios.

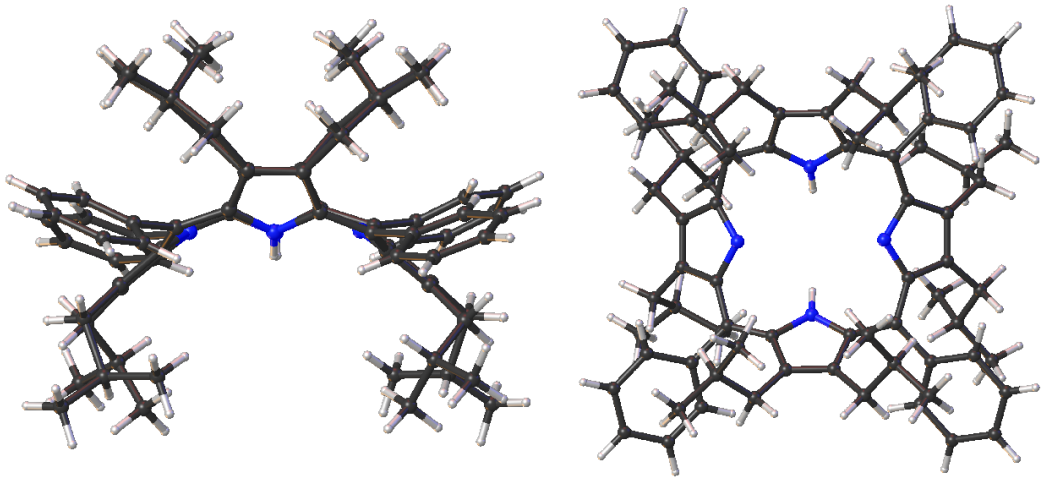

Figure A5. Side and top views of **174**. Thermal ellipsoids indicate 50% probability. *The corresponding crystallographic data was collected and solved by Dr. K. J. Flanagan.*

Influence of TEA on the Consumption of 2,3,7,8,12,13,17,18-Octaethyl-5,10,15,20-tetranitroporphyrin

Compound **95** (5.0 mg, 7.0 µmol, 1 equiv) was dissolved in 1.0 mL of deuterated chloroform and the appropriate amount of TEA was added with a high precision syringe. After the addition of 4-bromobenzenethiol (**HSAr[1]**, 5.9 mg, 31 µmol, 4.4 equiv), the reaction mixture was allowed to stir for 10 min at RT and a sample was taken for ^{1}H NMR analysis without further purification. The amount of unreacted **95** was calculated using the signal of residual chloroform as internal standard.

A blank sample containing only 5.0 mg of **95** in 1 mL of deuterated chloroform was also prepared in order to calibrate the integral of the signal of residual chloroform.

Since aliquots were analyzed without further purification, it was not feasible to directly calculate the amount of **188** formed in the mixture due to overlapping NMR signals, hence the consumption of **95** had to be investigated as an indicator for the progress of the reaction.

Table A1. Screening of the consumption of **95** in the presence of TEA.

entry	TEA (relating to thiol)	consumption of 95 after 10 min, %
1	blank sample	0
2	0 mol%	5
3	23 mol%	77
4	35 mol%	82
5	50 mol%	100

NMR Spectroscopic Studies on the Statistical Porphyrin Type Isomer Mixture Formed from 3-Methyl-4-phenylpyrrole and Benzaldehyde

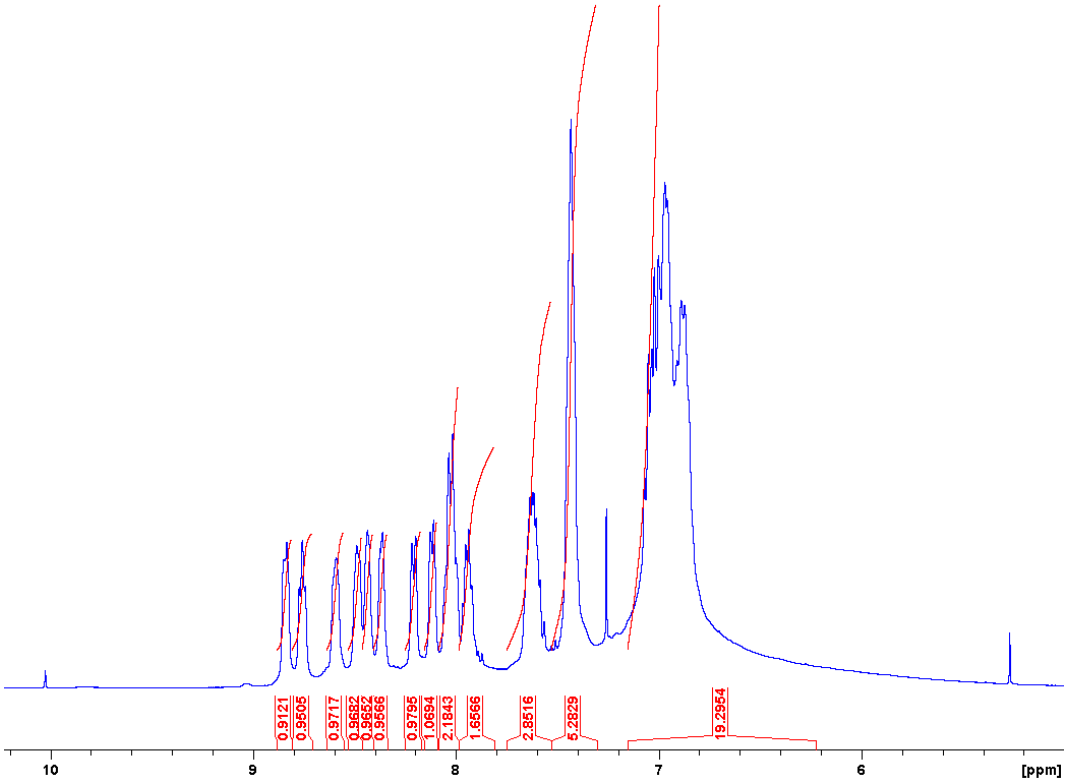

Figure A6. Excerpt of the ^{1}H NMR spectrum of the free base products: aromatic region.

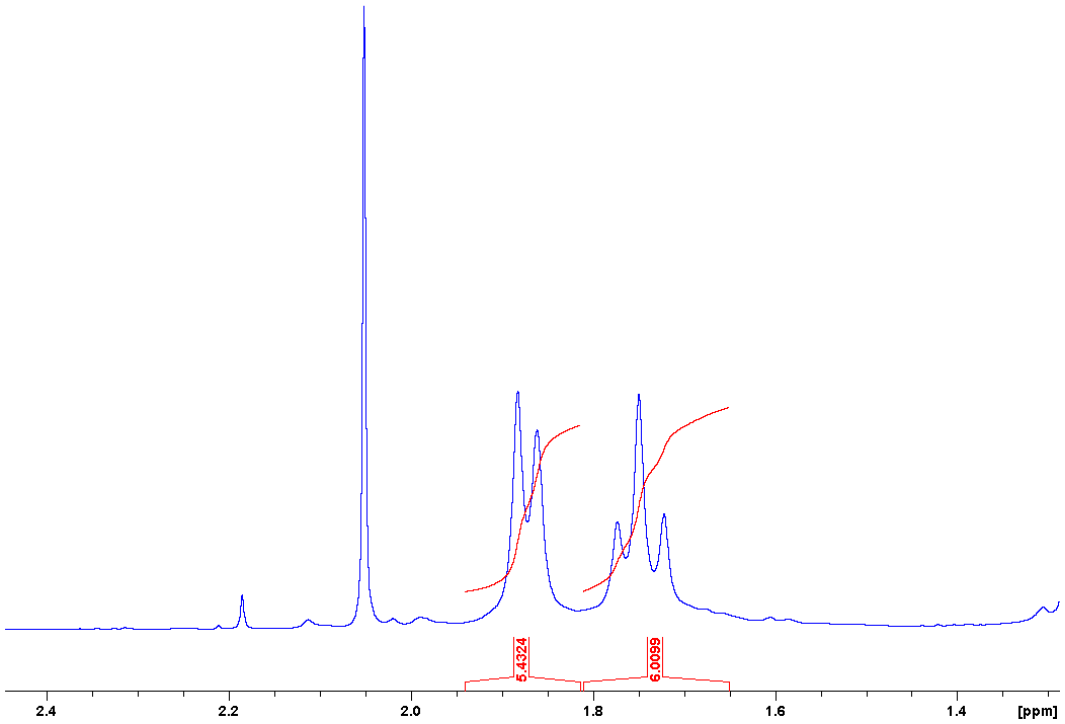

Figure A7. Excerpt of the ^{1}H NMR spectrum of the free base products: aliphatic region.

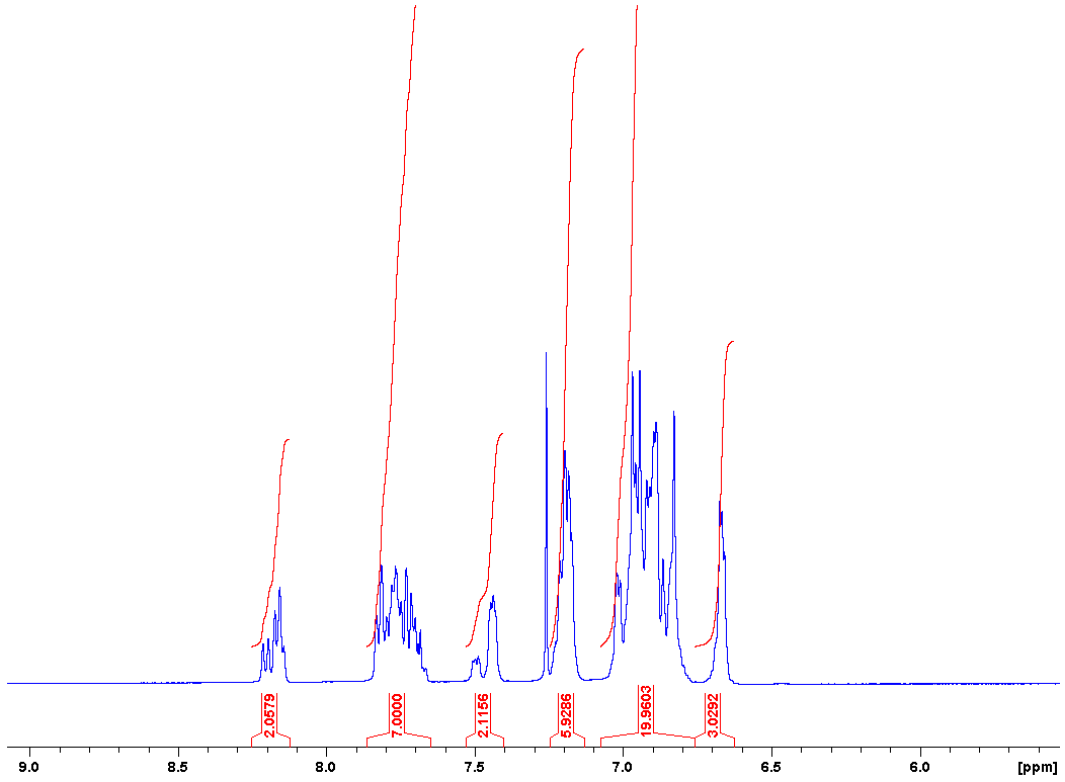

Figure A8. Excerpt of the ^{1}H NMR spectrum of the Ni(II) complex products: aromatic region.

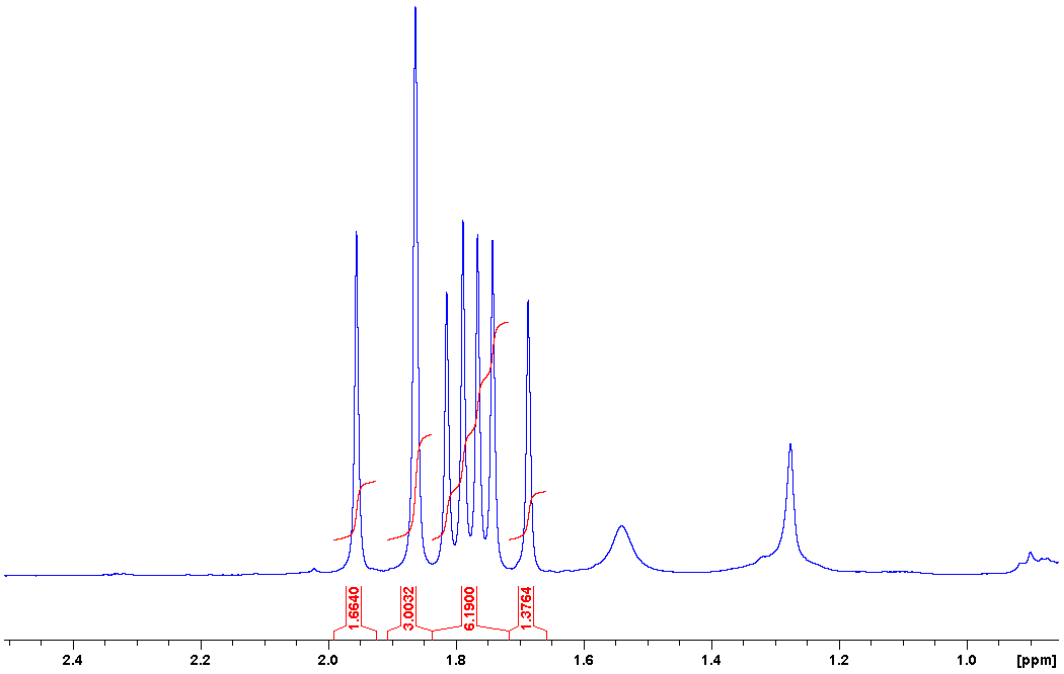

Figure A9. Excerpt of the ^{1}H NMR spectrum of the Ni(II) complex products: aliphatic region.

Determining the Ratio between 5,10-Bis[(4-bromophenyl)thio]-2,3,7,8,12,13,17,18-octaethylporphyrin and 5,15-Bis[(4-bromophenyl)thio]-2,3,7,8,12,13,17,18-octaethylporphyrin

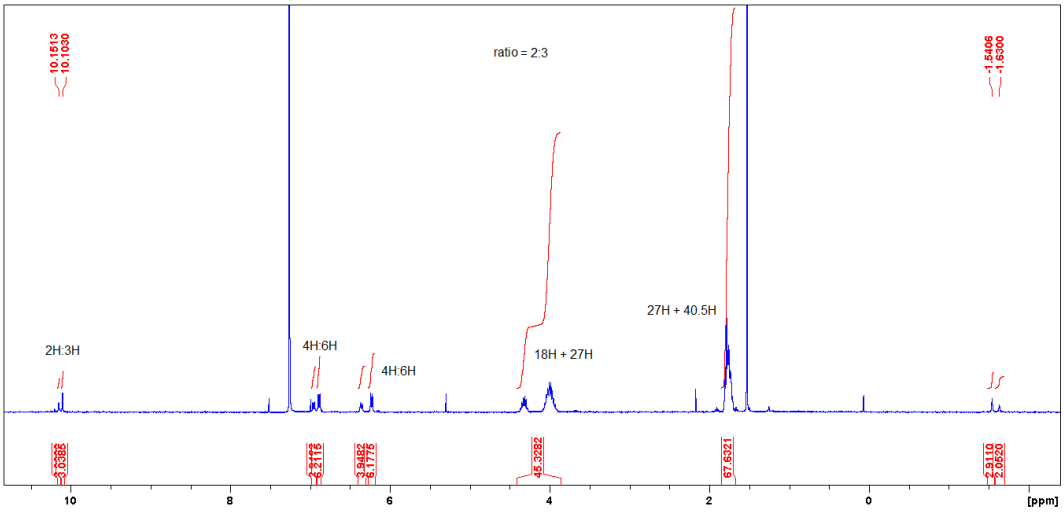

Figure A10. ^{1}H NMR spectrum of 5,10-bis[(4-bromophenyl)thio]-2,3,7,8,12,13,17,18-octaethylporphyrin (**190**) and 5,15-bis[(4-bromophenyl)thio]-2,3,7,8,12,13,17,18-octaethylporphyrin (**191**).

Integration of the N–H proton signals at −1.63 and −1.54 ppm and the meso-proton signals at 10.10 and 10.15 ppm indicate a 2:3 ratio of two porphyrins. Additionally, integration of the signals for aromatic hydrogen atoms confirms the suggested substitution pattern. HRMS analysis was in accordance with this result as only a single major *m/z* signal was detected and the isotope distribution was affirmative. Due to the chemical shifts and the fact that comparable S_NAr reactions showed a preference towards formation of the 5,10-disubstituted product,[162] it is proposed that **190** is the major compound.

^{1}H NMR Spectra of New Compounds

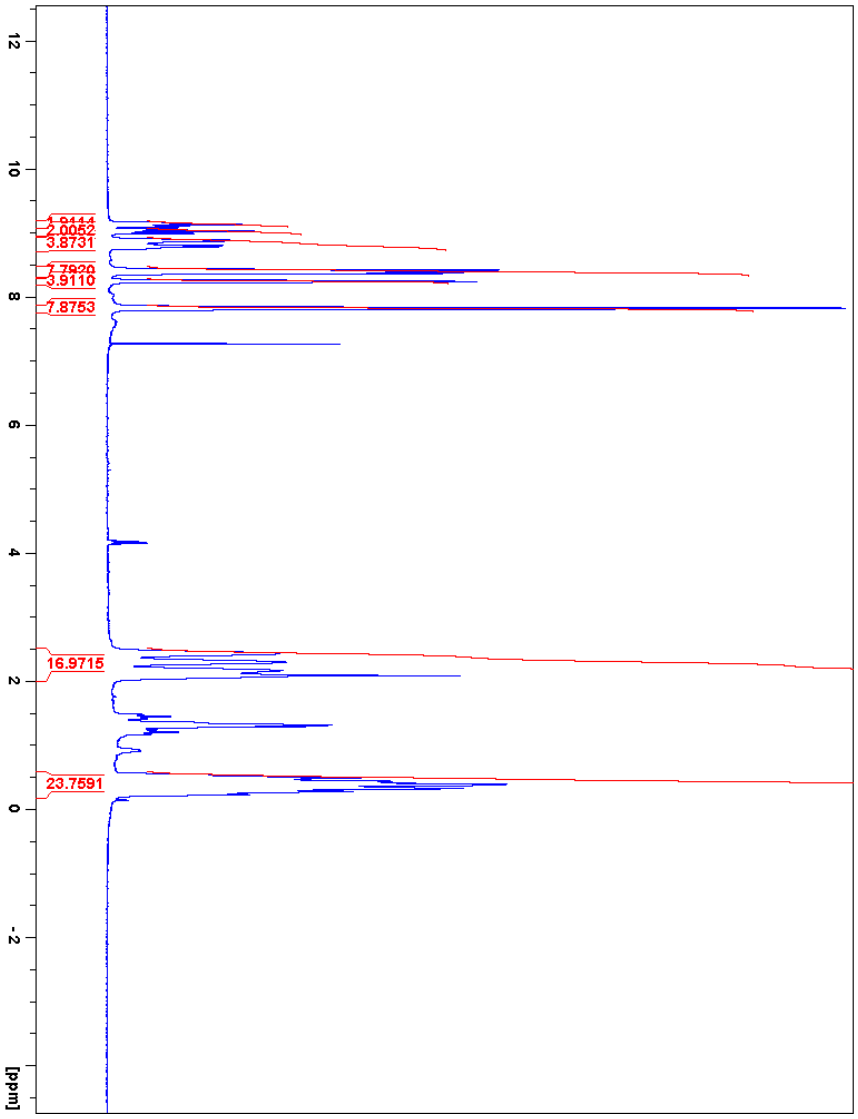

Figure A11: ^{1}H NMR spectrum of **162**.

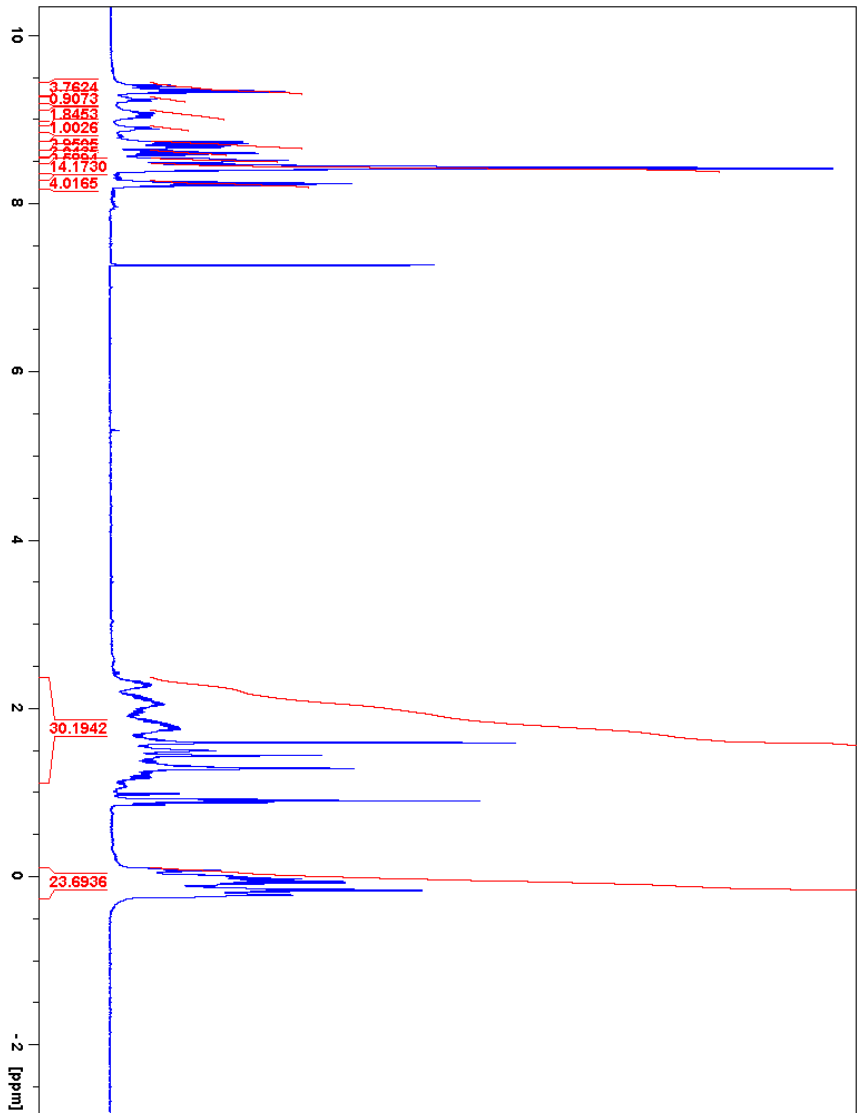

Figure A12: ^{1}H NMR spectrum of **164**.

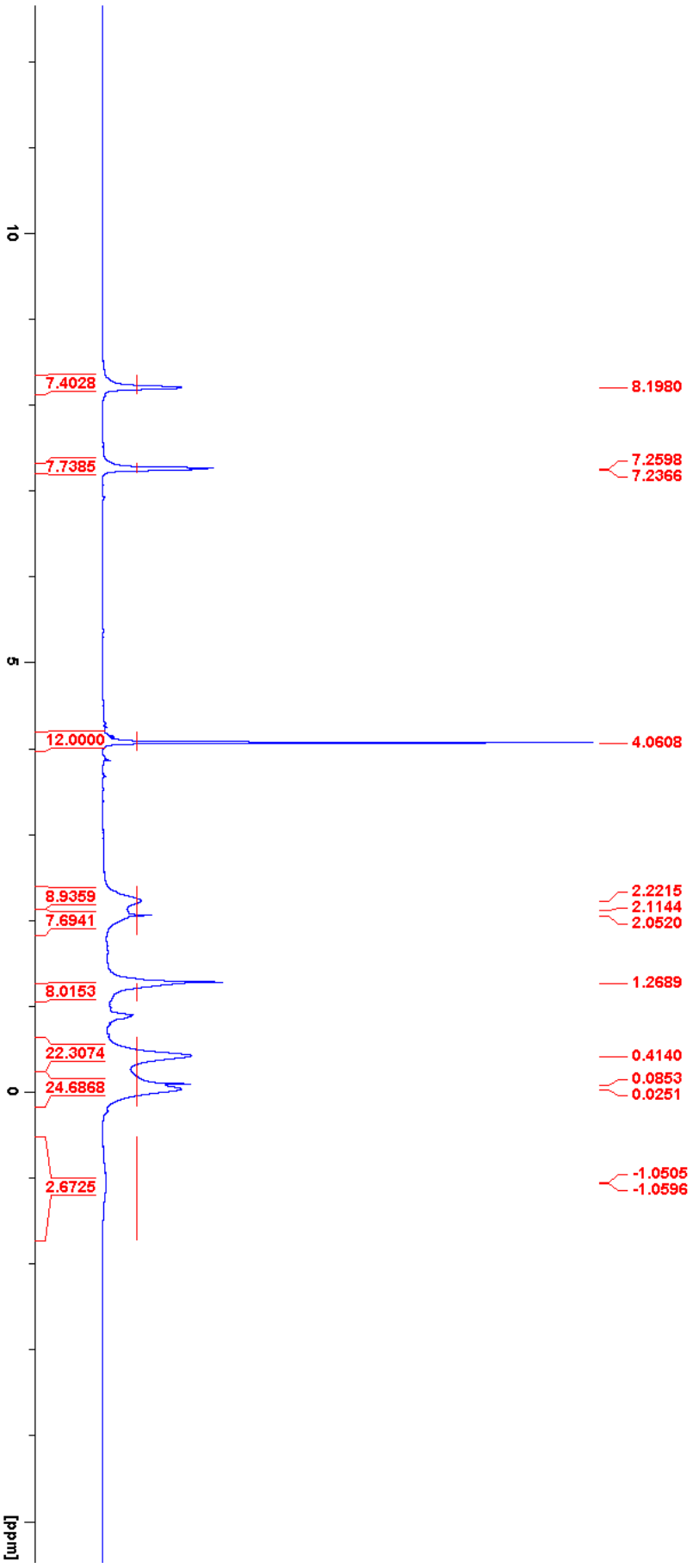

Figure A13: ^{1}H NMR spectrum of **175**.

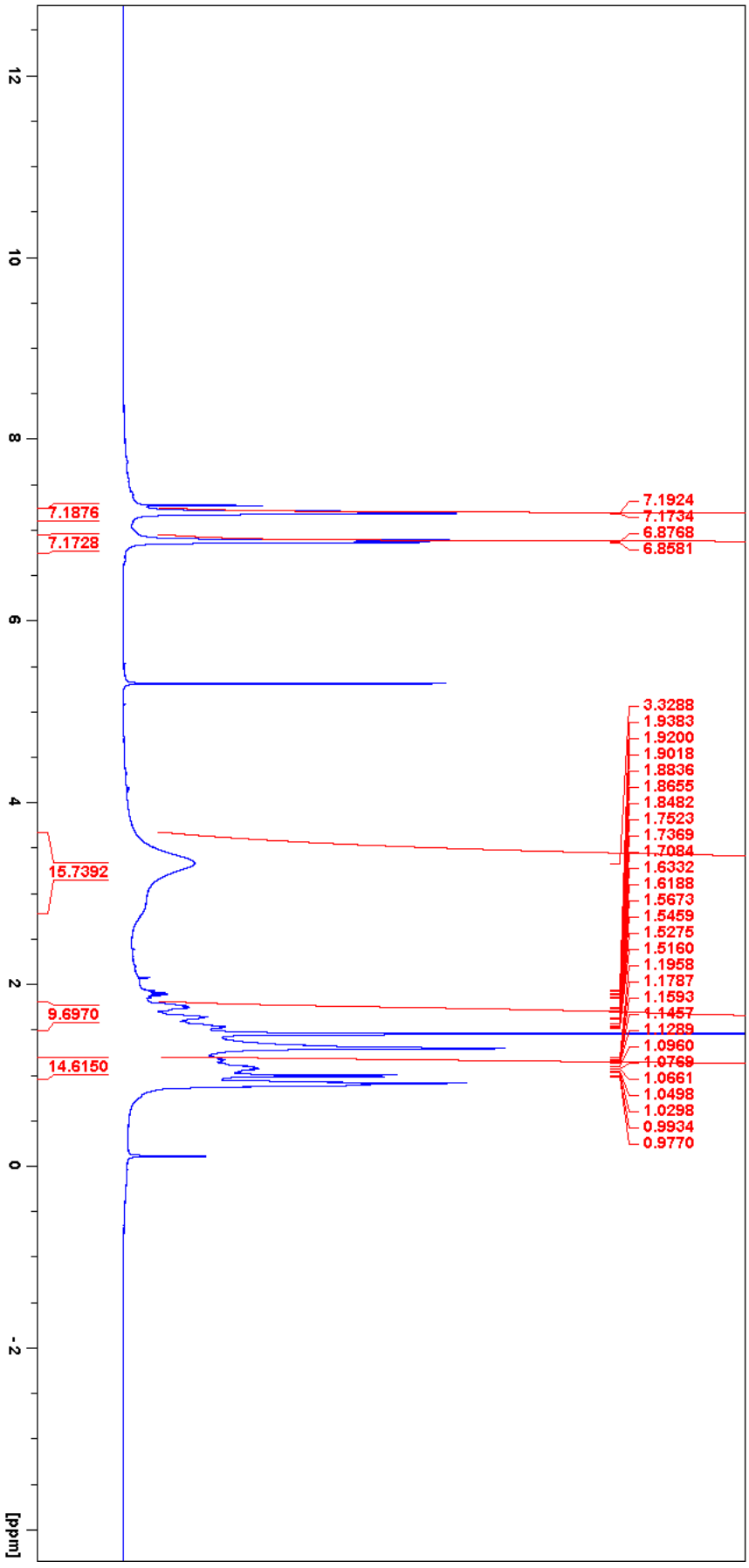

Figure A14: ^{1}H NMR spectrum of **188**.

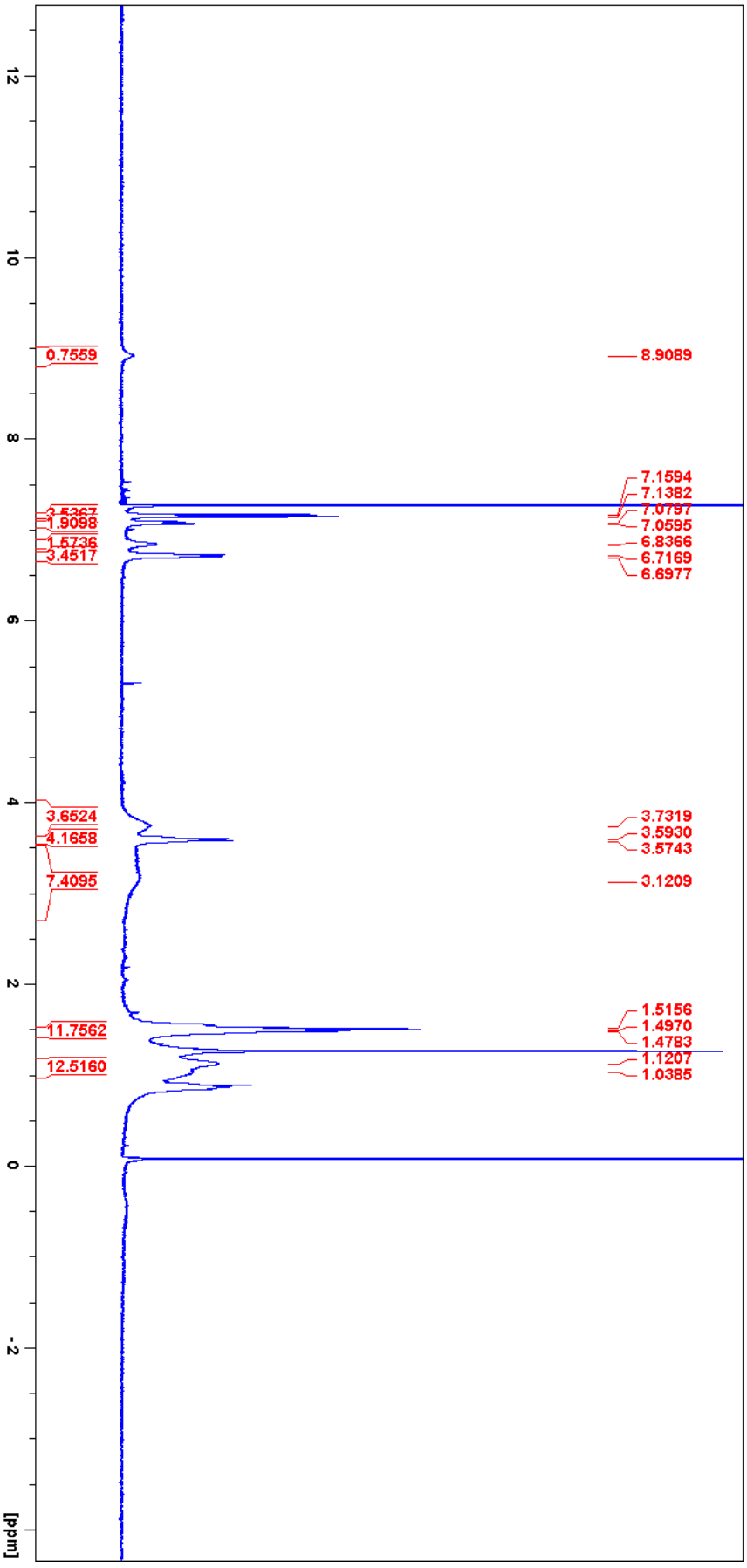

Figure A15: ^{1}H NMR spectrum of **189**.

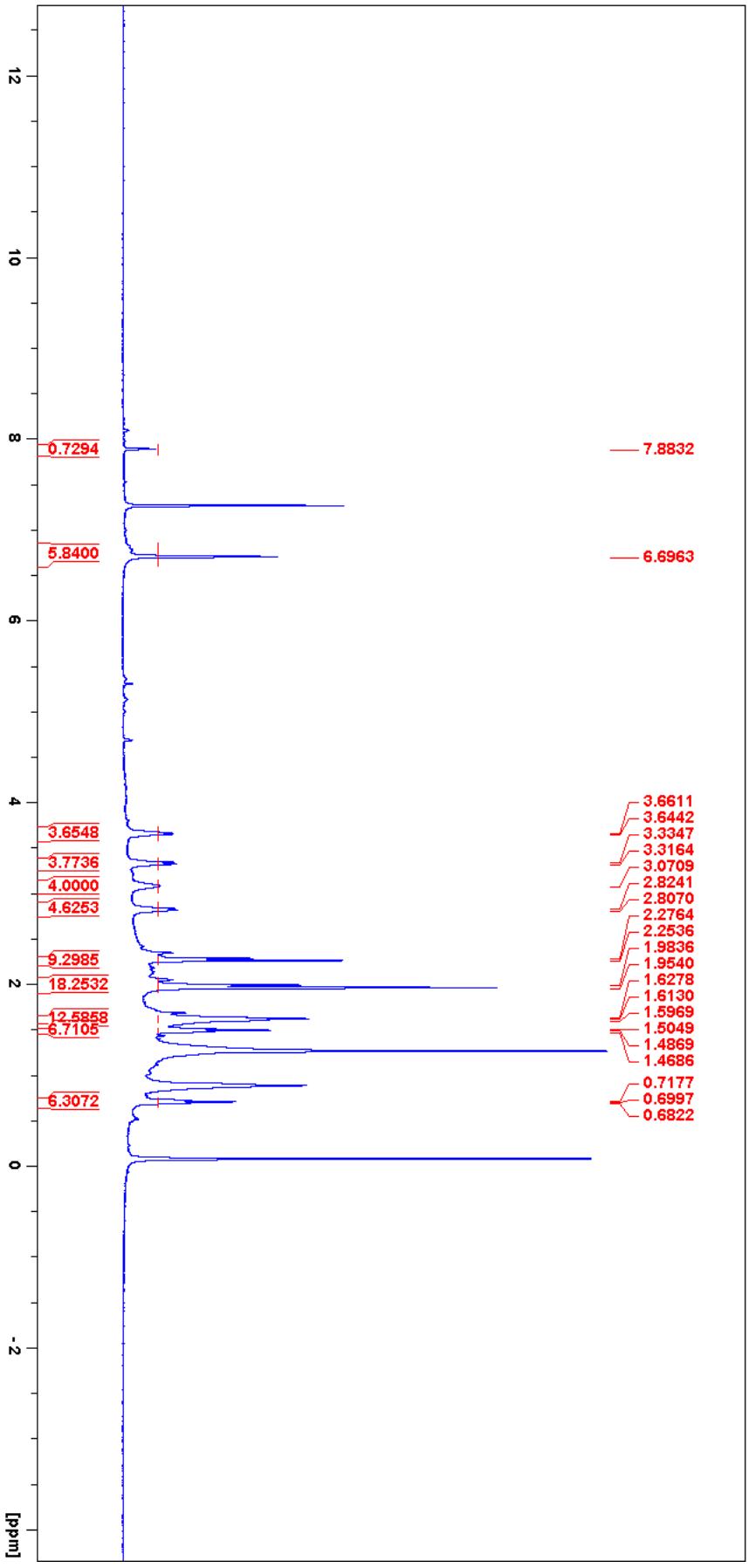

Figure A16: ^{1}H NMR spectrum of **192**.

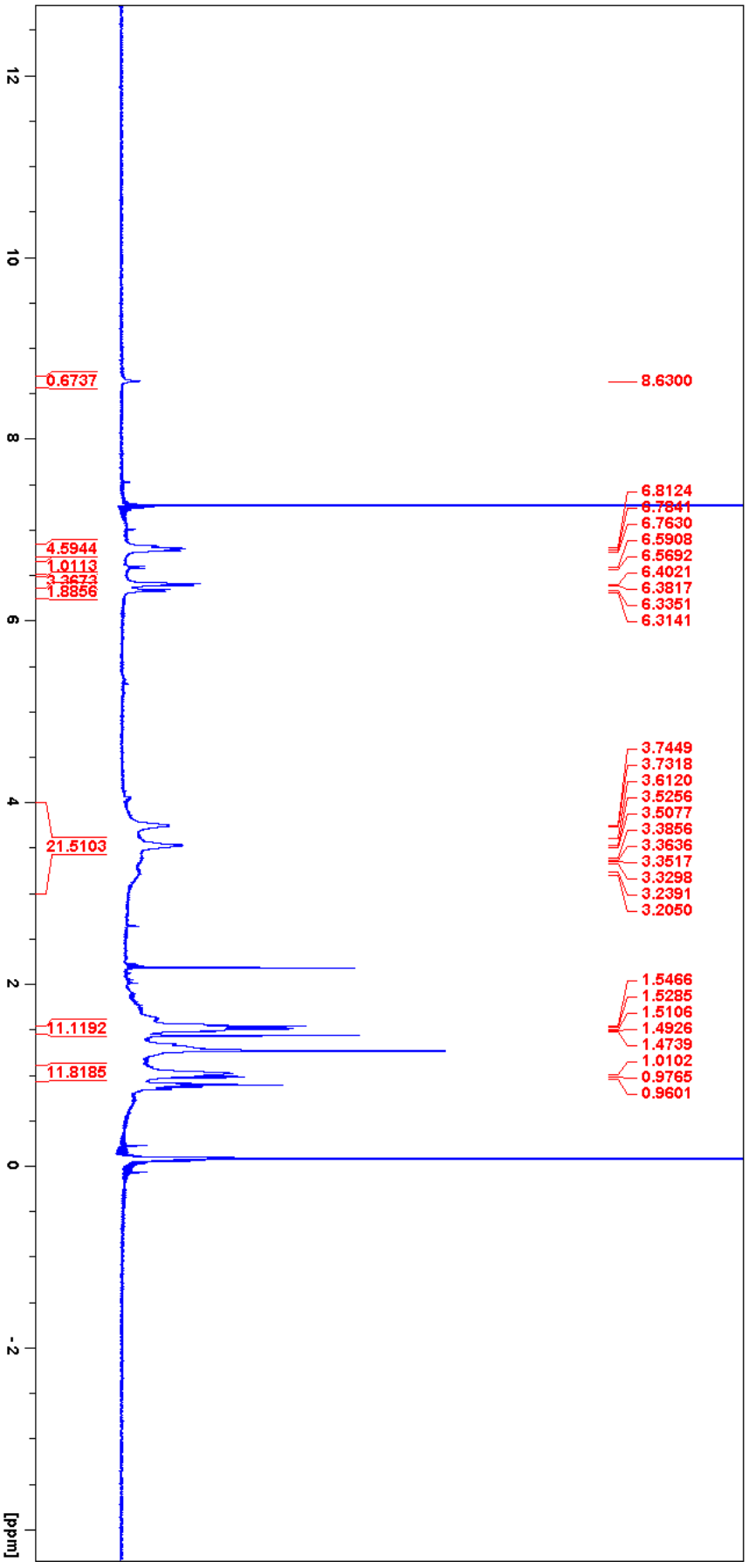

Figure A17: ^{1}H NMR spectrum of **193**.

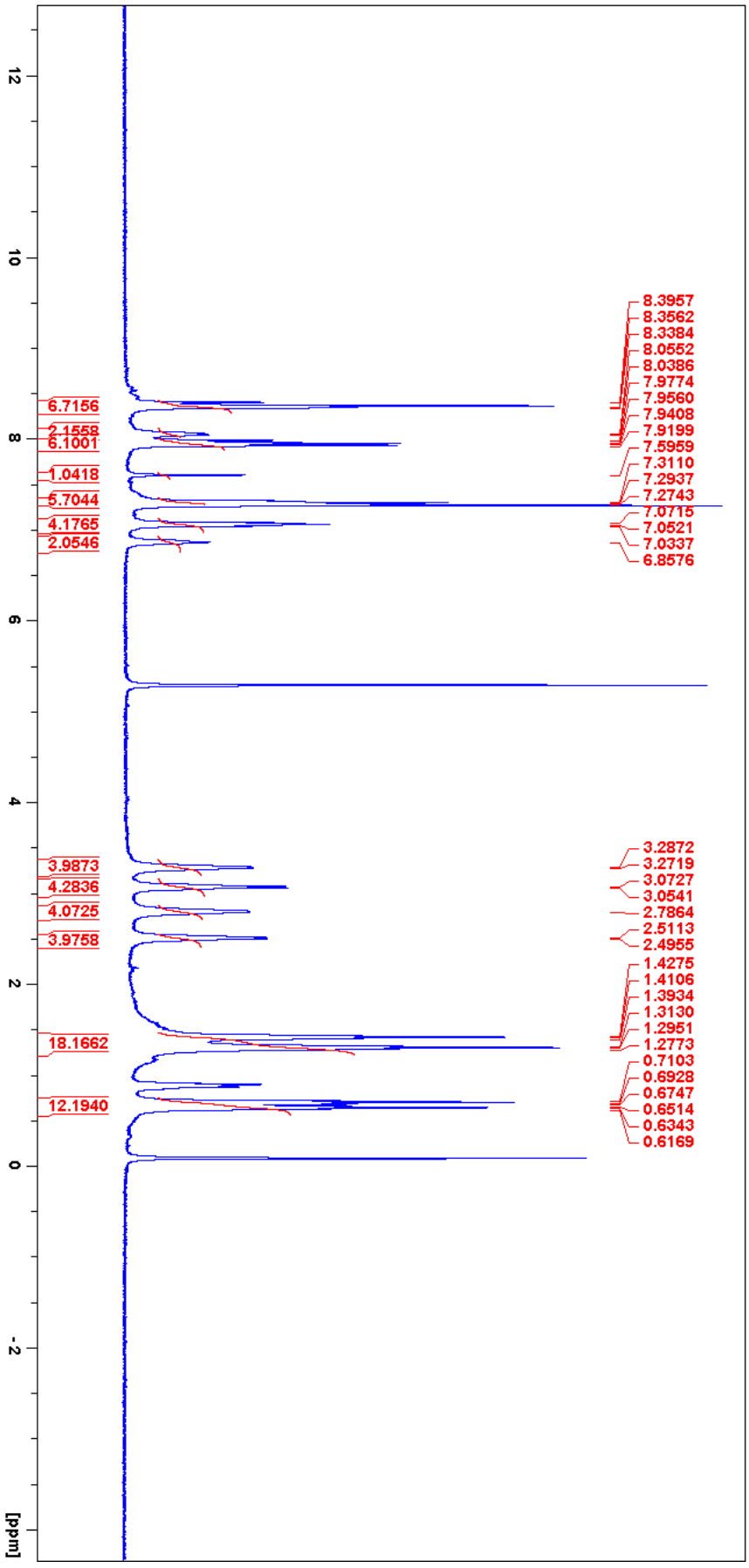

Figure A18: ^{1}H NMR spectrum of **194**.

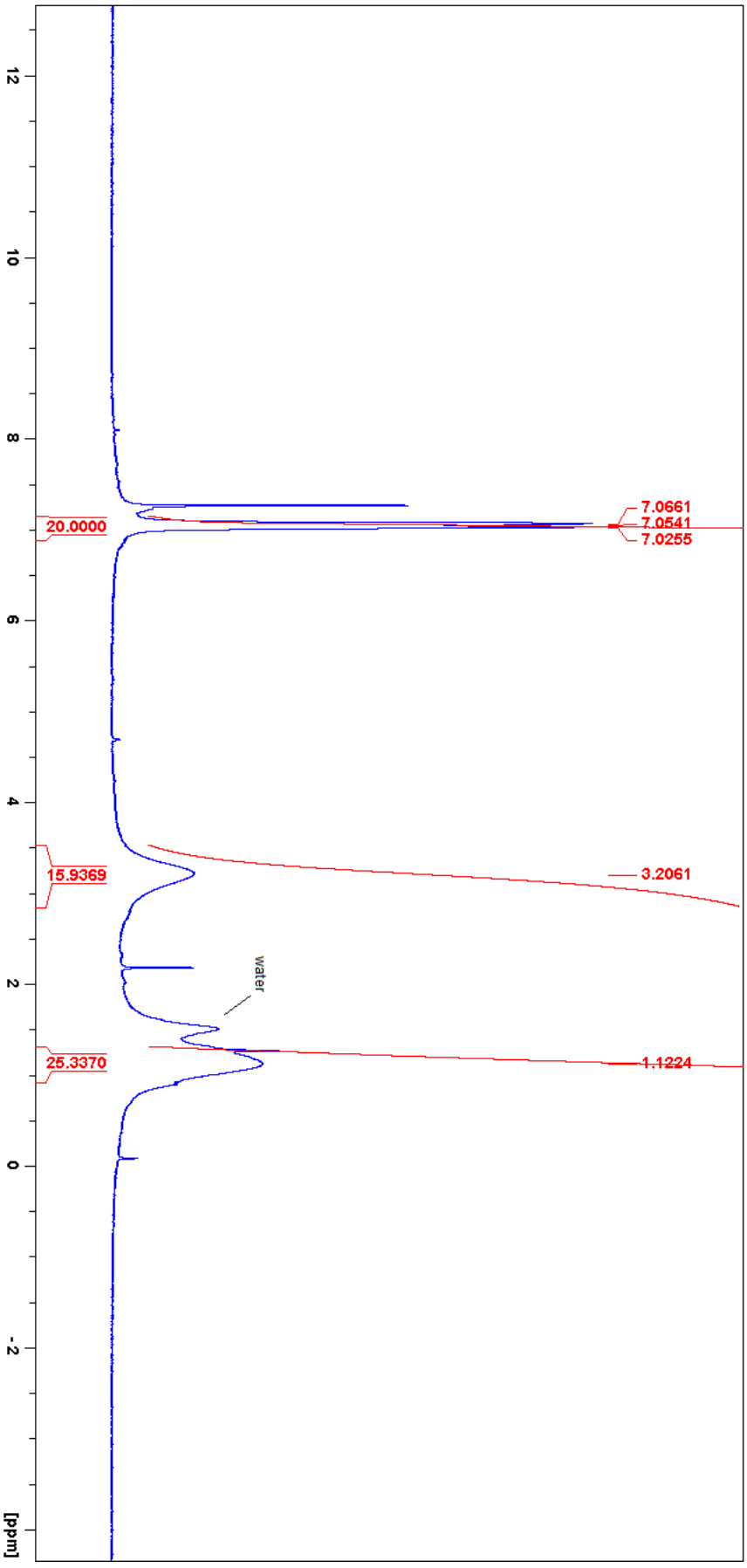

Figure A19: ^{1}H NMR spectrum of **195**.

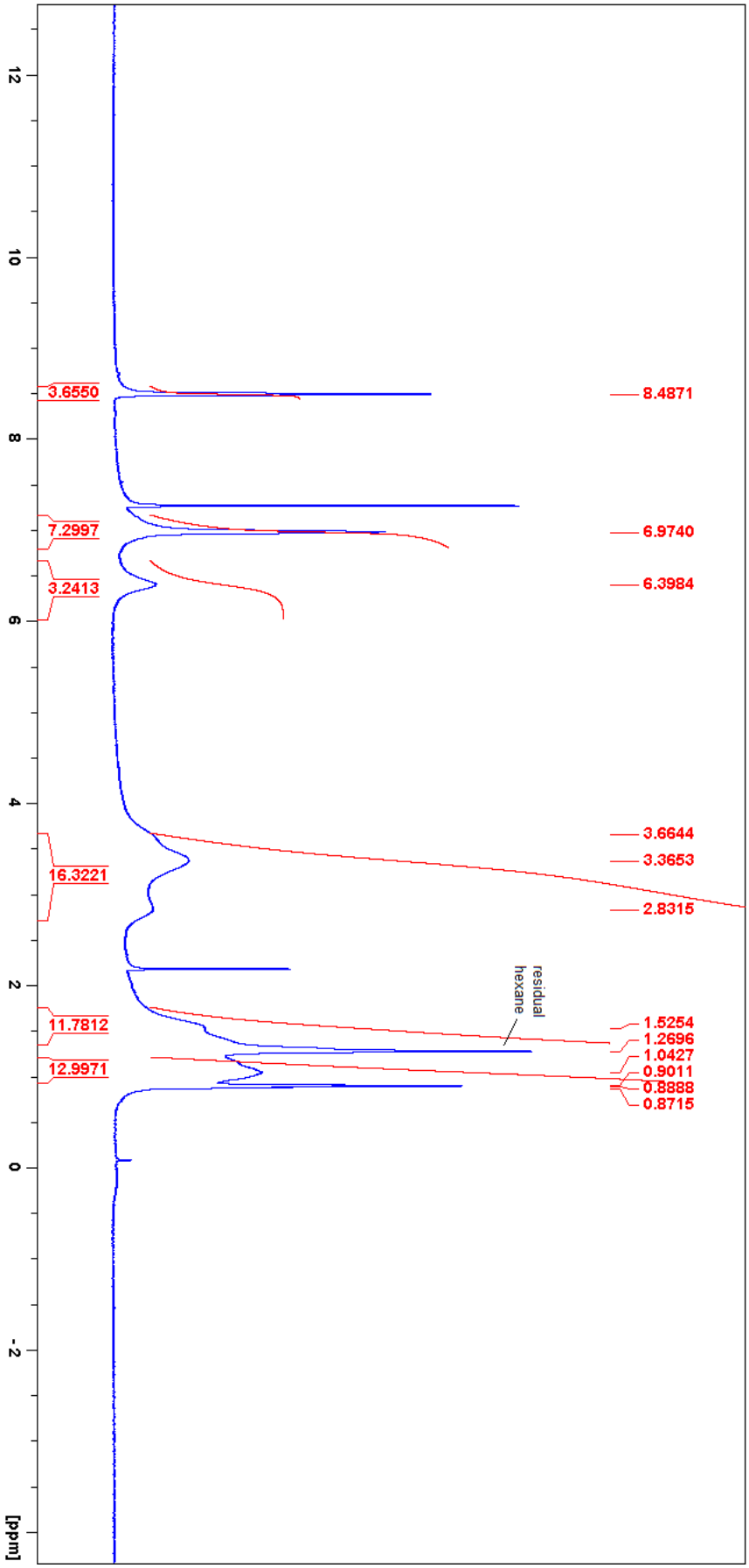

Figure A20: ^{1}H NMR spectrum of **196**.

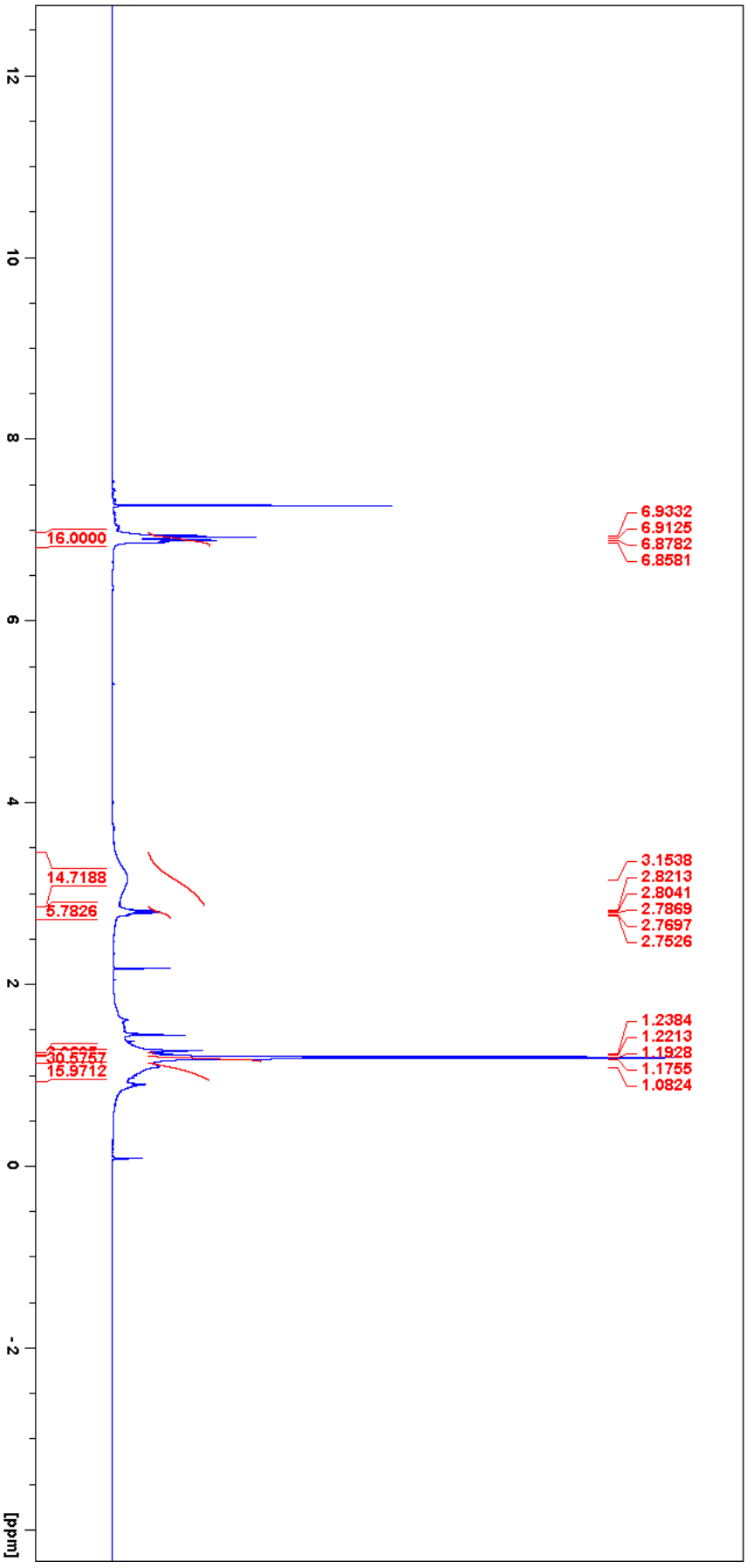

Figure A21: ^{1}H NMR spectrum of **197**.

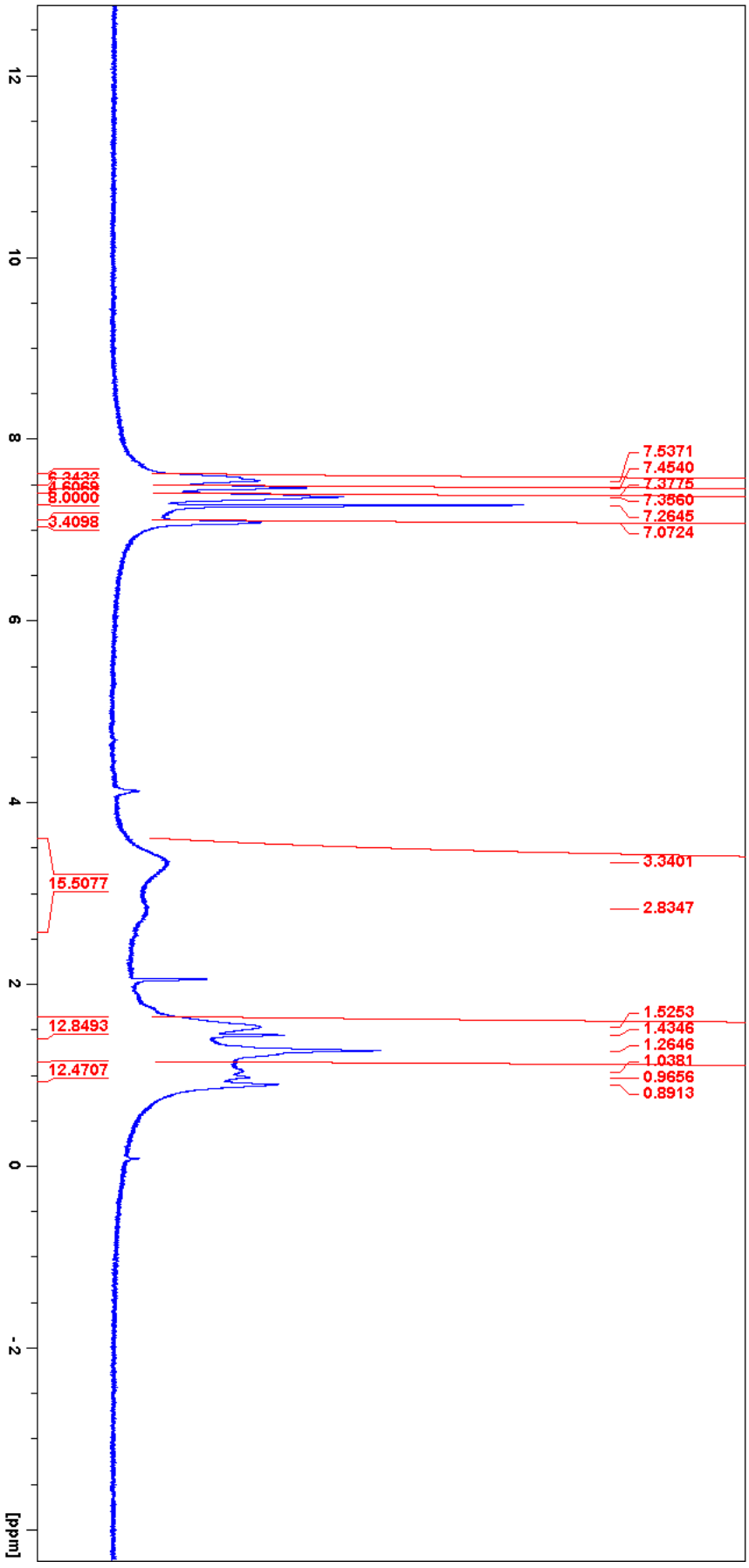

Figure A22: ^{1}H NMR spectrum of **198**.

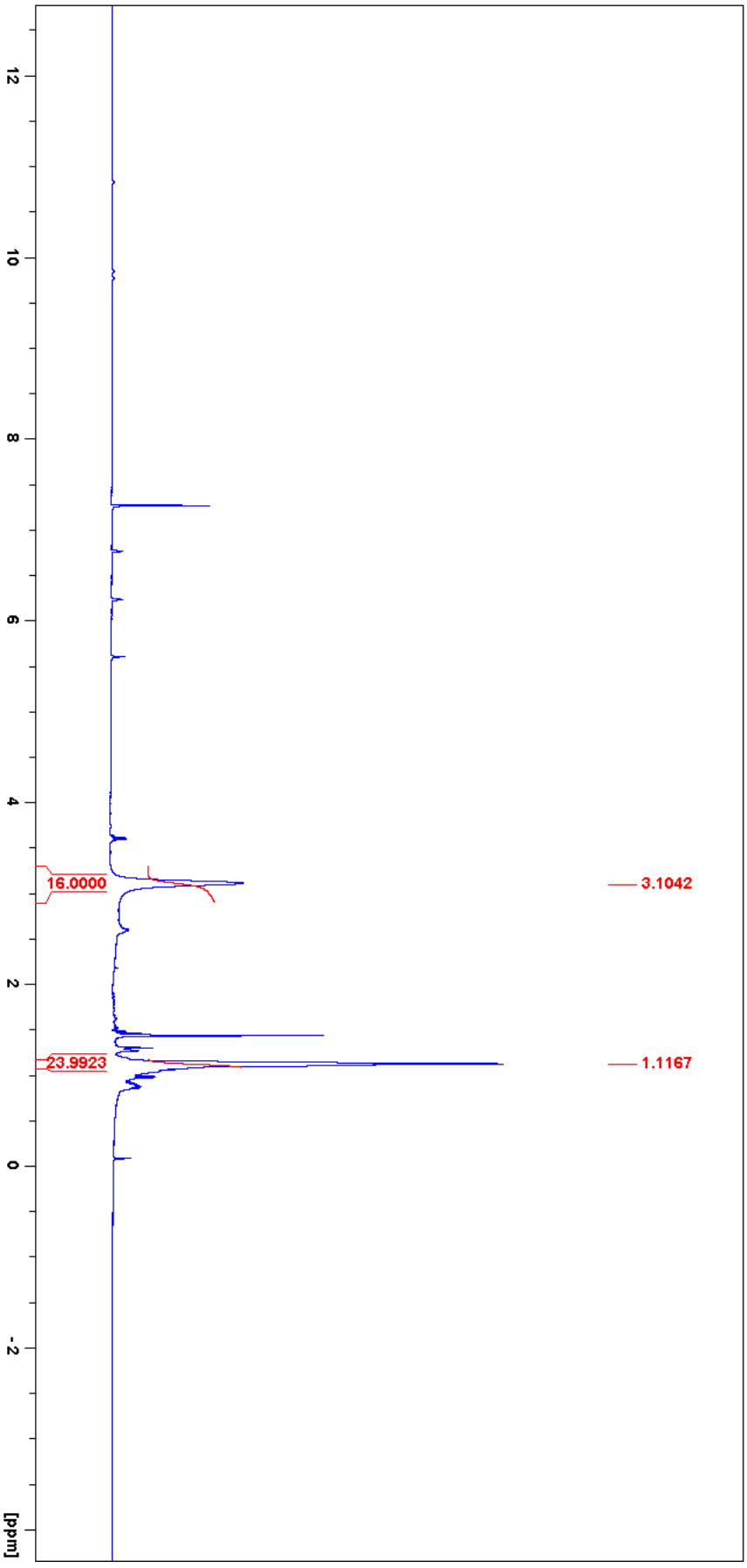

Figure A23: ^{1}H NMR spectrum of **199**.

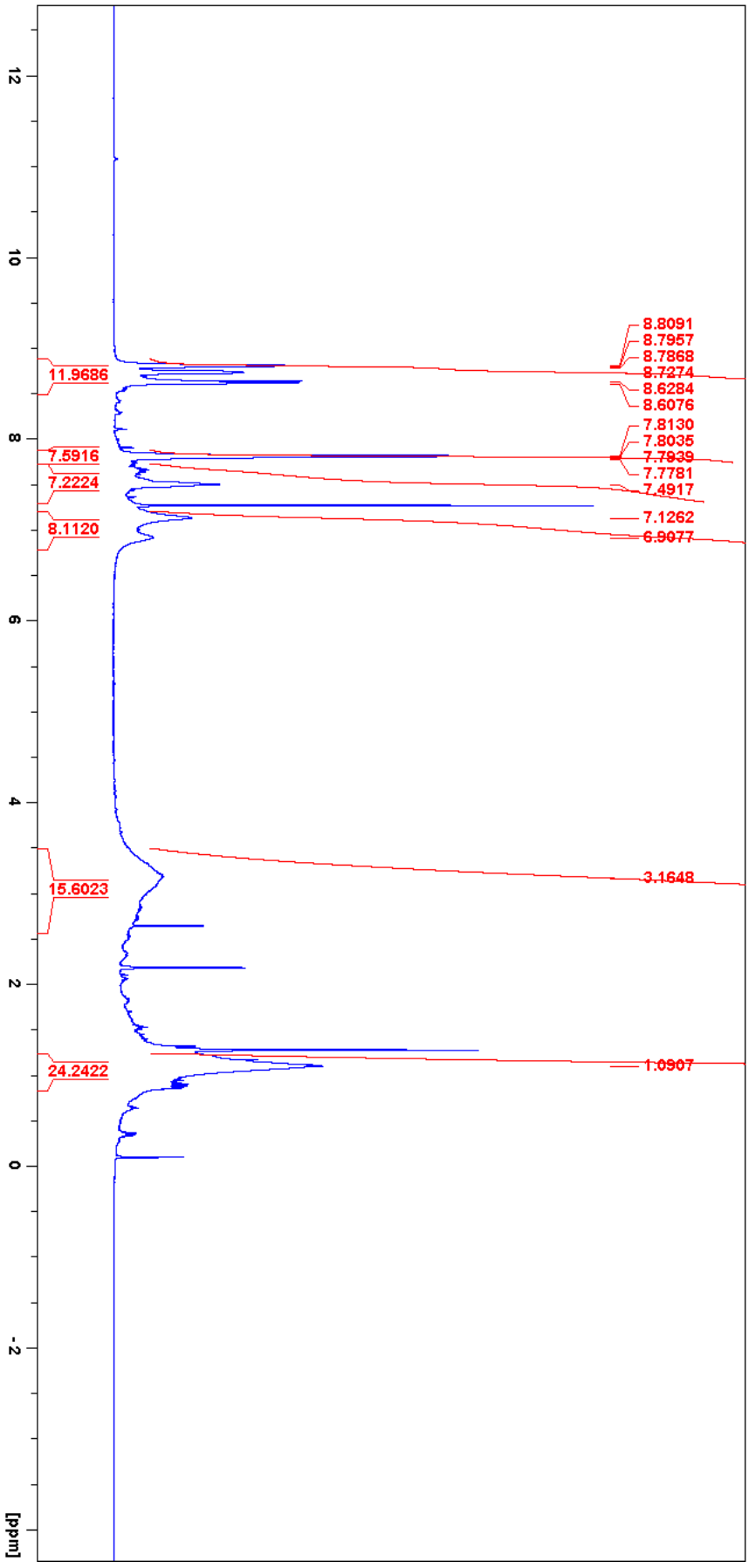

Figure A24: ^{1}H NMR spectrum of **200**.

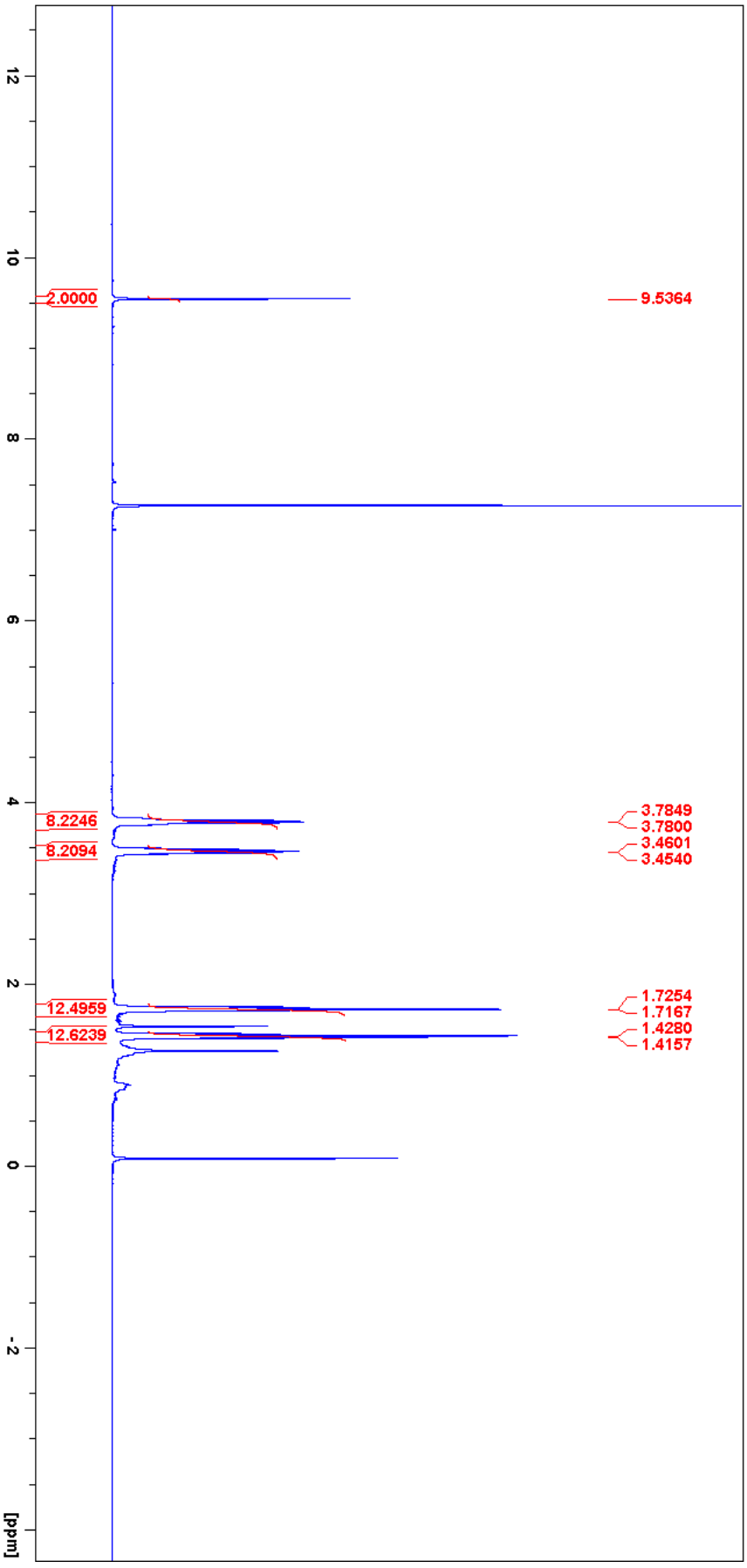

Figure A25: ^{1}H NMR spectrum of **204**.

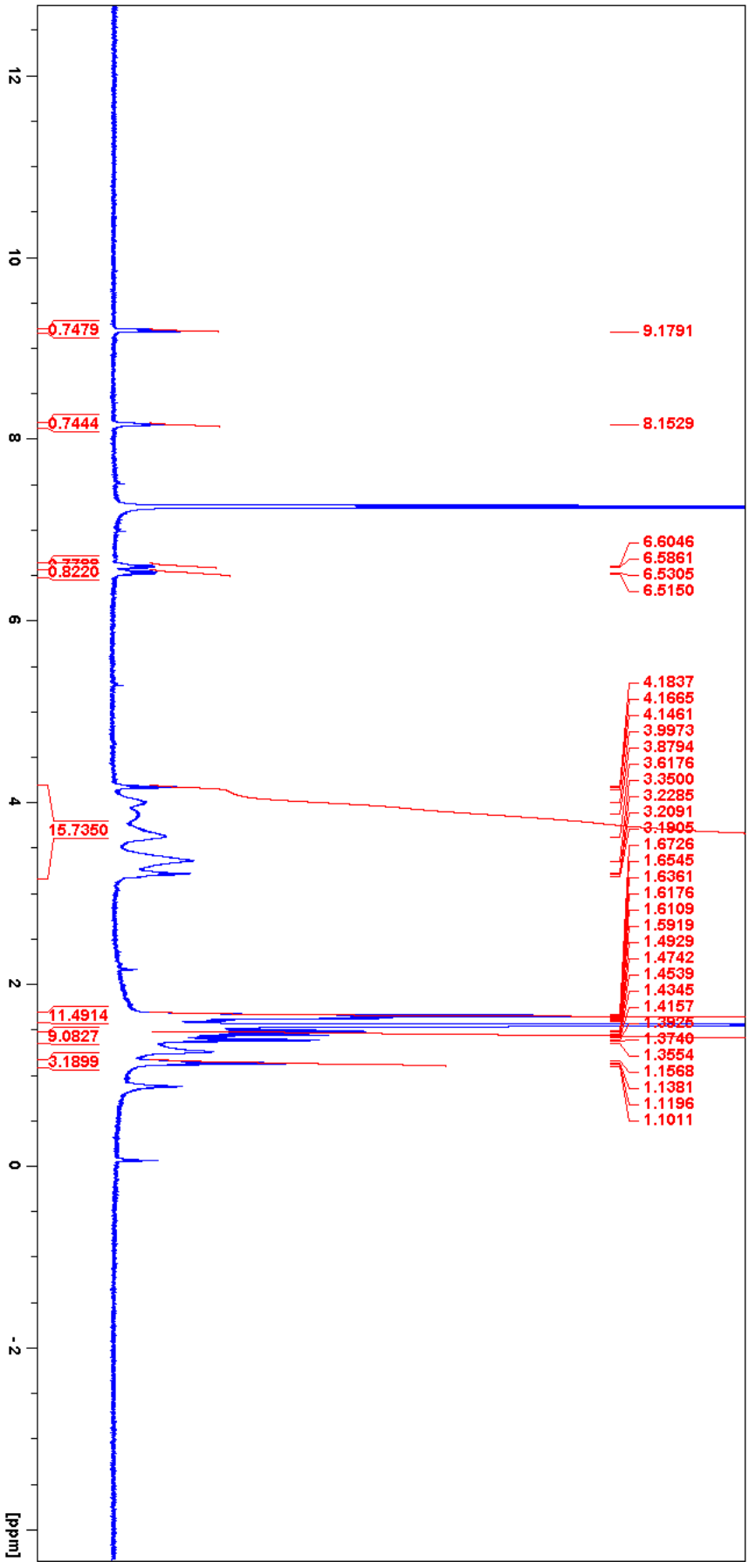

Figure A26: ^{1}H NMR spectrum of **205**.

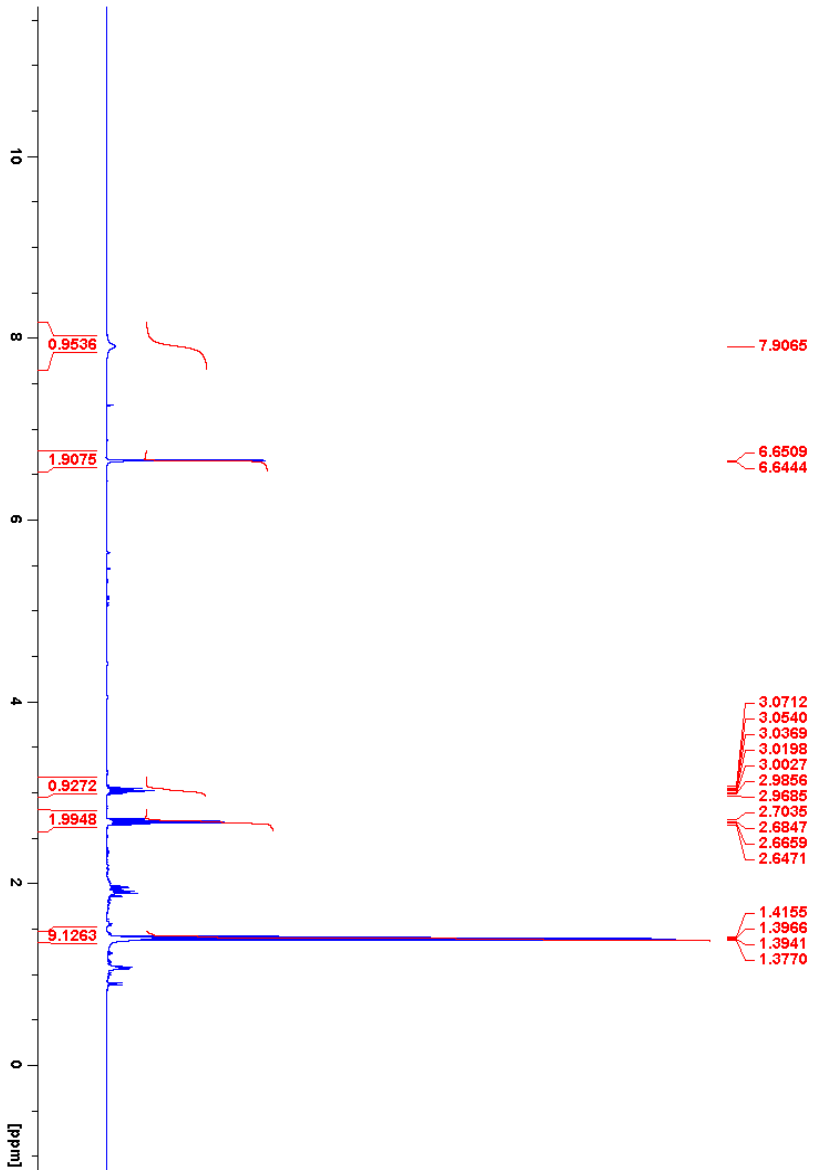

Figure A27: ^{1}H NMR spectrum of **182**.

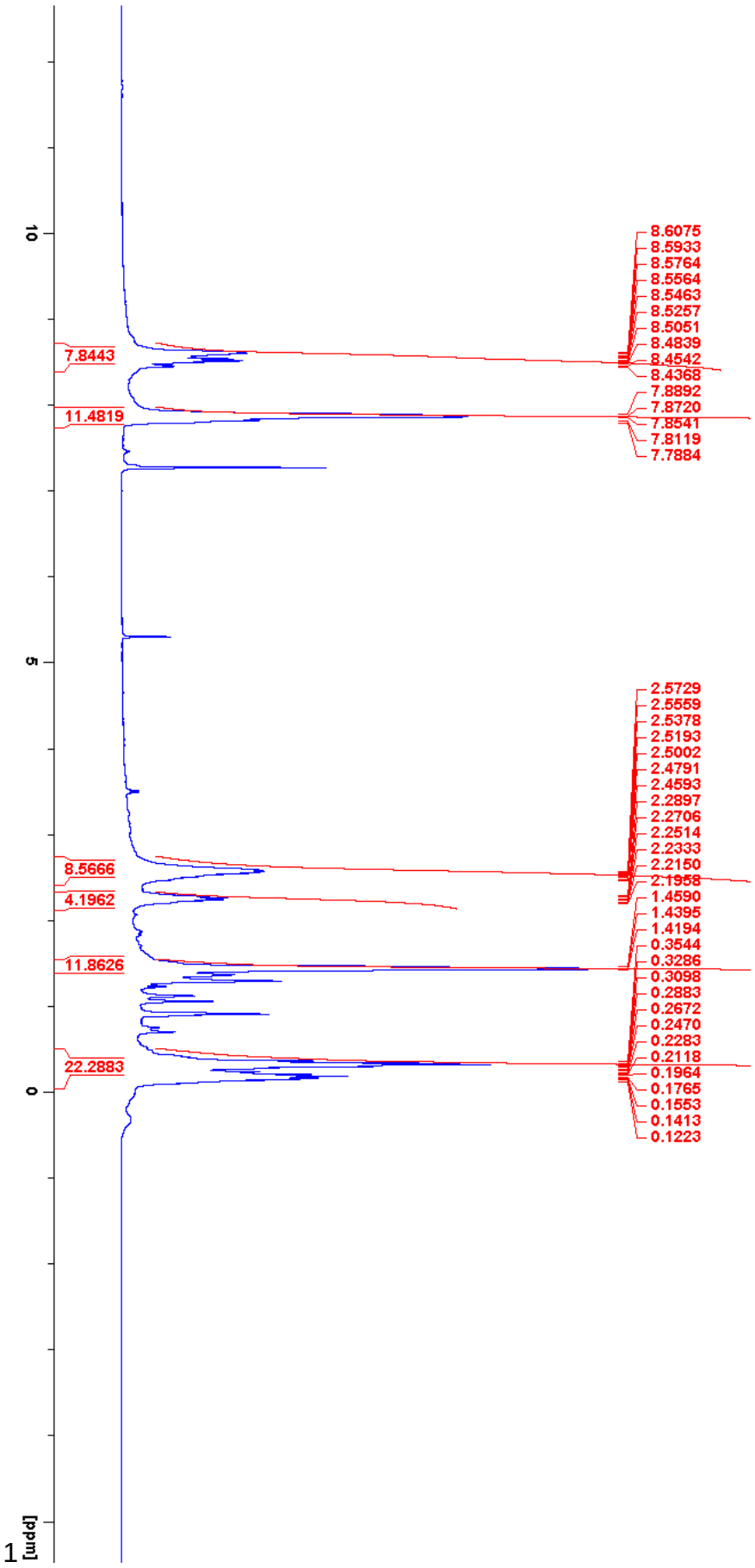

Figure A28: ^{1}H NMR spectrum of **243**·2HCl.

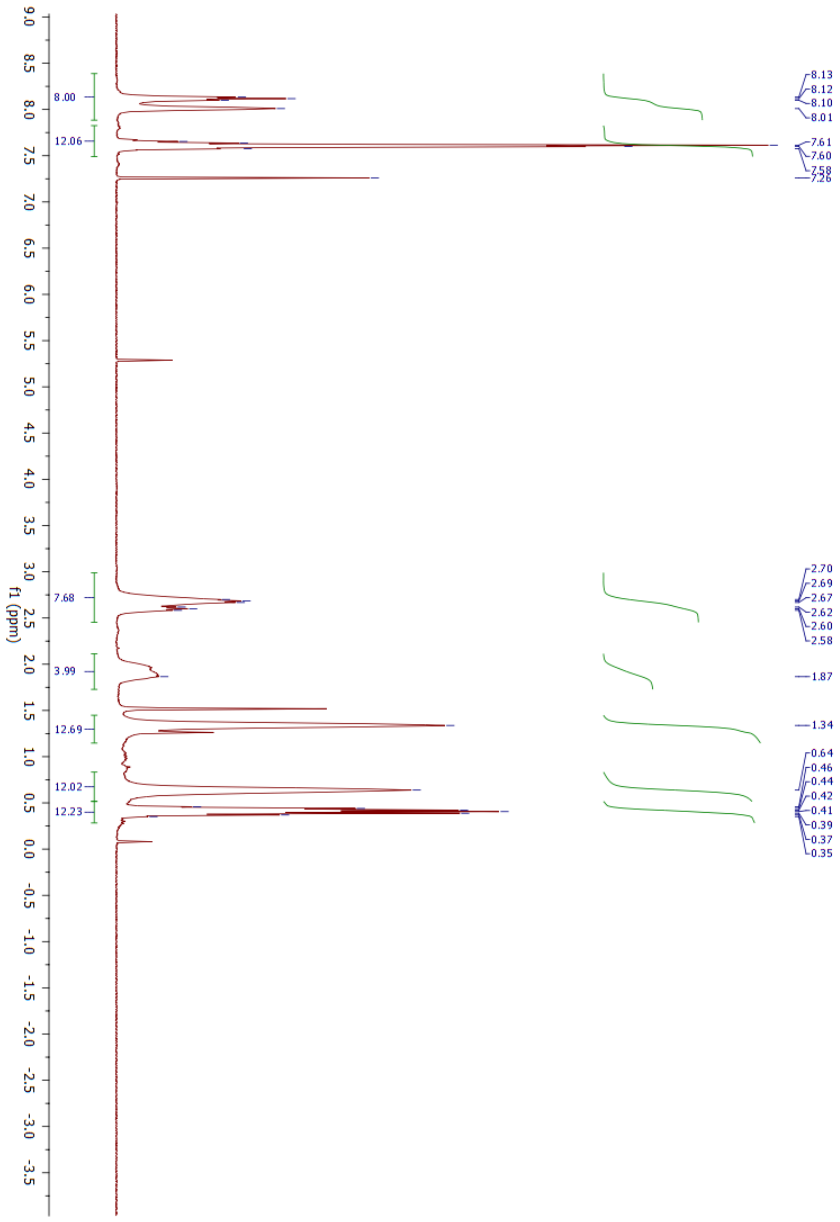

Figure A29: ^{1}H NMR spectrum of **244**.

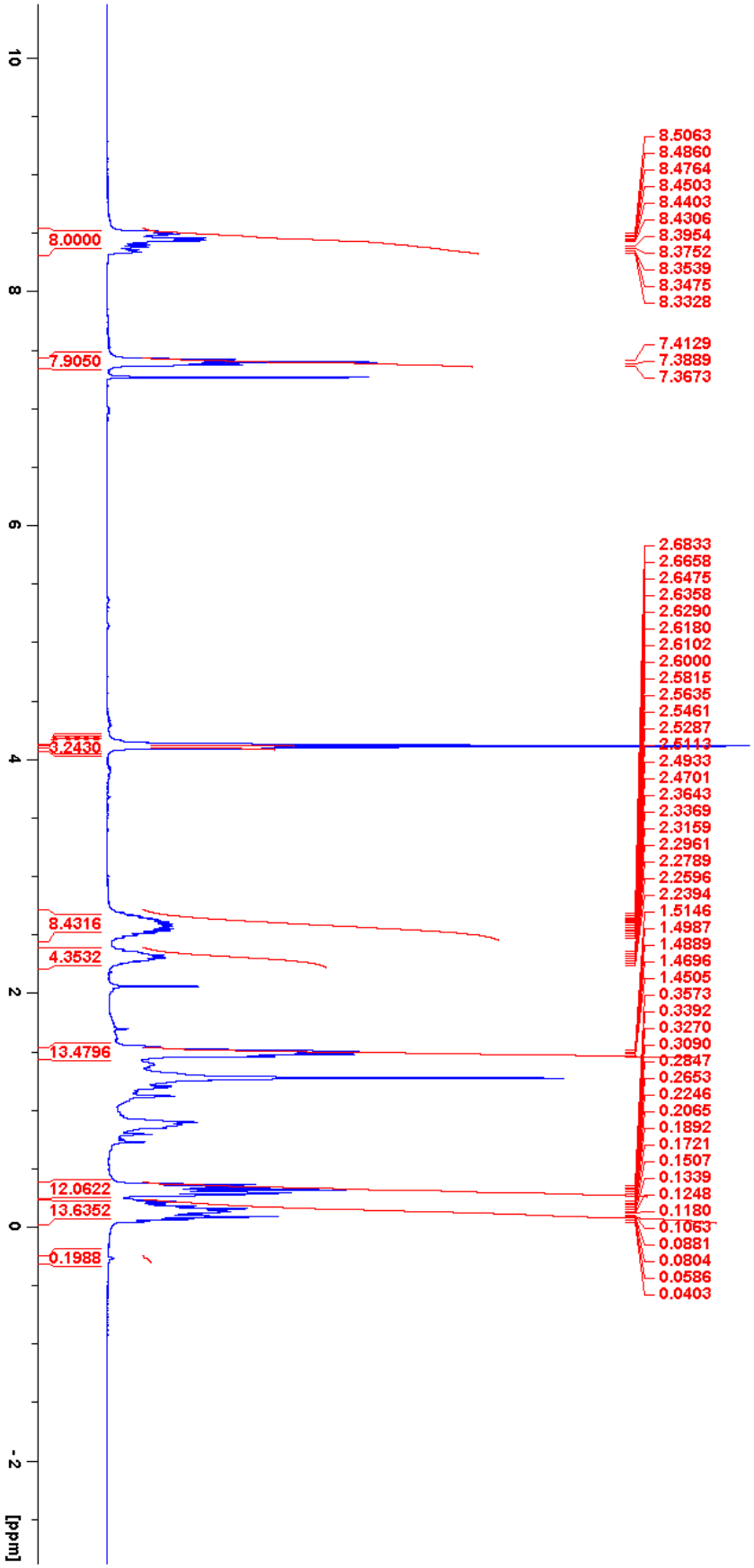

Figure A30: ^{1}H NMR spectrum of **245**·2HCl.

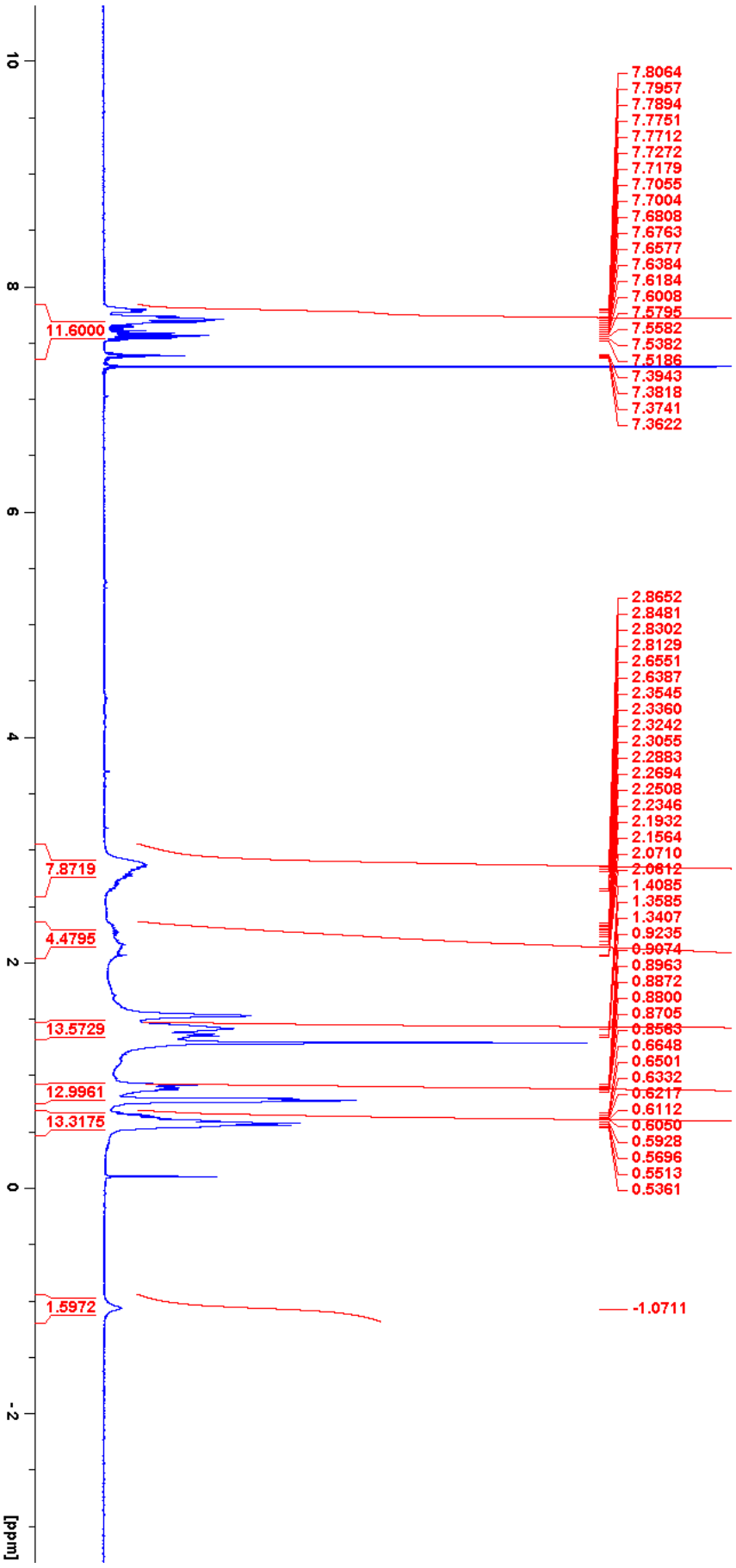

Figure A31: ^{1}H NMR spectrum of **246**.